

# CHARACTERISATION OF PLASMA CLOSING SWITCHES FILLED WITH DIFFERENT GASES

A thesis presented in fulfilment of the requirement for  
the degree of

**Doctor of Philosophy**

**Caron M<sup>c</sup>Garvey, BSc (Hons), MSc**

**2017**

**Department of Electronic and Electrical Engineering**

**University of Strathclyde**

**Glasgow, UK**

'This thesis is the result of the author's original research. It has been composed by the author and has not been previously submitted for examination which has led to the award of a degree.'

'The copyright of this thesis belongs to the author under the terms of the United Kingdom Copyright Acts as qualified by University of Strathclyde Regulation 3.50. Due acknowledgement must always be made of the use of any material contained in, or derived from, this thesis.'

Signed:

Date:

## Acknowledgements

I would like to acknowledge a few people who have provided help and support throughout this PhD project. I would like to thank Dr Igor Timoshkin for his supervision, support and guidance throughout the duration of this PhD project. Without your patience and suggestions this project and thesis most definitely would never have been completed. Thanks also should go to Dr Mark Wilson for always being willing to take time to help talk over issues and problems that came up with understanding the theory or in the lab.

Thank you must also go to Professor Scott MacGregor and the entire HVT/ROLEST group for the regular opportunities to discuss our research work at group meetings organised by Dr Michelle Maclean. Also my fellow PhD & post-doc colleagues who have made this PhD journey bearable; Michelle, Tracy, Laura, Michael, Karen, Dan, Jonah, Rachael, Laura, Sian, Justine, Sotiria & Athanasios,

Funding provided by AWE Aldermaston is gratefully acknowledged. Specific thanks must go to Mark Sinclair and Aled Jones of AWE Aldermaston for their input on various aspects of this PhD project throughout the duration of this project and the provision of a Tektronix Oscilloscope for conducting lab work.

Thanks must also go to the High-Voltage Mechanical Workshop for their assistance in producing the switch bodies used within this investigation and their assistance in troubleshooting issues when things inevitably went wrong. Thanks also go to Maureen Cooper for all of her administrative assistance over the course of these studies, especially in organising conference trips and the examination of this thesis.

Finally, the biggest thanks of all have to go to my family but in particular, my mum, dad & brother for putting up with me through all the highs and lows that trying to complete a PhD brings. I honestly don't know how you've done it, but thank you!

## ABSTRACT

Sulphur Hexafluoride ( $\text{SF}_6$ ) is one of the most commonly used gases within switching applications for pulsed power applications due to a large number of desirable properties, however, it is a greenhouse gas and global concerns over the emission of this gas into the atmosphere have led to an increase in research into potential environmentally friendly alternatives.

This study focused on an experimental investigation into the breakdown characteristics of two commonly used plasma closing switch topologies when filled with different gasses and gas mixtures not previously considered in as much depth for switching purposes (air,  $\text{N}_2$ , 60%/40%  $\text{N}_2/\text{O}_2$ , 90%/10%  $\text{Ar}/\text{O}_2$ , and  $\text{CO}_2$ ) as compared to the characteristics of the switches when filled with  $\text{SF}_6$ . A self-breakdown switch and a field-distortion triggered switch topology with varying inter-electrode gap lengths up to 9mm, filled with gasses at pressures in the range 0.1MPa-0.5MPa were studied and some key operational characteristics and switching parameters such as the self-breakdown voltage of the gases, the spread in self-breakdown voltage, time to breakdown and jitter of the switches were investigated and compared. Temperature of the plasma that forms during breakdown and the conductivity of plasma was extracted for each gas and in addition to this, analysis of post-breakdown waveforms allowed for obtaining values of inductance and resistance of the switches.

Experimental results have been used in the development of two computational models of Marx Generators which are used in the voltage erection stage of pulsed power systems. The models developed describe the switches as either having constant resistance or taking into account the transient plasma resistance which allows for a more accurate representation of the voltage and current behavior across the output load over the first quarter of the current oscillation after switch closure occurs.

# **Contents**

Acknowledgements.....	ii
List of Symbols .....	vii
Chapter 1. Introduction.....	1
Chapter 2. Background and Literature Review .....	5
2.1 Pulsed Power .....	5
2.2 Pulsed Power Switches .....	10
2.2.1 Self-Breakdown Switches .....	12
2.2.2 Triggered Switches.....	15
2.3 Basic principles of Gas Breakdown .....	23
2.4 Modelling of Transient Processes in Plasma Closing Switches .....	30
2.5 Insulating Gases used in Pulsed Power Switches.....	38
2.5.1 SF <sub>6</sub> as an Insulating gas.....	39
2.5.2 Alternatives to SF <sub>6</sub> already considered.....	41
2.6 Conclusions .....	43
Chapter 3. Characterisation of a Self-Breakdown Spark Gap Switch.....	45
3.1 Design and Development of Self-breakdown Switch.....	46
3.2 Experimental Setup and Methodology .....	50
3.3 Self-Breakdown Voltage: Results and Analysis .....	52
3.3.1 Self-Breakdown Voltages for an Air-Filled Switch vs pd.....	53
3.3.2 Self-Breakdown Voltages For a N <sub>2</sub> -Filled Switch vs pd.....	56
3.3.3 Self-breakdown Voltages for a 60% Nitrogen + 40% Oxygen Mix Filled Switch vs pd .....	58
3.3.4 Self-breakdown voltages for a CO <sub>2</sub> -filled switch vs pd.....	60
3.3.5 Self-breakdown voltages for a 90%/10% Ar/O <sub>2</sub> mix filled switch vs pd.....	62
3.3.6 Self-breakdown voltages for an SF <sub>6</sub> -filled switch vs pd.....	64
3.3.7 Comparison of self-breakdown voltages gases for all gases. ....	66
3.4 Analysis of Experimental Results .....	68
3.5 Discussion.....	73
Chapter 4 . Characterisation of a Field-Distortion Spark Gap Switch Triggered with “Slow” 0.45 kV/μs HV Impulses .....	75
4.1 Switch design and electrostatic modelling .....	75
4.2 Switch Construction and Test Set-up.....	82
4.3 Methodology.....	84
4.4 Time to Breakdown in a field distortion switch with variation in pressure and percentage of DC stress level.....	89
4.4.1 Time to Breakdown for an Air filled switch .....	90
4.4.2 Time to Breakdown for an N <sub>2</sub> filled switch.....	96

4.4.3	<i>Time to Breakdown for a switch filled with a 60% /40% N<sub>2</sub>/O<sub>2</sub> mixture.....</i>	101
4.4.4	<i>Time to Breakdown for a switch filled with a 90% /10% Ar/O<sub>2</sub> mix.....</i>	107
4.4.5	<i>Time to Breakdown for a switch filled with CO<sub>2</sub>.....</i>	113
4.4.6	<i>Time to Breakdown for a switch filled with SF<sub>6</sub>.....</i>	118
4.5	Statistical Analysis.....	119
4.5.1	<i>Weibull Analysis of Time to Breakdown.....</i>	121
4.6	Computational Analysis of Time to Breakdown Results .....	135
4.7	Conclusions. ....	138
<b>Chapter 5 . Characterisation of a Field-Distortion Spark Gap switch Triggerred with fast 1kV/ns HV impulses.....</b>		<b>140</b>
5.1	Experimental test set-up.....	141
5.2	Methodology.....	143
5.3	‘Time to Breakdown’ characteristics of the field-distortion switch triggered by a Blumlein pulse generator.....	144
5.3.1	<i>Time to Breakdown for an air-filled switch triggered with 1kV/ns HV impulses. ...</i>	144
5.3.2	<i>Time to Breakdown for a N<sub>2</sub>-filled switch triggered with 1kV/ns HV impulses.....</i>	151
5.3.3	<i>Time to Breakdown for a switch filled with a 60%/40% N<sub>2</sub>/O<sub>2</sub> mixture triggered with 1kV/ns HV impulses.....</i>	156
5.3.4	<i>Time to Breakdown for a switch filled with a 90%/10% Ar/O<sub>2</sub> mixture triggered with 1kV/ns HV impulses.....</i>	162
5.3.5	<i>Time to Breakdown for a CO<sub>2</sub>-filled switch triggered with 1kV/ns HV impulses.....</i>	167
5.3.6	<i>Jitter Analysis .....</i>	171
5.4	Statistical Analysis.....	172
5.4.1	<i>Weibull Analysis of a 2mm inter-electrode gap length.....</i>	173
5.5	Conclusions .....	190
<b>Chapter 6. Plasma Channel Characteristics .....</b>		<b>193</b>
6.1.	Plasma Temperature Evaluation.....	194
6.2	Conductivity of Plasma in Breakdown Channel .....	208
6.3	Discussion.....	210
<b>Chapter 7. Plasma Channel Characteristics .....</b>		<b>211</b>
7.1	<i>Post Breakdown Characteristics.....</i>	211
7.2	<i>Test-set-up and methodology .....</i>	212
7.3	<i>Results .....</i>	216
7.4	<i>Discussion.....</i>	223
<b>Chapter 8. Computational Model: 12 Stage Marx Generator .....</b>		<b>225</b>
8.1	Constant Resistance Model .....	226
8.1.1	<i>Development of Computational Model.....</i>	226
8.1.2	<i>Computational Results – Constant Resistance Model.....</i>	232
8.1.3	<i>Conclusions.....</i>	240
8.2	Dynamic Resistance Model .....	241
8.2.1	<i>Computational Results – Dynamic Resistance .....</i>	247

8.3 Discussion and Conclusions .....	254
Chapter 9 . Conclusions and Future Work.....	257
9.1 Conclusions .....	257
9.2 Future Work.....	262
Chapter 10. Publications .....	264
Chapter 11. References.....	265
Chapter 12. Appendix 1. Weibull Graphs.....	277
12.1 Field-Distortion Gap triggered with 0.45kV/ $\mu$ s HV impulse.....	277
12.2 Field-Distortion Gap triggered with 1 kV/ns triggering .....	286

## **List of Symbols**

$V$	Voltage (V)
$V_{DC}$	DC charging voltage
$R_{ch}$	charging resistor
$Sw$	<i>switch</i>
$C$	capacitance (F)
$L$	inductance (H)
$V_{br}, U$	breakdown voltage (V)
$R$	Resistance ( $\Omega$ )
$p$	gas pressure in the switch (Pa)
$d$	inter-electrode gap distance (m)
$E$	electric field strength (V/m)
$E_{max}$	peak electric field (V/m)
$\alpha$	Townsend's first ionisation coefficient
$\gamma$	Townsend's second ionisation coefficient
$c$	constant
$R_{pl}$	resistance of plasma channel ( $\Omega$ )
$R_{tot}$	Total circuit Resistance ( $\Omega$ )
$U$	Energy of breakdown channel per unit length (J/m)
$\sigma$	conductivity of plasma ( $1/\Omega.m$ )
$M, k$	phenomenological constants which fit to experimental data
$A_1$	fit coefficient applied to self-breakdown data (kV/Pa.m)
$\beta$	second fitting coefficient extracted from the best-fit applied to self-breakdown data (V)

$V_{DC\ stress}$	DC stress voltage applied across the inter-electrode gap space in triggered switch less than the self-breakdown voltage (kV)
$V_{trigger\ impulse}$	impulse voltage applied to the trigger electrode (V)
$A$	Einstein's transitional probability
$g_u$	statistical weight of the upper energy level (eV)
$k$	Boltzmann's constant
$T$	temperature of a plasma channel (K)
$\lambda$	wavelength of light emitted during breakdown event (nm)
$E$	energy applied across the inter-electrode gap (J)
$\gamma_E$	constant that takes into account electron-electron scattering
$Z$	mean ionic charge
$n_e$	number of electrons per unit volume of plasma (MKS)

## Chapter 1. Introduction

The search for potential alternative gases to be used as replacements for Sulphur Hexafluoride ( $\text{SF}_6$ ) as an insulation gas within industrial applications in the power and pulsed power industries has increased in recent years due to the ever tighter global restrictions and regulations governing emissions of greenhouse gases [1]. One particular component of high voltage (HV), pulsed power systems where  $\text{SF}_6$  gas is typically used, is within the spark switches that are a fundamental component of Marx Generators (which can be used within the voltage erection stage of much larger pulsed power systems), or spark switches used in Pulse Forming Lines.

The spark switches used within the Marx generator system are gas-filled and sometimes referred to as plasma closing switches as in their “off” state they are open until spark breakdown occurs, at which point they ‘close’ allowing a current to flow. There are many advantages to using plasma closing switches within the pulsed power research and industrial environments such as their ability to operate at high voltages and currents, their ability to handle high rates of change of currents and voltages, fast closing times have been achieved  $\sim 10$ 's of ns and the standard deviation in the closing time, referred to as the jitter of the switch can be incredibly low too and has been reported as low as  $\sim 2$  ns [2], [3].

The presented work looks at some of the key breakdown characteristics of two commonly used plasma closing switch topologies employed within industrial applications when the spark switches are filled with environmentally friendlier gases/gas mixtures than the more conventionally used  $\text{SF}_6$  gas. In order to compare key breakdown performance characteristics of these switch topologies when filled with different gases directly with the performance characteristics of a conventional  $\text{SF}_6$  filled switch, where possible, experimental results obtained with the potential alternative gases have been compared to the breakdown results obtained under identical experimental conditions when the switch is also filled with  $\text{SF}_6$ . The post-breakdown characteristics of different gases (electrical conductivity of plasma formed in the gas-filled switches) have then been used in the development of a computational model that takes into account the transient characteristics of plasma in the spark plasma closing switches. Thus the developed computational model

allows for investigation of the output characteristics of the pulsed power system (Marx impulse generator) with gas –filled plasma closing switches. The developed model has been used to study the influence of the pulsed power system parameters such as inductance and conductivity of gas plasma on the main parameters of the HV generated impulses: their rise time and wave shape. This information is essential for development and optimization of the pulsed power systems with desirable output parameters to satisfy requirements of the practical pulsed power systems.

In Chapter 2 of the presented thesis, a comprehensive literature review introduces pulsed power technology from its first military applications and progress made throughout the decades since the Second World War which have expanded the many applications into which pulsed power technologies are now employed. A discussion on commonly used switch topologies within the voltage erection stages of pulsed power systems is also provided with a focus on gas-filled plasma closing switches as these are the focus of the experimental research presented within this thesis. A description of the basic principles of gas breakdown is also covered within Chapter 2 as this provides the working mechanism of the gas-filled plasma closing switches. Global industrial applications require different operational parameters of their switches and as such, the gases employed within plasma closing switches vary depending upon the application. A review of commonly used gases as a dielectric media within plasma closing switches alongside their benefits and drawbacks are given within this chapter. The main findings of Chapter 2 establish the groundwork upon which this research is based and show that until now, there has not been an extensive investigation into the operational characteristics of commonly used plasma closing switch topologies when filled with environmentally friendly gases as compared to SF<sub>6</sub> gas which is restricted and of global environmental concern.

Chapter 3 provides a detailed outline of experimental work conducted concerned with the characteristics of six different gases/gas mixtures; air, nitrogen (N<sub>2</sub>), 60%/40% nitrogen/oxygen (N<sub>2</sub>/O<sub>2</sub>), 90%/10% argon/oxygen (Ar/O<sub>2</sub>), carbon dioxide (CO<sub>2</sub>) and SF<sub>6</sub>, within a self-closing spark gap switch. Key breakdown characteristics such as the self-breakdown voltage and the spread of the self-breakdown voltage have been investigated for a range of inter-electrode gap lengths and gas pressures within the switch body. It is shown comprehensively that for a sphere-sphere electrode topology switch filled with different gases, the self-breakdown voltage of air, N<sub>2</sub>, 60%/40% N<sub>2</sub>/O<sub>2</sub> and CO<sub>2</sub> are similar

as the product of the gas pressure within the switch and the inter-electrode gap distance,  $pd$ , increases. The breakdown voltage for  $SF_6$  remained higher than any of the other gases tested, however, the spread in breakdown voltage was also found to be large. It was found that for  $SF_6$  at smaller  $pd$  values, the same level of self-breakdown voltage could be achieved in all other gases tested (with the exception of the 90%/10% Ar/O<sub>2</sub> mixture) with smaller spread at slightly increased, but still reasonable  $pd$  values.

Chapter 4 presents the details of a field-distortion spark gap switch which has been designed and constructed. Within this chapter, the field distortion switch is filled with each of the same gases as used within Chapter 2 (with the exception of  $SF_6$ ) and the main inter-electrode gap space is stressed with 70% or 80% of the self-breakdown voltage before a  $\sim 30$ kV voltage impulse is applied at a rate of  $\sim 0.45$ kV/ $\mu$ s to the mid-plane electrode. The application of the voltage impulse to the mid-plane electrode initiates the breakdown within the switch and the time between the initiation of the trigger impulse and complete collapse of the voltage across the main-gap of the switch is recorded. The standard deviation in the recorded times is defined as the jitter of the switch and for each of the gases is found to be typically  $< 10\mu$ s and increases as the gas pressure within the switch increases.

In Chapter 5 operational parameters of the same field-distortion spark gap switch as described within Chapter 4 have been investigated. However, in place of the trigger generator which applies the voltage impulse at a rate of  $0.45$ kV/ $\mu$ s, a  $-30$ kV voltage impulse is applied to the mid-plane electrode within this experimental set-up via a Blumlein pulse generator at a much faster rate of voltage rise of  $\sim 1$ kV/ns. Again the time between the initiation of the triggering impulse and complete voltage collapse across the main gap of the switch has been recorded and the jitter of the switch obtained. When the trigger impulse is applied by the  $\sim 1$ kV/ns Blumlein pulse generator, it was found that the jitter of the switch filled with each of the five gases was significantly reduced and found to be typically  $< 5$ ns.

A lumped element R-L-C circuit which represents a basic practical pulsed power system is set up within Chapter 6 to simulate the post-breakdown behavior of the plasma channel in the plasma-closing switch. Utilising the plasma channel that forms during a breakdown event as the constant resistive component R, and the light emitted during a breakdown event, the constant resistance of the conductive plasma channel and the temperature of

plasma in the breakdown channel are obtained and analysed. By use of the Boltzmann method to estimate the temperature of the conductive plasma channel formed between the electrodes in the self-breakdown switch utilised and described within Chapter 3 it is possible to extract an estimated temperature of the plasma channel formed during breakdown. The temperature of the plasma channels formed during breakdown events for each of the six gases of interest within this investigation, including SF<sub>6</sub> are estimated over a range of breakdown parameters and obtained results are analysed and discussed.

Chapter 7 provides an analysis of the post-breakdown current within the system. Utilising the same RLC circuit as set-up within Chapter 6, the post-breakdown current flowing in the circuit after a breakdown event in the switch is analysed. Using the obtained current waveforms further fundamental properties of the plasma channel such as the resistance and inductance of the plasma channel that form during breakdown within the switch have been obtained. These parameters are required to develop a computational model of the switch and the pulsed power system; these models have been developed in Chapter 8.

Chapter 8 provides a detailed description of the computational model that has been developed within this project based on the obtained experimental values of plasma conductivity and inductance of plasma closing switches. This model allows for simulation of the output high voltage impulse of a Marx Generator across a practical load, thus this computational model can be used for optimization of the performance of the pulsed power machines used in practical applications. The development of the model is described from a constant resistance of the plasma closing switches, through to a model which considers the transient properties of the plasma channel formed during breakdown in plasma closing switches. The transient properties of the plasma channel have been obtained from experimental data obtained in other chapters of this thesis. The output of the developed model was compared with the measured output of currently-used Marx-generators employed within industry in order to determine how accurately and closely the model replicates the output of physical systems.

Finally, conclusions and suggestions for future research are discussed within Chapter 9. This includes overall recommendations that could be implemented to currently employed systems that utilize plasma closing switches filled with SF<sub>6</sub>.

## Chapter 2. Background and Literature Review

### 2.1 Pulsed Power

Pulsed power was developed during the Second World War and aided in the creation of radar systems. The main essence of “Pulsed Power”, sometimes referred to as ‘pulse power’ in older text is the storage of energy over some extended period of time, compression and then the release of the stored energy occurs over a comparatively far shorter period of time [4], [5] e.g. storing energy over a few seconds and releasing over ps- $\mu$ s timescales. This broad definition of pulsed power, however, is believed to fundamentally miss out a lot of what pulsed power has to offer to applications [6]. Another definition of Pulsed Power given by Bluhm [7] is that; we can consider power to be ‘pulsed power’ for energies discharged into a load for single short pulses or pulses with controllable repetition rates when the electrical power of these pulses is of the order of a few GW . The energy content of these pulses should be of the order of 1kJ or greater. This definition by Bluhm, that the electrical power of pulses should be of the order of a few GW may have applied to the original applications of pulsed power technologies, however, any application that makes use of pulsed power rather than continuous power is still considered pulsed power, regardless of the electrical power or energy content of the pulses.

The original intent of pulsed power technology was for military and defence applications and the output pulses were used to simulate bursts of radiation from exploding nuclear weapons, an application which is beyond day-to-day requirements and involves great amounts of electrical power (can be in the region of terraWatts [8]). Although the foundations of pulsed power technology sit firmly within military applications and many of the advances within pulsed power have arisen from military requirements technological advances which have arisen in the decades since the development of the first pulsed power systems within the world of pulsed power science and engineering have been driven by the many wide-ranging applications within which pulsed power is now utilised beyond military and defence applications. Some of the areas currently making use of pulsed power technologies within their research include, but are not limited to; contributions in fusion research [8], [9], medical applications [10]–[14], agricultural applications such as water

treatment [15] and other industrial applications such as treatment of exhaust gases and material processing [16], mineral processing and plasma channel drilling [17], [18] pulsed electric treatment of liquids and microorganism suspensions for lysis and disinfection [19], [20]. Within these applications and beyond it is noted that and that pulsed power is not and was not intended to ever be an alternative to the traditional ac/DC power sources, instead pulsed power is concerned with applications where power across a load must be pulsed or where the system performs better should the applied power be pulsed instead of continuous.

With a general overview of the many areas where pulsed power technologies are currently employed and a broad definition that pulsed power can be described as 'energy is stored over a long period of time, compressed in time and then rapidly released', it is necessary to describe the key components of pulsed power systems which are fundamental to this research project. There are two main ways in which the energy of a pulsed power system can be stored; this energy can be stored either in an inductive element or within a capacitive element. The energy densities available from inductive elements can be in the region of 3-40 MJ/m<sup>3</sup> compared to the 0.01-1 MJ/m<sup>3</sup> available from capacitive energy storage elements [21], [22]. However where the energy storage elements found in a system are inductive, plasma opening switches must be used rather than the plasma closing switches which are used when the energy storage elements are capacitive. Pulsed power systems employing inductive energy storage elements and the associated plasma opening switches are outwith the scope of this research project and thus only the plasma closing switches and systems making use of capacitive energy storage elements were considered within this research project.

Key components of pulsed power systems based upon capacitive energy storage include a single capacitor,  $C$ . This is charged by a DC voltage supply  $V_{DC}$  via a charging resistor,  $R_{CH}$ , before the switch  $SW$  closes and supplies the voltage pulse across some load. A schematic of a simple pulsed power system which is based upon a capacitive method of energy storage is shown within Figure 2-1

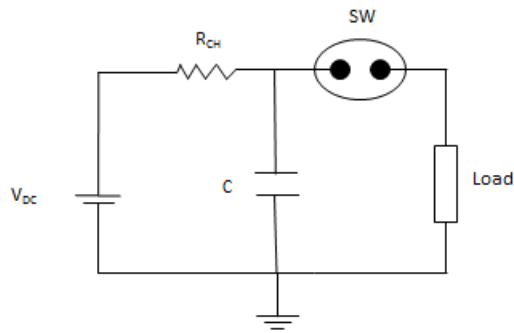


**Figure 2-1 Schematic of a pulsed power system that makes use of a capacitive energy storage method.**

A schematic of a pulsed power system is shown within Figure 2-1. The DC voltage supply,  $V_{DC}$ , applies of the same polarity as the supply voltage across the load. The voltage is applied across the load only when the capacitor discharges after the closure of the switch. The switch closure occurs either under a self-breakdown condition or under a triggered breakdown regime depending upon the nature of the switch.

If a voltage impulse is required to have a polarity that is the opposite polarity to the charging voltage, this can be achieved by swapping the position of the capacitor and the switch within Figure 2-1 so that the new circuit diagram would resemble that shown in Figure 2-2.

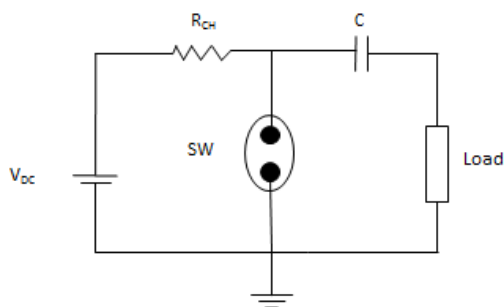


**Figure 2-2 Schematic of pulsed power system with capacitive energy storage method that will provide a voltage impulse across the load that is the opposite polarity to the DC charging voltage.**

During the discharge period, the DC power supply is decoupled from the load as the switch is closed, effectively shorting the circuit to ground.

If experimentally constructing a circuit from the schematic of the pulsed power circuits as shown within Figure 2-1 and Figure 2-2, the peak output voltage across the load will be nominally equal to the input charging voltage (some voltage will be dropped across the charging resistor). It is possible to achieve voltage multiplication by charging multiple capacitors in parallel and then discharging them in series. Within some pulsed power systems, the energy storage stage is also the voltage multiplication stage e.g. a Marx generator. In a Marx generator an arrangement of capacitors are charged in parallel as shown in Figure 2-3.

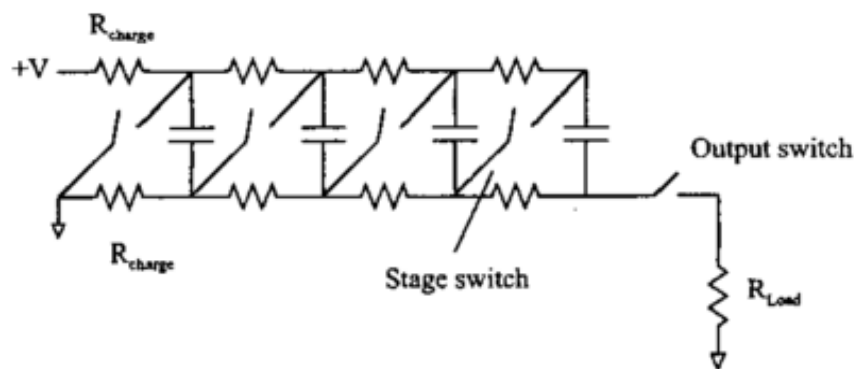


Figure 2-3 A schematic of a Marx Generator which shows the capacitors charging in parallel [23]

Once the capacitors have been charged, by causing the gas-filled switches to close (initiating breakdown within the switches by either self-breakdown or triggered breakdown mechanism), the capacitors are discharged in series which then gives a voltage nominally equal to  $N \times V$  across the load where  $N$  is the number of capacitor bank stages and  $V$  is the voltage to which they were charged. Marx generators are typically cascading systems in which once breakdown in the first gap the first gap has occurred, the second gap 'sees' a voltage twice the normal voltage which initiates breakdown within the second gap etc. This process rapidly flows down the entire stack of capacitor banks initiating breakdown in all the gaps [24].

The voltage multiplication stage is incredibly important for achieving the high, peak output voltages required for pulsed power applications. The switches used within the voltage multiplication stage need to operate reliably at the early voltage multiplication stages in order to erect the voltage pulses required in order for the rest of the system to operate.

Marx generators are used as primary energy drivers in large scale pulsed power systems, such as the Z-accelerator (Sandia National Labs,), high-current generator developed in High Current Electronics Institute (HCEI, Russia) used for Z-pinch research and the MAGPIE facility at Imperial College London. Z-pinch research is essentially an array of exploding wires orientated in the z-axis in order to produce intensive shock waves and plasmas.

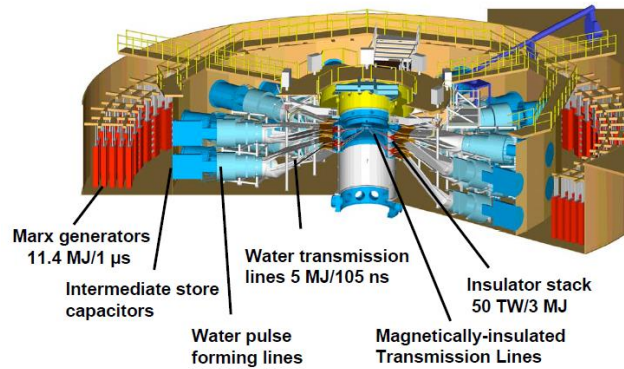


Figure 2-4 Sandia Z-accelerator [25]

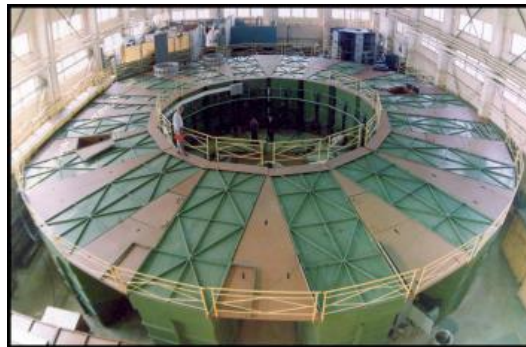
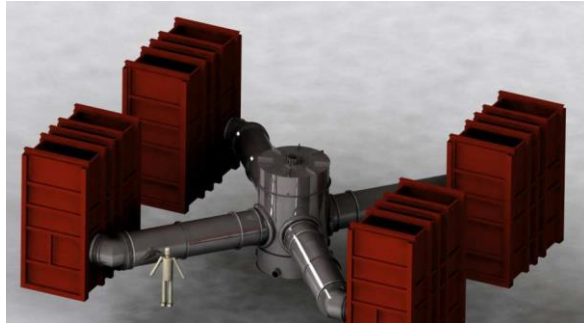


Figure 2-5 High power pulsed system which has been developed at the Institute of High Current Electronics [26]

The MAGPIE facility at Imperial College “consists of four 100 kV Marx banks which store a total of 336 kJ, and generate an output voltage of 2.4 MV. Each Marx bank is connected to a 5 Ohm, 100 ns, water-filled transmission line and subsequently attached to a trigatron switch. After the switches, the four lines join to a single, 1.25  $\Omega$  water-filled transfer line”. MAGPIE is used for Z-pinch research and generation of Megagauss magnetic fields. A diagram of MAGPIE is shown in Figure 2-6 [27].



**Figure 2-6 MAGPIE set-up from Imperial College London with the four 100kV Marx banks (in red) are shown. Each is attached to a transmission line and each of the four transmission lines join to a single line in the centre of the image.**

Marx generators are of particular interest within this thesis as they can be used as the primary charging device of many high-power nanosecond pulse generators as discussed by Mesyats [5]. Within Chapter 8 of this investigation two computational models are developed of a 12-stage Marx generator that factor in the dynamic characteristics of the spark switches in order to investigate the output of the 12 stage Marx bank across some load. The load in these computational models can easily be replaced by existing simulated models containing details of the rest of the pulsed power system beyond the initial charging stage where the Marx bank is situated.

## 2.2 Pulsed Power Switches

As mentioned within Section 2.1, the switches are a fundamental component of any pulsed power system. Switches used within pulsed power applications can be broadly divided into two main sub-categories depending upon whether the energy storage method is inductive or capacitive, and these are opening switches or closing switches respectively. This project is concerned with pulsed power systems where the method of energy storage makes use of a capacitive storage element and thus plasma closing switches are utilised within the experimental set-up. Naming conventions of pulsed power switches typically cover the switches intended use within a system such as an opening or closing switch or more specifically, switches will be named after some key aspect that describes one of their working features e.g switches may be named after the method by which they are triggered [24].

There are many different types of plasma closing switch, but many of these are not of interest within this research project, however, Burkes *et al* [28] provided a review of many different switching types available within the pulsed power community such as thyratrons, ignitrons, vacuum tubes, spark gaps, thyristors, transistors, mechanical switches, superconducting switches etc. The performance parameters and working limitations of each type of switch were presented and it was noted that the limitations of specific switches should be considered dependent upon the application within which the switches are to be used e.g. mechanical switches. Although conventional mechanical switches have been used since the 1700s in experiments as a means of controlling the electrical current, the rapid release of energy at the point of switching can result in switch failure due to erosion, burning or welding open/together of switch parts, since high temperatures can be produced from the high currents that flow [21]. Erosion and ultimate failure of the mechanical switch(es) led to failure of the pulsed power system or damage to load components, an undesirable and costly problem. For this reason, many pulsed power applications use spark gap switches where the topology consists of two (or more) electrodes separated by some distance and the space between the electrodes is filled with a dielectric media. The working media within these switches, that is, the dielectric media that fills the distance between the two electrodes is used to withstand the voltage applied across the gap until a threshold value is reached, initiating breakdown.

The dielectric media utilised within pulsed power plasma closing switches can be gaseous, liquid [29], [30], solid [31] or vacuum [32], [33] and the switches are filled with each (or in the case of vacuum have an absence of any of these) dependent upon the required application of the switch as each switch-filling media has different, desirable, properties. Gases and liquids are considered to be 'self-healing' and can recover their previous dielectric strength after breakdown when left for some period of time unlike solid dielectrics which are eroded and break due to application of voltage across them (solid insulation should be replaced between shots); liquid dielectrics are also preferred if heat needs to be removed; solid dielectrics are preferred when mechanical forces are required to be withstood and vacuum can be used as a dielectric for a wide range of triggering, rapid recovery and low energy losses [32]. This investigative project is concerned solely with gas-filled plasma closing switches and the performance characteristics of the switches when different gases are used to fill the inter-electrode gap space. The different gases used within the different switch topologies will be discussed within Section 2.5, for now, a

discussion on some of the different switch topologies and triggering mechanisms commonly used within pulsed power applications is presented.

### 2.2.1 Self-Breakdown Switches

The fundamental operation of all of the types of switches is transition from the insulation state to the conductive state by application of a voltage across the inter-electrode gap. In a self-breakdown switch, only two electrodes are utilised and are separated by a distance  $d$ . A voltage is applied across the inter-electrode gap length and is increased until it reaches the threshold of the dielectric media (the self-breakdown voltage) that occupies the space between the electrodes and initiates a breakdown within the gap. The self-breakdown voltage of the media that fills the space between the inter-electrode gap length, when the topology of the electrodes creates a uniform electric field between the electrodes can be given by Paschen's Gas Breakdown Law which links the breakdown voltage,  $V_{br}$ , gas pressure,  $p$ , and the inter-electrode distance,  $d$ , ( $V_{br}$  is a function of  $p \times d$ ), discussed within Section 2.3. For non-uniform fields within the switch which can be created due to the topology of the electrodes, Paschen's law is not valid anymore, however conditions that arise within non-uniform fields and which result in corona discharges can be used to enhance parameters which have been shown to stabilise the switch performance in the presence of a highly non-uniform field [34]–[36].

Three commonly used electrode topologies within self-breakdown switches used in pulsed power and high voltage applications are sphere-sphere, plane-plane and point-plane (sometimes referred to as cone-plane topology). The plane-plane topology is commonly used when a uniform electric field is required as this particular design of electrodes gives an (assumed) uniform electric field between the two electrodes where the only enhancement of the electric field occurs at the corners of the electrodes. In practical applications where parallel planes of infinite length are not achievable and therefore field enhancement may occur at the edges of the parallel plates, a small radius can be introduced to eradicate fringing effects and these electrode profiles are Rogowski profile electrodes [37]. Sphere-sphere topology switches are commonly used [38]–[41] where investigations into the breakdown voltage of gases are being investigated. Small regions where the electric field is enhanced occur between the two spheres at the 'tip' of the spheres. Low erosion rates for the electrodes are an advantage for both, plane-plane and the sphere-sphere electrode

topology switches as well as being easier to fabricate than the point-plane electrode configuration which requires precision in the radius of the point tip for calculating the enhanced electric field around the point electrode.

For the point-plane electrodes, a highly non-uniform electric field exists between the electrodes with the highest electric field existing at the tip of the point electrode. The electric field rapidly reduces as the distance increases away from the tip of the point electrode. Corona stabilisation can occur within the highly non-uniform field area of the point-plane switches filled with electronegative gases i.e. the generation of space charge which re-distributes the electric field within the inter-electrode gap space and in the case of negative energisation of the high voltage electrode in air, negative space charge may result in an increase in the breakdown voltage – corona stabilisation [42]. If multiple point electrodes are utilised within a single switch, this can also promote multi-channelling to reduce the overall inductance and control the rate at which current will flow through the gap.

Each of the different self-breakdown switch topology designs described is presented schematically within Figure 2-7.

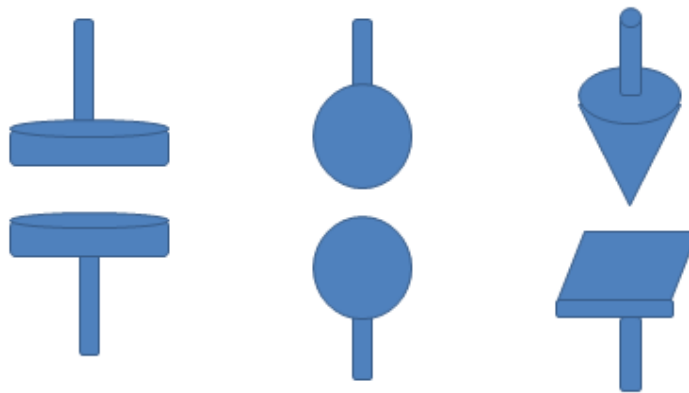


**Figure 2-7. Three different self-breakdown spark switch topologies (a) plane-plane (b) sphere-sphere and (c) point-plane / cone-plane.**

The electric field that exists between the electrodes in each of these configurations shown in Figure 2-7 is often compared to a perfectly uniform electric field. For an ideal uniform

electric field, as is the assumed case for the plane-plane electrode configuration, the value of the electric field is calculated by:

$$E = \frac{V}{d} \quad (2.1)$$

with  $E$  the electric field strength,  $V$  the voltage applied across the gap and  $d$  the inter-electrode gap separation.

For the sphere-sphere topology electrode system (Fig 2-7b) the maximum electric field is given by the following equation:

$$E_{\max} = 0.9 \left( \frac{V}{d} \right) \times \frac{\left( \frac{r+d}{2} \right)}{2} \text{ (MV/cm)} \quad (2.2)$$

Where  $V$  is the applied voltage (MV),  $d$  is electrode spacing (typically 3-7 cm for this Equation) and  $r$  is the radius of the sphere (cm).

In the point-plane topology, the maximum field at the tip of the cone (Fig 2-7 c) is given by:

$$E_{\max} = \frac{2V}{r \ln \left( \frac{4d}{r} \right)} \quad (2.3)$$

Where  $V$  is the applied voltage,  $r$  is the radius of the pointed electrode tip,  $d$  is the distance between the pointed electrode tip and the plane electrode.

For topologies such as the sphere-sphere and point-plane topologies presented within Figure 2-(b) and (c), the ratio of the peak electric field value to that of the uniform topology field gives the field enhancement factor denoted by  $\eta$ :

$$\eta = \frac{\text{Peak Electric Field}}{\text{Uniform Electric Field}} \quad (2.4)$$

The uniform electric field value can be calculated using Equation (2.1).

The operation of a self-breakdown closing switch involves increasing the voltage applied across the inter-electrode gap distance beyond the threshold voltage of whichever media is occupying the gap distance. Based on Pashen's law,  $V_{br}(pd)$ , discussed in Section 2.3, it is clear that there are only two ways to change the breakdown voltage of a self-breakdown switch filled with a specific medium and they are:

1. Altering the inter-electrode gap length,  $d$
2. Altering the gas pressure between the electrodes,  $p$ .

The altering of the inter-electrode gap length requires physical movement of the electrodes, making self-breakdown switches more complex and less robust. For this reason, typically the distance between the electrodes will be fixed and the gas pressure within the switch will be raised or lowered in order to alter the breakdown voltage of the switch.

Self-breakdown switches are popular within many areas of pulsed power research and in many applications due to being robust, reliable and cost-effective and most commonly the inter-electrode gap space of plasma closing switches will be filled with either gas or a liquid [5]. However, as self-breakdown switches as have been described are not triggered by an external means there is not a high level of control over when breakdown will occur within the switch. In practical applications, this high level of control is required over the operation of the switches in order to reliably know that the switches are triggering at a specific time and voltage within their system in order for later parts of the system to 'see' specific voltages that they require to operate. In order to have some determination and control over the time at which the breakdown within the switches will occur, which is important for systems such as Marx generators, triggered switches are commonly used.

### **2.2.2 Triggered Switches**

Spark gap switches are used within pulsed power applications due to their capabilities of being able to operate with high voltages, high current capabilities, fast  $dV/dt$ ,  $dI/dt$  and fast switching times with low jitter.

The switching time of a triggered switch is defined as the time required for the voltage applied across the switch to drop from the charging voltage to the minimum value. This

occurs as a thermalized breakdown channel develops across the inter-electrode gap length and current flows across the switch. Jitter can be defined as the standard deviation of the measured times taken for the voltage to drop from the nominal charging voltage to the minimum value. This is sometimes referred to as  $1\text{-}\sigma$  jitter which denotes that the jitter is obtained to 1 standard deviation and has been used as an accepted definition of jitter in the literature [43], [44].

Some switch designs have an external triggering mechanism which is utilised to initiate breakdown between the electrodes and therefore closure of the switch. This section briefly introduces and discusses a few of the more commonly used triggered switch designs found within the pulsed power community, covering the benefits and limitations of particular designs.

**Field Distortion Triggering** of spark switches is a simple yet effective method of triggering spark gaps when highly consistent breakdown events (at time, inductance etc) are required. The main electrodes within the switch are stressed with a voltage below the DC breakdown voltage to ensure no self-breakdown will occur within the main inter-electrode gap. A trigger impulse of opposite polarity to the applied DC stress voltage is applied to the mid-plane electrode. It should also be noted that the impulse applied to the mid-plane triggering electrode is not usually sufficient to initiate breakdown within the gap without the DC stress voltage also being applied across the gap [45], [46].

The electric field between the triggering electrode and one of the main electrodes is enhanced and initiates a discharge which then expands to form a full breakdown within the gap between the main electrodes.

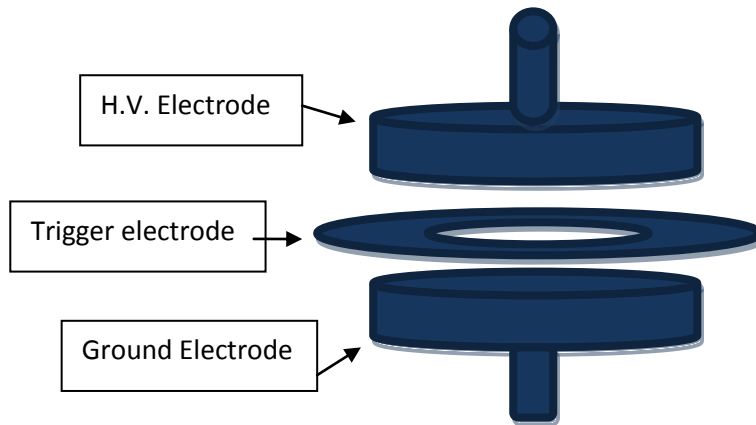


Figure 2-8 Schematic of a Field Distortion triggered switch

The electrodes of a field distortion switch can be arranged as shown within Figure 2-8 although the 'main' electrodes can also be spherical ball bearings in place of the plane electrodes. The mid-plane electrode where the external trigger impulse is applied is located mid-way between the two main electrodes although for some applications this can be moved closer to one of the main electrodes. The trigger electrode is placed along the equipotential lines and when the DC stress voltage is applied across the main inter-electrode gap but prior to the application of the trigger impulse, the trigger electrode does not influence the electric field within the switch.

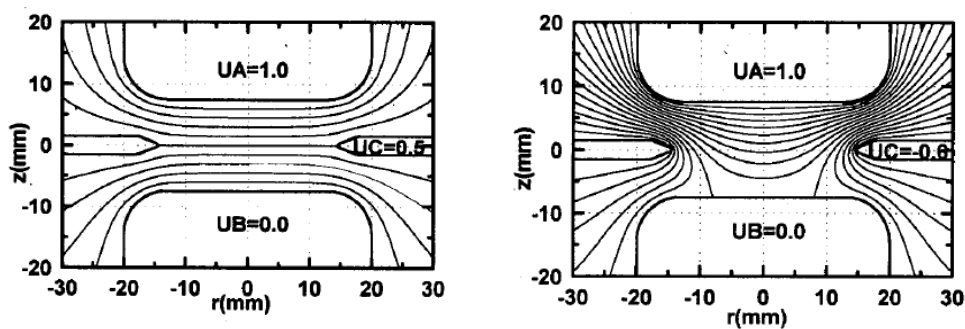


Figure 2-9 shows the electric field distribution within the field distortion switch after the application of a DC stress voltage across the main inter-electrode gap (a) prior to the trigger voltage being applied to the trigger electrode and (b) once the trigger impulse is applied to the mid-plane electrode [45].

Figure 2-9(a) shows the electric field distribution within a field-distortion switch prior to the trigger impulse being applied to the mid-plane electrode. It can be seen that the mid-plane

electrode lies along the equipotential lines and that the electric field is not disturbed by the mid-plane electrode. Figure 2-9(b) shows the distribution of the electric field within the switch once the trigger impulse has been applied to the mid-plane electrode. It can clearly be seen that the electric field is disturbed and enhanced in regions between the trigger electrode and the upper electrode which will lead to breakdown in this region before complete switch closure (which corresponds to a breakdown event across the main inter-electrode gap length) [45].

J.C. Martin commented that the design of a field distortion gap, typically filled with gases was incredibly simple to modify and is quoted noting “this form of construction is so simple as to be positively moronic” [24].

In addition to being robust, simple to build and modify and reliable, field distortion switches are commonly used within pulsed power applications due to their ability to operate over a wide range of voltages (10s-100s kV) and with low jitter capabilities (ns) [47], [48].

If the edges of the triggering electrode are sharp, erosion can occur over the operational lifetime of the switch which changes the geometry of the trigger electrode. Any changes to the geometry of the triggering electrode can reduce the operational reliability, and so minimising the erosion of the electrodes should also be considered when designing switches [49].

**Trigatrons** are another of the commonly used plasma closing switches within industry. Trigatrons typically have two electrodes separated by some distance  $d$  and are triggered by some electrical signal applied to a third electrode which is inserted inside one of the other two electrodes, as illustrated within Figure 2-10 [50].

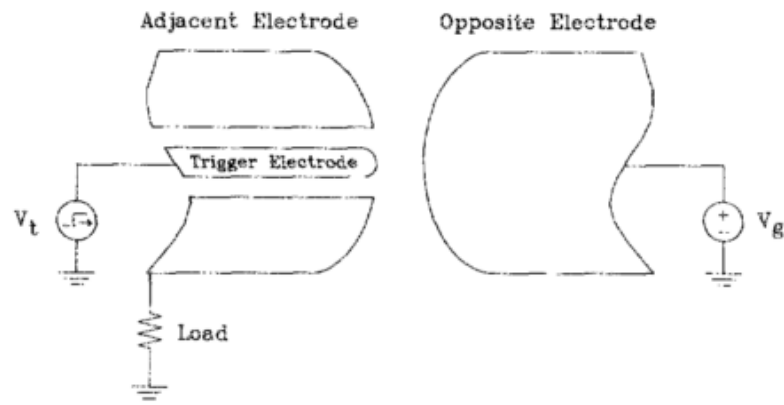


Figure 2-10 Schematic drawing of a trigatron spark gap [50]

Trigatrons are operated by having the two main electrodes applied with some voltage across them which is less than the self-breakdown voltage level of the dielectric medium filling the gap. By applying an impulse to the trigger electrode, breakdown is initiated between the trigger electrode and the adjacent electrode which in turn develops into breakdown within the main inter-electrode gap space between the two main electrodes.

Trigatrons are popular as they can be set to trigger from an external electrical signal, are reliable and are simple in their design. Limitations of trigatrons and their usage include the erosion of the trigger pin for high current applications and erosion of the trigger pin over time can lead to changes in closure time and other defining triggering characteristics of the switch [51].

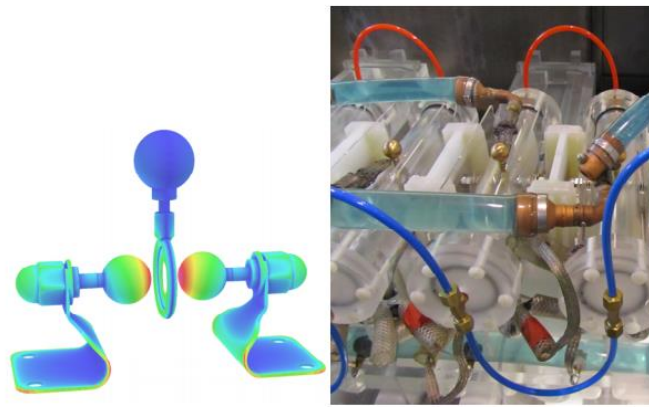
**Laser triggering** is another common method of triggering within certain pulsed power applications where very precise control over the breakdown of the switch is required instead of allowing the switch to operate within the self-breakdown regime. There are many different geometrical set-ups when triggering spark gas with lasers, however, they all fundamentally operate on the basis that the laser pulse provides the initial stimulation to initiate breakdown within the inter-electrode gap space. Guenther and Bettis [52] provided schematics and an extensive discussion on the laser triggering of switches for use within high voltage systems. The main advantages of triggering a spark gap with a laser is that it allows for a high degree of control over the operation of the switch and the time when breakdown will occur. Sandia's Z accelerator is one large machine which requires very

precise co-ordination of breakdown of the switches and as a result uses laser triggering for many of their switches [25], [53], [54].

Laser triggered SF<sub>6</sub> filled switches can provide a low jitter, for example in paper [55] jitter of 1.2 ns has been reported, the switch was operated “at a SF6 pressure of 0.36 - 0.69 MPa”

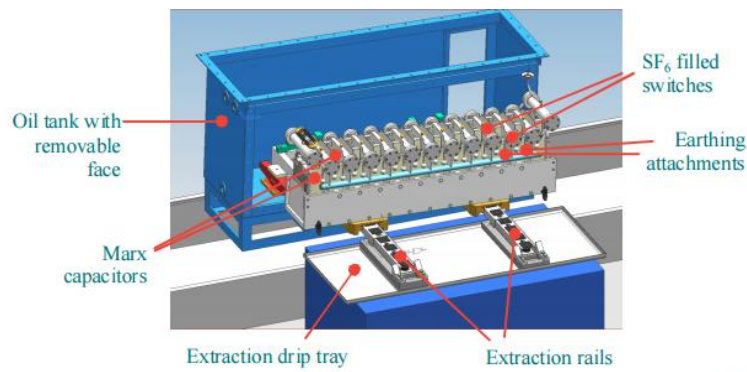
In SF<sub>6</sub> filled switches, it is typically an ultraviolet pulsed laser which is used to initiate the breakdown within the spark gap as this has been shown to improve the jitter (~1-10 ns for laser triggered switches at Sandia [56], [57] although this can be reduced to tens of ps [58]) and have smaller variations on delay time with varied applied voltages in the spark gaps. One limitation of laser-triggered spark gaps however is that they are not ideal for applications requiring high pulse repetition rates as they typically are only able to achieve 10 - 15 Hz [54], [57]. The most prohibitive reasons for not using laser triggering within more pulsed power systems is the vast size that the laser system takes up and the cost associated with purchasing the lasers.

Field distortion switches, trigatrons and laser triggered switches are probably the most commonly used typed of triggered switches within industrial applications however other exist too. It is worth discussing the advantages and limitations of the commonly used triggered switch topologies within experimental set-ups as switches are typically chosen for desirable performance characteristics e.g the switch which provides the lowest jitter may not necessarily also capable of performing at high repetition rates or vice versa. Within the research presented in this thesis a self-breakdown spark gap switch and a field-distortion switch are used as these are the topologies used within the Marx bank of the MEVEX pulsed power machine at AWE [59], [60].



(a)

(b)



(c)

**Figure 2-11** Field-distortion switch from AWE's MEVEX pulsed power machine [59]

Within the voltage erection stage of AWE's MEVEX pulsed power system, the Marx bank employs 13 plasma closing switches, 2 'self-breakdown' switches and 11 field-distortion triggered switches. Figure 2-11(a) shows a schematic of the field-distortion switches that are used within the MEVEX machine, Figure 2-11(b) is a photograph of a small number of the actual switches and Figure 2-11(c) provides a diagram showing the Marx bank of the MEVEX machine and the key components that make it up including the switches.

**Commercially available** plasma closing switches for pulsed power applications include switches developed by the Institute of High Current in Tomsk (Russia), Kinetech Ltd USA and Sandia National Laboratories (L-3 switch) USA. Figure 2-12 shows a picture of these

three low inductive switches which can be, and are, used in linear transformer drivers alongside schematics of their internal cross sections [3].

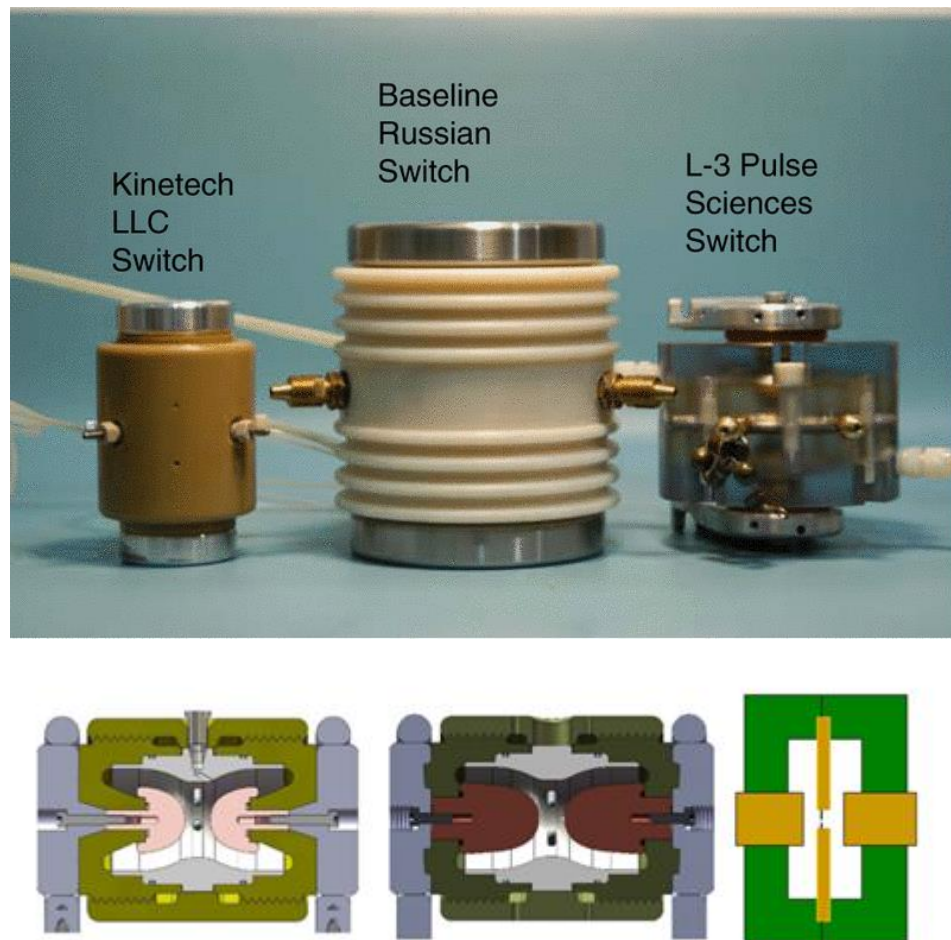


Figure 2-12 a photograph of three commercially available switches and underneath each, a schematic of their internal cross sections. Picture is taken from [44].

These commercially available switches vary greatly in lifetime (number of breakdowns; 2000 for the HCEI switch to >7000 for the L3 switch), their jitter capabilities ( $\sim 0.5\text{ns}$  -  $1\text{ns}$  in the L3 switch to  $\sim 2.2\text{ns}$  in the Kinetech switch) and other features such as delay in switching time which would need to be considered for the application within which they are to be used.

## 2.3 Basic principles of Gas Breakdown

In all of the switches described above, the electrodes are separated from each other by a distance  $d$  and the closure of the switch occurs when ‘breakdown’ is initiated across the gap. Although solids and liquid dielectrics have desirable properties for certain switching applications, this investigation deals solely with plasma closing switches which utilise different gases as the dielectric media within the inter-electrode gap space. This section aims to provide a detailed description of what is meant by “breakdown” specific to the events that occur within gas-filled switches.

Breakdown in a gas, is the transition from a non-self-sustaining discharge a self-sustained discharge. One of the main characteristics of breakdown in a gas-filled spark gap is the presence of a voltage across the gap and the simultaneous flow of current through the gap.

There are several different classifications of gas discharges which are related to the development of spark breakdown in practical plasma closing switches: Townsend discharges (based on the development of electron avalanches), streamer discharges (fast ionisation wave propagating in the gas) and corona discharges (incomplete discharges formed in the areas where the electric field is higher than the value of the critical electric field). The two main mechanisms for breakdown considered in the spark switches are Townsend and streamer breakdown, both of which govern under different conditions [61]. The avalanche (Townsend) breakdown can be transformed into the streamer breakdowns if specific conditions in the spark gap are met.

As with each of the switch designs described within Section 2.2 above, the spark gap switches have electrodes separated by distance  $d$  (a cathode and anode separated by some distance), a voltage applied across the gap and the gap is filled with a gas, a free electron may be emitted from the cathode or it may originate somewhere within the gas that fills the gap between cathode and anode. If the electron can gain sufficient energy from the electric field present such that the electron energy is greater than the ionizing energy of the gas molecules it will be capable of ejecting an electron from a molecule that it may collide with. The new electron and the impacting electron are then accelerated by the field and can cause further electron emissions – an electron avalanche is created.

For Townsend breakdown it is considered that each electron that leaves the cathode will produce a number of ionising collisions  $[e^{\alpha d} - 1]$  where  $\alpha$  is Townsend's first ionisation coefficient which is "the number of ionising collisions made by one electron per unit drift in the direction of the field" and depends on the gas filling the gap [62] and  $d$  is the gap length.

The total current that flows across the device can be given by:

$$I = \frac{I_0 e^{\alpha d}}{1 - \gamma(e^{\alpha d} - 1)} \quad (2.5)$$

where  $I$  is the current flowing in the device,  $I_0$  is the photoelectric current generated at the cathode surface,  $\gamma$  is known as Townsend's second ionisation coefficient (and also depends on the gas filling the gap) the number of secondary electrons produced by each positive ion which hits the cathode.

When the voltage applied across the gap increases, and if there are no external ionisation sources (i.e.  $I_0 \rightarrow 0$ ) the discharge current,  $I$ , can flow through the discharge gap only if the following condition (which is called Townsend breakdown condition) is met:

$$\gamma(e^{\alpha d} - 1) = 1 \quad (2.6)$$

This condition defines the breakdown voltage in electropositive gases. The high dielectric strength of some gases is due to the affinity of free electrons to attach to neutral atoms or molecules and in doing so, forming negative ions. Attachment within these ions represents the effective way of removing electrons which would have led to breakdown at low voltages and the gases where attachment is the key role are referred to as electronegative gases [63]. For switching purposes, electronegative gases are typically used as their affinity of free electrons to attach to neutral atoms means they can withstand applications of much higher voltages, a desirable property for high voltage switching.

For highly electronegative gases such as  $\text{SF}_6$ ,  $\text{CO}_2$  and  $\text{O}_2$  which are highly attaching, the Townsend current growth Equation (Equation 2.5) can be modified to Equation 2.7:

$$I = I_0 \frac{\left[ \frac{\alpha}{\alpha - \eta} e^{(\alpha - \eta)d} \right] - \left[ \frac{\eta}{\alpha - \eta} \right]}{1 - \left[ \gamma \frac{\alpha}{\alpha - \eta} e^{(\alpha - \eta)d} - 1 \right]} \quad (2.7)$$

where  $\eta$  is the number of attaching collisions made by one electron drifting one centimetre in the direction of the field. Townsend's breakdown criterion given by Equation 2.6 in [63] can also be modified for electronegative gases and is given by:

$$1 - \left[ \gamma \frac{\alpha}{\alpha - \eta} e^{(\alpha - \eta)d} - 1 \right] = 0 \quad (2.8)$$

The range of operation for Townsend and streamer mechanisms depends on and can be distinguished by the critical length of the avalanche discharge and the gap spacing. The critical length of an avalanche is defined as the length at which the discharge of a single avalanche can sufficiently distort (enhance) the electric field in front of the avalanche head and thus the slow electronic avalanche (which propagates with the drift velocity of electrons) can transform into a significantly faster moving ionisation wave (streamer). It is established experimentally that the field ahead of the avalanche front is sufficiently strong for formation of streamers if the avalanche head contains  $10^{18} - 10^{20}$  electrons. Thus for transformation of electronic avalanche into plasma streamer the following condition should be satisfied:

$$\alpha \ell_{crit} > (18-20) \quad (2.9)$$

where  $\ell_{crit}$  is the critical length of the avalanche.

If the critical length of the electron avalanche,  $\ell_{crit}$ , is greater than the length of the gap,  $d$ , the electric field in the gap will not be distorted by the space charge of the avalanche and thus only Townsend breakdown can occur. Conversely, if the critical length of the electron avalanche is shorter than the gap space, the development of the avalanche may change into a plasma streamer and this is what is also known as a streamer discharge [5].

The Townsend breakdown mechanism can be used to explain static breakdown in the gap, with its transition to pulsed breakdown depending on the specific topological, electrical and

thermodynamic conditions in the gas switch. Townsend's breakdown depends on the second ionisation process i.e. positive ions should have sufficient time to return back from the anode to the cathode to generate secondary electrons by hitting the cathode. The minimum transit time (time of ionic flight from the anode to the cathode) can be introduced into the breakdown model and this time can be used to establish the electrical, topological and thermodynamic conditions for different categories of discharges in spark gaps: the Townsend (static) discharge and the impulsive (streamer) discharge.

This analysis was conducted in [64] and Figure 2-13 shows conditions for Townsend and impulsive streamer discharges. The area along line 1 in the  $\tau^*p$ -  $D^*p$  diagram is attributed to an area where the discharges do not have well defined characteristics to satisfy either avalanche or impulsive streamer characteristics. The conditions above line 1 are where the characteristics for static Townsend discharges are prevalent and anything below the line is when the conditions define impulsive streamer discharges.

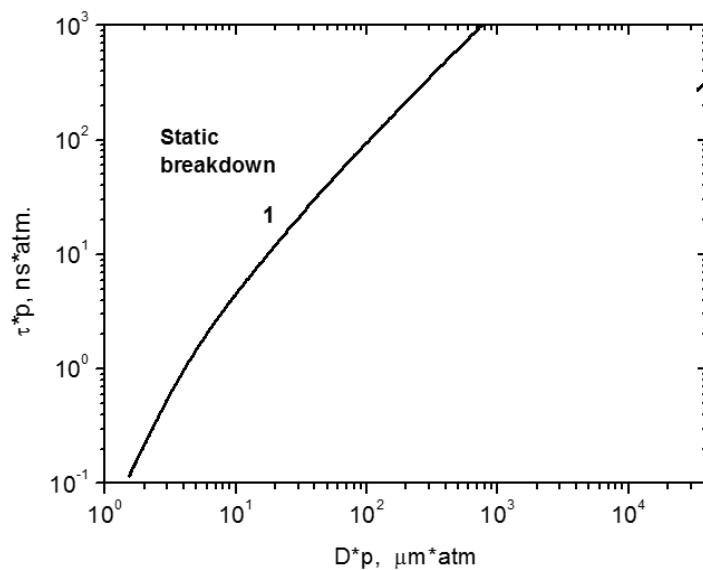


Figure 2-13  $\tau^*p$  vs  $D^*p$  showing breakdown conditions for static or impulsive breakdown conditions depending upon if the conditions fall above or below the boundary line indicated from [64]

The boundary Line 1 in Figure 2-13 allows the evaluation of the parameter ranges which are required for the Townsend (static) mechanism of breakdown to occur. For the parameters  $\tau p(dp)$  which describe the area above Line 1, the breakdown will be the Townsend static

breakdown. For the parameters which are below Line 1 the breakdown can be impulsive (streamer) breakdown.

This line is described by the following Equation:

$$p\tau > 10Dp / \left( \frac{E_{br}}{p}(Dp) \right)^{0.53} \quad (2.10)$$

where  $E_{br}$  is the breakdown field strength,  $p$  is the pressure in atm,  $D$  is the distance between cathode and anode,  $\tau$  is the time of application of the voltage [64].

The main performance characteristics of a spark switch are characteristics such as the self-breakdown voltage, the triggered breakdown voltage, voltage spread, jitter etc. The self-breakdown voltage in a gas-filled switch is the maximum voltage that can be applied across the gap before the gas ionizes and ultimately a current will be able to flow through the gap.

When electrons and ions in a gap filled with gas at pressure  $p$  are moving in a field  $E$  are applied to calculate  $\alpha$  and  $\gamma$ , the breakdown voltage can be calculated as a function of  $pd$ , the product of the pressure of the gas and the gap spacing using condition (2.3). This Equation for the maximum voltage which can be withstood by the gas before breakdown, will be initiated, referred to as the self-breakdown voltage, was derived by Paschen [65] and relates the breakdown voltage of gases to the product  $pd$  and is given by:

$$V_{br} = \frac{Bpd}{\ln(Apd) - \ln\left(\ln\left(1 + \frac{1}{\gamma}\right)\right)} \quad (2.11)$$

where  $V_{br}$  is the breakdown voltage of the gas in  $V$ ,  $p$  is the gas pressure in Pa,  $d$  is the electrode separation in m  $\gamma$  is the secondary Townsend emission coefficient which relates the number of secondary electrons emitted per incident positive ion, and  $A$  and  $B$  are experimentally determined constants.

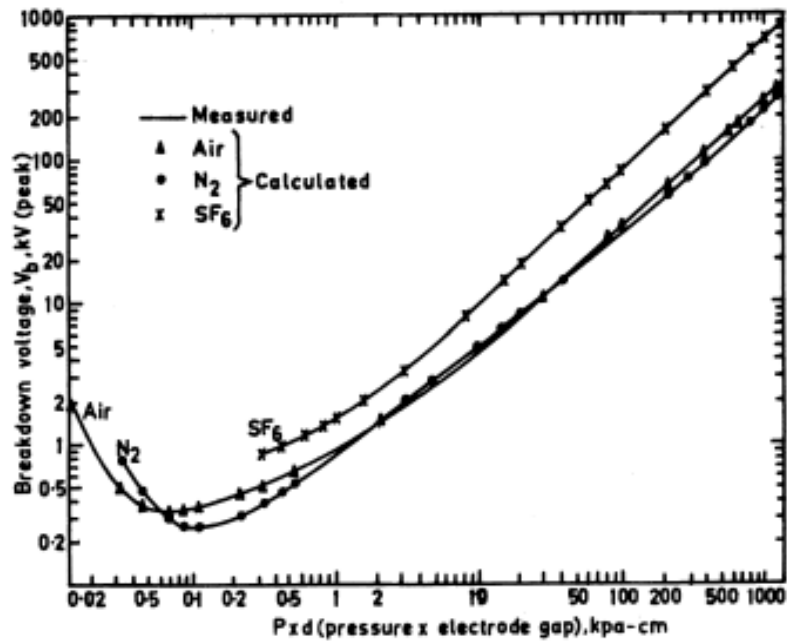
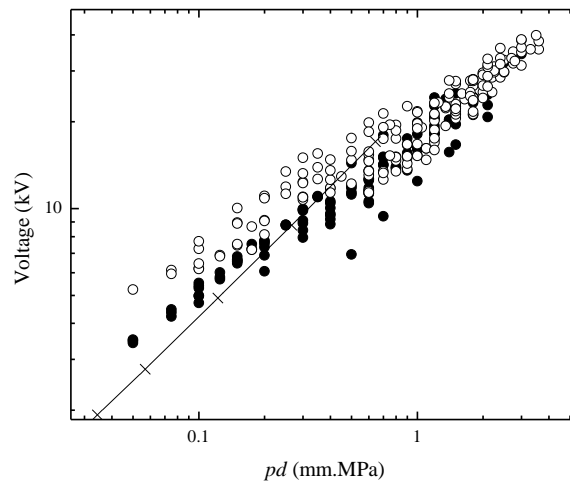


Figure 2-14 Paschen Breakdown Curves for Air, N<sub>2</sub> and SF<sub>6</sub> as measured by [66].

Figure 2-14 provides a graph showing Paschen breakdown curves for Air, N<sub>2</sub> and SF<sub>6</sub> and clearly shows that on the right hand side of the Paschen minimum, the breakdown voltage of SF<sub>6</sub> is higher than that of Air and N<sub>2</sub> and increases more rapidly as a function of  $pd$  than both air and N<sub>2</sub>. The Paschen curves can be split into two distinct sections, the left hand side (LHS) and the right hand side (RHS) around a minimum point on the curve which is known as the Paschen minimum. The Paschen minimum represents the  $pd$  value at which an electron avalanche will occur at the lowest voltage causing breakdown.

Paschen's law derived within [65] and described by Equation 2.11, was strictly for ideally uniform electric field conditions and the data that exists to date covers standard gases. The number of gas mixture combinations are too numerous to be able to have Paschen curves for every combination of gases in existence. This means that for any topology of electrode where a perfectly uniform electric field does not exist, the prediction of self-breakdown voltage of gases for which Paschen curves already exist may not hold true. However, it has been shown that the breakdown curves  $V_{br}(pd)$  in highly divergent electric fields in air follows the Paschen's law obtained for uniform electric field [67]. It has been stated by Hogg et al. [67] that the breakdown voltages obtained in a point plane electrode topology filled with air "closely follows the conventional Paschen's law, and there is a strong scaling

tendency for breakdown voltages in highly divergent electric fields which can be utilised in the design of plasma closing switches and other component parts of compact high-voltage systems". Figure 2-15 shows the breakdown data obtained by Hogg et al in a point plane configuration stressed with both positive and negative electric potential (open and closed circles) and the classic Paschen's breakdown curve obtained in the uniform electric field.



**Figure 2-15 Experimental results obtained in [67] examining the breakdown voltage of air under the influence of positive and negative electric potential (open and closed circles respectively) within a point-plane topology switch in comparison to paschen breakdown curves where perfectly uniform field is assumed.**

By showing the agreement of the breakdown voltage of air under highly non-uniform conditions with 'classic Paschen' breakdown data, this allows for further work to be conducted into investigating the breakdown voltage of gases or gas mixtures which have not already been considered for use within switches and shows that a reasonable estimation of the breakdown voltage can come from a switch topology where the electric field within is not perfectly uniform.

Paschen's law has also been shown to have limitations: when the inter-electrode gap distance has been reduced significantly while gas pressure is held constant at around 0.1MPa [68]; or when the  $pd$  value is incredibly high, deviations from the predicted values have been seen to occur [69]. This shows that if experimental conditions to determine the self-breakdown voltage of a gas do not meet the perfectly uniform field conditions as required by Paschen, it cannot reasonably be expected that Equation 2.11 will accurately

describe or predict the self-breakdown voltage of the gas. Therefore, if another equation can be suggested that more accurately described any trend in the behaviour of the self-breakdown voltage as a function of  $pd$  under non-uniform conditions, this may provide a better fit to experimental data than a classic Paschen curve for the same gas under perfectly uniform electric field conditions.

## 2.4 Modelling of Transient Processes in Plasma Closing Switches

The interest in developing a computational model of switches such as plasma closing switches can be considered as a method of changing operational parameters in order to quickly investigate the influence on the output of currently employed systems or as a means to aid development of new systems. While the idea of developing a computational model that can accurately describe the performance of pulsed power systems seems simplistic, the factors which must be considered and included within the model are numerous and complex, such as providing an accurate representation of the time-varying resistance and inductance of the plasma channel that forms during a breakdown event. This is a particular area of interest as the resistance and inductance of the plasma channel influence the operation of the pulsed power system and being able to computationally model this will allow for optimisation of currently employed systems or development before construction of any future systems.

For some approaches such as that presented within [70][71], the simplification made whereby the resistance and inductance of the plasma are deemed to be time independent allows for estimations of both the resistance and inductance values of the plasma as constant values. It is also reported within this paper that typical values for inductance are within the nH range and resistances on the order of an  $\Omega$  to m $\Omega$ . Modelling plasma closing switches in this way as simplified RLC circuits, as part of larger pulsed power systems such as Marx banks, has been shown to produce results over long timescales ( $\mu$ s) that are comparable with experimentally obtained results [60][59][72].

It has been reported that the inductance can still be considered constant over time [33], however, in practice the behaviour of the resistance of the plasma channel that forms during a breakdown event is complex and does vary with time, which needs to be

considered when developing a representative computational model. The change in plasma resistance, however, is observed to drop from a high value pre-breakdown until it stabilises to some lower, constant value during the conduction phase, when current is flowing through the plasma channel. Being able to understand this behaviour allows for deeper understanding of the energy dissipated within the switches and many studies have suggested ways to describe the behaviour of the plasma resistance [73]–[81].

The starting point for all models to date within the literature aiming to estimate a plasma channel resistance is the reasonable assumption that the resistance of a plasma channel is directly related to the resistance due to the conductivity of the gas which is dependent upon the mobility of charged particles within the gas. The simplest form of Ohm's law, where  $V=IR$ , considers only the case where the plasma resistance is a constant value. In order to consider temporal conditions across the breakdown channel in a switch that contain a non-constant time-dependent resistance, this would become  $V(t)=I(t)R(t,I)$ .

As breakdown develops within the inter-electrode gap length, the dynamics of the plasma channel change in terms of the radius of the plasma channel expanding, temperature increasing and pressure increasing and any model for the dynamic plasma resistance should include coefficients to consider these factors in order to increase the accuracy of the model. Within the established literature where models have attempted to describe the behaviour of the plasma resistance,  $R_{pl}$ , two main approaches have been taken:

- The resistance,  $R$ , is proportional to the inverse of the current,  $i$ , to the power,  $n$ :

$$R_{pl} \propto \frac{1}{i^n} \quad (2.10)$$

- Or the resistance is proportional to the inverse of the integral of the current  $i$ :

$$R_{pl} \propto \frac{1}{\int i dt} \quad (2.11)$$

Both of these approaches cover the first quarter of the current oscillation, or when the plasma resistance goes from its open circuit resistance value (maximum resistance) to its minimum value as the current flow through the plasma reaches its maximum value. An

approach, using a hydrodynamic model suggested by Braginskii [82], for estimating the radius of the plasma channel has been shown by Maas [29], to correspond closely to experimental results.

The different methods of describing the resistance of plasma that have been presented within the literature such as those mentioned by Rompe and Weizel [79], Toepler [81], Vlastos [73], Barannik [74], Kushner [75] and Popovic [78] are based on the main physical mechanisms of breakdown such as the energy balance equation and satisfaction of the principles of thermodynamics but where they all differ is in the phenomenological constant(s) used to fit to analytical data sets under set experimental conditions. Each of these presented methods have been derived under sets of assumptions or manipulated or normalised in order to align with resistances curves which may have been obtained under different sets of experimental conditions.

Toepler's suggested equation, Equation 2.12, to describe the plasma resistance proposed [81] as an inverse to the integral of the current flow through the plasma channel was derived empirically from experimental data.

$$R_{pl}(t) = \frac{C_1 l}{\int i dt} \quad (2.12)$$

where:  $R_{pl}(t)$  is the dynamic plasma resistance [ $\Omega$ ],  $C_1$  is a proportionality constant that depends upon the gas,  $l$  is the plasma channel length [m] and  $i$  is the current [A]. The experimental data used to obtain Toepler's expression for the plasma resistance made use of a plasma channel 9mm – 10mm in length and using air at a pressure of  $P_0 = 10^5$  Pa. Toepler's Equation includes a constant of proportionality which will change dependent upon the gas in which the plasma forms, however no suggestions are made by the author within the paper as to values for this constant.

Another suggestion as to an Equation which can describe the dynamic plasma resistance during a breakdown event was presented by Vlastos [84] as in Equation 2.13:

$$R_{pl}(t) = \frac{C_1 l a^{2/5}}{\left(\int i^2 dt\right)^{3/5}} \quad (2.13)$$

where each of the symbols have same meaning as previously used within Equation (2.12) and  $a$  is the plasma channel radius (m). The experimental conditions from which this expression for the plasma resistance was obtained were that the length of the plasma channel was 130mm and under exploding wire restrike conditions. Exploding wire restrike conditions are a method of creating long plasma channels up to 9m in length by applying high power impulses to a thin copper wire allowing a column of plasma to form along the axis of the wire [73], [85]. In addition to the fixed experimental conditions, the author made assumptions about the arc channel such as no radiative or thermal losses. The conductivity of the plasma channel was assumed using Spitzer's conductivity and related to the temperature by  $\sigma \propto T^{3/2}$ . The Spitzer conductivity and the temperature dependence are discussed within Chapter 7 of this thesis when the Spitzer model of conductivity is used to extract a value of conductivity of the plasma from temperature measurements obtained through optical emission spectroscopy.

Popovic *et al* provided another expression for estimating the plasma resistance, given by Equation 2.14 and is derived empirically from experimental data and presented as another dependence upon the inverse integral of the current flowing through the channel [78].

$$R_{pl}(t) = \frac{C_1 l}{\left[ \int i^2 dt \right]^n} \quad (2.14)$$

The symbols in the expression above have the same meanings as within the previously presented equations and  $n$  is a constant. The test conditions used to derive this expression made use of a channel length of 0.02m, gas pressure of  $0.5 \times 10^5$  Pa, a unipolar pulse and for different gases (air, CO<sub>2</sub>, O<sub>2</sub>, Ar and Xenon (Xe)). Within the investigation a constant  $n = 0.33$  is suggested.

The following three suggested models by Rompe and Weizel, Barannik and Braginskii all have all been derived from the energy balance equation and, in a manner similar to those proposed and described already, suggest that the resistance of the plasma channel has a relationship that is inversely proportional to the integral of the current flow through the breakdown channel. Derived from hydrodynamic equations, the energy balance equation can be expressed as:

$$\frac{dU}{dt} = p \frac{l}{dt} [\pi a^2] = \frac{i^2}{\sigma \pi a^2} \quad (2.15)$$

where  $i$ ,  $a$  and  $l$  are as previously defined,  $U$  is the energy of the channel per unit length [J/m],  $p$  is the pressure of the shock front [Pa], and  $\sigma$  is the conductivity of the plasma [1/Ω.m]. The energy balance equation has been used as a basis for the plasma resistance equation suggested by Rome and Weizel in 1944, Barannik *et al* in 1975 and Braginskii in 1958.

The Equation for plasma resistance suggested by Rompe and Weizel [79] derived from the energy balance Equation is given as:

$$R_{pl}(t) = \left[ \frac{P_0 l^2}{2C_1 \int i^2 dt} \right]^2 \quad (2.16)$$

where the symbols all have the same meanings as previously stated and  $P_0$  is the initial gas pressure (Pa). Within the Rompe and Weizel paper [79] some the pressure reported was for  $P_0=1.6 \times 10^5$  Pa and the gap separation was reported as  $l < 0.035$  m. Thermal and radiative losses have been neglected within this model as well as any consideration of effects due to the arc radius, however this proposed method has been confirmed experimentally by Mesyats [86].

Barannik *et al* proposed model for estimating the resistance of a plasma channel also has proportionality dependent upon the inverse integral of the current flow and is derived from Equation (2.15) the energy balance equation. Barannik *et al* proposed the following expression for the resistance of the plasma channel [74]:

$$R_{pl}(t) = \frac{C_1 l \rho_0^{1/3}}{\int i^{2/3} dt} \quad (2.17)$$

and again, each of the symbols have the same definitions as previously outlined within the other possible plasma resistance equations with the addition of  $\rho_0$  being the gas density (kg/m<sup>3</sup>). Barannik's proposed model is suggested to fit with experimental results for current values of  $i \leq 10$  kA, pressures  $P_0 \leq 12 \times 10^5$  Pa,  $l \leq 0.4$  m and for air, SF<sub>6</sub> and N<sub>2</sub> gas. The assumptions and conditions included by Barannik *et al* within the paper are those of no

radiative or thermal losses in the model and that neither the conductivity or the temperature of the plasma change with time.

Braginskii's hydrodynamic model based on the energy balance equation, Equation (2.15), gives the radius of the breakdown channel as a function of time and current:

$$a^2(t) = \left( \frac{4}{\pi^2 \rho_0 \xi \sigma} \right)^{1/3} \int i^{2/3} dt \quad (\mu\text{m}) \quad (2.18)$$

with :  $a(t)$  the radius of the plasma channel [ $\mu\text{m}$ ],  $i$  is the current [A],  $\rho_0$  is the initial gas density [ $\text{kg}/\text{m}^3$ ],  $\xi$  is a constant associated with the gas,  $\sigma$  is the conductivity of plasma [ $1/\Omega\cdot\text{m}$ ] and  $t$  is the time [s]. Braginskii's model is based on the physical processes which occur within the gas i.e. the electrical energy which is deposited into the channel increases the internal energy of the plasma and the work associated with expanding the radius of the plasma channel. The radius of the plasma channel has been described by Equation 2.18 as a time dependent parameter which must also satisfy the energy balance equation given by Equation 2.15.

Thus in the framework of Braginskii's proposed model, the expression for the resistance of a plasma channel is given by:

$$R_{pl}(t) = \frac{l}{a(t)^2 \sigma \pi} \quad (2.19)$$

where each of the symbols are as previously defined. The expression for the radius of the plasma channel  $a(t)$  is given by Braginskii as in Equation (2.18) and is a function of the gas density, conductivity and a constant which depends upon the gas type. Braginskii's work [82] only gave values for the constant for hydrogen ( $\xi=4.5$ ), however Martin [87] provided a value for other gases, also  $\xi=4.5$ , which is discussed further within Chapter 8 of this thesis.

Each of these models for estimating the resistance of the plasma channel presented thus far has proposed that the resistance is proportional to the inverse integral of the current. Some investigations though, such as that undertaken by Kushner *et al* [75] propose a dependence of the plasma resistance upon an inverse exponent of the current. The expression for the resistance of the plasma channel given by Kushner *et al* is:

$$R_{pl}(t) = C_1 l \left[ \frac{P_0^3}{A^2 t^6} \right]^{1/5} \quad (2.20)$$

where the coefficients are the same as previously defined in Equations (2.12-2.19). The experimental constraints given by Kushner *et al* were for  $l \leq 0.012\text{m}$ , gas pressure  $P_0 = 0.5 \times 10^5 \text{ Pa}$  and current density of  $j = 2 \times 10^4 \text{ MA/m}^2$ . The gases used within [75] were  $\text{H}_2$ ,  $\text{N}_2$ ,  $\text{SF}_6$ ,  $\text{CH}_4$ ,  $\text{Xe}$ .

A review and comparison of many of these plasma resistance Equations has been presented by Engel *et al* [80]. The authors provide details of the assumptions made by each author within their respective studies, which have been outlined within this section, as well as providing recommendations for the value of  $C_1$ , the proportionality constant which appears in all of the above suggested expressions for the plasma resistance. Where no value for the constant was provided by the author within the original research paper Engel *et al* have suggested suitable values to fit with data, however, it should be noted that values for  $C_1$  presented were all normalised for gas pressure  $P_0 = 0.85 \times 10^5 \text{ Pa}$  and where more than one value for  $C_1$  is reported, these values have been obtained dependent upon which expression for the radius of the plasma channel has been used by the author within their original investigation.

Table 2-1 shows the values of the constant(s) of proportionality suggested by Engel *et al* for each of the author's papers where an equation to describe the resistance of the plasma channel that forms during a breakdown has been suggested. Values for the constant of proportionality  $C_1$  are given for a normalised gas pressure to account for differences in experimental test conditions in some of the papers. It can clearly be seen that there is a wide range of values (across orders of magnitude) of which  $C_1$  can take.

**Table 2-1 Values for C the constant(s) of proportionality suggested by Engel *et al* for each of the proposed methods of describing the plasma resistance outlined**

<u>Reference</u>	<u>Normalised Constant, C<sub>1</sub></u>
<i>Barannik</i> [74]	$C_1 = 1.7 \times 10^{-3}$
<i>Kushner</i> [75]	$C_1 = 24.7$ $C_1 = 19.1$
<i>Popovic</i> [78]	$C_1 = 30$ (for $n=0.33$ )
<i>Rompe and Weizel</i> [79]	$C_1 = 9.7$
<i>Toepler</i> [81]	$C_1 = 4.5 \times 10^{-2}$
<i>Vlastos</i> [84]	$C_1 = 876$ $C_1 = 1003$

Many of the proposed equations to describe the temporal behaviour of the plasma resistance over time which have been discussed have proportionality constants attached to them which have been extracted under specific experimental conditions. It can therefore reasonably be assumed that any value of plasma resistance obtained using these equations will only hold true provided identical experimental conditions are going to be replicated.

Within Chapter 8 of this thesis, two computational models of 12-stage Marx bank systems are developed. For the dynamic resistance model, the Braginskii expression for plasma resistance as given by Equation (2.19) is utilised. Braginskii's equation for the plasma resistance was chosen as this was developed from the energy balance equation, includes the expression for a changing radius of plasma channel with time, given by Equation (2.18), and was not dependent upon specific experimental conditions in order to derive this expression. By using Braginskii's expression for the resistance of a plasma channel, this also allowed for more user input in order to determine the model's sensitivity to changing physical parameters (e.g the conductivity of the gas) and is comprehensively outlined within Chapter 8.

## 2.5 Insulating Gases used in Pulsed Power Switches

As already outlined briefly in Section 2.2, gases are typically used as the insulation medium within pulsed power switches due to their dielectric strength, ability to recover their dielectric strength after a discharge event, rate at which they can recover their dielectric strength and cost amongst other reasons. From an review of available literature [88]–[92] it has been seen gases used within spark gap switches of pulsed power devices include; Air, SF<sub>6</sub>, CO<sub>2</sub>, N<sub>2</sub>, Helium (He), hydrogen (H<sub>2</sub>), argon and many mixtures of gases such as SF<sub>6</sub>-CO<sub>2</sub>, SF<sub>6</sub>-Air and SF<sub>6</sub>-N<sub>2</sub>.

Gases can be split into two broad categories dependent upon their ability to attract electrons and to form stable negative ions (electronegative gases) or to be ionised by electron impact with formation of positive ions (electropositive gases). Generally speaking, the more electronegative a gas is, the higher the breakdown voltage of that gas will be due to the attachment of electrons and the formation of negative space charge – thus the highly electronegative gases tend to have higher dielectric strengths than electropositive gases.

**Table 2-2 Dielectric Strength of the gases used within this investigation. Table created with data taken from [93]**

Gas	Dielectric Strength (relative to air)	Electron Attaching
Air	1	Weakly attaching
N <sub>2</sub>	1.15	Weakly attaching
CO <sub>2</sub>	0.95	Weakly Attaching
SF <sub>6</sub>	3	Strongly Attaching
Ar	0.2	Non-attaching

Each of the gases provides different advantages to the application within which it is used e.g. air and SF<sub>6</sub> can provide high voltage hold-off capabilities under pressure, argon has been shown to promote multi-channelling [94] which reduces the inductance of the switch and can reduce the electrode erosion [6], [95]. He, neon (Ne) and Ar have also been

reportedly used to provide faster switching times [96], [97]. The most important factors for switching can include; the voltage hold off capability, the recovery rate (for high repetition rate switching capabilities) or any other experimentally determined characteristic which should be suitable for the application within which the switch will be used.

Many of the gases used within pulsed power switching have had environmental concerns attached to them and within recent years under climate change regulations have had their usage tightly bound under strict conditions [98], [99]. The most commonly used gas as an insulating media within the switches of many pulsed power systems is SF<sub>6</sub> [8], [59], [60], [100] and the aim of this project was to suggest an alternative to SF<sub>6</sub> that can be used within the switches of pulsed power systems.

### **2.5.1 SF<sub>6</sub> as an Insulating gas**

SF<sub>6</sub> is a man-made gas which was first made commercially available in 1947 [101] and, due to its high dielectric strength, it has become the most commonly used gas within pulsed power systems. SF<sub>6</sub> has a dielectric strength approximately 2.5-3 times higher than the dielectric (breakdown) strength of air and as a result can withstand voltages approximately three times larger than air under DC conditions [102]–[105]. Literature has reported that pressurised SF<sub>6</sub> can withstand pulsed voltages within the range of 10 kV-5MV for single shot applications, [106]. This high dielectric strength achieved by SF<sub>6</sub> is able to almost fully self-recover.

Degradation of SF<sub>6</sub> does occur over time and as the number of breakdown events increases and therefore the gas must be replaced periodically to maintain the full dielectric strength.

Under pulsed voltage conditions and when under pressure, it is reported within the literature that SF<sub>6</sub> at ~0.8MPa (absolute) the field gradient can reach as high as 1MV/cm [24]. In addition to the desirable switching properties of SF<sub>6</sub> due to its high dielectric strength, is also considered to be chemically inert, non-flammable, non-explosive, thermally stable and non-toxic [107], [108].

Despite these desirable switching properties including non-toxicity, it has been reported [109] that under the influence of:

- i. Partial corona discharges
- ii. Spark discharges or switching operations
- iii. Switching arcs and power circuit breakers
- iv. Failure arcs due to insulation breakdown

the decomposition of SF<sub>6</sub> can occur and the by-products that remain after any of these events are considered to be toxic and hazardous to human health and the environment [98].

Using SF<sub>6</sub> within high voltage switches has been reported to enhance electrode erosion which reduces the lifetime of the device [110]. A reduced lifetime of devices means that they will need replaced more frequently, requiring money to be spent on replacing the electrodes and money lost due to associated system down-time. In addition to the cost of periodic replacing of the electrodes due to the degradation caused by SF<sub>6</sub>, the cost of obtaining SF<sub>6</sub> has substantially increased since it was first made commercially available. It has been found from the literature [111] that from 1960 – 1994 the cost of SF<sub>6</sub> remained constant at ~ \$3/lb, by 1997 this had increased to \$12 - \$37/lb and in 2017 to purchase SF<sub>6</sub> the cost is ~\$35 - \$60/lb [112], around 20 times the cost that it was even in 1994. This increase in cost, while possibly due to demand is more likely due to the restrictions now in place on the usage and emissions of SF<sub>6</sub>.

The Kyoto protocol in 1997 [98], the Doha amendment [113] and the Paris agreement [114] were made by global leaders to discuss the problems faced in tackling climate change as a result of global warming and the depletion of the ozone layer due to the emission of gases from industrial applications. As a result of the initial summit held in Kyoto, restrictions on the usage and emissions into the atmosphere of hydrofluorocarbon gases (HFCs), perfluorocarbons (PFCs), N<sub>2</sub>O, CO<sub>2</sub> and SF<sub>6</sub> amongst others were agreed to by the European Community and 37 other industrialised countries. The Doha amendment and the Paris agreement are a second phase and more recent update to the initial Kyoto protocol respectively and the industrial communities where the gases that are the main consumers of these 'restricted gases' are being asked to further reduce their consumption or remove the requirement for them entirely.

## 2.5.2 Alternatives to SF<sub>6</sub> already considered

As an initial step towards removing SF<sub>6</sub> from pulsed power systems, research was conducted into using mixtures of SF<sub>6</sub> with other gases and comparing the performance of these gases within pulsed power systems to the conventional systems that are filled with pure SF<sub>6</sub>. The work was carried out with the intentions of seeing if by reducing the amount of SF<sub>6</sub> within the systems by combining it with some other, environmentally friendlier gas, it would be possible to retain the performance characteristics of the SF<sub>6</sub> filled switches. Smaller percentages of SF<sub>6</sub> would ultimately reduce environmental impacts as well as running costs. Environmentally friendlier gases such as N<sub>2</sub>, air, CO<sub>2</sub>, Ar and He have all been mixed with SF<sub>6</sub> [88], [90], [115]–[120] and compared under identical experimental conditions to pure SF<sub>6</sub>.

The idea of mixing SF<sub>6</sub> with other gases, while reducing the amount of SF<sub>6</sub> required within pulsed power systems and reducing the impact on the environment, does not entirely provide a solution to the problem posed of finding “an alternative to SF<sub>6</sub>”. An alternative gas to SF<sub>6</sub> to use within the switches of the pulsed power systems would require that the switches, when filled with this potential alternative, perform identically, or even in some areas, such as the voltage hold-off capabilities,  $dV/dt$  or current handling capabilities, improved performance may be desirable. Under identical experimental test conditions for various applications, gases have been considered as potentials to replace SF<sub>6</sub> entirely within switches [47], [111], [121]. Some of the gases which have been considered as potentials for replacing SF<sub>6</sub> within power and pulsed power systems have included CF<sub>3</sub>I [93], [122], [123], CF<sub>4</sub>, C<sub>3</sub>F<sub>8</sub> and CF<sub>2</sub>Cl<sub>2</sub> [121]. Gases such as C<sub>3</sub>F<sub>8</sub> and CF<sub>4</sub> and have shown comparable or higher dielectric strengths when compared under similar test conditions and thus have been suggested as possible alternatives to SF<sub>6</sub>. Some of which are shown in Table 2-3. These gases would provide a suitable alternative to SF<sub>6</sub> under certain conditions if the request was to simply seek out alternative gases that would provide a dielectric strength comparable to, or better than that of SF<sub>6</sub>.

**Table 2-3 from [124] comparing properties of different gases including the dielectric strength (relative to SF<sub>6</sub>), the atmospheric lifetime and the global warming potential.**

Chemical formula	c-C <sub>4</sub> F <sub>8</sub>	1-C <sub>3</sub> F <sub>6</sub>	C <sub>3</sub> F <sub>8</sub>	C <sub>2</sub> F <sub>6</sub>	N <sub>2</sub>	CO <sub>2</sub>	CF <sub>4</sub>	SF <sub>6</sub>
Chemical name	Perfluorocyclobutane	Perfluoropropylene	Perfluoropropane	Perfluoroethane	Nitrogen	Carbon dioxide	Perfluoromethane	Sulfur hexafluoride
Molecular weight	200.04	138.02	150.0	138.01	28.01	44.01	88.05	146.06
Molecular structure					N≡N	O=C=O		
Dielectric strength (vs. SF <sub>6</sub> )	1.27	0.92-1.0	0.97, 0.40-1.12	0.78, 0.67-0.90	0.34-0.43	0.32-0.37	0.4, 0.39-0.6	1.0
Liquefaction temperature in °C	-5.99	-29.6	-36.7	-78.1	-195.8	-78.5	-128	-63.8
GWP: 100-year value (vs. SF <sub>6</sub> gas)	10,300 (45%)	100 (0.44%)	8,830 (39%)	12,200 (54%)	0	1 (0.0044%)	6,500 (29%)	22,800 (100%)
Atmospheric lifetime (years)	3200	10	2,600	10,000	-	-	100,000	3,200
Price per gas pressure, vs. SF <sub>6</sub> (p.u. / MPa, SF <sub>6</sub> ), gas purity	9.1 (99.5%)	3.1 (99.5%)	1.8 (99.9%)	2.5 (99.99%)	0.003 (99.99%)	0.02 (99)	1.1 (99.999)	1.0 (99.99)

Many of the suggested gases found by the authors to have dielectric properties greater than (or comparable to) SF<sub>6</sub> are also considered to be greenhouse gases with global warming potential (GWPs) of ~7000-8000, seen in Table 2-3 and [98], [113] which are also restricted under the Montreal Protocol which governs the substances that deplete the ozone layer [125].

Two of the gases investigated of interest within recent years for possible use within high voltage applications are HFO1234ze and CF<sub>3</sub>I. HFO1234ze has a GWP of 6 compared to SF<sub>6</sub>'s GWP of 22,800 meaning that while it still has a more negative impact on the environment than CO<sub>2</sub> (GWP = 1 and the reference from which all other GWPs are measured), it is remarkably less impacting on global warming than SF<sub>6</sub>. It has previously only been used as a refrigerant gas although now it is being looked at for its potential as an insulation gas and its breakdown properties are currently being studied [126]. CF<sub>3</sub>I has been a gas with considerable research conducted on it as a potential replacement for SF<sub>6</sub> within the power industry such as switchgear and gas insulated systems [93], [122], [123], [127], [128] and has shown a dielectric strength 1.2 times greater than that of SF<sub>6</sub> and is considered slightly toxic. Studies into the by-products of CF<sub>3</sub>I after high voltage discharges have occurred within the gas have shown that CF<sub>3</sub>I also produces harmful and toxic by-products [129] or non-toxic by-products such as C<sub>2</sub>F<sub>6</sub> which has a global warming potential of ~6200 and is also a listed gas of concern under the Kyoto protocol [98].

Gases such as air and N<sub>2</sub> have been used within spark switches [47], [66], [102], [103], [130]–[133] although in order to be able to replicate the performance of the conventional SF<sub>6</sub>-filled switches in terms of voltage hold-off capabilities, runtime, jitter (in the case of triggered switches),  $dV/dt$ ,  $dI/dt$  and other key operational characteristics that are required when considering any gas as a replacement for SF<sub>6</sub>, the pressure required of these gases often has to be substantially higher due to their lower dielectric strength.

## 2.6 Conclusions

This chapter has provided a discussion on the basic principles of pulsed power and how it has developed from technologies used predominantly within defence applications into wide-reaching, applications which are utilised on a daily basis across the globe. A brief description of the set-up of a pulsed power system which utilises a capacitive method of energy storage has been provided and an in-depth look at different kinds of plasma closing switches used in different areas of pulsed power research for different applications is given and the differences between these alongside the operational limitations are discussed.

An overview of the mechanisms of gas breakdown, which are the mechanisms that occurs within the plasma closing switches during operation, is provided covering Townsend and streamer discharges and Paschen's law. Limitations of Paschen's law are discussed in detail as are suggestions of equations to predict the self-breakdown voltage for non-standard gases and gas mixtures at specified inter-electrode gap distances and gas pressures are investigated within this thesis.

A comparison of methods describing the time-dependent resistance of the plasma channel that forms during a breakdown event is presented alongside the experimental restrictions and any assumptions made by the author in extracting the expression for the resistance. Being able to accurately describe and computationally model the time-dependent plasma resistance is of huge importance within the pulsed power research community as this can lead to the development of models of larger pulsed power systems which are accurate and can allow for optimisation of current systems or aid the development of future systems. This thesis presents a PSpice simulation of a 12 stage Marx generator which includes at

each switch stage, an expression for the time-dependent resistance, thus, a comparison of models from literature was conducted.

Finally, as this thesis will predominantly focus on the operational characteristics of plasma closing switches when filled with different gases a review of the gases which are conventionally used within research and industry was presented. The most commonly used gas within the switches of pulsed power systems is SF<sub>6</sub> and so a discussion on SF<sub>6</sub>, the advantages and what makes it the gas of choice is presented. The disadvantages of SF<sub>6</sub> usage being the growing environmental concern have led to a desire to remove this gas entirely from any and all applications where it is currently utilised. The research into finding a suitable replacement gas for SF<sub>6</sub> is not a new topic and a brief review of the alternative gases which have been suggested to date is given.

Within this thesis, the experimental chapters provide a discussion on some of the operational characteristics of two commonly used plasma closing switch topologies used within industry when filled with different environmentally friendly gases. The self-breakdown voltages of 6 different gases are compared within a self-breakdown switch with a sphere-sphere topology. A field-distortion triggered switch was also filled with each of the different gases and breakdown initiated under the influence of two different trigger impulses, in order to compare the time to breakdown and jitter of the switch. During the breakdown events conducted within the self-breakdown switch, the light emissions were obtained and analysed and characteristics of the plasma channel, such as the temperature of the plasma and conductivity of the plasma, are extracted. Post-breakdown current waveforms were also obtained and analysed to extract values of total resistance and inductance of the plasma channel. From the experimental work conducted and the values extracted and measured, two models of plasma closing switches are developed within the computational software PSpice, one assuming constant resistance over time and one including temporal changes of the resistance.

## Chapter 3. Characterisation of a Self-Breakdown Spark Gap Switch

A key component of any pulsed power system that plays a large role in the reliability and repeatability of the output pulse(s) formed is the switch or switches. The design of the switches in this investigation have been based upon the dimensions and topology of the switches used within the MEVEX Marx generator at AWE which was going through a period of regeneration and upgrade at the time of this study [59], [60]. The aim of this Chapter is to investigate the breakdown characteristics of spark gap switches when filled with different gases which can be used as alternative to SF<sub>6</sub>, therefore a switch with topology similar to the original MEVEX switch should be designed, filled with any alternative gas and its operational characteristics should be established.

This chapter discusses a sphere-sphere, self-breakdown spark gap switch topology, which is based on the 'half-gap' switches used in the Marx generator of AWE's MEVEX machine [59], [60]. In this Chapter six different gases; air, N<sub>2</sub>, 60%/40% N<sub>2</sub>/O<sub>2</sub> mixture, CO<sub>2</sub>, 90%/10% Ar/O<sub>2</sub> mixture and SF<sub>6</sub> and self-breakdown voltages were recorded for a variety of inter-electrode gap spaces and gas pressures within the switch. In each test 20 breakdown events for each combination of gas, gap space and gas pressure were conducted and the mean self-breakdown voltage as well as its standard deviation, were obtained, presented and discussed in this Chapter.

Some of the results obtained in Chapter 3, i.e. breakdown characteristics of a sphere-sphere self-breakdown plasma closing switch when filled with different gases, have previously been published [39]–[41]. It is shown that, in terms of voltage hold-off capabilities, for environmentally friendly gases, such as air, N<sub>2</sub> and a mixture of 60%/40% N<sub>2</sub>/O<sub>2</sub>, there are some conditions, such as elevated pressures or longer gap spaces which would provide similar levels of self-breakdown voltages to conventional SF<sub>6</sub>-filled switches but however these gases have lower voltage spread and are thus more reliable and stable during breakdown operation. Another advantage to using these gases is shown in terms of the spread of breakdown voltage, which is observed to be much narrower for the

environmentally friendlier gases than for SF<sub>6</sub> or CO<sub>2</sub> and in all cases was seen to decrease as both gas pressure and gap space increased.

### **3.1 Design and Development of Self-breakdown Switch**

In order to design a self-breakdown, sphere-sphere topology spark gap switch, the electric field in this topology was modeled within the electrostatic software package QuickField before construction took place. Performing an electrostatic simulation of the proposed design of the switch allowed for analysis of the field distribution between the upper (high voltage) and lower (grounded) spherical electrodes. The proposed switch body is axisymmetric: it is a glass reinforced tube which is 60mm in diameter; the electrodes were made of 16mm diameter brass spheres, and can be separated by a maximum distance of 9mm.

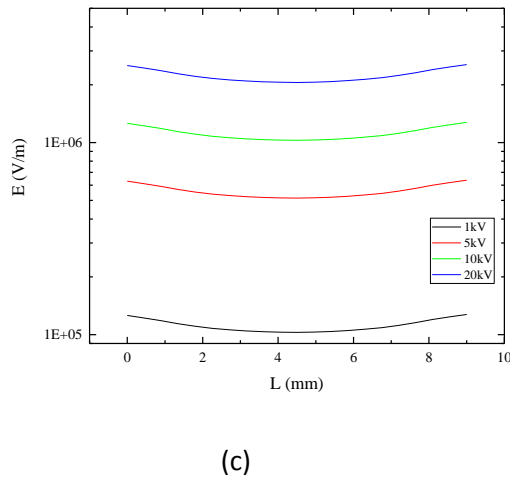
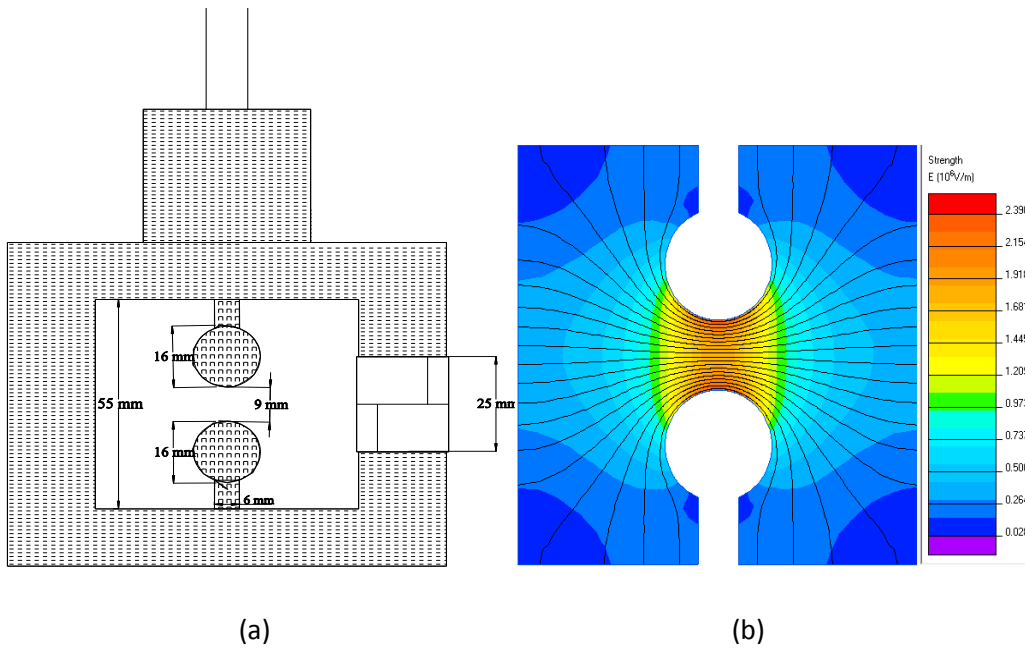


**Figure 3-1(a)** Schematic diagram of the self-breakdown switch with the key dimensions of the proposed design for the switch. **Figure 3-1(b)** the QuickField simulation result of the electric field within the proposed switch design under normal operational conditions. **Figure 3-1(c)** shows the strength of the electric field between the upper (HV) electrode and the lower (grounded) electrode when 1kV, 5kV, 10kV and 20kV DC voltage is applied to the upper electrode.

The computational model which was run simulated the electrostatic field distribution in the switch under normal conditions before breakdown. The space between the spherical electrodes would be set to the desired inter-electrode gap length and the gap space filled with a dielectric (gas) of known permittivity. The lower of the two spherical electrodes would be grounded throughout experimental conditions while voltage would be applied to the upper electrode, increasing until breakdown occurs. The results of this electrostatic

modelling are presented within Figure 3-1. This field distribution is produced when two simulated, 16mm diameter spherical brass electrodes are separated by 9mm and the inter-electrode gap space is filled with air,  $\epsilon_r=1$ . The results of the Quickfield simulation of the electric field are shown in Figure 3-1(b) and show that the proposed switch design, when operating under the desired conditions would provide, as expected, the peak value of the electric field directly between the spherical electrodes with no unwanted field enhancements occurring elsewhere within the switch body under normal operational conditions. Figure 3-1(c) presents a graph comparing the magnitude of the electric field strength in the region directly between the upper and lower spherical electrodes for increasing applied voltage to the upper electrode (simulating the increasing voltage required to initiate breakdown within a 9mm gap as the gas pressure increases) and it can clearly be seen that as the voltage applied to the upper electrode increases (corresponding to the increase in breakdown voltage required for closure due to the increase in gas pressure), the electric field will increase. This is in line with analytical results predicted by Equation (2.2) for the maximum electric field in the sphere-sphere topology.

It was from this simulation model with specified dimensions that the physical switch was designed and constructed. Figure 3-1 shown the cross-section of the practical switch which was used to study the self-breakdown characteristics of different gases. Figure 3-2 is a photograph of the self-breakdown switch which has been constructed from the dimensions and schematic provided in Figure 3-1(a).

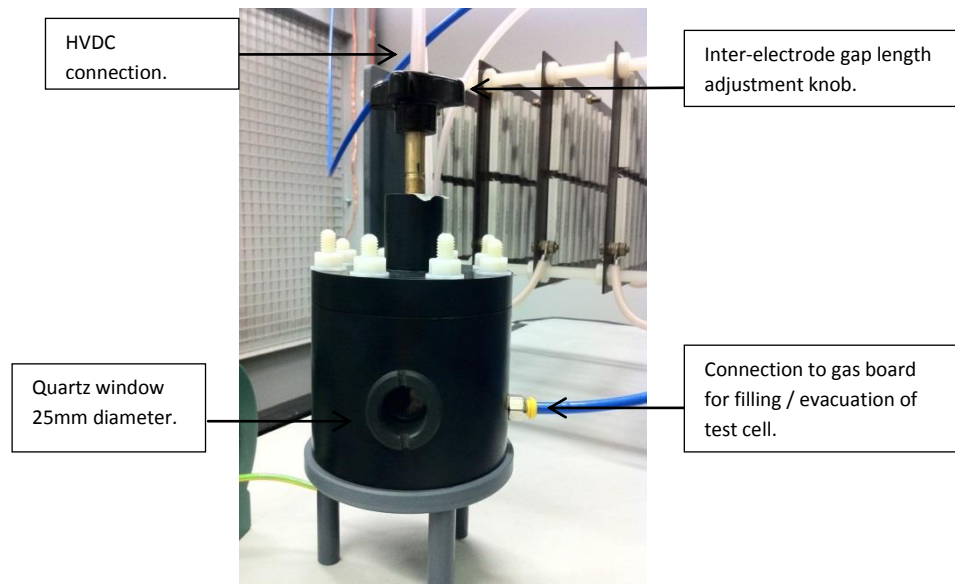


**Figure 3-2 Photograph of the constructed self-breakdown switch**

The body of the practical switch was constructed from a solid glass-reinforced nylon (GRN), rod. The switch body has 102mm external diameter/60 mm internal diameter and is 90mm in height (65mm main body plus 15mm lid).

The spherical electrodes within the test cell are machined brass spheres 16mm in diameter, mounted onto a 3mm diameter brass rod. The lower spherical electrode is held in a fixed position throughout the experimental procedure and thus the inter-electrode gap space within the switch is altered by movement of the upper electrode. This alteration of inter-electrode gap space is achieved by rotating the knob attached to the shaft and upper electrode pointed out in the diagram in Fig 3-2. Each 360° rotation of the knob corresponds to a vertical adjustment of 1mm within the switch.

Within the body of the test-cell, a 25mm diameter quartz window was mounted to allow for analysis of optical emissions during breakdown events, for evaluation of plasma temperature, which is discussed in Chapter 6. A 6mm push-in gas connection is also mounted into the side of the test cell for evacuating gas, filling the switch and monitoring the gas pressure within the test-cell before, during and between experiments.

One other design requirement of the spark gap switch was that it should be able to withstand pressures of up to 0.5MPa absolute. The lid of the test-cell is held in place by

eight nylon bolts and o-rings have been placed at each point within the test-cell where connections are fit together to ensure the switch can be pressurised and hold gas pressure over the length of time required to conduct experiments.

### 3.2 Experimental Setup and Methodology

The experimental requirements of the desired test-set were that once the inter-electrode gap space had been set and the test-cell filled with gas to the desired pressure, there should be continual monitoring of the voltage being applied across the inter-electrode gap until the point where a breakdown event was seen to occur.

Self-breakdown voltage and the voltage hold-off capabilities for six different gases were to be tested for each combination of:

- Gas
  - Air (BOC bottled, 12% relative humidity)
  - N<sub>2</sub> (99.9% N<sub>2</sub>, BOC Ltd)
  - 60% N<sub>2</sub> + 40% O<sub>2</sub> (BOC Ltd)
  - 90% Ar + 10% O<sub>2</sub> (BOC Ltd)
  - CO<sub>2</sub> (BOC Ltd)
  - SF<sub>6</sub> (BOC Ltd)
- Inter-electrode gap space
  - 1mm – 9mm
- Gas pressure
  - 0.1MPa–0.4MPa

A 'zero point' for determining the inter-electrode gap space was defined as the point when the upper and lower spherical electrodes were in contact creating a short circuit across the switch. It is from this point that the inter-electrode gap space is determined as each full rotation of the knob equates to a 1mm vertical displacement of the upper electrode inside the switch. The gap between spherical electrodes was 'set' to the required distance before the gas within the switch was changed.

In dealing with gas-filled switches, adequate gas safety and gas handling must be undertaken. A gas distribution board was set-up for the process of evacuating then refilling

the test-cell with the different gases. A digital pressure gauge, manual valves with 6mm gas tubing that connect the test cell to the gas cylinders, vacuum pump and gas exhaust pipes were all connected via the gas board.

A Glassman high voltage DC power supply was used to apply DC voltage to the upper electrode through a 100k $\Omega$  charging resistor and the voltage applied across the gap is monitored by a North Star PVM-5 high voltage probe (60kV impulse/100 kV DC, 80 MHz bandwidth) connected to a Tektronix Tektronix TDS 3054C digitising oscilloscope (500MHz bandwidth, 5GS/s sampling rate). Figure 3-3 is a schematic of the experimental test set-up for the self-breakdown experiments.

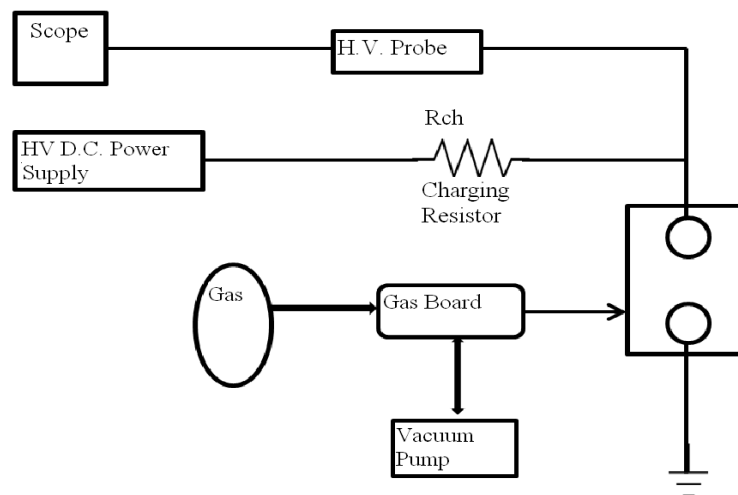


Figure 3-1. Schematic of Experimental set-up with self-breakdown switch

After the inter-electrode gap space had been set, the ambient air was evacuated from the test cell by the vacuum pump before the switch was then filled to 0.1MPa with the bottled gas under test. A positive polarity DC voltage was applied manually at a rate of  $\sim 2$  kV/s to the upper electrode while the lower electrode was held at ground until a breakdown event was seen to occur on the screen of the scope at which point, the applied voltage was reduced to zero again. The magnitude of voltage applied at the point where breakdown occurred was recorded as the breakdown voltage and this was repeated for 20 events before the gas was evacuated from the test cell and filled again with the same bottled gas to an increased pressure in 0.05MPa increments. This process was repeated for each

pressure in the range 0.1 – 0.4MPa for each of the 6 bottled gases tested and for each inter-electrode gap space in the range 1 – 9mm (in 1mm increments).

The mean self-breakdown voltage value was calculated for each combination of gas tested, gap space and gas pressure and, where possible, experimental data has been compared to standard Paschen data taken from literature as discussed in Chapter 2. Where novel gases have been used for switching purposes or new mixtures had been used, suitable fittings have been suggested to describe and predict breakdown events by extrapolation of experimental data obtained.

The standard deviation in the self-breakdown voltage was calculated and is considered to represent the spread in the self-breakdown voltage.

### **3.3 Self-Breakdown Voltage: Results and Analysis**

This section presents the experimentally obtained and analysed results for the self-breakdown voltages of the 6 different gases tested within the sphere-sphere topology switch. A discussion on the interesting results observed and the industrial impact of the results obtained, as well as any practical implications on currently employed systems, follows on from experimental work.

The self-breakdown voltages for each of the six different gases tested are presented individually alongside the comparison with Paschen data for gases where available. In the cases where novel gases in terms of switching applications have been considered, analysis of the results are extracted from the experimental data and fittings are applied to the data.

For each graph presented, each symbol represents an average value of 20 breakdown events conducted for each specific combination of inter-electrode gap length and gas pressure where breakdown was able to be initiated. The error bars represent the standard deviation for each individual set of breakdown experiments conducted.

Following on from the self-breakdown voltages of each individual gas considered, a comparison of these voltages for all six gases together is presented and interesting conclusions are drawn.

### 3.3.1 Self-Breakdown Voltages for an Air-Filled Switch vs $pd$

Experimental breakdown data obtained for an air-filled switch has been plotted using the OriginPro 2015 software package.

Alongside the experimentally obtained results, a classic Paschen fit for air has been applied to the experimental data and for the inter-electrode gap-space and the gas-pressure used throughout experiments. The range of operation of the self-breakdown spark gap switch falls on the right hand side of the Paschen curve, well away from the Paschen minimum and the breakdown voltage of a gas-filled gap. The breakdown voltage can be described by Equation (2.5). It was proposed that a modified form of this equation using phenomenological constants  $M$  and  $k$ , which provides a reasonable fit to experimental breakdown data in the self-breakdown electrode topology filled with air [66] can be given by Equation 3.1 :

$$V_{br} = \frac{M(pd)}{\ln(pd) + k} \quad (3.1)$$

where  $M = 2.74$  and  $k = 3.51(pd)^{0.06}$  are related to the breakdown of air at given  $pd$  [66].

When the Paschen fitting (3.1) is plotted alongside the experimentally obtained results (solid fit line) it was noted that the self-breakdown results obtained in the sphere-sphere topology switch in which spark discharge occurs, for all values of  $pd$  tested, fit closely to those described in literature for a breakdown event in air in uniform field conditions.

The literature Paschen data used to describe and predict the breakdown voltage of a gas for a specified value of  $pd$ , is considered valid for breakdown conditions in a uniform electric field. As already outlined in section 3.1, the design of the self-breakdown switch makes use of a non-ideal uniform electric field which provides an electric field utilisation factor of  $\eta = 2.25$  between the spherical electrodes. Therefore, potentially in the case of electric fields with a high field utilisation factor  $\eta$  (Equation 2.4) in some gases it could be expected that the Paschen Equations 2.5 or 3.1 will not be valid. Therefore in order to describe experimental breakdown voltage  $V_{br}(pd)$  for all gases under these test conditions a

phenomenological fitting can be used. In this work it is suggested to use an allometric fit and to apply this fit to the experimental data:

$$V_{br} = A(pd)^\beta \quad (3.2)$$

where  $A_1$  (kV/Pa.m) and  $\beta$ (kV) are fitting coefficients extracted from the experimental data. This power Equation describes the breakdown voltage of gases as a function of the product of the inter-electrode gap space and the gas pressure and constants of proportionality calculated from experimental results.

Figure 3-4 shows the behaviour of self-breakdown voltage of an air-filled switch as the product of the gas pressure and the inter-electrode gap space,  $pd$ , increases.

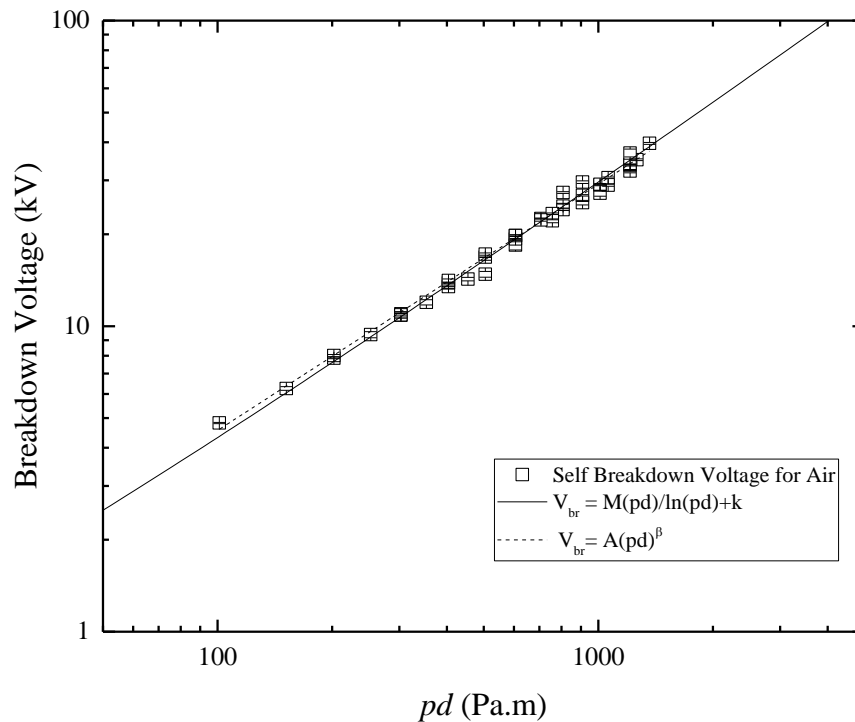


**Figure 3-2 The average breakdown voltages for an air-filled switch as a function of the product of the gas pressure and the inter-electrode gap length.**

As can be seen from the results in Figure 3-4, the self-breakdown voltage increases proportionally as the product  $pd$  also increases. The standard deviation, or the spread in the obtained self-breakdown voltage, is relatively small for an air-filled switch, in the range 0.02kV – 1.09kV and was observed to decrease as the product  $pd$  increased. For practical applications, this means that for switches operating with larger gaps, higher gas pressures or some combination of the two, the performance of the switch is more stable and the self-breakdown operation of an air-filled switch can be more reliably predicted.

In the case of breakdown events in an air-filled switch, the value of the fitting coefficients have been obtained using the best fit procedure in Origin graphing software package and it was found that  $A_1 = 0.11$  kV/Pa.m and  $\beta = 0.81$  kV. Thus it is established that for bottled air in the sphere-sphere electrode configuration used within the present work, both the Paschen fitting (Equation 3.1) and the phenomenological fitting (Equation 3.2) fit reasonably well with the experimental self-breakdown voltage.

When a fit with Equation (3.2) is plotted (dashed line in Fig. 3.4) alongside the experimental data, it was observed that the allometric fit in the range of  $pd$  values tested, provides very close match to experimentally obtained results. Also it can be seen that using phenomenological fitting Equation (3.2) to describe the self-breakdown voltage of air in the sphere-sphere topology can therefore give a more accurate description of the behaviour of the self-breakdown voltage of air for low  $pd$  values as compared with the Paschen fitting 3.1.

Later in this chapter Equation (3.2) will be used together with Paschen fitting, Equation 3.1, for each of the 6 gases tested, as this approach may give a more accurate description of the behaviour of the self-breakdown voltage of each gas which is important from practical engineering point of view. This fitting with Equation 3.2 can be used in the design of plasma closing switches for Pulsed Power applications or any other application in which switching is utilised and where the classic Paschen description may not prove accurate due to non-uniformity of field or the development of spark discharge.

### 3.3.2 Self-Breakdown Voltages For a N<sub>2</sub>-Filled Switch vs $pd$

This section presents the results of measuring of, self-breakdown voltages in the the sphere-sphere switch topology filled with nitrogen. The same experimental procedure was used in these tests as previously outlined in section 3.3.1. The obtained results are presented in Figure 3-5 as  $V_{br}(pd)$  for N<sub>2</sub> gas.

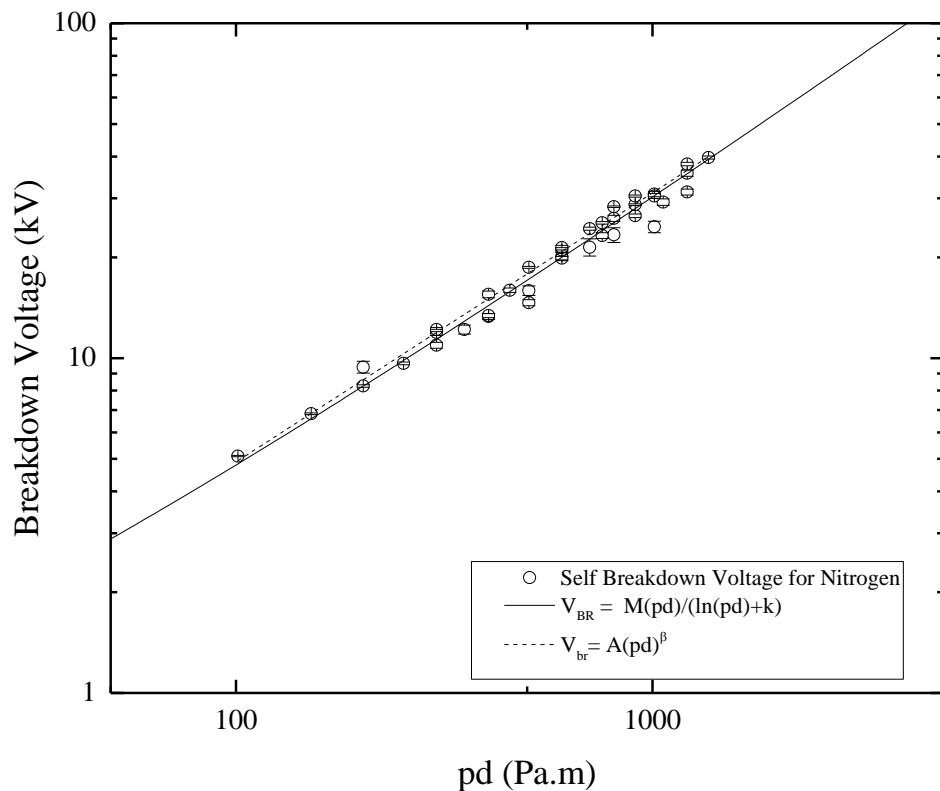


**Figure 3-3 The average breakdown voltages for a nitrogen-filled switch as a function of the product of the gas pressure and the inter-electrode gap length.**

As can be seen from the results presented in Figure 3-5, there is a proportional increase in the self-breakdown voltage in a N<sub>2</sub>-filled switch as the product  $pd$  increases as was seen in the case of breakdown events for an air-filled switch. The error bars in Figure 3-5 above shows that the standard deviation in breakdown voltage will decrease as the product  $pd$  is

increased. For self-breakdown events in a nitrogen-filled switch the value of standard deviation was observed to be in the range 0.02kV - 1.26kV. This is also considered to be a relatively small standard deviation, meaning more reliable prediction of self-breakdown voltage as the value of  $pd$  increased.

The Paschen curve for  $N_2$  was plotted using Equation 3.1 (solid line) alongside the experimentally obtained self-breakdown data. For self-breakdown events occurring in  $N_2$  within the  $pd$  range of interest, the constants in the Paschen Equation (3.1) are given by  $M=2.565$  and  $k = 2.4 \cdot (pd)^{0.103}$ . It can be seen that for the  $N_2$  filled switch, the Paschen description of the self-breakdown voltage fits well with the experimentally obtained results.

The approach used in applying an allometric fit with Equation (3.2) to the experimental data was applied to the self-breakdown nitrogen data. The coefficients  $A$  and  $\beta$  for Equation 3.2 have been obtained in Origin Pro 10 graphing software using the best fit procedure and it was found that these coefficients are:  $A_1= 0.12$  kV/Pa.m and  $\beta= 0.80$  kV. Fitting Equation 3.2 with these coefficients has been plotted (dashed line) in Figure 3-5 above and sits very close to the classic Paschen description of the breakdown voltage for  $N_2$  as well as the experimental results.

### 3.3.3 Self-breakdown Voltages for a 60% Nitrogen + 40% Oxygen Mix Filled Switch vs $pd$

This section presents the self-breakdown voltages obtained in the sphere-sphere topology filled with a gas mixture consisting of 60%/40%  $N_2/O_2$ . The obtained results in the form of  $V_{br}(pd)$  are shown in Figure 3-6.

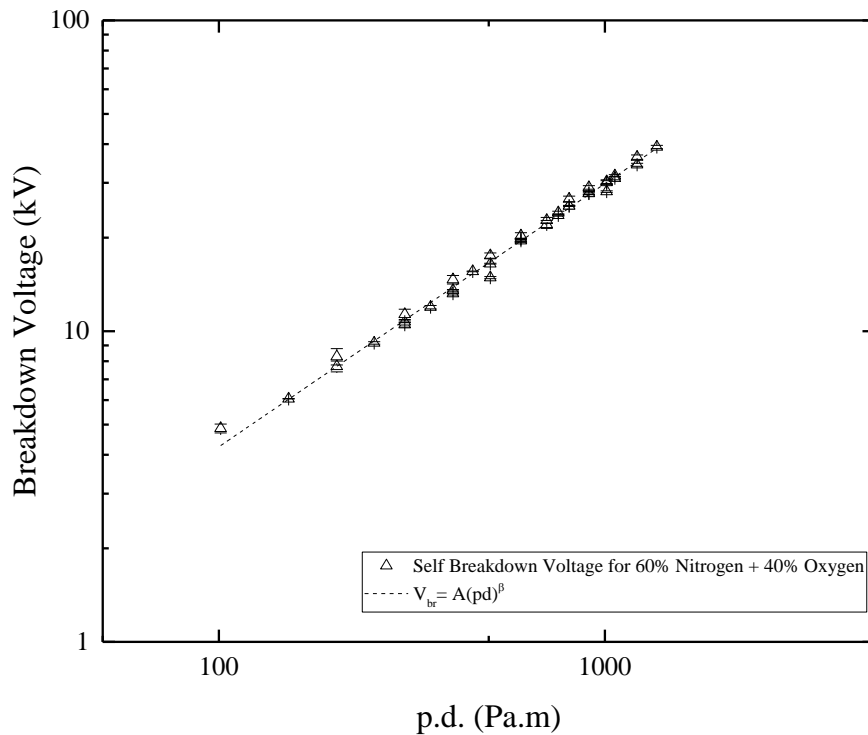


Figure 3-4 The average breakdown voltages for a switch filled with a 60%/40% nitrogen/oxygen mixture as a function of the product of the gas pressure and the inter-electrode gap length..

For a switch filled with a mixture of 60%/40%  $N_2/O_2$  it was observed that the level of breakdown voltage increased almost linearly as the product  $pd$  increases. Practical benefits which would be applicable to industrial applications in using this mixture come from the small standard deviation of the self-breakdown voltage observed which fell in the range 0.01 – 0.65kV, the smallest standard deviation values observed for any of the gases tested. For practical applications this shows that the most reliable prediction of self-breakdown

voltage occurs in the switch filled with a mixture of 60%/40% N<sub>2</sub>/O<sub>2</sub> at increasing values of  $pd$ .

While many mixtures of gases making use of oxygen and nitrogen have previously been considered for switching applications [66], [89], [102], [111], a mixture ratio of 60%/40% N<sub>2</sub>/O<sub>2</sub> has not previously been considered for use in plasma closing switches for industrial switching applications. The reason for selecting a mixture of 60%/40% N<sub>2</sub>/O<sub>2</sub> is that, when compared to air as (crudely approximated to) 80%/20% N<sub>2</sub>/O<sub>2</sub> it approximately doubles the percentage of oxygen (an electronegative gas) in the mixture and would therefore allow for an investigation to see if there was any significant alteration to the obtainable voltage hold-off capability of the switch due to the electronegativity of increasing percentages of oxygen.

With this specified ratio of 60%/40% N<sub>2</sub>/O<sub>2</sub> having not previously been considered for the purposes of switching, investigations into previous published literature have yielded no self-breakdown data for comparison of the experimental data obtained within this investigation. As there is no previous data of any kind for this specified gas mixture, there can be no Paschen curve plotted for this gas mixture and therefore the allometric fitting with Equation (3.2) has been applied to the experimental data obtained. The coefficients for  $A$  and  $\beta$  were found using the best fit procedure conducted in Origin Pro 10 graphing software, and they found to be :  $A_1=0.09\text{kV}/\text{Pa.m}$  and  $\beta=0.85\text{ kV}$ .

The fit line obtained using Equation (3.2) with these  $A_1$  and  $\beta$  coefficients are plotted (dashed line) in Figure 3-6 alongside the experimentally obtained self-breakdown results for this gas mixture.

### 3.3.4 Self-breakdown voltages for a CO<sub>2</sub>-filled switch vs $pd$

Another gas of interest within industrial applications is CO<sub>2</sub>. Although not environmentally friendly as such, the standards upon which the global warming potentials are ranked are all compared to the impact of CO<sub>2</sub> on the environment. CO<sub>2</sub> is ~23,000 times less harmful to the environment than SF<sub>6</sub>. Figure 3-7 presents the results of the sphere-sphere topology, self-breakdown for a switch filled with CO<sub>2</sub>.

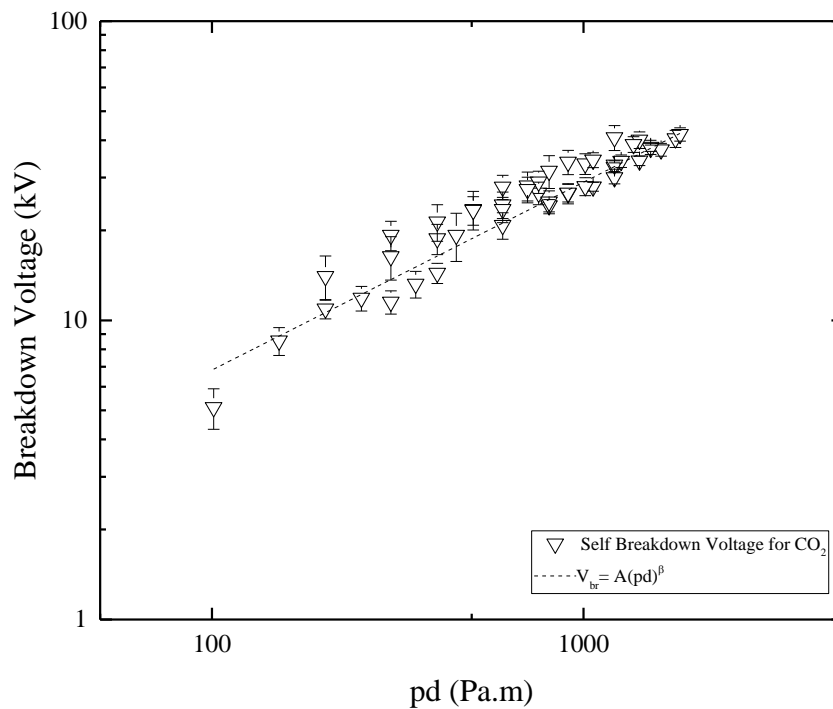


Figure 3-5. The average breakdown voltages for a switch filled with a CO<sub>2</sub> as a function of the product of the gas pressure and the inter-electrode gap length.

The level of voltage hold-off was seen to increase as  $pd$  increased, however, the standard deviation for a CO<sub>2</sub> filled switch was the largest of all 6 gases tested and fell within the range 0.79-3.97kV. As the value of  $pd$  increased, the standard deviation in the CO<sub>2</sub> filled switch was not seen to change significantly leading to an unreliable prediction of self-breakdown voltages across the entire range of  $pd$  values.

It was concluded that the larger standard deviation values were observed for smaller  $pd$  values and negated the potential benefit in using  $\text{CO}_2$  to withstand slightly higher voltages for lower  $pd$  values.

The allometric fit applied (Equation 3.2) to the experimental data for all gases was applied to the experimental results for a  $\text{CO}_2$  filled switch and the constants found using the best fit procedure in Origin graphing software are  $A_1 = 0.38 \text{ kV/Pa.m}$  and  $\beta = 0.63\text{kV}$ .

When the allometric fit line 2, Equation 3.2, with these coefficients is plotted alongside the experimental results in Figure 3-7 (dashed line) it can be seen that for larger values of  $pd$  there is a more accurate fit to the experimental data.

### 3.3.5 Self-breakdown voltages for a 90%/10% Ar/O<sub>2</sub> mix filled switch vs $pd$

This section discusses the self-breakdown capabilities of a mixture of 90%/10% Ar/O<sub>2</sub> oxygen, a mixture which has not previously been considered for switching purposes. Figure 3-8 shows the self-breakdown voltage as a function of  $pd$  for the switch when filled with 90%/10% Ar/O<sub>2</sub> mix.

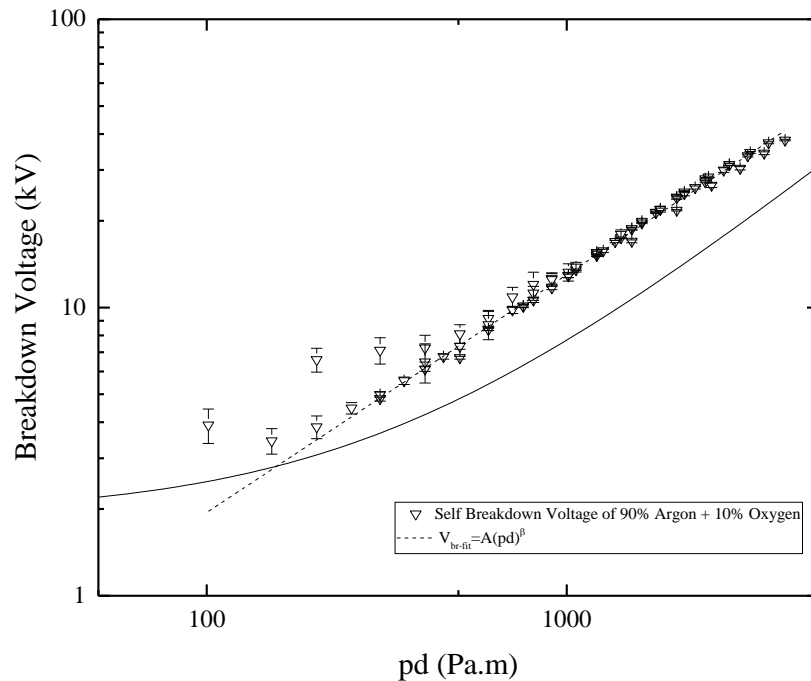


Figure 3-6. The average breakdown voltages for a switch filled with a 90%/10% Ar/O<sub>2</sub> mixture as a function of the product of the gas pressure and the inter-electrode gap length.

Argon gas has previously been used in a wide range of applications, both as a pure gas or added as part of a mixture for some enhanced properties such as to promote multi-channeling to reduce inductance [116], [134]–[138]. The mixture of 90%/10% Ar/O<sub>2</sub> provided the lowest breakdown voltages of all the gases tested as is evident from Figure 3-8 but was also observed to increase proportionally as  $pd$  increased.

It was found that the standard deviation in a switch filled with a 90%/10% Ar/O<sub>2</sub> mixture fell within the range 0.07kV-1.23kV, the a relatively wide range considering the

lower self-breakdown voltages, and therefore also one of the less reliable gases for predicting self-breakdown voltage in self-breakdown operation.

A mixture of 90%/10% Ar/O<sub>2</sub> has not previously been investigated for its suitability of use as an insulation gas within switching devices and there is no classic Paschen information for this particular mixture either. Figure 3-8 does however show the self-breakdown data for this particular gas mixture plotted alongside the Paschen curve for pure argon (solid line) which is extracted from work presented in [136], [137].

As is clearly seen in Figure 3-8, when using a mixture of 90%/10% Ar/O<sub>2</sub>, the experimentally obtained self-breakdown results are widely varied from the classic Paschen description of the breakdown voltages of pure argon.

By fitting the experimentally obtained results with an allometric fit as in Equation 3.2, the coefficients extracted using Origin graphing software (best fit procedure) are  $A_1 = 0.04$  kV/Pa.m and  $\beta = 0.82$  kV. This allows for a more accurate description of the breakdown voltage capabilities of a 90%/10% Ar/O<sub>2</sub> mixture to be described by Equation (3.2).

When Equation (3.2) with the corresponding coefficients  $A_1$  and  $\beta$  is plotted (dashed line) alongside the experimental results and the classic Paschen data for pure argon, it is noted to have a very close fit to obtained results and thus can be used to accurately predict the breakdown voltage of this particular gas mixture for the defined range of  $pd$  values.

### 3.3.6 Self-breakdown voltages for an SF<sub>6</sub>-filled switch vs $pd$

This section describes the self-breakdown voltage results obtained from the switch filled with SF<sub>6</sub>. SF<sub>6</sub> being the most commonly used gas, its properties as a gas for use in switching are well established. Figure 3-9 presents the results of an experimental investigation into the performance of SF<sub>6</sub> in this particular switch body for direct comparison to other gases.

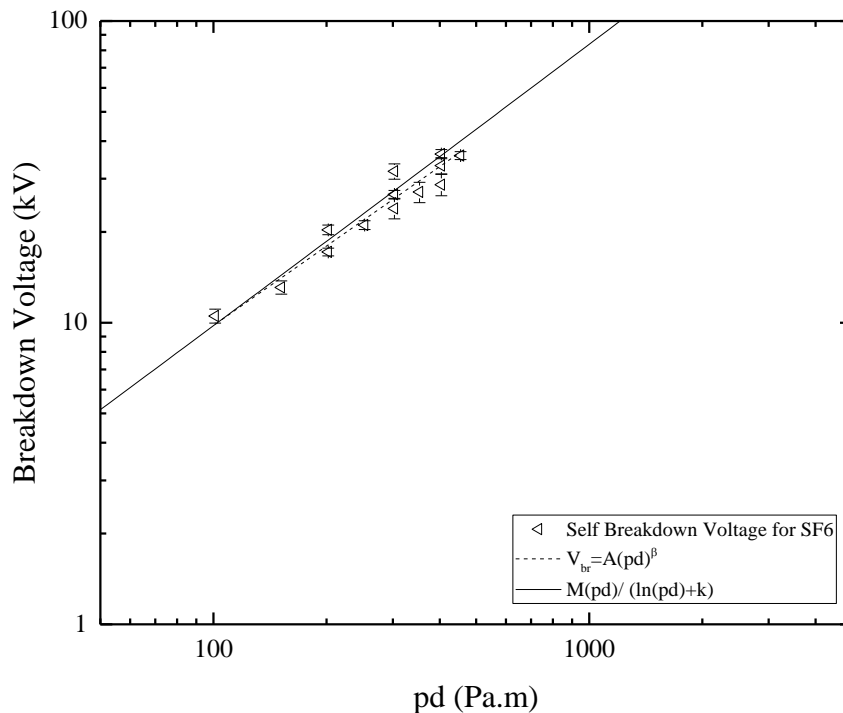


Figure 3-7 The average breakdown voltages for a switch filled with SF<sub>6</sub> as a function of the product of the gas pressure and the inter-electrode gap length.

Due to the dielectric strength of SF<sub>6</sub> being around 3 times that of air, a smaller range of  $pd$  values where breakdown could be initiated were found due to experimental equipment limitations. Where breakdown events were initiated, it was observed that as  $pd$  increased, the voltage required to initiate breakdown also proportionally increased.

The standard deviation for the self-breakdown voltage in an SF<sub>6</sub> filled switch was observed to be quite large, falling within the range 0.51kV – 2.32kV.

SF<sub>6</sub> being a well-established gas and one of the most commonly used gases for switching within the pulsed power community, its breakdown characteristics are well known and described throughout literature. Figure 3-9 plots the classic Paschen curve for SF<sub>6</sub> (solid line) with Equation given by Equation (3.2) and constants given by  $M=2.19$  and  $k=6.45(pd)^{0.84}$ . As can be seen in Figure 3-9, this classic Paschen curve for SF<sub>6</sub> fits well with the experimentally obtained results particularly at lower  $pd$  values. It is not clear if the experimental data would continue to fit quite so well at  $pd$  values increased beyond the capabilities of the experimental equipment.

When considering the allometric fitting of Equation 3.2 applied to experimental data, the best fit procedure in Origin software allow extraction of the coefficients  $A_1=0.17$  kV/Pa.m and  $\beta = 0.87$ kV. The breakdown voltage of SF<sub>6</sub> can be described by Equation (3.2) with these coefficients and when this allometric fit line is plotted (dashed line) in Figure 3-9 it appears that Equation 3.2 fits closely to all of the experimental data as  $pd$  increases.

### 3.3.7 Comparison of self-breakdown voltages gases for all gases.

This section provides a comparison of the breakdown voltage capabilities of all 6 of the gases tested. Figure 3-10 shows a comparison graph of the self-breakdown voltage for all 6 of the gases/gas mixtures tested as a function of the product  $pd$ .

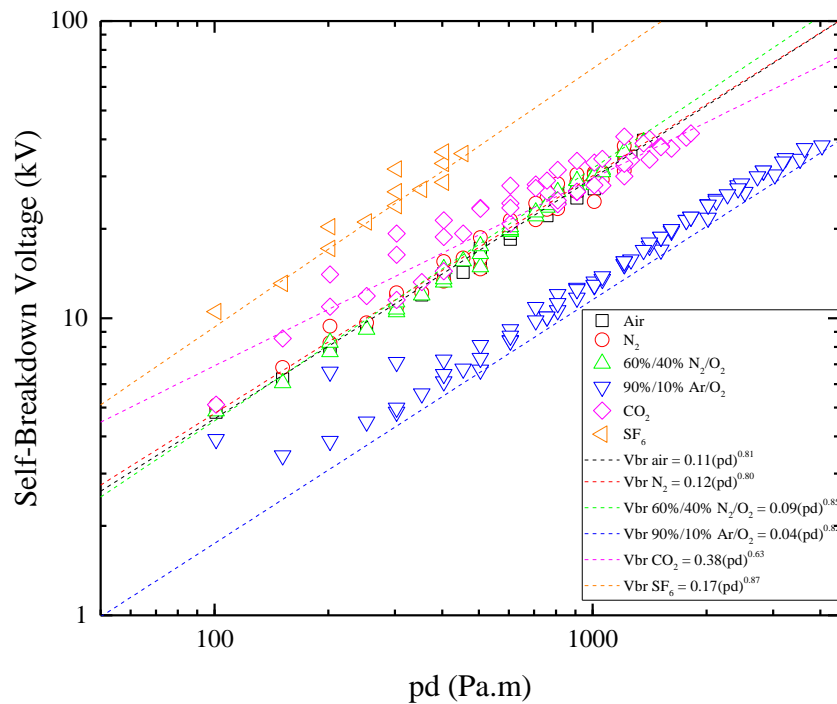


**Figure 3-8** A comparison graph for the average calculated self-breakdown values obtained for each of the six gases/gas mixtures tested.

It is evident from Figure 3-10 that  $\text{SF}_6$  still provides the self-breakdown voltage of all the gases while the mixture of 90%/10%  $\text{Ar}/\text{O}_2$  provided the lowest self-breakdown voltages. The four gases; air,  $\text{N}_2$ ,  $\text{CO}_2$  and the 60%/40%  $\text{N}_2/\text{O}_2$  mixture have similar performance in terms of self-breakdown voltages as  $pd$  increases. At lower  $pd$  values,  $\text{CO}_2$  was seen to have slightly higher self-breakdown voltage capabilities than air,  $\text{N}_2$  or the 60%/40%  $\text{N}_2/\text{O}_2$  mix. It can be seen from Figure 3-10 that the self-breakdown voltages

A key finding from this investigation in relation to  $\text{SF}_6$  filled switches currently in operation, is that for  $pd$  values in the ranges tested, the self-breakdown levels reached can easily be

achieved with air, N<sub>2</sub> or a 60%/40% N<sub>2</sub>/O<sub>2</sub> mixture with a reasonable increase in  $pd$  (300-1200 Pa.m). Where breakdown was observed to occur within an SF<sub>6</sub>-filled switch, the  $pd$  values were within the range 100-500 Pa.m, the same breakdown voltage can be achieved in the other mentioned gases for  $pd$  values of 300-1200 Pa.m. This increase in  $pd$  values of around three times can correspond to an increase in pressure, increase in inter-electrode gap length or a both.

Another result of note came from the spread in self-breakdown voltages of each of the different gases. CO<sub>2</sub> was observed to have the largest spread in self-breakdown voltage of all gases tested which negated any small benefit being able to withstand higher voltages at lower  $pd$  values than air, N<sub>2</sub> or the 60%/40% N<sub>2</sub>/O<sub>2</sub> mixture. The second largest spread in self-breakdown voltages came from the switch filled with SF<sub>6</sub>. This means that where possible, SF<sub>6</sub> could be replaced in currently operating systems with air, N<sub>2</sub> or the 60%/40% N<sub>2</sub>/O<sub>2</sub> mixture at an increased  $pd$  value and will be operationally more predictable and reliable at the voltages where breakdown will occur.

Where classic Paschen breakdown data was available, the experimental results obtained were plotted alongside the literature data for comparison, however, due to the non-uniformities of the electric field within the switch and the nature of the transition into a spark breakdown between two spherical electrodes, the Paschen curves used to predict the breakdown voltage of gases have been determined to not be the most accurate prediction of achievable voltage hold-off capabilities within this self-breakdown switch topology. For the six gases/gas mixtures tested, an allometric fit with Equation (3.2) has been fit to experimental data and has been shown to more accurately predict the self-breakdown voltage of the six gases/mixtures tested.

The fitting coefficients  $A_1$  (kV/Pa.m) and  $\theta$  (kV) obtained using the best fit procedure in Origin graphing software for the allometric fit of each of the gases/gas mixtures tested are presented within Table 3-1 to provide a comparison. 95% confidence intervals for the obtained coefficients are also provided.

**Table 3-1 A and  $\beta$  coefficients of the allometric fit applied to the experimental self-breakdown voltage data obtained for each of the six gases/gas mixtures tested and the 95% confidence bands**

	AIR	N <sub>2</sub>	60% N <sub>2</sub> + 40% O <sub>2</sub>	90% Ar + 10% O <sub>2</sub>	CO <sub>2</sub>	SF <sub>6</sub>
<b>A<sub>1</sub></b>	0.11	0.12	0.09	0.04	0.38	0.17
95% confidence interval	0.10-0.12	0.10-0.13	0.08-0.10	0.035-0.045	0.27-0.49	0.17-0.27
<b><math>\beta</math></b>	0.81	0.80	0.85	0.82	0.63	0.87
95% confidence interval	0.80-0.82	0.78-0.82	0.84-0.86	0.81-0.83	0.59-0.67	0.77-0.97

Table 3-1 compares the  $A_1$  and  $\beta$  coefficients of Equation (3.2), the allometric fit applied to the experimentally obtained self-breakdown voltage data for each of the six different gases/gas mixtures tested. As has already been shown within this chapter, the allometric fit provides a closer fit to experimental data than the Paschen curve (where Paschen data has been available from literature) and for the gases which have previously not been considered for switching purposes in the proposed mixed quantities (60%/40% N<sub>2</sub>/O<sub>2</sub> and 90%/10% Ar/O<sub>2</sub>) an allometric fit only, has been applied as a way means of predicting the self-breakdown voltage for these gas mixtures at  $pd$  values outwith the scope of this experimental investigation.

### 3.4 Analysis of Experimental Results

The experimental results presented show the average values of the self-breakdown voltage calculated from the 20 breakdown events conducted for each inter-electrode gap space, gas pressure and gas tested. A factor of interest which can arise from an experimental test set-up is whether there are any apparent conditioning effects on the electrodes or within the gas over a number of breakdown events.

The measured self-breakdown voltage value for each of the 20 breakdown events was plotted as a function of the breakdown number to view if any obvious conditioning effects were taking place throughout each of the experimental sets conducted. Figure 3-11(a)-(f) shows the self-breakdown voltage levels as a function of breakdown number for a fixed

inter-electrode gap length of 3mm. Each plot presents the self-breakdown voltages measured of one of the six gases/gas mixtures tested within the self-breakdown switch as a function of the breakdown number for each of the different gas pressures tested.

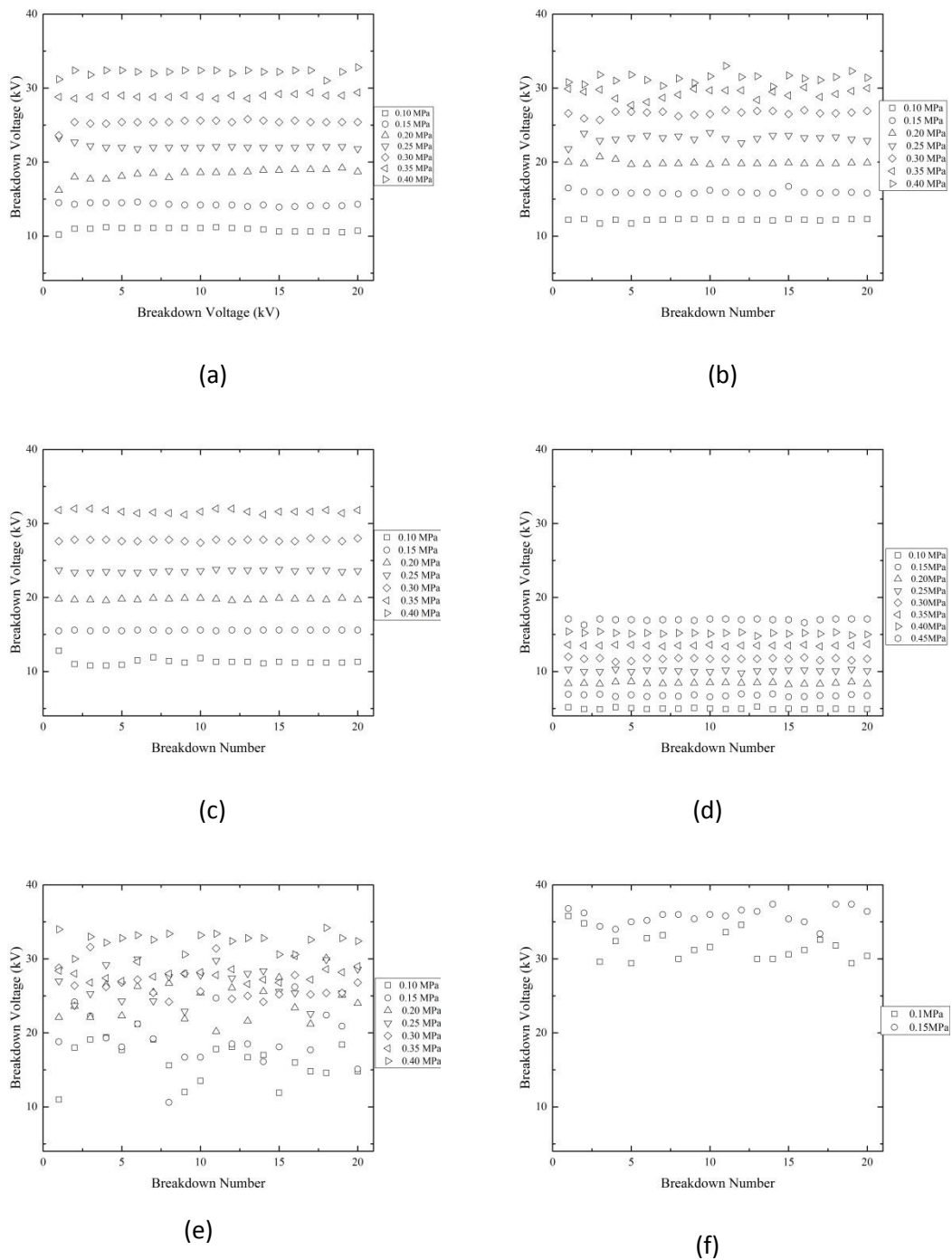


**Figure 3-9 Measured self-breakdown voltage as a function of the breakdown number for (a) air (b) N<sub>2</sub> (c) 60%/40% N<sub>2</sub>/O<sub>2</sub> (d) 90%/10% Ar/O<sub>2</sub> (e) CO<sub>2</sub> (f) SF<sub>6</sub> respectively within a fixed 3mm inter-electrode gap length. The measured self-breakdown voltages are shown for each gas as the gas pressure within the switch increases.**

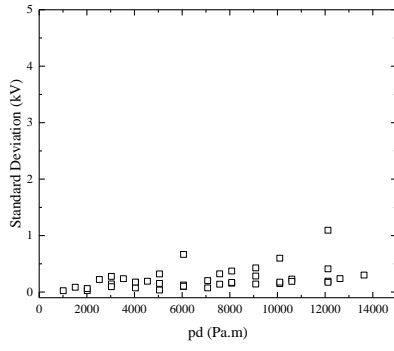
By plotting the self-breakdown voltage as a function of the breakdown number, it is possible to observe any potential conditioning effects acting upon the electrodes or taking place within the fresh portion of gas in the switch which may affect the performance of the switches and would need to be considered within industrial applications.

It can be seen in Figure 3-11(a)-(d) that there is no functional variation in the self-breakdown voltage as the breakdown number increases i.e. between the first breakdown observed and the 20<sup>th</sup> breakdown observed for each gas and gas pressure, the self-breakdown voltage was consistent. It can also be seen for these gases that as the gas pressure within the switch increased, the change between the self-breakdown voltages measured for each individual breakdown event is wider spread.

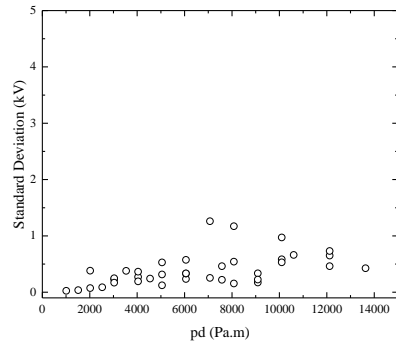
Another interesting result, evident from Figures 11(e) and (f), the CO<sub>2</sub> filled switch and the SF<sub>6</sub> filled switch, is the wide spread in breakdown voltages recorded for both gases. Neither of these gases at the pressures tested showed consistent levels of breakdown voltage during testing. This resulted in both of these gases providing the largest values of standard deviation in the self-breakdown tests conducted.

Aside from the standard deviation in the self-breakdown of each of the gases changing as the gas pressure changes (and thus assuming it will change as the product  $pd$  changes, which will be discussed within the next section), there were no evident conditioning effects observed when monitoring the self-breakdown voltage for any of the gases tested as a function of the breakdown number which confirms the self-breakdown voltage results previously presented within this chapter without having to consider or discard breakdown events conducted due to conditioning of the experimental set-up.

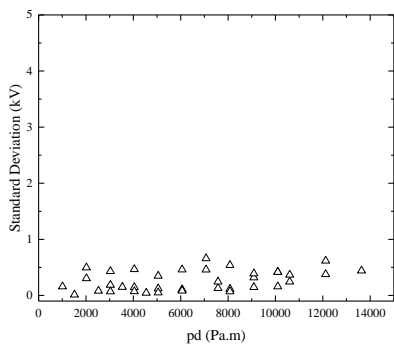
Within Figure 3-11(a)-(f), for a fixed 3mm inter-electrode gap length, as the gas pressure increased, it could be seen that the variation in the self-breakdown voltage grew as the gas pressure increased. In Figure 3-12(a)-(f), the standard deviation in the self-breakdown voltage for each of the data sets was plotted as a function of the product  $pd$ .



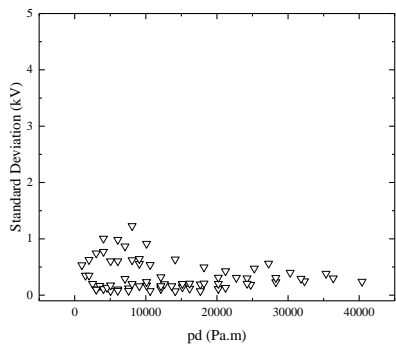
(a)



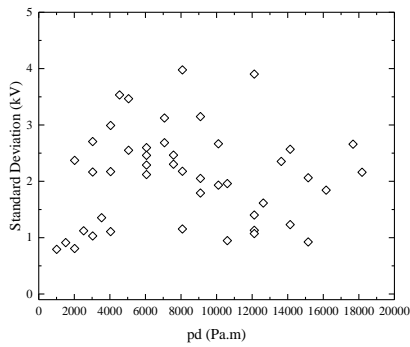
(b)



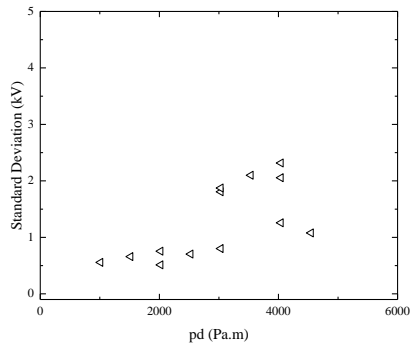
(c)



(d)



(e)



(f)

**Figure 3-10(a)-(f) standard deviation in the self-breakdown voltage as a function of  $pd$  for for (a) air (b)  $N_2$  (c) 60%/40%  $N_2/O_2$  (d) 90%/10%  $Ar/O_2$  (e)  $CO_2$  (f)  $SF_6$  respectively.**

It can be seen within Figure 3-12(a) the air-filled switch, Figure 3-12(b) the N<sub>2</sub> filled switch, Figure 3-12(c) the switch filled with the 60%/40% N<sub>2</sub>/O<sub>2</sub> mixture and Figure 3-12(f) the SF<sub>6</sub> filled switch, as the  $pd$  value increases, the calculated standard deviation in the self-breakdown value was also generally seen to increase. This result is in agreement with the self-breakdown result presented as a function of the breakdown number in Figures 3-11(a)-(f) which showed that within the fixed 3mm inter-electrode gap length, as the gas pressure within the switch increased, the self-breakdown voltage for each of the gases was observed to vary more widely.

In the switch filled with the 90%/10% Ar/O<sub>2</sub> mixture, the standard deviation was able to be calculated for much higher values of  $pd$  than the other gases tested due to the lower self-breakdown voltage of the 90%/10% Ar/O<sub>2</sub> gas mixture and a far wider range of self-breakdown voltages measured and the corresponding calculated standard deviation of those measurements are available.

Figure 3-12(e) presents the calculated standard deviation of the measured self-breakdown voltages within the switch when filled with CO<sub>2</sub>. As already discussed within section 3.3.4, CO<sub>2</sub> provided the largest values of standard deviation in self-breakdown voltage of all the six gases/gas mixtures tested and when plotted as a function of  $pd$ , there are no distinct trends as appear with the other gases tested within this experimental investigation. For all possible  $pd$  values where breakdown was initiated, regardless of the experimental inter-electrode gap length or gas pressure combination required to achieve this  $pd$  value, the standard deviation within a CO<sub>2</sub>-filled switch was found to be significantly larger than the other gases.

For all gases tested, it was found that there could be a wide spread in the calculated values of the standard deviation for the same  $pd$  value. This is due to different combinations of inter-electrode gap lengths and gas pressures giving the same product  $pd$ .

### 3.5 Discussion

This investigation into the breakdown performance of different gases in a self-breakdown switch with a uniform electric field distribution has produced important results which can be used in practical applications.

A self-breakdown sphere-sphere topology spark gap switch was designed from operational requirements provided by AWE. An electrostatic simulation of pre-breakdown electric field in the proposed switch was conducted before construction took place, to ensure that under normal operational procedures there would be no abnormal field enhancements occurring within the switch. Post-simulation development and construction of the switch a simple circuit was developed which allowed the self-breakdown voltages of 6 different gases/gas mixtures to be monitored, recorded and compared. SF<sub>6</sub> was one of the gases used within the experimental investigation and was used as a baseline to compare all other gases to. This baseline was created as any gas considered as a potential replacement gas for switching applications should be able to provide similar performance characteristics to those of SF<sub>6</sub>.

It was found that air, N<sub>2</sub> and a mixture of 60%/40% N<sub>2</sub>/O<sub>2</sub> all provide similar levels of self-breakdown voltage suggesting that the percentage of the electronegative O<sub>2</sub> mixed with the electropositive N<sub>2</sub> does not strongly contribute to the overall self-breakdown strength of these gases / gas mixtures. However the 60%/40% N<sub>2</sub>/O<sub>2</sub> mixture had the lowest standard deviation of all the gases tested (0.05 kV-0.65 kV) and so proved to be the most stable and reliable in terms of breakdown voltage level predictions, a desirable trait for industrial applications.

It was found that a mixture of 90%/10% Ar/O<sub>2</sub>, although used in some industrial pulsed power applications, provides far lower voltage hold-off capabilities than any of the other gases tested (voltages approximately 50-60% of that achieved by air, N<sub>2</sub>, 60%/40% N<sub>2</sub>/O<sub>2</sub> or CO<sub>2</sub> for the same *pd* values) and the standard deviation in self-breakdown voltages is significantly large. In self-breakdown applications where the *pd* values fall in the range 100 – 1500 Pa.m, as was tested, there is no evidence to support suggesting that a 90%/10% Ar/O<sub>2</sub> mixture would make a suitable alternative gas for use in plasma closing switches.

CO<sub>2</sub>-filled switches at lower tested  $pd$  values (100-300 Pa.m) provided higher breakdown levels than the switches filled with air, N<sub>2</sub> and the 60%/40% N<sub>2</sub>/O<sub>2</sub> mixture. It was found, however, that as the  $pd$  values increased, the self-breakdown levels in a CO<sub>2</sub>-filled switch were at a similar level to those switches filled with air, N<sub>2</sub> and the 60%/40% N<sub>2</sub>/O<sub>2</sub> mixture. Another finding of this experimental investigation was that the standard deviation in a CO<sub>2</sub>-filled switch had the largest values (0.79-3.97 kV compared to the ~0.65-1.3 kV for all other gases although SF<sub>6</sub> has a breakdown voltage spread around 1-2 kV) and, as such, suggests that the self-breakdown voltages are the least predictable of all tested gases. Despite the slight advantage in the increase in breakdown voltage at smaller  $pd$  values, a gas with more reliable breakdown characteristics is desirable in practical applications. No conditioning effects were observed throughout each set of breakdown tests run and no significant decrease in standard deviation as pressure increased was apparent under the experimental conditions available.

The calculated standard deviation of the self-breakdown voltages measured was investigated as a function of the product  $pd$  within the switch and was shown to increase as  $pd$  increases for all gases/gas mixtures tested, with the exception of the CO<sub>2</sub> filled switch which had no discernible trends.

Much of the research into alternative gases for use within pulsed power devices comes from a desire to replace SF<sub>6</sub>. The self-breakdown experiments conducted using SF<sub>6</sub> showed that, despite providing a breakdown voltage level ~2.5 times that of most of the other gases, the standard deviation of SF<sub>6</sub> was also large.

The breakdown voltage level and breakdown voltage spread of self-breakdown switches are two key characteristics of interest for many industrial applications. It has been shown that the self-breakdown voltage of SF<sub>6</sub> in a switch can be replicated in a switch filled with a 60%/40% N<sub>2</sub>/O<sub>2</sub> mixture at a  $pd$  value which would require minimal retrofitting of current systems and would also improve on the spread of breakdown voltage, ensuring the switching is more reliable.

The next section of this thesis will be focussed on the design and investigation of a field-distortion, triggered spark gap topology switch filled with 6 different gases/gas mixtures.

## **Chapter 4 . Characterisation of a Field-Distortion Spark Gap Switch Triggered with “Slow” 0.45 kV/μs HV Impulses**

This chapter presents an experimental investigation into time to breakdown and jitter of a field-distortion triggered spark gap switch. The field-distortion spark gap is the second of the two switch topologies of interest throughout this investigation and is of particular interest due to the large number of these topology of switches that can be used in erecting Marx generators e.g. within the Mevex machine at AWE, of the 13 switches used to erect the Marx, 11 of them are of a field-distortion design [59], [60].

Within this chapter a discussion on the design of a field-distortion, triggered spark gap switch is presented followed by the results of an experimental investigation into the breakdown characteristics of the field-distortion switch filled with six gases previously investigated; air, N<sub>2</sub>, 60%/40% N<sub>2</sub>/O<sub>2</sub>, 90%/10% Ar/O<sub>2</sub>, CO<sub>2</sub> and SF<sub>6</sub>. The key breakdown characteristics in a field-distortion switch triggered with HV impulses with a “slow”, ~0.45kV/μs rate of voltage rise have been studied in this Chapter, these key characteristics, including the time to breakdown and the switch jitter, have been investigated with respect to their dependence upon inter-electrode gap space, gas pressure within the switch and the level of DC stress voltage applied across the main inter-electrode gap distance. Statistical analysis of the experimental results is conducted and the main findings are presented and discussed in this Chapter.

### **4.1 Switch design and electrostatic modelling**

The basic concept and principle of operation of field distortion plasma closing switches are described in Chapter 2. Based on this basic concept a field-distortion switch has been designed and developed in this study. When designing the field-distortion spark gap switch, some of the desirable operational characteristics which had to be taken into consideration were that, similar to the self-breakdown switch, this switch body should also

be able to withstand and contain gas pressures up to 0.5MPa absolute. The triggering voltage impulse applied during the experimental procedure is designed to be applied to a mid-plane electrode which would remain in a fixed position at an equidistant point between the two spherical electrodes throughout the experimental procedure.

Prior to construction of the switch, a model of the switch has been developed in the electrostatic software package Quickfield in order to simulate the pre-breakdown electric field distribution inside the proposed switch design.

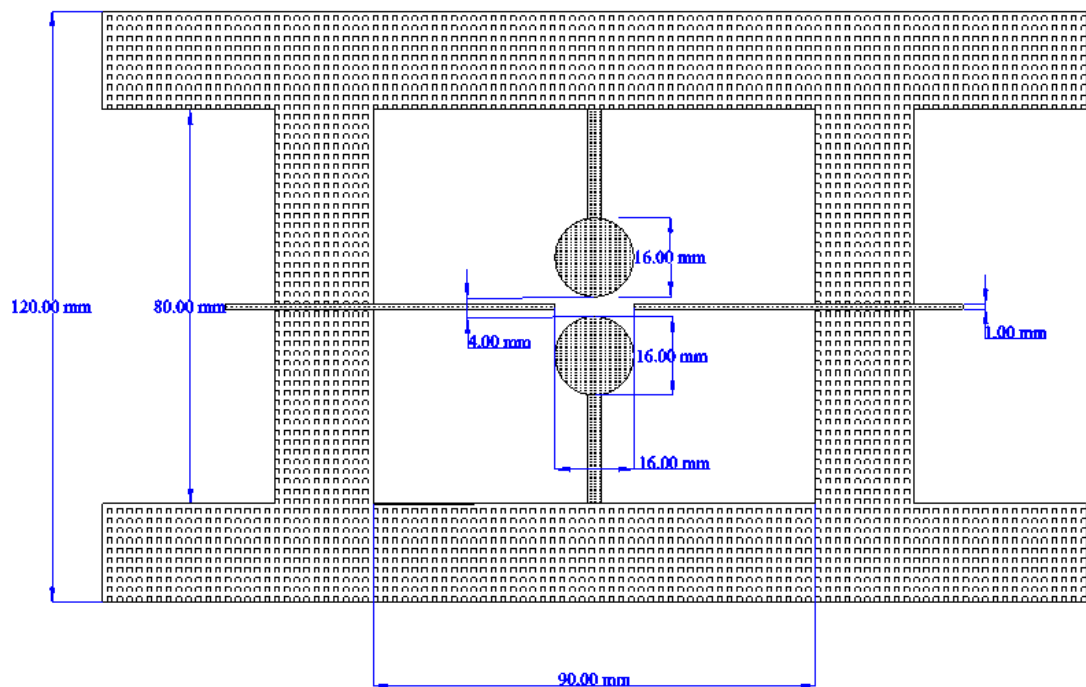


**Figure 4-1** The proposed design for a field-distortion spark gap switch to investigate the time to breakdown and jitter characteristics of different gases.

Figure 4-1 shows the proposed design for the field-distortion spark gap switch which was modelled within the QuickField electrostatic software for analysis of the electric field distribution before breakdown events. The proposed design in Figure 4-1 makes use of a 90mm diameter cylindrical test cell comprised of two halves. A 1mm thick brass plate, 150mm in diameter with a 16mm aperture in the centre is utilised as the mid-plane triggering electrode and this is held in place between the upper and lower halves of the test cell body. This location of the trigger plate which follows the equipotential lines in the

switch is selected to avoid distortion of the field within the switch before application of the trigger impulse. The 'main electrodes' used within this test cell are the upper and lower 16mm diameter, spherical brass electrodes, identical to those used in the self-breakdown topology switch as described within Chapter 3.

When simulated within QuickField software, two different experimental conditions have been modelled. Both simulations conducted have made use of a DC stress voltage of 10kV applied to the upper spherical electrode and the lower spherical electrode is grounded throughout experiments. One of the conditions modelled considered the mid-plane electrode when assigned to be a floating potential voltage and another condition where a fixed voltage of -30kV is applied to the mid-plane electrode.

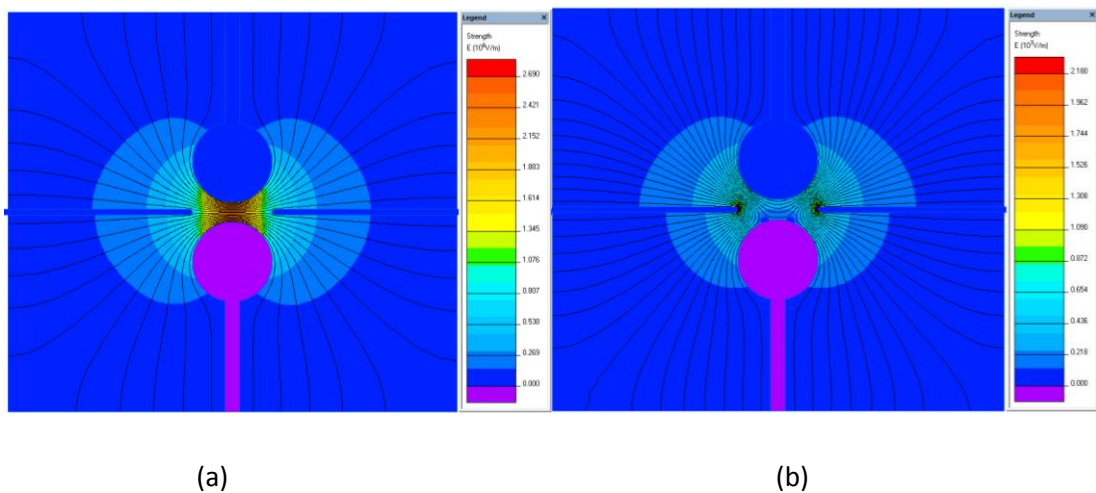


**Figure 4-2(a) QuickField cross section of the switch and the electric field distribution between the electrodes under operational conditions when a DC stress voltage of 10kV is applied to the upper electrode, the lower spherical electrode is grounded and the mid-plane electrode is a floating potential. Figure 4-2(b) QuickField cross section of the switch and the electric field distribution between the electrodes under operational conditions when a DC stress voltage of 10kV is applied to the upper electrode, the lower spherical electrode is grounded and a -30kV voltage is applied to the mid-plane electrode.**

It is shown in Figure 4-2(a) above, the electric field strength within the proposed switch design during operational conditions for a 4mm inter-electrode gap (considered to be the gap between the upper and lower spherical electrodes) when a DC stress level of +10 kV is applied to the upper spherical electrode, the lower spherical electrode is grounded and the mid plane electrode is considered at floating potential. It can be seen that the electric field

reaches its maximum value in the region between the upper and lower spherical electrodes similar to the case of the self-breakdown topology switch as discussed within Chapter 3.

It is seen from Figure 4-2(b) that when a -30kV voltage is applied to the mid-plane electrode, the electric field is at a maximum around the mid-plane electrode, in the region between the mid-plane electrode and the upper-electrode where the DC stress voltage is applied.

This proposed switch topology enhances the electric field in the region surrounding the mid-plane where the trigger impulse with polarity opposite to the polarity of the DC stress is applied and upper electrode where the DC stress voltage across the gap is applied. The magnitude of the electric field will also be enhanced although to a lesser extent between the mid-plane electrode and the lower spherical electrode which is grounded throughout experimental procedure as is shown in Figure 4-3 below.

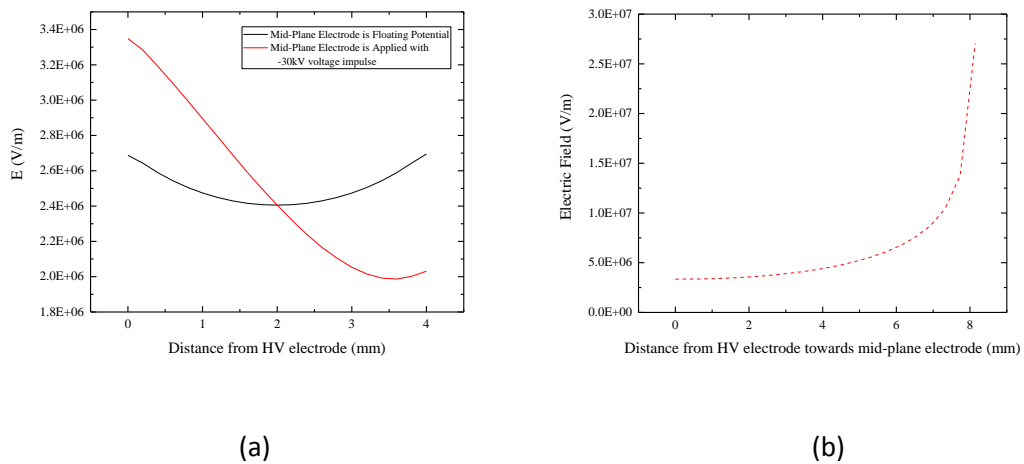


**Figure 4-3 (a) The magnitude of the electric field between the upper and lower spherical electrodes when the midplane electrode is at a floating potential and when it has a -30kV voltage applied moving from the upper electrode which is applied with 10kV DC as a voltage stress towards the lower spherical electrode which is grounded. (b) The magnitude of the electric field in the region between the upper electrode where the high voltage DC stress is applied and the mid-plane triggering electrode where -30kV is applied moving from the HV electrode towards the mid-plane triggering electrode.**

Figure 4-3(a) shows a comparison of the magnitudes of the electric field between the upper spherical electrode which is stressed with 10kV DC and the lower spherical electrode held at ground potential (black line). When the mid-plane electrode is modelled to be at a floating potential, it is seen that the peak magnitude of the electric field is  $\sim 2.7\text{MV/m}$  in the regions immediately around the electrodes and a minimum electric field value of

~2.4MV/m, which occurs at precisely the mid-point between the upper and lower electrode (indicated at the 2mm point of the 4mm distance between the upper and lower electrodes). In Figure 4-3(a) when the modelled switch is stressed with +10kV DC and the mid-plane triggering electrode has -30kV voltage applied (red line), the peak magnitude of the electric field in the region between the two main spherical electrodes is seen to have increased to ~ 3.4MV/m in the region directly surrounding the upper electrode stressed with the high voltage. The magnitude of the minimum electric field is seen to be lower, ~ 2MV/m than that of the conditions when the mid-plane electrode is at a floating potential.

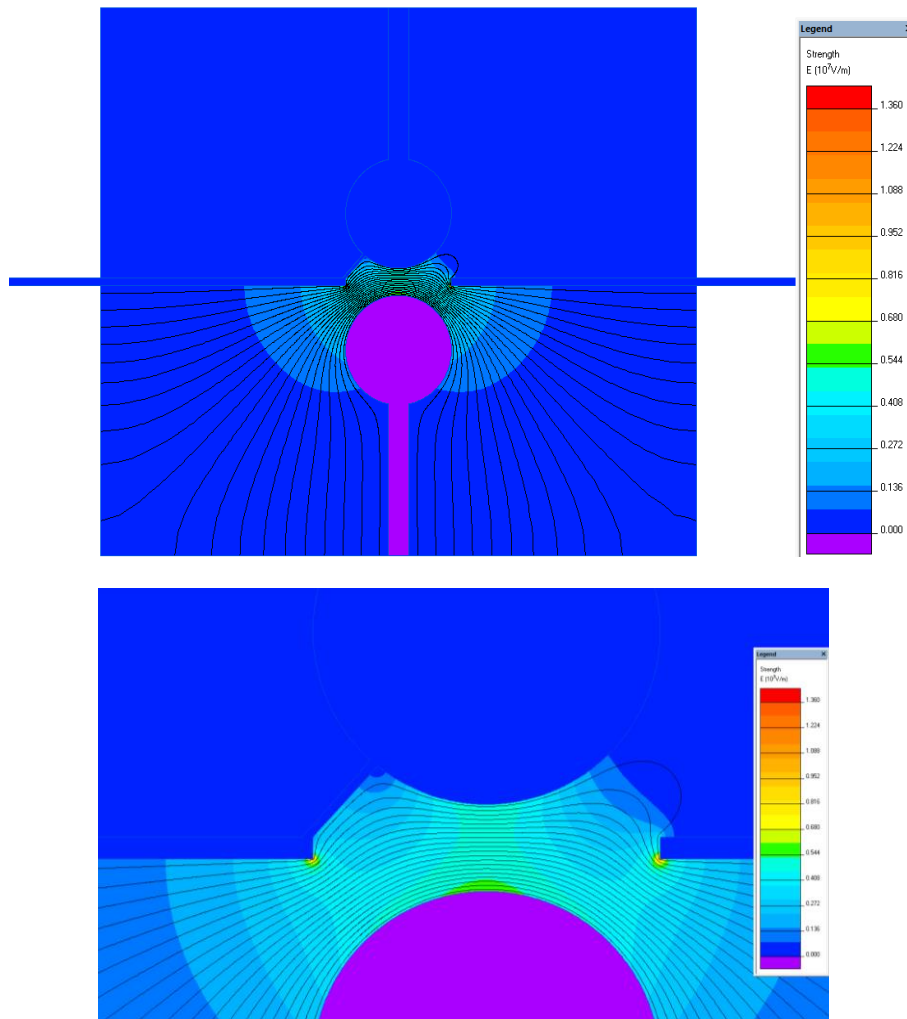
However, when the mid-plane electrode provides -30kV voltage, as seen in Figure 4-2(b), the electric field strength is increased in the region between the high-voltage electrode and the mid-plane electrode, with the intense electric field strength in the region surrounding the mid-plane electrode. Figure 4-3(b) plots the magnitude of the electric field strength in moving from the high voltage spherical electrode with +10kV DC voltage applied to the edge of the mid-plane triggering electrode where the -30kV trigger impulse is applied. It is clearly seen from Figure 4-3(b) that the electric field strength increases by an order of magnitude in the region around the mid-plane triggering electrode when compared to the electric field strength in the main inter-electrode gap of the switch. This significant increase in the strength of the electric field in the region surrounding the mid-plane electrode suggests that under experimental conditions, where a DC stress voltage is applied to the upper spherical electrode (and is smaller in magnitude than the voltage impulse which is to be applied to the mid-plane trigger electrode) and the mid-plane electrode supplies a trigger voltage of the opposite polarity to the DC stress voltage, the magnitude of the electric field within the switch is an order of magnitude higher in the region surrounding the mid-plane electrode and thus the breakdown event within the switch will initiate within this region before complete breakdown of the main gap occurs.

Once a breakdown event has been initiated between the mid-plane triggering electrode and the upper spherical electrode where the high voltage DC stress has been applied, a net 'post-initiation' voltage is established at the high voltage electrode and trigger electrode when a spark connects the two electrodes. The two initially separate electrodes, independently stressed with DC and impulse voltages of opposite polarities, become stressed with the post-initiation voltage after the spark bridges the gap between the two:

$$|V_{post-initiation}| = |V_{trigger-impulse}| - |V_{dc-stress}| \quad (4.1)$$

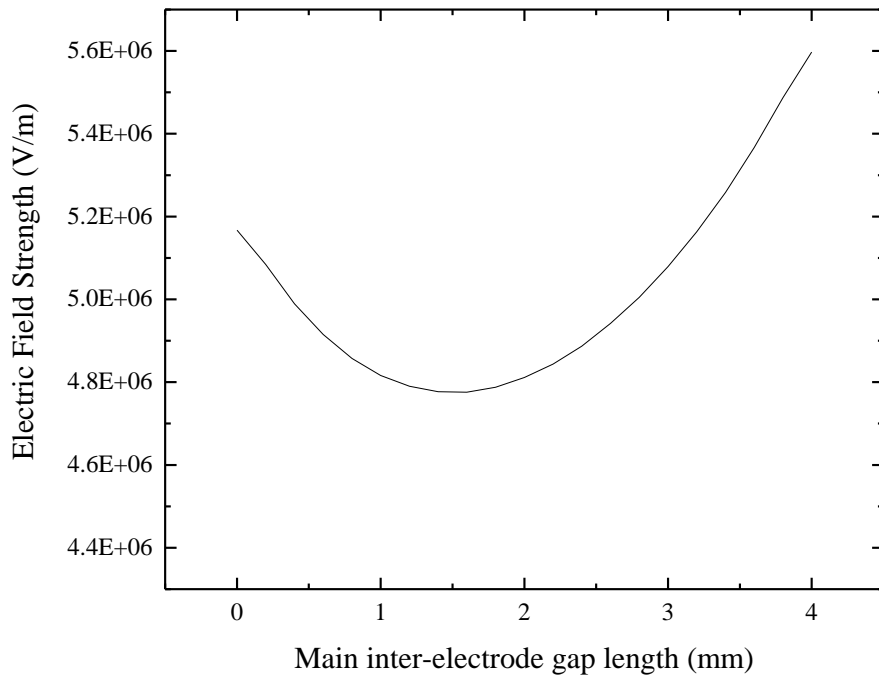
where  $V_{trigger-impulse}$  is the magnitude of the trigger impulse applied to the mid-plane electrode and  $V_{DC-stress}$  is the voltage applied to the upper spherical electrode as the DC stress across the main gap of the switch.

The field distribution in the switch has been obtained after a conductive plasma channel is formed between the upper spherical electrode and one part of the mid-plane triggering electrode, this field distribution has been obtained using Quickfield electrostatic software. The conductive plasma channel was modelled as a thin conductor placed between the top HV electrode and the trigger plate, thus the top HV electrode and the trigger electrode have the same electrical potential,  $V_{post-initiation}$ , after formation of the conductive plasma channel (assuming that the plasma resistance and the voltage drop across the plasma channel are negligible for the purpose of this analysis).



**Figure 4-4 Electric Field strength within the switch post-initiation of breakdown between the two electrodes. The net voltage equal to the magnitude of the trigger voltage minus the DC stress voltage is applied and the electric field strength within the main-inter-electrode gap length is observed.**

Figure 4-4 presents the result of the electric field strength simulation in Quickfield for a post-initiation condition when a spark channel has bridged the gap between the upper spherical electrode and the mid-plane electrode and the net post-initiation voltage is manually applied on what had previously been the high voltage electrode, the mid-plane electrode and the spark channel which now has formed connecting the two electrodes. In the simulation in Figure 4-4,  $V_{\text{post-initiation}}$  is applied as a net voltage of 20kV (equal to 30kV-10kV, the magnitude of the trigger impulse voltage minus the DC stress voltage applied across the main gap) from the upper spherical electrode, the mid-plane electrode and the channel formed between the two electrodes. Figure 4-5 shows the resulting electric field strength within the switch post-initiation of breakdown.



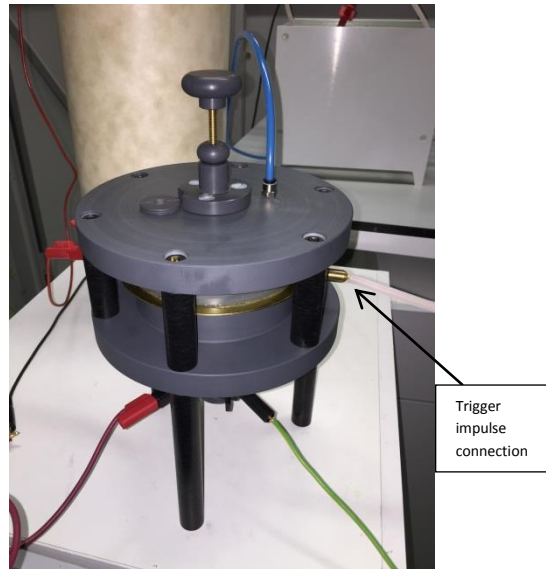
**Figure 4-5. The electric field strength in the region between the upper, spherical electrode and the lower, grounded electrode when the net post-initiation voltage is applied to the upper electrode and mid-plane electrode. The switch simulates the post-initiation condition where a spark has bridged the gap between the mid-plane electrode and the upper spherical electrode which initially had opposite polarity voltages applied to them. The spark bridging the gap between the two electrodes become stressed with a single, net post-initiation voltage after the spark has bridged between the two electrodes.**

Figure 4-5 shows the electric field strength in the main inter-electrode gap length when a net-post initiation voltage of 20kV is applied to the mid-plane, upper electrode and the spark channel that bridges the two electrodes, simulating the conditions after breakdown has been initiated but before complete closure of the switch has occurred.

## **4.2 Switch Construction and Test Set-up**

The proposed switch design as described within Section 4.1 has been shown through electrostatic simulation to encourage breakdown events within the switch to initiate between the upper electrode where the DC stress voltage is applied and the mid-plane electrode upon which the high voltage trigger impulse is applied, before complete closure

of the switch will occur. No unwanted field enhancements were seen to occur at points elsewhere within the proposed design and, as such, a physical switch was constructed based upon the model design.



**Figure 4-6 Photograph of the field-distortion topology switch.**

The schematic diagram in Figure 4-6 above shows a photograph of the constructed switch built from the schematic provided in Figure 4-1. The main body of the test cell was constructed in two halves from a grey PVC rod, the mid-plane triggering electrode is constructed from a 1mm thick brass sheet and is held in place between the two halves of the switch body, a connection for applying the voltage impulse to this mid-plane electrode is screwed onto one side of the trigger plane as indicated in Figure 4-6. The location of the trigger-plane is firmly fixed and cannot move throughout the experimental procedure and both halves of the test cell are fixed together, compressed and held in place with six bolts, three of which fix into the legs of the test cell.

The main electrodes within the field-distortion spark gap switch were two spherical electrodes, identical to those used in the self-breakdown switch (16mm diameter, brass attached to 3mm thick shaft) and within the design of this switch topology, the inter-electrode gap distance is fully adjustable by raising or lowering both the upper and lower spherical electrodes. The upper and lower electrodes are simultaneously adjusted and each

360° rotation of the shaft corresponds to a 1mm vertical adjustment of each electrode, resulting in an increase or decrease of the gap space by 2mm.

A 2mm incremental increase in gap space was chosen as this keeps the separation between the upper electrode with the mid-plane and the lower-electrode with the mid-plane uniform ensuring that no breakdown between mid-plane and one of the main electrodes will be favoured due to uneven gap spacing.

By allowing both the upper and lower electrodes to be moved, provides more control over the gap separation under experimental conditions.

In Section 4.3 of this thesis, the methodology and description of the experimental procedure followed to conduct the breakdown tests within the field-distortion spark gap switch is provided.

### **4.3 Methodology**

This section describes the experimental test set-up and methodology for conducting breakdown tests carried out with the field-distortion triggered switch and making use of a trigger generator to provide the trigger impulse to the mid-plane electrode.

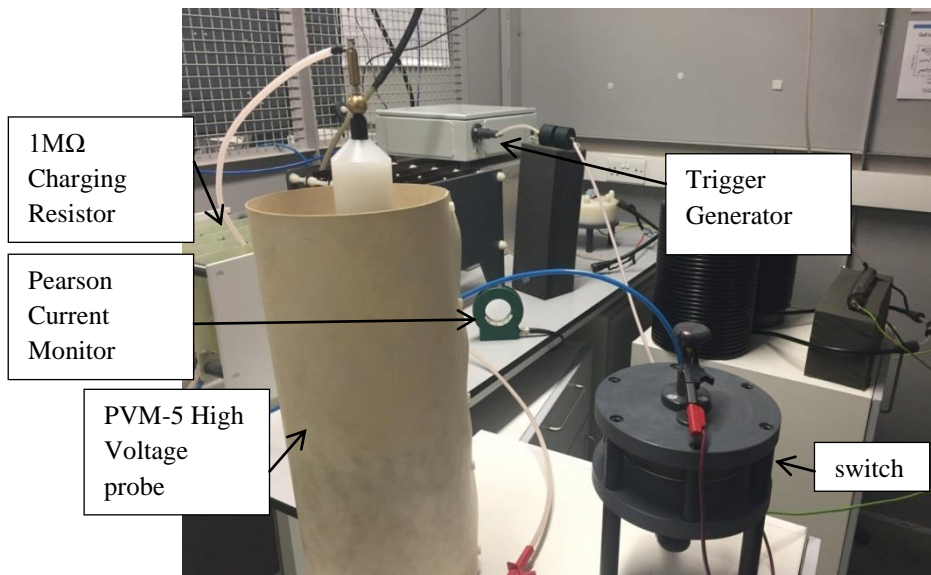


**Figure 4-7. Experimental test set-up for measuring time to breakdown in the Field distortion spark gap switch when the -30kV trigger impulse is applied to the mid-plane electrode by the trigger generator. The voltage across the main gap is monitored by HV voltage probe, a DC stress voltage applied to the upper spherical electrode via a 1MΩ charging resistor. To ensure complete breakdown occurs, the current across the switch is monitored via Pearson current monitor.**

The experimental test set-up for the breakdown experiments conducted is shown in Figure 4-7 and consists of a Glassman high voltage DC power supply (EH series 0-60kV) which provides a DC stress voltage across the inter-electrode gap space in the switch via a 1MΩ charging resistor. A maximum trigger impulse of ~30kV with a rate of rise ~0.45kV/μs is applied by means of a trigger generator via a decoupling resistor to the mid-plane electrode of the switch. A North Star PVM-5 high voltage probe (1000:1 division ratio, 80 MHz nominal bandwidth) is used to monitor the voltage across the 'main gap' of the switch i.e. the total gap between the two spherical electrodes. A Tektronix P6015A probe (1000:1 division ratio, 75 MHz nominal bandwidth) is used to monitor the trigger impulse provided by the trigger generator to the mid-plane of the switch. The voltage signals from both probes were monitored using a Tektronix TDS 3054 digitising oscilloscope (500MHz bandwidth, 5GS/s sampling rate). A TesTec HVP-40 probe (1000:1 division ratio, 300 Hz) was also used for the purpose of determining the level of DC stress voltage applied to the upper spherical electrode.

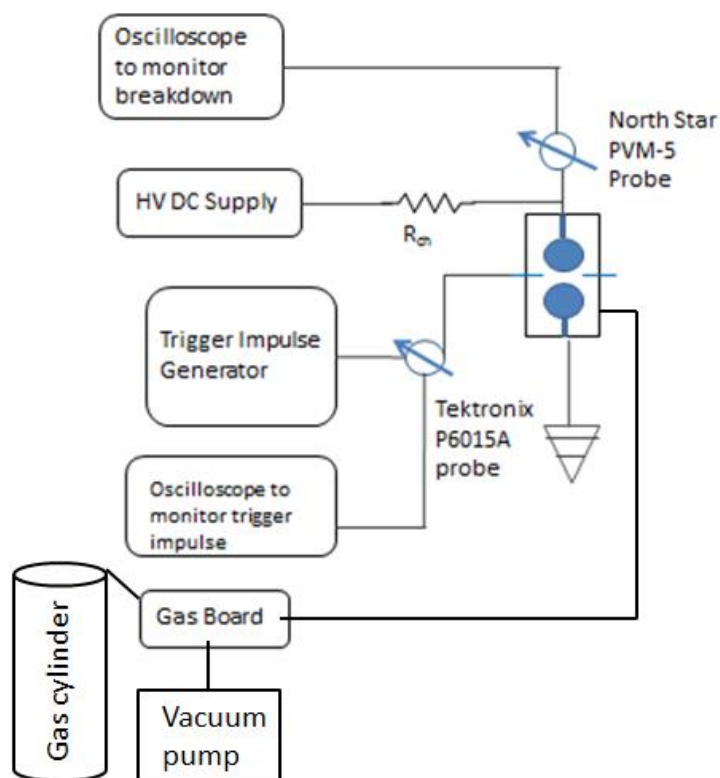


Figure 4-8 Schematic of the experimental test set-up created for field distortion switch experiments

For the field-distortion topology switch, the inter-electrode gap space during experimental procedures is defined from a 'zero point' where a short circuit is observed across the entire switch. By measuring the resistance across the switch from the upper electrode to the lower electrode by using a digital multi-meter, the gap is space is defined from the point where the upper electrode no longer makes contact with the mid-plane electrode and the lower spherical electrode no longer makes contact with the mid-plane electrode. The shortest inter-electrode gap space where triggered breakdown experiments were conducted was with a 2mm gap – achieved by adjusting both the upper and lower electrodes by 1mm each from the zero point.

To measure the time to breakdown for each gas tested for a range of pressures at different inter-electrode distances, an initial evaluation of the self-breakdown voltage level for each gas at each pressure tested for the different inter-electrode gap distances was required.

Once the gap distance had been set, gas was evacuated from the switch by means of the vacuum pump in the same steps taken outlined in Section 3.0 for evacuating and refilling

the switch with gas. The self-breakdown voltage of each gas at different pressures was measured within this switch topology and this was conducted as described in Section 3.0 by manually increasing the DC voltage applied at a rate of  $\sim 2\text{kV/s}$  to the upper spherical electrode until a complete voltage collapse across the switch was observed to occur on the screen of the oscilloscope. The breakdown voltage level was recorded and the self-breakdown voltage level for each gas, inter-electrode distance and gas pressure was used in determining the DC stress voltage level required for the triggered breakdown experiments. Typically when gaps are stressed with a DC voltage to minimise the jitter, the DC stress applied is in the region of 60%-90% of the self-breakdown voltage and as the gap becomes increasingly stressed, typically the operation of the switch is seen to become more stable with jitter seen to decrease.

The process for carrying out the time to breakdown experiments involved setting of the inter-electrode gap length as previously outlined, evacuating the test cell of gas and filling with gas to an initial pressure of 0.1MPa with air and manually applying a DC stress voltage to the upper spherical electrode of 70% of the self-breakdown voltage for this gas at this pressure.

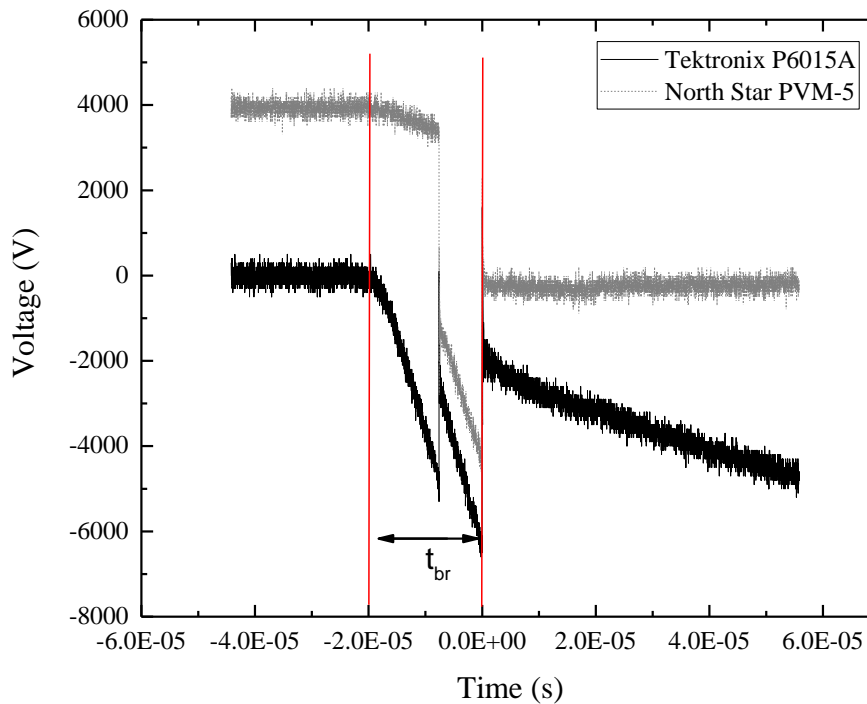


**Figure 4-9 Voltage waveforms from both the Tektronix and the North Star voltage probe indicating the measured time to breakdown in an air-filled switch at 0.15MPa with 70% V<sub>br</sub> DC stress applied.**

Figure 4-9 shows the obtained voltage waveforms from the Tektronix probe monitoring the voltage impulse applied to the mid-plane electrode and the North Star PVM-5 probe which monitored the voltage across the main gap of the switch. The time to breakdown is marked and is taken to be the time between the start of the voltage impulse on the trigger plane and the complete collapse of voltage across the main gap. As can also be seen from Figure 4-9, the DC stress voltage applied across the inter-electrode gap length equating to 70% of the self-breakdown voltage is below the 10kV that was modelled within Quickfield. The trigger impulse that is applied to the mid-plane electrode that initiates the breakdown within the gap does not reach the full -30kV before breakdown is initiated. The values of 10kV dc stress and a -30kV voltage application to the mid-plane triggering electrode were simply maximum expected values, however under experimental conditions, different values of DC stress will be applied and the magnitude of the trigger voltage that is required to initiate breakdown will change for each data set. It is therefore reasonable to conclude that

the magnitude of the electric field in the region between the electrodes will be smaller than the values obtained from the simulations.

The start of the voltage impulse was measured on the screen of the oscilloscope and defined as the last point at which the voltage was measured to be zero before negative value, non-zero voltage measurements were taken. The end point of the 'time to breakdown' is measured as the moment when the voltage across the entire switch collapses to zero as indicated on Figure 4-4 above. For the triggered switch experiments outlined, 30 breakdown events were conducted before the test cell was evacuated and refilled to the same pressure with a fresh portion of gas. The experiment was then conducted with an increased DC stress level across the main inter-electrode gap length of 80% of the self-breakdown voltage.

This procedure was repeated for each of the six gases that had previously been investigated in the experiments; air, N<sub>2</sub>, 60%/40% N<sub>2</sub>/O<sub>2</sub>, 90%/10% Ar/O<sub>2</sub>, CO<sub>2</sub> and SF<sub>6</sub> within the self-breakdown topology switch. For each of the gases investigated the switch was stressed with 70% of the DC self-breakdown voltage level and 80% of the DC self-breakdown voltage level for each gas pressure within the range 0.1MPa-0.4MPa. The gas pressure within the switch was increased from 0.1MPa (absolute) in 0.05MPa increments to a maximum pressure of 0.4MPa or until breakdown between the electrodes was not observed. Inter electrode gap lengths of 2mm and 4mm were investigated.

The next section of this chapter will present the results of the breakdown experiments conducted for each of the gases tested under the experimental conditions. The time to breakdown as a function of increasing pressure has been obtained and presented in this Section for each inter-electrode gap length tested individually.

#### **4.4 Time to Breakdown in a field distortion switch with variation in pressure and percentage of DC stress level.**

Within this section, the results of the experimental investigation focused on the time to breakdown of each of the gases which had previously been investigated for self-breakdown properties within Chapter 3 are presented. The time to breakdown measurements are presented separately for each gas and inter-electrode gap space and within each of the

graphs, a comparison of the effect of stressing the main inter-electrode gap length with either 70% or 80% of the self-breakdown voltage level is shown.

This triggered switch was filled with each of the 6 gases used in previous experiments shown; bottled air, N<sub>2</sub>, 60/40% N<sub>2</sub>/O<sub>2</sub>, 90%/10% Ar/O<sub>2</sub>, CO<sub>2</sub> and SF<sub>6</sub>. The results of the time to breakdown experiments for each gas are presented below.

A linear fit is applied to the experimental data as a means of comparing the time to breakdown characteristics of the switches at different gas pressures for different levels of DC stress voltage applied across the switch.

#### 4.4.1 Time to Breakdown for an Air filled switch

The results presented within this section show the time to breakdown as a function of gas pressure for an air-filled switch and the jitter (standard deviation of the time to breakdown) as a function of the gas pressure within the switch. The standard deviation in time to breakdown, (typically depicted the Greek letter  $\sigma$  is used for standard deviation calculated using a normal distribution assumption) is obtained from experimental results: this is referred to as the jitter (or 1- $\sigma$  jitter) of the switch and is another key characteristic of interest which has been investigated and is presented. The jitter calculated for each variation of experimental parameters is shown in the context of the time to breakdown but also presented independently as a function of gas pressure within the switch.

A linear phenomenological fitting has been applied to the experimental data and is plotted on the figure alongside the experimental results as a means of evaluating the relationship between the time to breakdown and the  $pd$  value. The linear fit applied to the experimental data has equation:

$$t_{br} = ap + b \quad (4.2)$$

Where  $t_{br}$  is the time to breakdown,  $a$  is the gradient of the line ( $\mu\text{s}/\text{MPa}$ ),  $p$  is the gas pressure within the switch (in MPa) and  $b$  is a constant ( $\mu\text{s}$ ).

Coefficients  $a$  and  $b$  have been obtained using the best fit procedure in Origin Pro graphing, by fitting Equation (4.2) to the experimental data points. Equation 4.2 for 70% DC breakdown stress voltage and 80% DC breakdown stress voltage with numerical coefficients

$a$  and  $b$  are provided in graphs presented in this Section and summarised in Table 4-1. For each figure presented within this Chapter, the solid symbols represent the experimental conditions where 70% of the self-breakdown voltage is applied as the DC stress across the inter-electrode gap length, the open symbols represent the conditions for 80% of the self-breakdown voltage applied as DC stress and the error bars represent the jitter in the time to breakdown.

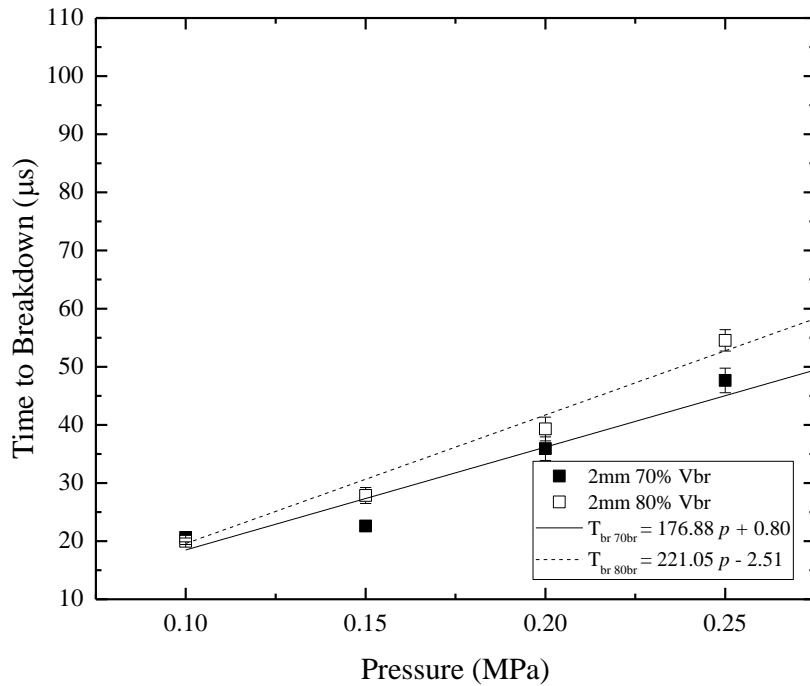


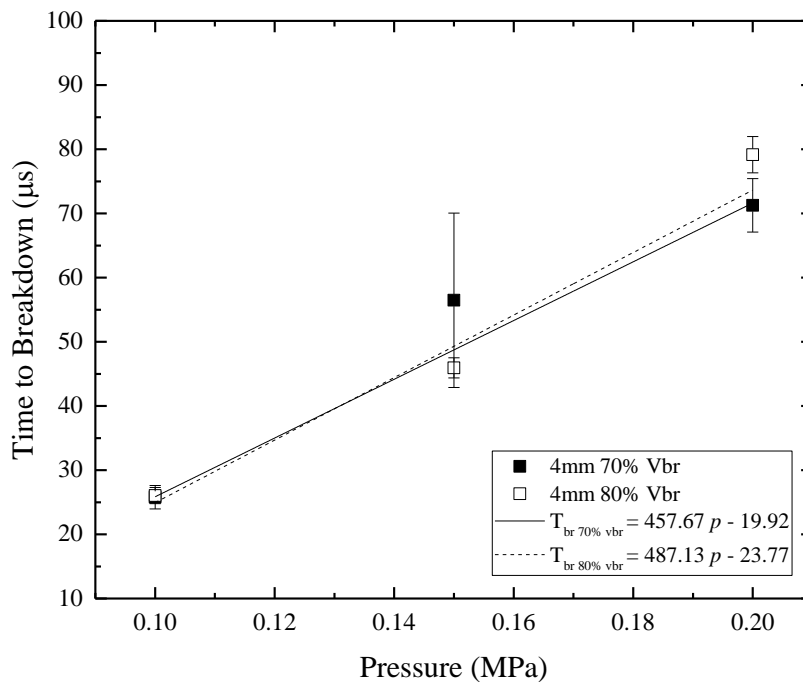
Figure 4-10. Average time to Breakdown vs pressure in an Air-filled switch with a 2mm inter-electrode gap length.

Figure 4-10 above shows the time to breakdown in a 2mm gap for an air-filled switch stressed with 70% of the self-breakdown voltage and for experiments conducted with the gap stressed with 80% of the self-breakdown voltage. It was observed that as the gas pressure within the switch increases, there is also an increase in the time between the initiation of breakdown and complete voltage collapse across the switch.

An interesting result from Figure 4-10 is that for a 2mm inter-electrode gap length in air-filled switch, when the switch gap was stressed with 80% of the self-breakdown voltage,

the time to breakdown was observed to be longer than the time to breakdown under the conditions where the switch was stressed with 70% of the self-breakdown voltage. It was found that when the gap was stressed with 80% of the self-breakdown voltage potential, the time to breakdown was 9% - 34% longer than the total time to breakdown when the gap was stressed with 70% of the self-breakdown voltage potential. This experimental observation may seem counter-intuitive, however it is discussed and explained with computational modelling of these results within Section 4.6 when the electric field strength is modelled within the switch and a plasma channel formed between the upper spherical electrode and the mid-plane triggering electrode is taken into consideration.

Once the work in a 2mm gap had been completed, the inter-electrode gap space was increased to 4mm gap length between the main spherical electrodes.



**Figure 4-11 Average time to Breakdown vs pressure in an Air-filled switch with a 4mm inter-electrode gap length.**

As is shown in Figure 4-11, in a 4mm inter-electrode gap space also shows the proportional increase in time to breakdown as gas pressure within the switch increases. The standard

deviation in the time to breakdown for both switches stressed with 70% or 80% of the self-breakdown voltage level appeared to decrease slightly as the pressure increased. The exception to this being the 4mm gap stressed with 70% of the self-breakdown voltage capability which provided the largest standard deviation (jitter).

The experiments conducted with a 4mm inter-electrode gap length, as also seen in the case of the 2mm inter-electrode gap space, show that the time to breakdown generally is longer when a DC stress level of 80% of the self-breakdown voltage level is applied across the main gap. An exception being at 0.15MPa, however this point also showed the largest standard deviation value and statistically can be considered to fall in-line with the other results. Experiments conducted for a 2mm gap filled with air at 0.15MPa pressure however also showed the largest standard deviation values. For 0.1MPa and 0.2MPa experiments conducted, the increase in time to breakdown for a gap stressed with 80% of the self-breakdown voltage potential were 1% and 11% longer than the time to breakdown observed in the experiments conducted with 70% of the self-breakdown voltage potential applied as DC stress across the gap.

The coefficients  $a$  and  $b$  derived for Equation 4.2 for each of the inter-electrode gap lengths and DC stress voltage combinations is presented within the Table 4-1 below.  $A$  and  $b$  together with their 95% confidence intervals, have been obtained using the best fit procedure in Origin Pro graphing software.

Table 4-1 provides a comparison of the coefficients  $a$  and  $b$  of Equation (4.2) which describe the dependence of the time to breakdown measured on the product  $pd$  of the inter-electrode gap length and the gas pressure within the switch.

**Table 4-1 linear fit coefficients for air-filled switch**

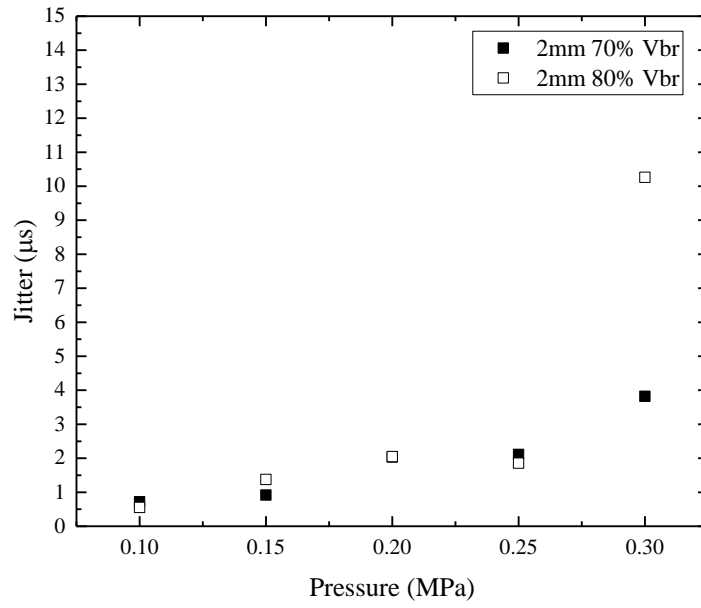
<b><u>AIR</u></b>	<b><u><math>a</math> (<math>\mu\text{s}/\text{MPa}</math>)</u></b>	<b><u><math>b</math> (<math>\mu\text{s}</math>)</u></b>
-------------------	--	---

<b>2mm 70% DC stress</b>	176.88	+0.80
95% confidence interval	100.54 - 253.22	-10.21 - (+) 11.81
<b>2mm 80% DC stress</b>	221.05	-2.51
95% confidence interval	180.80 – (+) 261.30	-7.73 - (+) 2.71
<b>4mm 70% DC stress</b>	457.67	-19.92
95% confidence interval	413.43-501.91	-25.34 – (-)14.50
<b>4mm 80% DC stress</b>	487.13	-23.77
95% confidence interval	346.79 – 627.47	-42.39 – (-)5.15

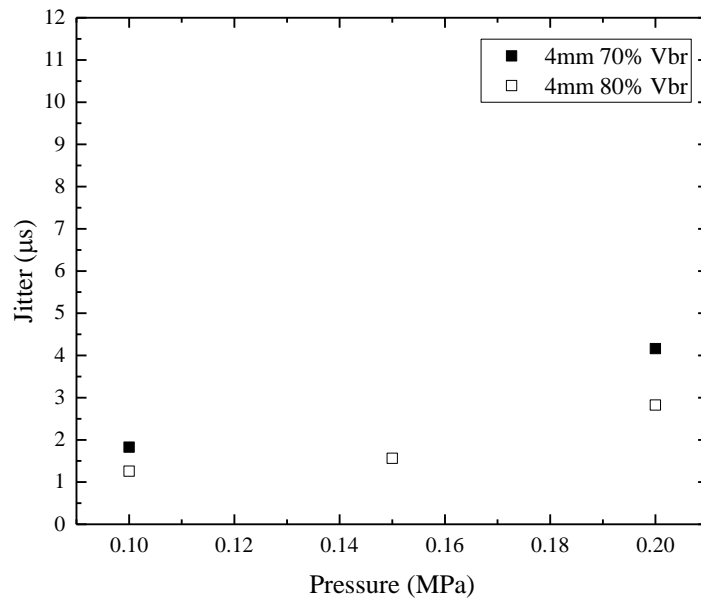
For both the 2mm inter-electrode gap length and the 4mm inter-electrode gap lengths it can be clearly seen that for the experimental conditions where the test cell is stressed with 80% of the self-breakdown voltage, the gradient of the linear fit is larger than the values obtained when the gap is stressed with 70% of the self-breakdown voltage, confirming that as  $pd$  increases, the switch when stressed with 80% of the self-breakdown voltage will continue to take longer to achieve breakdown than the switch which has been stressed with 70% of the self-breakdown voltage.

This is an intriguing result which again as discussed within Section 4.6 is due to the topology of the spark switch itself. The longer time to breakdown for gaps stressed with 80% of the self-breakdown is apparent from the steeper gradient of the fit applied to the experimental data.

Figure 4-12 shows the behaviour of the jitter as a function of the gas pressure within the switch.



(a)



(b)

Figure 4-12 Calculated Jitter for the field-distortion spark switch as a function of gas pressure for the air-filled switch when the main inter-electrode gap length is (a) 2mm and (b) 4mm and for both 70% and 80% of the self-breakdown voltage level applied across the main gap as a DC stress voltage.

As can be seen, for an air filled switch for both the 2mm and the 4mm inter-electrode gap lengths tested, the jitter was observed to increase as the gas pressure within the switch also increased overall within the switch.

Interestingly, for the lower pressures tested 0.1MPa-0.2MPa the jitter of the switch was calculated to be statistically the same as gas pressure increases. It is as the gas pressure is increased further (0.25MPa and above) that the jitter was calculated and observed to increase. This was observed within both the 2mm and 4mm inter-electrode gaps lengths.

For the air-filled switch, the role of the DC-stress voltage level on the jitter performance of the switch did not appear to play a statistically significant role on the jitter performance of the switch. Generally, it was observed that jitter in the air-filled switch was in the region of 4 $\mu$ s or less for the high voltage, trigger impulses applied to the mid-plane electrode with a rate of voltage rise of 0.45kV/ $\mu$ s.

#### **4.4.2 Time to Breakdown for an N<sub>2</sub> filled switch**

This section presents the results of the experiments conducted for both the 2mm and 4mm inter-electrode gap lengths within the main switch body when filled with N<sub>2</sub> gas. The N<sub>2</sub> gas used (BOC Ltd, 99.9% purity) is from the same cylinder which had been used in previous self-breakdown experimental work. Figure 4-13 presents the time to breakdown results for the 2mm inter-electrode main gap length within the switch as a function of the gas pressure.

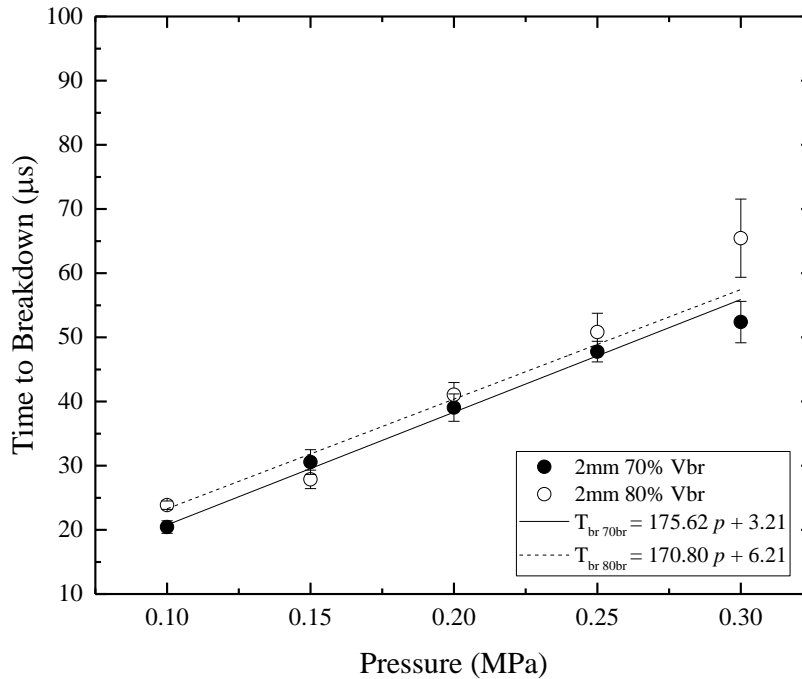


**Figure 4-13 Average time to Breakdown vs pressure in an N<sub>2</sub>-filled switch with a 2mm inter-electrode gap length.**

Within Figure 4-13, it can be seen that the time to breakdown of the switch when filled with nitrogen was observed to increase linearly as the gas pressure within the switch increases and the standard deviation in calculated time to breakdown values also was observed to increase when observed as a function of gas pressure.

Within the 2mm nitrogen-filled gap switch, it was also observed that for all bar one of the pressures tested (0.15MPa) the time to breakdown in a switch stressed with 80% of the self-breakdown voltage potential was longer than the time to breakdown observed in experiments conducted with 70% of the self-breakdown voltage potential applied as a DC stress voltage.

It was found that by increasing the DC stress applied across the gap from 70% to 80% of the self-breakdown voltage level the total time to breakdown of the switch was somewhere in the region of 5% - 25% longer than the total time to breakdown observed when the gap had been stressed with 70% of the self-breakdown voltage potential.

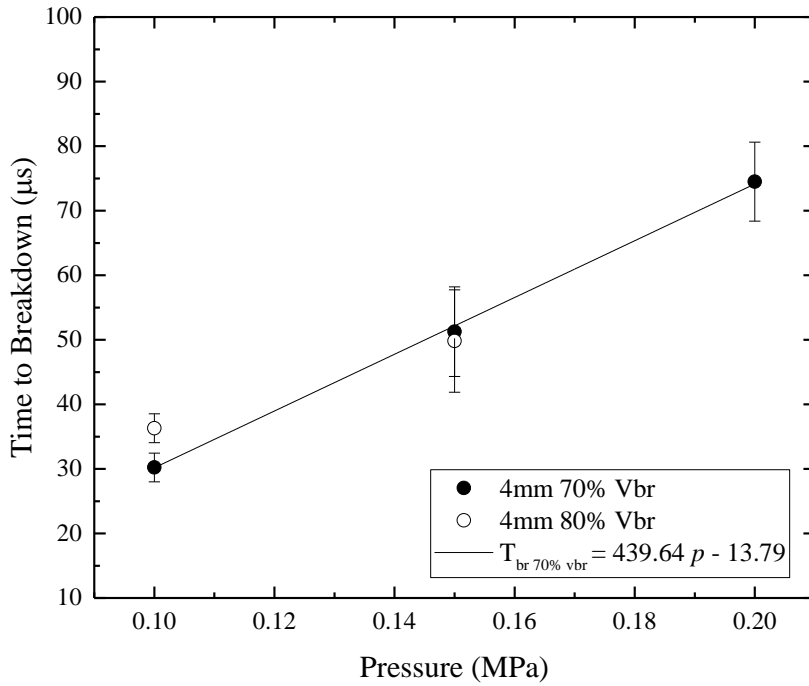


**Figure 4-14 Average time to Breakdown vs pressure in an N<sub>2</sub>-filled switch with a 4mm inter-electrode gap length.**

As Figure 4-14 shows, within the 4mm N<sub>2</sub> filled inter-electrode gap, the increase in time to breakdown of the switch is also linear with pressure.

When stressed with 80% of the self-breakdown voltage potential, no breakdown events were observed to occur in the switch for gas pressures of 0.2MPa or above. This means that an accurate comparison of the performance of the time to breakdown characteristics of the switch when stressed with either 70% of the self-breakdown voltage or 80% of the self-breakdown voltage could not be conducted for this combination of 4mm inter-electrode gap length, DC stress levels and gas pressures in a N<sub>2</sub>-filled switch.

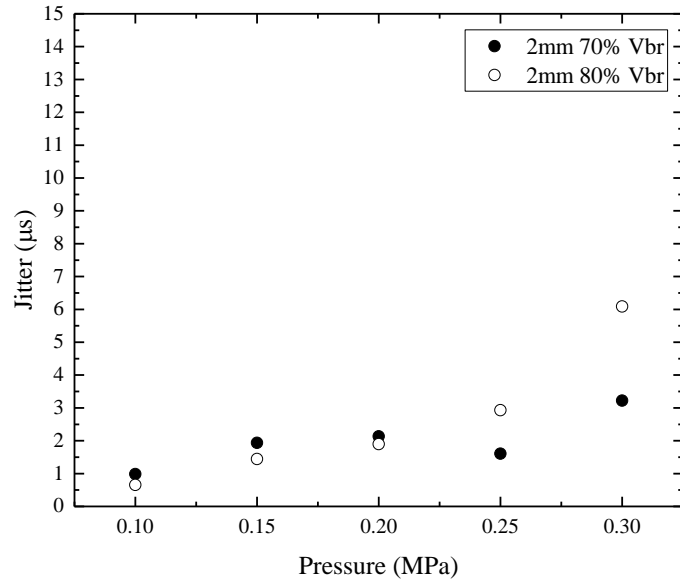
A linear fit was applied to the experimental data where breakdown events were observed to occur for at least three different gas pressures within the switch. The coefficients of the linear fittings of Equation (4.2) for a N<sub>2</sub> filled switch are given in Table 4-2:

**Table 4-2 linear fit coefficients for the N<sub>2</sub>-filled switch**

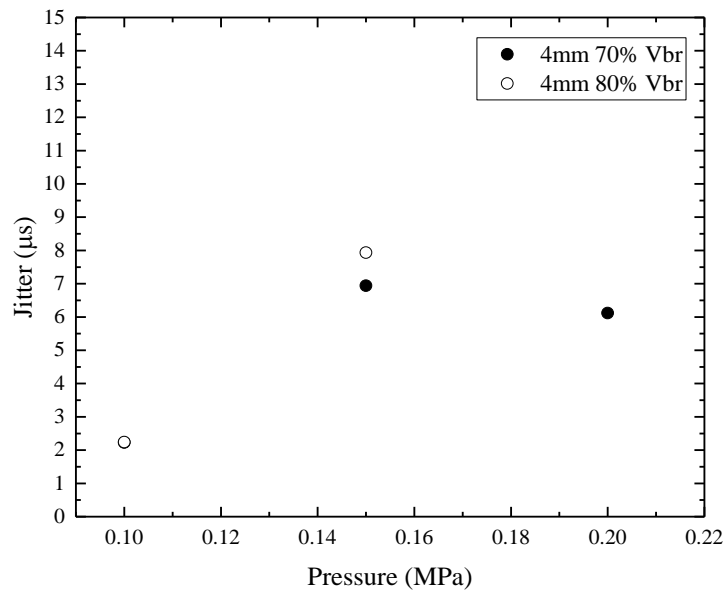
<u>Nitrogen</u>	<u>a (μs/MPa)</u>	<u>b (μs)</u>
<b>2mm 70% DC stress</b>	175.62	3.21
95% confidence interval	161.59 – 189.65	0.81 – 5.61
<b>2mm 80% DC stress</b>	170.80	6.21
95% confidence interval	129.60 – 212.00	0.84 – 11.58
<b>4mm 70% DC stress</b>	439.67	-13.79
95% confidence interval	424.77 – 454.57	-15.57 – (-)12.01

The coefficients of the linear fit applied to experimental data of the N<sub>2</sub>-filled switch suggest that for the gas pressures tested, the time to breakdown measurements in a 2mm gap length stressed with 80% of the self-breakdown voltage potential would again be longer than those under conditions where 70% of the self-breakdown voltage potential is applied as DC stress voltage. The coefficients suggest that as the gas pressure increases beyond the scope of this project in a switch filled with N<sub>2</sub> gas, the 70% DC stressed switch may take longer to breakdown than the 80% of self-breakdown voltage stressed switch. However, this is not a reasonable deduction which could be made from the experimental data and the pressures at which this may occur are above those which were able to be used within the scope of this research project.

Another key breakdown characteristic of the nitrogen-filled switch to be considered is the jitter of the switch. Figure 4-15 presents the jitter as a function of the gas pressure within the switch.



(a)



(b)

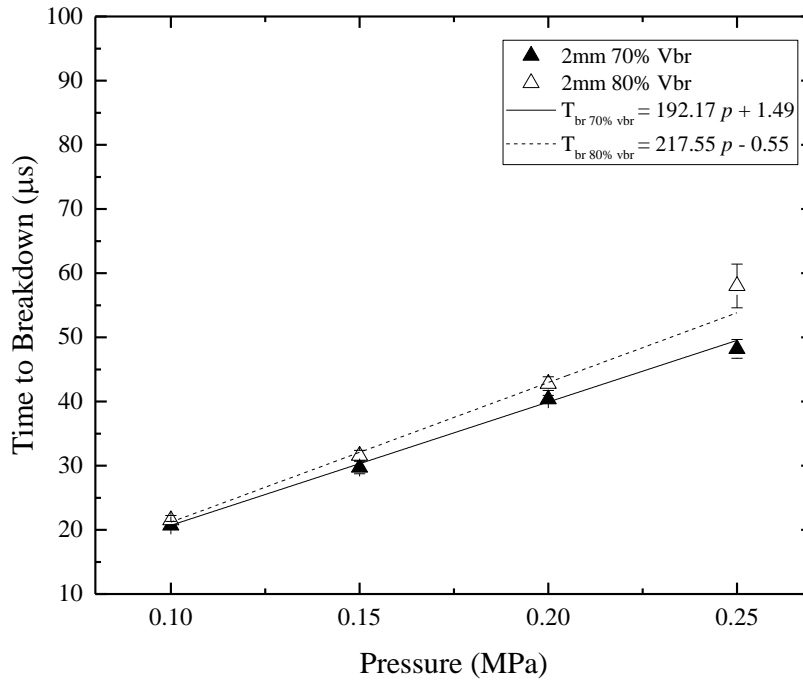
Figure 4-15 Calculated Jitter for the field-distortion spark switch as a function of gas pressure for the  $N_2$ -filled switch when the main inter-electrode gap length is (a) 2mm and (b) 4mm and for both 70% and 80% of the self-breakdown voltage level applied across the main gap as a DC stress voltage.

Figure 4-15 shows the jitter performance of the switch when filled with nitrogen as a function of the gas pressure within the switch. It is shown that in the nitrogen-filled switch as was observed in the air-filled switch, the jitter increases as gas pressure increases although in the switch with the 2mm inter-electrode gap, for the lower gas pressures (0.1MPa-0.2MPa) the jitter remains largely the same  $\sim 2\mu\text{s}$ . For the 2mm  $\text{N}_2$ -filled inter-electrode gap, the jitter remains  $3\mu\text{s}$  or less however when the inter-electrode gap space is increased to 4mm, the jitter of the switch increases dramatically to around  $8\mu\text{s}$  for the same gas pressures.

#### **4.4.3 Time to Breakdown for a switch filled with a 60% /40% $\text{N}_2/\text{O}_2$ mixture.**

A mixture of 60%/40%  $\text{N}_2/\text{O}_2$  was the next gas tested in the field-distortion switch to investigate the time to breakdown characteristics. Again this gas was chosen as the mixture containing 40% oxygen is approximately double the concentration of oxygen than in air. This allows for a comparison of increasing quantities of electronegative oxygen to electropositive nitrogen gas and the effect that this has on the breakdown characteristics, specifically the time to breakdown characteristics of a field distortion gap stressed with different levels of the self-breakdown voltage potential.

As shown in Figure 4-16, for a 2mm inter-electrode gap space filled with the 60%/40% oxygen/nitrogen gas mixture a linear increase in the time to breakdown as a function of increasing gas pressure was observed which is in agreement with both the air-filled switch and the switch filled with nitrogen (99.9% purity) gas.



**Figure 4-16 Average time to Breakdown vs pressure in a switch filled with 60%/40% N<sub>2</sub>/O<sub>2</sub> gas mixture with a 2mm inter-electrode gap length.**

It was observed that for this particular gas mixture, when the main inter-electrode gap is stressed with 80% of the self-breakdown voltage potential the time to breakdown was measured to be longer than that using 70% of the self-breakdown voltage. The increase in time to breakdown was calculated to be between 3%-20% longer in the experiments conducted with 80% of the self-breakdown voltage DC stress than in the 70% self-breakdown voltage experiments and was observed to increase as gas-pressure increased.

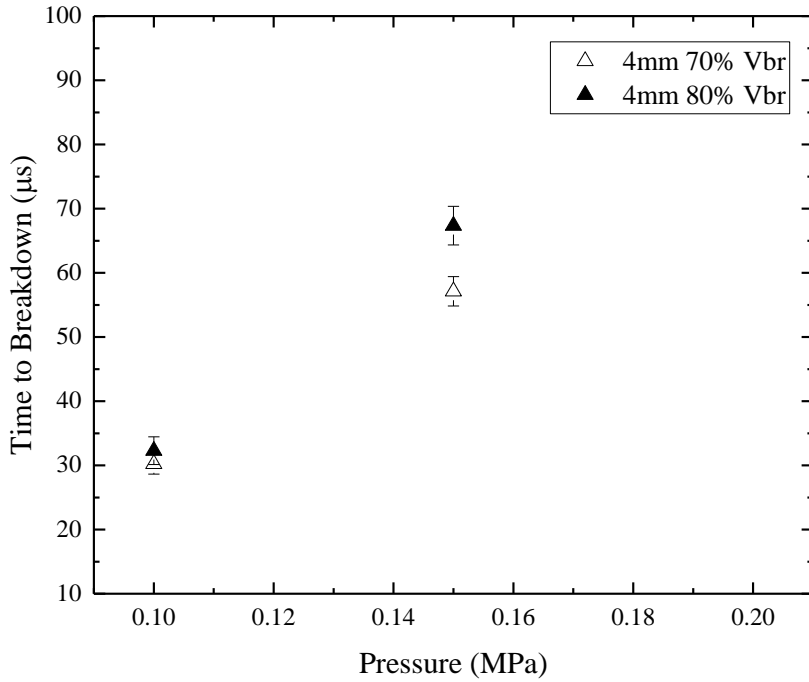


**Figure 4-17 Average time to Breakdown vs pressure in a switch filled with 60%/40% N<sub>2</sub>/O<sub>2</sub> gas mixture with a 4mm inter-electrode gap length.**

Within Figure 4-17, the average time to breakdown for the conditions where a 4mm inter-electrode gap was filled with the mixture of gas comprised of 60%/40% N<sub>2</sub>/O<sub>2</sub> are presented. It was observed that for 0.1MPa and 0.15MPa pressure within the switch, the time to breakdown was observed to increase as gas pressure increases in the expected manner as had been observed for previous gases and in the 2mm gap and for previous gases tested.

As the gas pressure within the switch for the 60%/40% N<sub>2</sub>/O<sub>2</sub> mixture was increased to 0.2MPa or above, when applying a voltage impulse with a voltage rise rate of 0.45kV/μs to the mid-plane electrode, no breakdown events were observed across the switch. This was confirmed by monitoring both the voltage across the switch, no collapse of voltage across the main inter-electrode gap occurred, and by monitoring of the current in the switch where there was no current flow observed after the trigger impulse had been applied indicating that no breakdown event had occurred.

Of the results obtained i.e. the time to breakdown measured in the switch at 0.1MPa and 0.15MPa, as had been shown in the previous gases, the higher level of DC stress voltage (80% of the self-breakdown voltage) applied across the gap has been shown to result in a longer time to breakdown of the switch. For 0.1MPa and 0.15MPa gas pressure within the switch, the time to breakdown was calculated to be 7%-18% longer for the higher DC voltage stress level applied across the gap due to the design topology of the switch as is later discussed fully within Section 4.6.

A linear fit with Equation (4.2) has been applied to the experimental data obtained for the 2mm inter-electrode gap filled with the 60%/40% N<sub>2</sub>/O<sub>2</sub> mixture, the fitting was unable to be applied to the data obtained for the 4mm inter-electrode gap space experimental conditions due to a small number of pressures where breakdown could be initiated. The coefficients of the fitting lines which were able to be fit to experimental data are provided for the 60%/40% N<sub>2</sub>/O<sub>2</sub> gas mixture in Table 4-3.

**Table 4-3 Linear fit coefficients for the switch filled with a mix of 60%/40% N<sub>2</sub>/O<sub>2</sub>**

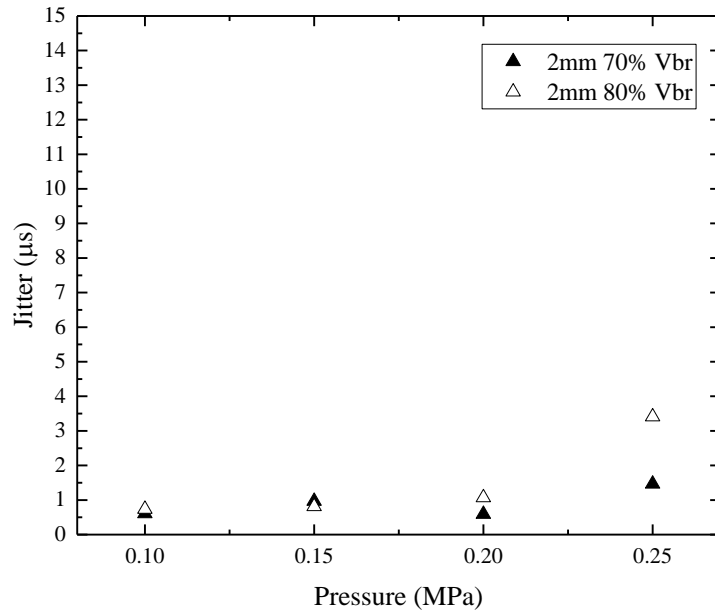
<b><u>60%/40% Nitrogen/Oxygen</u></b>	<b><u>a (μs/MPa)</u></b>	<b><u>b (μs)</u></b>
<b>2mm 70% DC stress</b>	192.17	1.49
95% confidence interval	180.46 - 203.88	-0.45 – 3.43
<b>2mm 80% DC stress</b>	217.55	-0.55
95% confidence interval	197.15 – 237.96	-3.54 – 2.44
<b>4mm 70% DC stress</b>	N/A	N/A
<b>4mm 80% DC stress</b>	N/A	N/A

Analysis of the coefficients of the linear fit applied to the experimental data shows for the 2mm inter-electrode gap that clearly a DC stress level of 80% of the self-breakdown voltage level resulted in time to breakdown measurements that were observed to increase as the

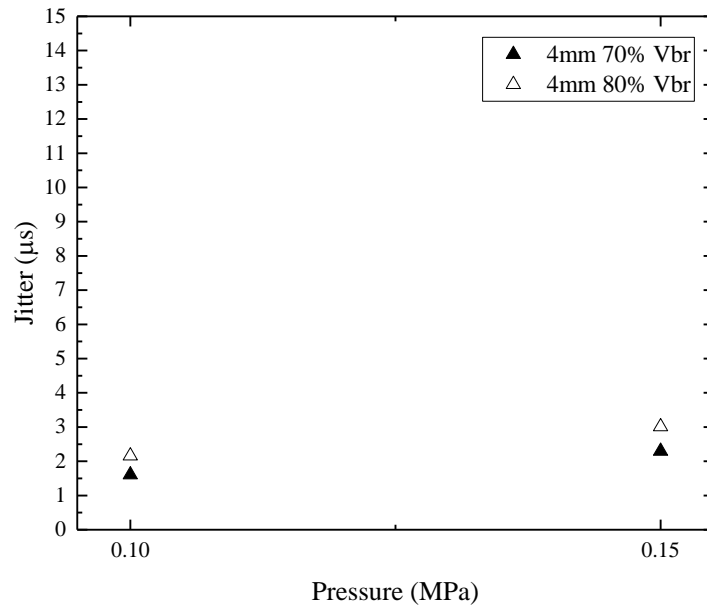
gas pressure within the switch further increased. The rate of increase of the time to breakdown measurements, evaluated by the magnitude of at a steeper gradient than the DC stress conditions of 70% of the self-breakdown voltage.

As for the 4mm inter-electrode gap distance, it is clear that it is not possible to apply linear fit lines to the experimental data obtained. It does appear that between 0.1MPa and 0.15MPa gas pressure, the time to breakdown increases as expected and the experimental conditions where 80% of the self-breakdown voltage is applied as a stress across the gap results in an increase in the time to breakdown for the same gas pressure when compared to the gap stressed with 70% of the self-breakdown voltage.

The jitter of the switch filled with the 60%/40% N<sub>2</sub>/O<sub>2</sub> mixture is presented as a function of gas pressure in Figure 4-18.



(a)



(b)

**Figure 4-18** Calculated Jitter for the field-distortion spark switch as a function of gas pressure for the 60%/40% N<sub>2</sub>/O<sub>2</sub>-filled switch when the main inter-electrode gap length is (a) 2mm and (b) 4mm and for both 70% and 80% of the self-breakdown voltage level applied across the main gap as a DC stress voltage.

In the self-breakdown experiments conducted and presented within Chapter 3, the 60%/40% N<sub>2</sub>/O<sub>2</sub> mixture had been shown to be the most stable gas in terms of the smallest spread in self-breakdown voltage measured. As can be seen in Figure 4-18 above, for both the 2mm 4-17(a) and 4mm inter electrode gap in Figure 4-18(b), the jitter obtained for this gas mixture is low ( $\leq 1\mu\text{s}$  for 0.1MPa-0.2MPa in the 2mm inter-electrode gap space) and although also observed to increase as gas pressure increases as was observed with other gases tested, still generally remains low for each combination of inter-electrode gap length and gas pressure combination tested, typically  $\leq 4\mu\text{s}$ .

#### 4.4.4 Time to Breakdown for a switch filled with a 90% /10% Ar/O<sub>2</sub> mix.

Within this section, the results of the time to breakdown analysis of results of the field-distortion spark gap switch filled with the gas mixture comprised of 90%/10% Ar/O<sub>2</sub> are presented.

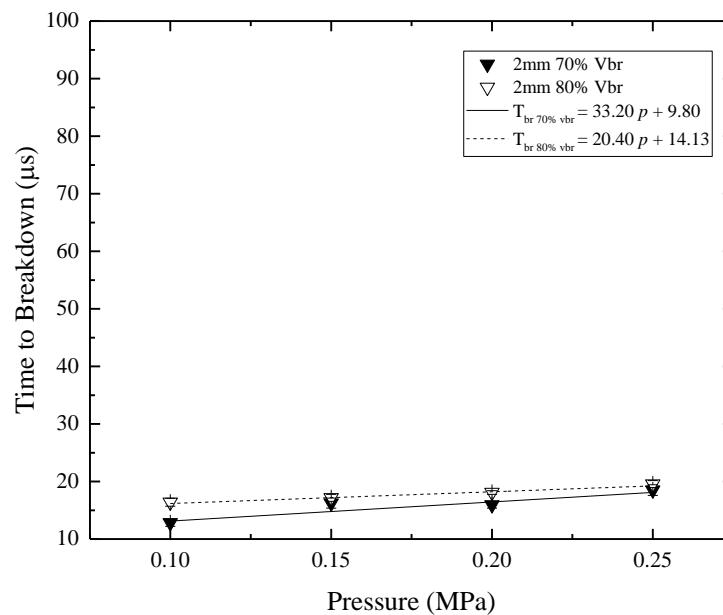


Figure 4-19 Average time to Breakdown vs pressure in a switch filled with 90%/10% Ar/O<sub>2</sub> gas mixture with a 2mm inter-electrode gap length.

The time to breakdown measured for the 2mm gap field-distortion switch filled with the 90%/10% Ar/O<sub>2</sub> mixture is shown in Figure 4-19. A small increase in the time to breakdown measured is observed as the gas pressure was increased from 0.1MPa to 0.25MPa, however on further increasing the gas pressure within the switch to 0.25MPa, the time to breakdown was observed to have significantly increased for both levels of applied DC stress voltage.

In line with the results previously presented within this chapter for the other gases tested, when the switch test-cell was filled with the mixture of 90%/10% Ar/O<sub>2</sub>, it was observed that the switch stressed with 80% of the self-breakdown voltage potential would take longer to reach complete breakdown than the switch which was stressed with 70% of the self-breakdown voltage potential e.g. in the experiments conducted with 80% of the self-breakdown voltage applied as a DC stress voltage, the time to breakdown of the switch was found to be 6% - 28% longer than the time to breakdown observed for the same gas pressure and the same inter-electrode gap space stressed with 70% of the self-breakdown voltage due to the design of the switch encouraging breakdown to initiate between the mid-plane electrode and the upper spherical electrode where the DC stress voltage is applied before complete breakdown across the main gap of the switch.

The increase in time to breakdown as the gas pressure within the switch increases appears linear as shown in Figure 4-19 and thus a linear fitting with Equation (4.2) was applied to the experimental data obtained.

Figure 4-20 shows the results of the increased inter-electrode gap length to 4mm when filled with the 90%/10% Ar/O<sub>2</sub> gas mixture.

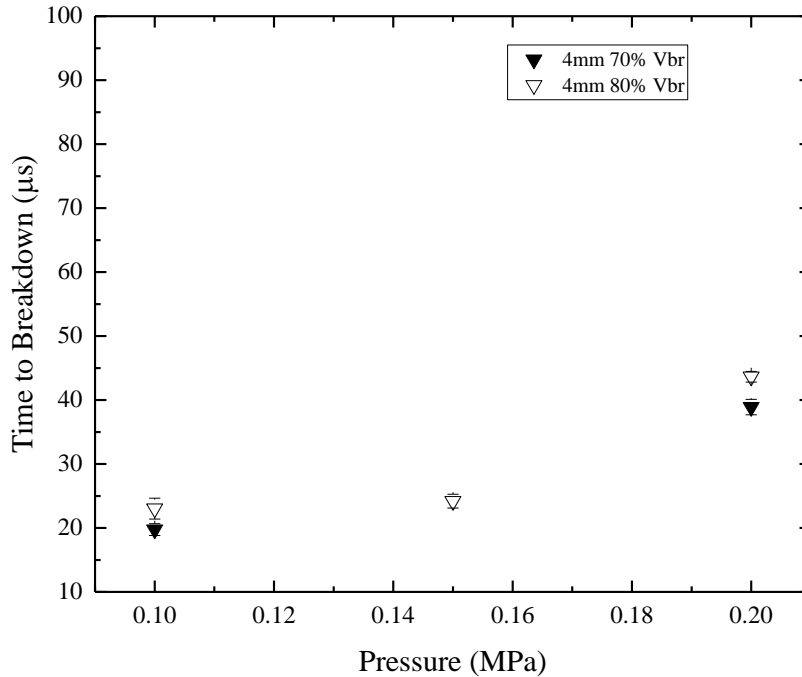


**Figure 4-20 Average time to Breakdown vs pressure in a switch filled with 90%/10% Ar/O<sub>2</sub> gas mixture with a 2mm inter-electrode gap length.**

An increase in time to breakdown was observed between 0.1MPa and 0.2MPa gas pressure although at the intermediate 0.15MPa pressure tested, the difference in time to breakdown was considered to be statistically the same as the time to breakdown calculated for 0.1MPa gas pressure within the switch.

For the switch filled with 90%/10% Ar/O<sub>2</sub> mixture and a 4mm inter-electrode gap length it is again shown that under experimental conditions when the main inter-electrode gap is stressed with 80% of the self-breakdown voltage, the time taken between the initiation of the voltage impulse and the complete collapse of the voltage across the gap is between 12% and 20% longer than when the gap is stressed with 70% of the self-breakdown voltage.

As applied to other gases within this chapter, the linear fit with Equation (4.2) was applied to the experimental data allows for a comparison of the coefficients of the experimental data for different DC stress levels applied across the switch.

Where measured time to breakdown increased linearly as the pressure within the switch body also increased, the linear fit with Equation (4.2) was applied and the coefficients  $a$  and  $b$  are given in Table 4-4.

**Table 4-4 linear fit coefficients for the switch filled with the 90%/10% argon/oxygen mix**

<b><u>90%/10% Argon/Oxygen</u></b>	<b><u><math>a</math> (<math>\mu\text{s}/\text{MPa}</math>)</u></b>	<b><u><math>b</math> (<math>\mu\text{s}</math>)</u></b>
<b><i>2mm 70% DC stress</i></b>	33.20	9.80
95% confidence interval	17.30 – 49.10	7.00 – 12.60
<b><i>2mm 80% DC stress</i></b>	20.40	14.13
95% confidence interval	17.44 – 27.36	13.18 – 15.08
<b><i>4mm 70% DC stress</i></b>	N/A	N/A
95% confidence interval	N/A	N/A
<b><i>4mm 80% DC stress</i></b>	N/A	N/A
95% confidence interval	N/A	N/A

Table 4-4 show that for the 2mm inter-electrode gap, at increased pressure, the steepest gradient of the fitting line is on the data from the 70% DC stress suggesting that as pressure increases, the time to breakdown may be longer for this level of DC stress. This however is not backed up by experimental results obtained and the increased pressures again would be out with the scope of this research project.

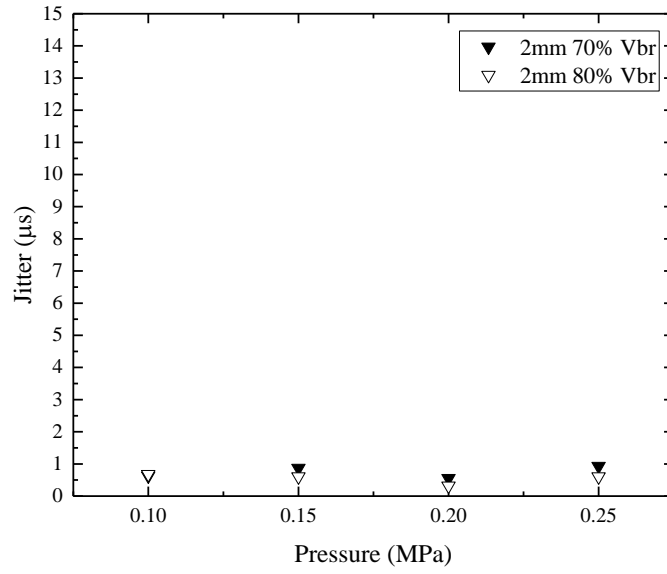
No linear fit was applied to the time to breakdown results for the 4mm inter-electrode gap space as from Figure 4-20, the time to breakdown does not appear to increase linearly with pressure.

In the self-breakdown switch results, the 90%/10% Ar/O<sub>2</sub> mixture showed the lowest voltage hold-off capabilities and the spread of the self-breakdown voltages were one of the

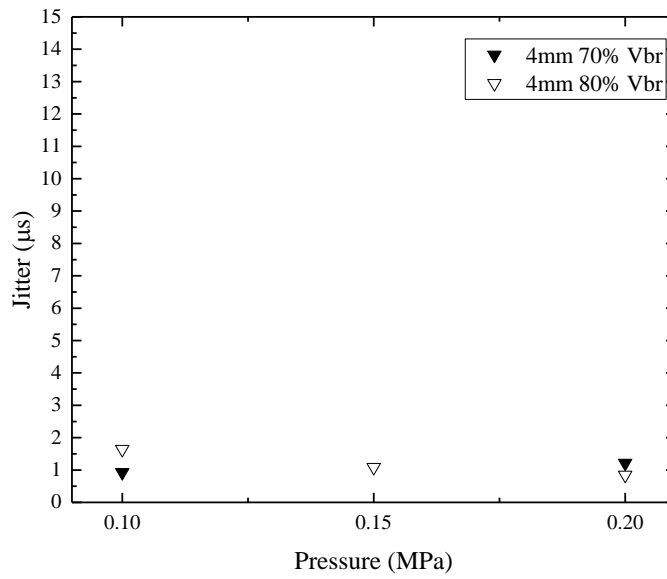
highest leading it to be deemed one of the least reliable gases of those tested for use in self-breakdown switches.

These results in the triggered regime show that although the time to breakdown is generally short for the 90%/10% Ar/O<sub>2</sub> mixture, there is very little variation for short inter-electrode gap lengths in the time to breakdown as gas pressure changes. This suggests that specific applications that may make use of short gaps, a range of pressures but require similar time to breakdown as gas pressure in the system changes, this gas mixture may be considered.

The jitter of the switch filled with 90%/10% Ar/O<sub>2</sub> is difficult to determine from the plotted Figures above, Figure 4-21(a) and (b) presents the jitter performance of both the 2mm and the 4mm inter-electrode gap lengths respectively as a function of gas pressure within the test cell.



(a)



(b)

Figure 4-21 Calculated Jitter for the field-distortion spark switch as a function of gas pressure for the 90%/10% Ar/O<sub>2</sub>-filled switch when the main inter-electrode gap length is (a) 2mm and (b) 4mm and for both 70% and 80% of the self-breakdown voltage level applied across the main gap as a DC stress voltage.

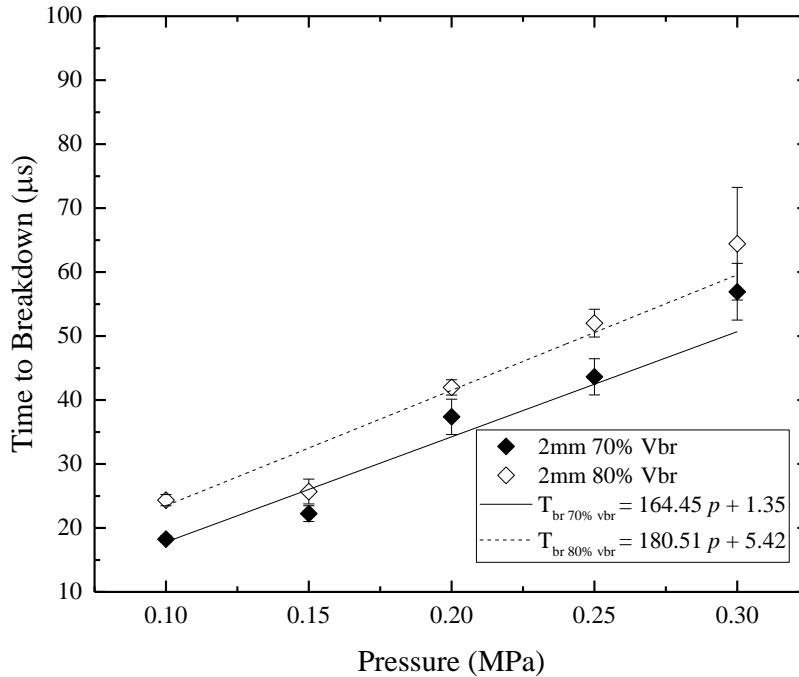
In the 2mm inter-electrode gap length switch, the jitter performance can clearly be seen to be  $<1\mu\text{s}$  for all pressures up to up to 0.25MPa and remains statistically the same regardless of an increase in pressure.

For the experimental conditions of a 4mm inter-electrode gap length, the results are less cohesive and do not give a defined trend on the jitter performance for this gas mixture under the triggered conditions described. In a 4mm inter-electrode gap length when stressed with 70% of the self-breakdown voltage, the jitter was observed to increase as the gas pressure increased. Conversely, under experimental conditions where a 4mm inter-electrode gap is stressed with 80% of the self-breakdown voltage, the jitter was observed to decrease as the gas pressure increased.

#### **4.4.5 Time to Breakdown for a switch filled with CO<sub>2</sub>**

This section contains the experimental results of the experimental investigation into the time to breakdown characteristics when the field-distortion spark gap switch was filled with CO<sub>2</sub>. In the self-breakdown results CO<sub>2</sub> had been shown at low pressures to provide slightly higher breakdown voltage capabilities than air, nitrogen and the 60%/40% N<sub>2</sub>/O<sub>2</sub> mixture. However it was also shown to have the largest spread in breakdown voltages observed and thus deemed less reliable for use in self-breakdown switching. In a triggered switching regime however, CO<sub>2</sub> has previously been used in industrial applications [102] .

The field-distortion switch was filled with CO<sub>2</sub> and the time to breakdown measurements as a function of the gas pressure are presented within Figure 4-22.



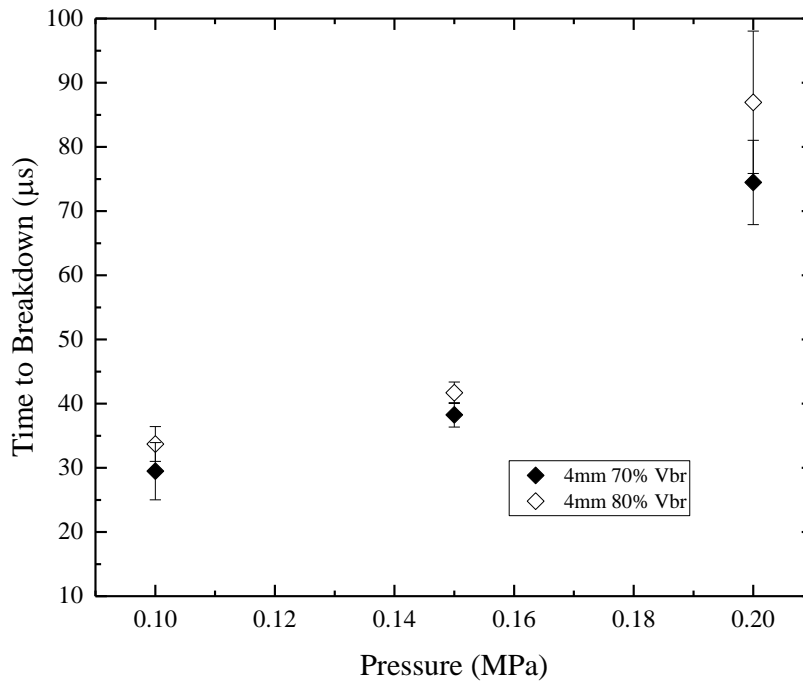
**Figure 4-22 Average time to Breakdown vs pressure in a switch filled with CO<sub>2</sub> with a 2mm inter-electrode gap length.**

Figure 4-22 shows that, when breakdown increases in a linear fashion as the gas pressure within the switch also increases. It can also be seen from Figure 4-22 that the jitter appears to increase as the gas pressure increases and this is discussed after Figure 4-24.

Another result of note is the agreement of these CO<sub>2</sub> results showing that the experiments conducted with the different levels of DC stress applied across the main gap of the switch appear to show that when the main inter-electrode gap is stressed with 80% of the self-breakdown voltage potential, the time it takes for complete voltage collapse across the gap to appear is 12%-33% longer than the time taken for complete closure of the switch when 70% of the self-breakdown voltage is applied across the gap.

The linear fit with Equation (4.2) has been applied to experimentally obtained data and is also shown on Figure 4-22. The coefficients of the fit Equation are in Table 4-5 for comparison.

Figure 4-23 presents the average time to breakdown measured in a 4mm inter-electrode gap length for a CO<sub>2</sub>-filled switch.



**Figure 4-23 Average time to Breakdown vs pressure in a switch filled with CO<sub>2</sub> with a 4mm inter-electrode gap length.**

It can be seen that although there is an increase in the time to breakdown as the gas pressure within the switch increases, the behaviour is non-linear and at 0.2MPa pressure, the highest pressure at which breakdown was observed the standard deviation of the time to breakdown measurements is large.

It can also be seen, however, that in the CO<sub>2</sub> filled switch with a 4mm inter-electrode gap-length, the time to breakdown measured in a gap stressed with 80% of the self-breakdown voltage is ~9%-16% longer than the measured time to breakdown when the gap is stressed with 70% of the self-breakdown voltage.

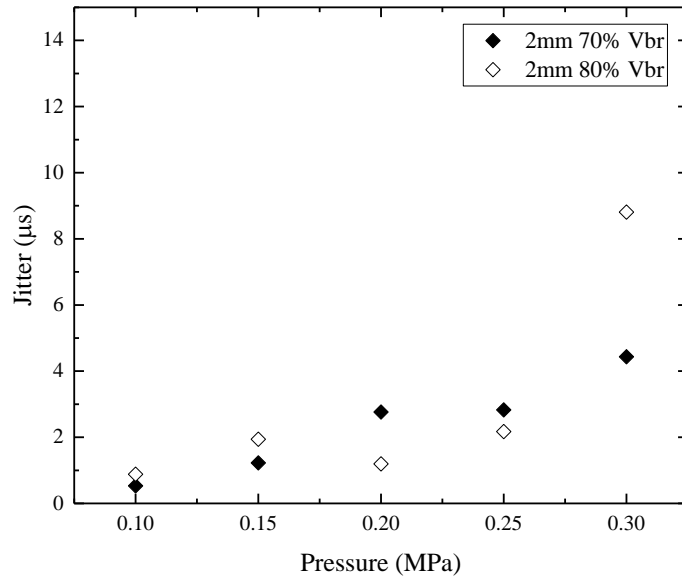
Where the measured time to breakdown increased linearly as the pressure within the switch body increased (the 2mm inter-electrode gap length conditions), the linear fit with Equation (4.2) was applied and the coefficients of Equation are given in Table 4-5.

Table 4-5 linear fit coefficients for the CO<sub>2</sub>-filled switch

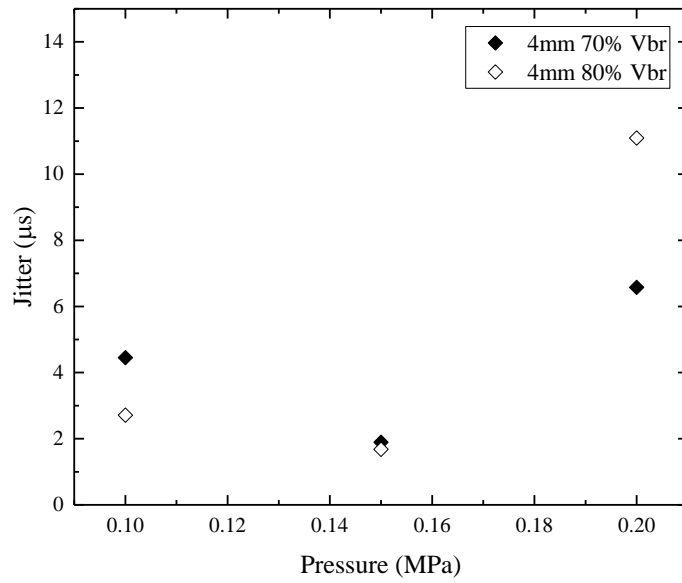
<u>Carbon Dioxide</u>	<u>a (μs/MPa)</u>	<u>b (μs)</u>
<b>2mm 70% DC stress</b>	164.45	1.35
95% confidence interval	119.66 – 209.24	-4.14 – 6.84
<b>2mm 80% DC stress</b>	180.51	5.42
95% confidence interval	137.30 – 223.72	-1.34 – 12.18
<b>4mm 70% DC stress</b>	N/A	N/A
<b>4mm 80% DC stress</b>	N/A	N/A

Table 4-5 provides the linear fit coefficients for the 2mm inter-electrode gap length when the gap space is filled with CO<sub>2</sub> gas. The 'a' coefficient which determines the sensitivity to change in pressure is larger for the condition of 80% of the self-breakdown voltage applied as the DC stress across the gap than for 70% of the self-breakdown voltage. This confirms that even at increased pressures beyond the scope of this investigation, the time to breakdown measured will be increased when the inter-electrode gap length is stressed with a higher level of voltage. This is further discussed in section 4.6.

The jitter of the CO<sub>2</sub>-filled switch is of key importance in this analysis as in the self-breakdown investigation. CO<sub>2</sub> had shown the largest value of breakdown voltage spread of all the gases tested. Figure 4-24 plots the jitter of the CO<sub>2</sub>-filled switch as a function of the gas pressure within the switch.



(a)



(b)

Figure 4-24 Calculated Jitter for the field-distortion spark switch as a function of gas pressure for the CO<sub>2</sub>-filled switch when the main inter-electrode gap length is (a) 2mm and (b) 4mm and for both 70% and 80% of the self-breakdown voltage level applied across the main gap as a DC stress voltage.

In agreement with the other gases tested and presented within this investigation, the jitter of the CO<sub>2</sub>-filled switch was calculated and observed to generally increase overall as the pressure of the gas within the switch also increased.

The jitter in the 2mm gap was typically less than 4μs while in the 4mm inter-electrode gap the jitter was calculated to be < 10μs. The values of jitter calculated for CO<sub>2</sub> are slightly above those calculated for the other gases tested within this investigation however, under triggered conditions, the difference in jitter between CO<sub>2</sub> and the other gases tested is not as significant as the difference in the spread of the breakdown voltage which was observed in self-breakdown investigations, suggesting that under triggered conditions CO<sub>2</sub> performs more reliably than it does under self-break conditions.

#### **4.4.6 Time to Breakdown for a switch filled with SF<sub>6</sub>**

In the interest of a complete dataset comparing all six gases which had been tested in the self-breakdown switch topology, the field-distortion switch was also filled with all six of the gases which had previously been used within experimental investigations.

The nature of SF<sub>6</sub> and its high dielectric strength and thus its higher breakdown voltage means that under the exact same experimental test conditions with the same experimental equipment as described above, no breakdown events were observed to occur.

This means that for a field-distortion spark-gap switch that is triggered by a trigger generator with a relatively long rise-time of the voltage impulse (0.45kV/μs), no direct comparisons can be made with SF<sub>6</sub> under identical experimental conditions.

## 4.5 Statistical Analysis

This section gives a brief side-by-side comparison of the measured time to breakdown in the triggered switch stressed when filled with all five gases tested (air, N<sub>2</sub>, 60%/40% N<sub>2</sub>/O<sub>2</sub>, 90%/10% Ar/O<sub>2</sub> and CO<sub>2</sub>) under DC stress and when a voltage impulse of 0.45kV/μs is applied to the mid-plane trigger electrode. The most appropriate way found to compare the gases in this manner was to take the coefficient 'a' from the linear fit applied to the experimental data obtained from the 2mm inter-electrode gap length tests conducted which is a measure of how sensitive the measured time to breakdown will be to any change in gas pressure within the switch. Figure 4-25 presents the value 'a', in Equation 4.2, the coefficient determining the gradient of the fitting line applied to the data set for experimental conditions of both 70% and 80% of the self-breakdown voltage applied across the gap.

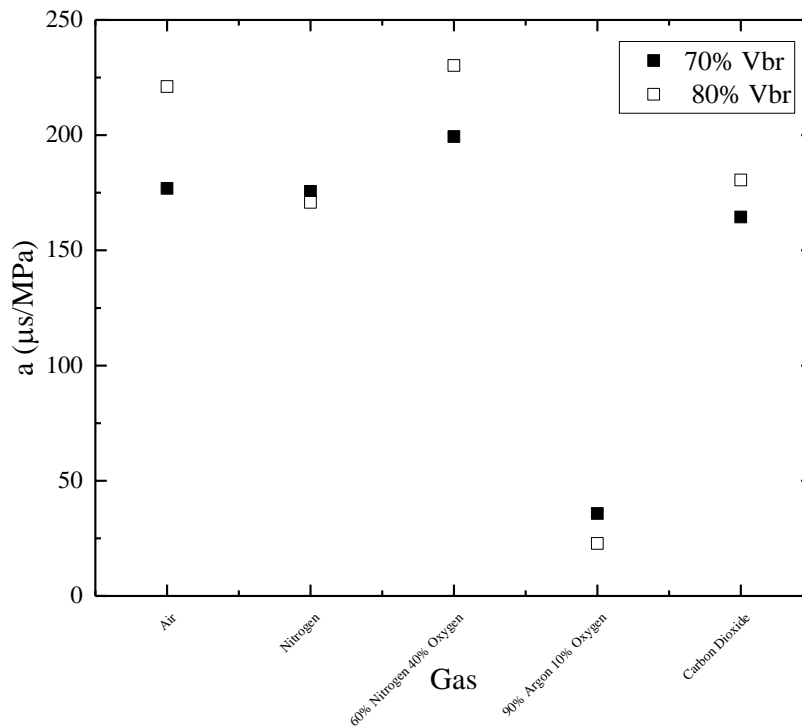


Figure 4-25. A comparison of the Linear fit coefficient 'a' (Eq. 4.2) for the 2mm inter electrode gap space which determines the sensitivity of the time to breakdown of each of the gases to any change in gas pressure within the switch for both 70% and 80% of the self-breakdown voltage applied as a DC stress across the main inter-electrode gap.

Figure 4-25 shows that under the application of 80% of the self-breakdown voltage across the switch gap in an air filled gap, a gap filled with CO<sub>2</sub> and a gap filled with a mixture of 60%/40% N<sub>2</sub>/O<sub>2</sub> results in a larger value of 'a' which can be considered to correspond to a longer time to breakdown since 'a' describes the sensitivity to changing pressure. For the N<sub>2</sub>-filled switch, the application of 70% or 80% of the self-breakdown voltage as the DC stress across the gap length provided similar values for 'a' (175.62 and 170.80 respectively).

The switch filled with the mixture of 90%/10% Ar/O<sub>2</sub> was observed to be the least sensitive to changes in pressure, i.e. the smallest 'a' values however this is more due to the far lower breakdown voltages achievable with the mixture of Ar/O<sub>2</sub>. It was also found that under experimental conditions, as discussed previously within Section 4.3.4, the switch stressed with 70% of the self-breakdown voltage at higher pressures than those in the scope of this project may take longer to achieve breakdown than the gap stressed with 80% of the self-breakdown voltage. This result is due to the nature of the Ar/O<sub>2</sub> mixture and has consistently been found and shown throughout Chapter 3 and 4 to have significantly different performance in terms of switching properties than any of the other gases tested.

An interesting result shown within Figure 4-25 is that, despite providing slightly higher self-breakdown voltages than the other gases tested (excluding SF<sub>6</sub>) in Chapter 3 and within Chapter 4 when determining levels of DC stress voltage, the time to breakdown in a CO<sub>2</sub> – filled was observed to be in line with the time to breakdown measured in air, N<sub>2</sub> or the 60%/40% N<sub>2</sub>/O<sub>2</sub> mixture. Figure 4-25 also shows that in terms of sensitivity of the time to breakdown measured to the changing gas pressure within the switch, CO<sub>2</sub> is one of the more stable gases with a smaller 'a' value than air or the 60%/40% N<sub>2</sub>/O<sub>2</sub> mixture and is comparable to the values for N<sub>2</sub>.

### 4.5.1 Weibull Analysis of Time to Breakdown

Each of the sets of experimental results obtained and presented within Section 4.3 have been analysed with a Weibull statistical analysis in order to compare the probability that breakdown events will occur for each of the gases tested and will take a specified amount of time deemed “time to breakdown” which shall be determined by the experimental conditions. A Weibull distribution is a statistical distribution which can be used for analyzing the reliability of dielectric media such as gas or liquid [139], [140] stressed with high voltage impulses.

A three-parameter Weibull distribution function was used following industrial standard IEC 62539 [141] as this is used within engineering to describe the distribution of experimental failure data, where the probability of a failure event (electric breakdown in the case of dielectric media) at a specific time  $F(t)$  is given by Equation (4.3) [141]

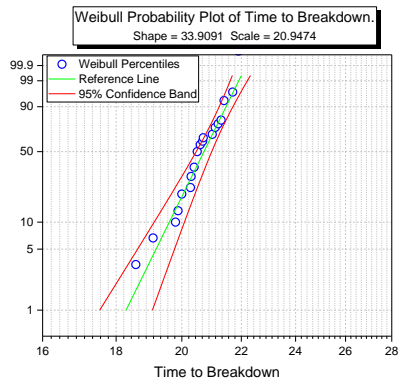
$$F(t; \alpha, \beta) = 1 - \exp\left\{-\left(\frac{t - \gamma}{\alpha}\right)^\beta\right\}; t \geq \gamma \quad (4.3)$$

where  $t$  is the time to breakdown,  $F(t)$  the Weibull probability distribution function (which provides the reliability of the system),  $\alpha$  ( $\mu\text{s}$ ) is a positive scale parameter which represents the time at which 63% of breakdowns will have occurred on the cumulative distribution curve and  $\beta$  is the shape parameter which is a measure of the range of breakdown times which is also positive. The larger the value of  $\beta$  is, the smaller the range of times in which a breakdown event is likely to occur. The term of  $\gamma$  ( $\mu\text{s}$ ) is known as the location parameter and is the minimum time at which breakdown events may occur, i.e. the probability of breakdown events occurring is zero for  $t < \gamma$ .

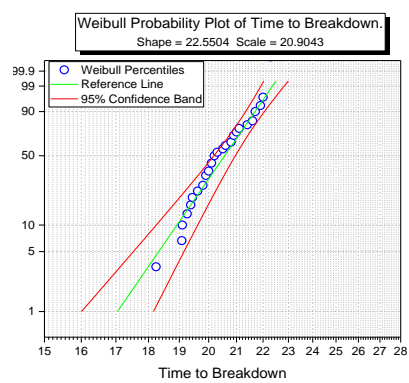
The breakdown in the plasma closing switch takes place at specified time under any given set of experimental conditions. Therefore, the output of a Weibull analysis can be utilised to estimate the probability that a breakdown will occur at a given time under specified operational conditions, such as gas pressure, inter-electrode gap length and level of DC stress applied across the main inter-electrode gap.

This section presents the Weibull analysis conducted for both the 2mm and 4mm inter-electrode gap lengths stressed with 70% and 80% of the self-breakdown voltage potential. The Weibull analysis has been conducted using Origin Pro graphing software which allows to fit the Weibull probability distribution function given by Equation 4.3 to the experimental time to breakdown data and to obtain the Weibull distribution parameters,  $\alpha$ ,  $\beta$  and  $\gamma$ . The fitting procedure in Origin Pro graphing software provides 95% confidence intervals for the obtained Weibull parameters. A comparison of  $\alpha$  ( $\mu\text{s}$ ),  $\beta$  and  $\gamma$  ( $\mu\text{s}$ ) for the different combinations of experimental conditions is given and this allows for a direct comparison of all gases tested.

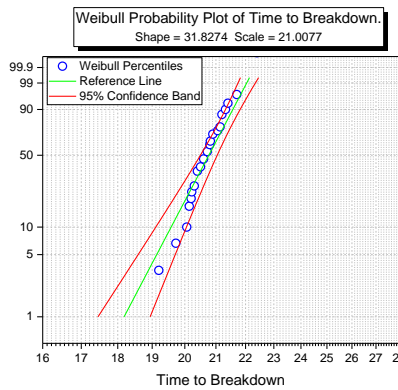
Weibull distribution graphs of the 2mm inter-electrode gap length under 70% and 80% of the self-breakdown voltage potential for each of the five gases tested; for each of the gas pressures tested where breakdown was able to be initiated, is presented. A table of coefficients for each of the respective gas pressures and inter-electrode gap lengths is compiled which provides a direct comparison of the scale and shape coefficients of each of the gases and the 95% confidence intervals for breakdown occurring at a specified time.



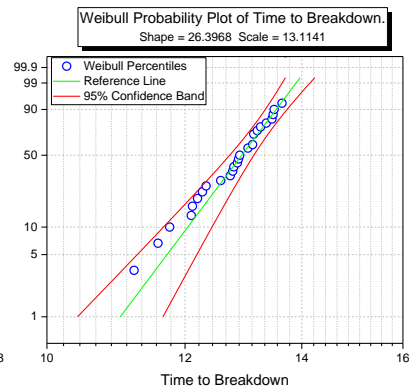
(a)



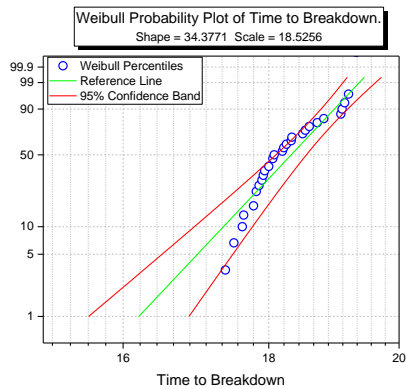
(b)



(c)



(d)



(e)

**Figure 4-26 Weibull analysis graphs for a 2mm inter-electrode gap length at 0.1MPa (a) Air (b) N<sub>2</sub> (c) 60%/40% N<sub>2</sub>/O<sub>2</sub> (d) 90%/10% Ar/O<sub>2</sub> (e) CO<sub>2</sub> with 70% of the self-breakdown voltage applied across the main inter-electrode gap length as DC stress. 95% confidence bands are also plotted. The vertical axis represents the reliability of breakdown events occurring (%) and the horizontal axis is the time to breakdown (ns). Each of the open circle symbols plotted on the graph represent breakdown events occurring at a specified time. The green line on each graph is a reference line with parameters of the shape and scale extracted from the Weibull fit of the plotted open symbols. The red lines on either side of the green line represent the 95% confidence band, that is, the band within which 95% of the breakdown events are predicted to occur.**

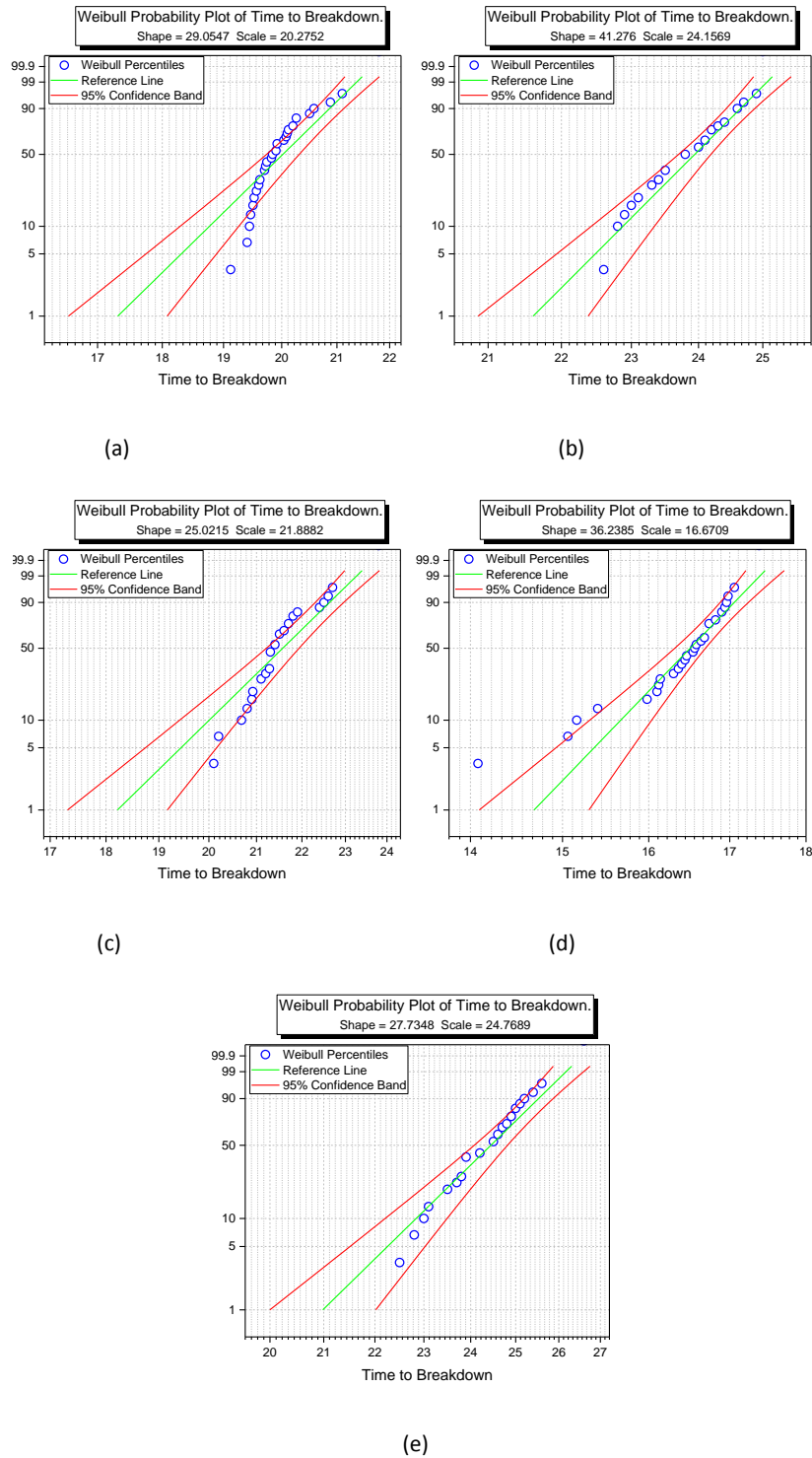


**Figure 4-27 Weibull analysis graphs for a 2mm inter-electrode gap length at 0.1MPa (a) Air (b) N<sub>2</sub> (c) 60%/40% N<sub>2</sub>/O<sub>2</sub> (d) 90%/10% Ar/O<sub>2</sub> (e) CO<sub>2</sub> with 80% of the self-breakdown voltage applied across the main inter-electrode gap length as DC stress. 95% confidence bands are also plotted. The vertical axis represents the reliability of breakdown events occurring (%) and the horizontal axis is the time to breakdown (ns). Each of the open circle symbols plotted on the graph represent breakdown events occurring at a specified time. The green line on each graph is a reference line with parameters of the shape and scale extracted from the Weibull fit of the plotted open symbols. The red lines on either side of the green line represent the 95% confidence band, that is, the band within which 95% of the breakdown events are predicted to occur.**

**Table 4-6 Weibull Parameters for time to breakdown events measured in a 2mm inter-electrode gap for each of the 5 gases tested at 0.1MPa pressure when 70% and 80% of the self-breakdown voltage are applied across the main inter-electrode gap length as DC stress voltage respectively.**

0.1MPa	Air	Nitrogen	60%/40% N <sub>2</sub> /O <sub>2</sub>	90%/10% Ar/O <sub>2</sub>	CO <sub>2</sub>
<b><i>2mm 70% V<sub>br</sub></i></b>					
<i>Scale - α (μs)</i>	33.91	22.55	31.83	12.93	34.38
95% confidence interval	25.83 – 41.99	17.23 – 27.87	25.08 – 38.58	-9.67 – 35.53	26.48 – 42.28
<i>Shape - β</i>	20.95	20.90	21.01	13.11	18.53
95% confidence interval	20.75 – 21.15	20.59 – 21.21	19.79 – 20.23	12.94 – 13.28	18.36 – 18.70
<i>Intercept- γ (μs)</i>	3.04	3.04	3.04	2.57	2.92
95% confidence interval	3.02 – 3.06	3.02 – 3.06	3.02 – 3.06	2.55 – 2.59	2.90 – 2.94
<b><i>2mm 80% V<sub>br</sub></i></b>					
<i>Scale - α (μs)</i>	29.05	41.28	25.02	27.73	36.24
95% confidence interval	23.14 – 34.96	31.37 – 51.19	19.86 – 30.18	21.66 – 33.80	27.10 – 45.38
<i>Shape - β</i>	20.28	24.16	21.89	24.77	16.67
95% confidence interval	20.04 – 20.52	24.35 – 23.97	21.60 – 22.18	24.48 – 25.06	16.52 – 16.82
<i>Intercept- γ (μs)</i>	3.01	3.18	3.09	3.21	2.81
95% confidence interval	2.99 – 3.03	3.16 – 3.20	3.07 – 3.11	3.19 – 3.23	2.79 – 2.83

Figures 4-26(a)-(e) present the Weibull probability plots for time to breakdown events for each of the gases tested; air, N<sub>2</sub>, 60%/40% N<sub>2</sub>/O<sub>2</sub>, 90%/10% Ar/O<sub>2</sub> and CO<sub>2</sub> respectively at 0.1MPa when 70% of the self-breakdown voltage is applied across the inter-electrode gap. Figures 4-27(a)-(e) present the Weibull probability plots of time to breakdown in a 2mm inter-electrode gap also under 0.1MPa pressure for the same gases however under a DC stress level equal to 80% of the self-breakdown voltage for each of the respective gases.

Table 4-6 presents a comparison of the three Weibull parameters obtained from the statistical analysis of the time to breakdown measurements in the switch filled to 0.1MPa with each of the gasses and stressed with 70% and 80% of the DC self-breakdown voltage level respectively. This allows for a direct comparison of each of the Weibull parameters  $\alpha$  ( $\mu$ s),  $\beta$  and  $\gamma$  ( $\mu$ s).

As described, the shape parameter  $\beta$ , is related to the size of the range of times over which a breakdown can be expected to occur. The gas with corresponding largest value(s) of  $\beta$  will have the smallest range in terms of measured times to breakdown and thus can be reasonably described as the most predictable and stable gas in terms of measuring the time to breakdown. Table 4-6 shows that the value of  $\beta$ , is largest under the 70% of self-breakdown voltage as DC stress application for the gas mixture comprised of 60%/40% N<sub>2</sub>/O<sub>2</sub> although the value of  $\beta$  obtained for both the air and N<sub>2</sub> filled switch are close in magnitude. When the level of DC stress voltage is increased to 80% of the self-breakdown voltage in the 2mm inter-electrode gap length for 0.1MPa gas pressure, the smallest range of breakdown voltages predicted, i.e. the highest value of  $\beta$  obtained was found in the 90%/10% Ar/O<sub>2</sub> mixture closely followed by the N<sub>2</sub> filled switch. This means that under experimental conditions where the gap is stressed with 70% of the DC stress level, the range of times over which breakdown is likely to occur is smaller for the 60%/40% N<sub>2</sub>/O<sub>2</sub> gas mixture than any of the other gases tested, however, when the level of DC stress voltage is increased to 80% of the self-breakdown voltage potential, the range of times over which a breakdown may occur is found to be smallest for the gap filled with the 90%/10% Ar/O<sub>2</sub> mix.

Another parameter of interest to come from Weibull analysis is the value of  $\gamma$  ( $\mu$ s). In the context of this experimental investigation,  $\gamma$  represents the minimum time ( $\mu$ s) where the probability of a breakdown occurring is non-zero. For any time  $t < \gamma$ , the probability of

breakdown occurring is zero and any time  $t \geq \gamma$ , the probability of breakdown occurring is non-zero. For all gases tested at 0.1MPa under DC stress of either 70% and 80% of the self-breakdown voltage, when the Weibull statistical analysis has been applied to the experimental data, it can be seen as in Table 4-6 that the minimum time where the probability of a breakdown occurring is non-zero is  $\sim 2.5\text{-}3.2\mu\text{s}$ .

The Weibull probability plots have been obtained for each of the other combinations of inter-electrode gap distance, gas pressure, gas type and DC voltage stress level applied across the gap. These probability plots can be found within Appendix 1, however, the key values of scale,  $\alpha$ , shape,  $\beta$ , and the intercept,  $\gamma$ , have been extracted and are presented within tables and discussed.

**Table 4-7 Weibull Parameters for time to breakdown events measured in a 2mm inter-electrode gap for each of the 5 gases tested at 0.2MPa pressure when 70% and 80% of the self-breakdown voltage are applied across the main inter-electrode gap length as DC stress voltage respectively.**

0.2MPa	Air	Nitrogen	60%/40% N <sub>2</sub> /O <sub>2</sub>	90%/10% Ar/O <sub>2</sub>	CO <sub>2</sub>
<b><i>2mm 70% V<sub>br</sub></i></b>					
<u>Scale - <math>\alpha</math></u> <i>(<math>\mu</math>s)</i>	22.96	16.96	65.87	40.03	21.39
95% confidence interval	17.23 – 28.69	13.43 – 20.49	51.65 – 80.01	30.14 – 49.92	15.73 – 27.04
<u>Shape - <math>\beta</math></u>	36.79	40.08	40.65	16.17	38.44
95% confidence interval	36.26 – 37.31	39.30 – 40.86	40.45 – 40.85	16.03 – 16.31	37.86 – 39.01
<u>Intercept- <math>\gamma</math></u> <i>(<math>\mu</math>s)</i>	3.61	3.69	3.70	2.78	3.65
95% confidence interval	3.59 – 3.62	3.67 – 3.71	3.68 – 3.72	2.76 – 2.80	3.63 – 3.67
<b><i>2mm 80% V<sub>br</sub></i></b>					
<u>Scale - <math>\alpha</math></u> <i>(<math>\mu</math>s)</i>	20.17	22.04	65.87	57.88	46.11
95% confidence interval	15.46 – 24.88	17.21 – 26.87	51.64 – 80.09	44.78 – 70.98	34.57 – 57.65
<u>Shape - <math>\beta</math></u>	40.28	41.95	40.65	18.24	42.50
95% confidence interval	39.62 – 40.94	41.32 – 42.58	40.44 – 40.85	18.13 – 18.34	42.19 – 42.81
<u>Intercept- <math>\gamma</math></u> <i>(<math>\mu</math>s)</i>	3.70	3.74	8.37	2.90	3.75
95% confidence interval	3.68 – 3.72	3.72 – 3.76	8.35 – 8.39	2.87 – 2.93	3.73 – 3.77

Table 4-7 compares the values of the three Weibull parameters obtained for each of the five gases tested under experimental conditions of a 2mm inter-electrode gap length, 0.2MPa gas pressure and 70% or 80% of the self-breakdown voltage applied as the DC stress across the main gap length within the field-distortion triggered switch triggered with a voltage impulse with a voltage rise-time of 0.45kV/ $\mu$ s.

The value of  $\beta$ , the shape parameter is again largest under the 70% of self-breakdown voltage as DC stress application for the gas mixture comprised of 60%/40% N<sub>2</sub>/O<sub>2</sub> and similarly to the lower pressure (0.1MPa evaluation) the value of  $\beta$  obtained for the N<sub>2</sub> filled switch is close in magnitude. This suggests that while the 60%/40% N<sub>2</sub>/O<sub>2</sub> gas mixture may have the shortest range of times over which a breakdown is predicted to occur, the switch, when filled with N<sub>2</sub> gas (99.9% purity) also has a comparatively short range over which there will be measured times to breakdown. When the level of DC stress voltage is increased to 80% of the self-breakdown voltage in the 2mm inter-electrode gap length for 0.2MPa gas pressure, the smallest range of breakdown voltages predicted, i.e. the highest value of  $\beta$  obtained was found in N<sub>2</sub> filled switch under the DC stress level of 80% of the self-breakdown voltage level.

Another parameter of interest to come from Weibull analysis is the value of  $\gamma$ . It can be seen from Table 4-7 that the minimum time where the probability of a breakdown occurring is non-zero is  $\sim$ 2.8-3.8 $\mu$ s, however, the shortest time where the probability of a breakdown is non-zero under the DC stress equal to 80% of the self-breakdown voltage in a switch filled with the mixture of 60%/40% N<sub>2</sub>/O<sub>2</sub> is  $\sim$ 8.3 $\mu$ s which is  $\sim$ 3 times the duration of any of the other gases tested.

**Table 4-8 Weibull Parameters for time to breakdown events measured in a 2mm inter-electrode gap for each of the 5 gases tested at 0.3MPa pressure when 70% and 80% of the self-breakdown voltage are applied across the main inter-electrode gap length as DC stress voltage respectively.**

0.3MPa	Air	Nitrogen	60%/40% N <sub>2</sub> /O <sub>2</sub>	90%/10% Ar/O <sub>2</sub>	CO <sub>2</sub>
<b><i>2mm 70% V<sub>br</sub></i></b>					
<i>Scale - α</i> ( <i>μs</i> )	24.85	19.63	24.29	7.54	13.61
95% confidence interval	18.63 – 31.06	14.94 – 24.32	18.67 – 29.91	5.64 – 9.44	10.53 – 16.69
<i>Shape - β</i>	69.97	53.81	69.94	35.05	58.96
95% confidence interval	69.05 – 70.89	52.91 – 54.71	68.99 – 70.89	33.53 – 36.56	57.53 – 60.39
<i>Intercept- γ</i> ( <i>μs</i> )	4.25	3.99	4.25	3.56	4.08
95% confidence interval	4.23 – 4.27	3.97 – 4.01	4.23 – 4.27	3.53 – 3.59	4.06 – 4.09
<b><i>2mm 80% V<sub>br</sub></i></b>					
<i>Scale - α</i> ( <i>μs</i> )	10.07	15.77	13.97	8.94	10.34
95% confidence interval	7.67 – 12.47	11.56 – 19.98	11.13 – 16.81	6.77 – 11.11	7.55 – 13.13
<i>Shape - β</i>	96.32	67.94	80.77	38.66	67.99
95% confidence interval	93.18 – 99.46	66.55 – 69.33	78.85 – 82.69	37.25 – 40.07	65.87 – 70.11
<i>Intercept- γ</i> ( <i>μs</i> )	4.57	4.22	4.39	3.65	4.22
95% confidence interval	4.54 – 4.60	4.20 – 4.24	4.37 – 4.41	3.62 – 3.68	4.20 – 4.24

Table 4-8 compares the values of all three Weibull parameters obtained for each of the five gases tested under experimental conditions of a 2mm inter-electrode gap length, 0.3MPa gas pressure and 70% or 80% of the self-breakdown voltage applied as the DC stress across the main gap length.

The value of  $\beta$ , the shape parameter is largest for the air-filled switch under the DC stress conditions where 70% or 80% of the self-breakdown voltage is applied across the gap. It was also noted that the value of  $\beta$  for the gas mixture made up of 60%/40%  $N_2/O_2$  was large for both the experimental conditions when the inter-electrode gap length was stressed with 70% or 80% of the self-breakdown voltage.

The value of  $\gamma$ , for the 2mm inter-electrode gap length when the gas pressure within the switch is 0.3MPa (absolute) was found to be  $\sim 4\mu s$  when the inter-electrode gap length is stressed with 70% of the self-breakdown voltage and  $\sim 4.4\mu s$  when stressed with 80% of the self-breakdown voltage of each of the gases. Under both DC stress level conditions of 70% and 80% of the self-breakdown level, the 90%/10%  $Ar/O_2$  gas showed the smallest value of  $\gamma$  corresponding to the shortest minimum time at which the probability of breakdown occurring would be non-zero. This can be regarded as a result of the lower voltage hold-off capabilities of the  $Ar/O_2$  mixture than the other gases tested. The largest  $\gamma$  values, i.e. the gases which have the longest time before the probability of a breakdown is non-zero are air and the mixture of 60%/40%  $N_2/O_2$ .

**Table 4-9 Weibull Parameters for time to breakdown events measured in a 4mm inter-electrode gap for each of the 5 gases tested at 0.1MPa pressure when 70% and 80% of the self-breakdown voltage are applied across the main inter-electrode gap length as DC stress voltage respectively.**

0.1MPa	Air	Nitrogen	60%/40% N <sub>2</sub> /O <sub>2</sub>	90%/10% Ar/O <sub>2</sub>	CO <sub>2</sub>
<b><i>4mm 70% V<sub>br</sub></i></b>					
<u>Scale - <math>\alpha</math></u> <i>(<math>\mu</math>s)</i>	16.37	14.44	25.66	26.53	8.36
95% confidence interval	12.62 – 20.12	11.09 – 17.79	19.03 – 32.29	20.09 – 32.97	6.24 – 10.48
<u>Shape - <math>\beta</math></u>	26.58	31.27	30.94	20.16	31.31
95% confidence interval	26.05 – 27.11	30.56 – 31.98	30.55 – 31.33	19.91 – 20.41	30.09 – 32.53
<u>Intercept- <math>\gamma</math> (<math>\mu</math>s)</u>	3.28	3.44	3.43	3.00	3.44
95% confidence interval	3.26 – 3.30	3.42 – 3.46	3.41 – 3.45	2.98 – 3.02	3.41 – 3.47
<b><i>4mm 80% V<sub>br</sub></i></b>					
<u>Scale - <math>\alpha</math></u> <i>(<math>\mu</math>s)</i>	23.17	18.85	15.55	15.42	13.40
95% confidence interval	17.70 – 28.64	14.34 – 23.35	12.22 – 18.88	11.82 – 19.02	10.31 – 16.49
<u>Shape - <math>\beta</math></u>	26.62	37.32	33.27	23.78	34.95
95% confidence interval	26.25 – 26.99	36.67 – 37.97	32.57 – 33.97	23.27 – 16.49	34.10 – 35.80
<u>Intercept- <math>\gamma</math> (<math>\mu</math>s)</u>	3.28	3.62	3.50	3.17	3.55
95% confidence interval	3.26 – 3.30	3.60 – 3.64	3.48 – 3.52	3.15 – 3.19	3.53 – 3.57

Table 4-9 provides a comparison of the values of the three Weibull parameters obtained for each of the five gases tested under experimental conditions (4mm inter-electrode gap length, 0.1MPa gas pressure and 70% or 80% of the self-breakdown voltage applied as the DC stress across the main gap length).

The values of  $\beta$  can be compared for each of the different gases from Table 4-9 and it is evident that  $N_2$  generally shows the largest  $\beta$  value at 0.1MPa pressure within the 4mm inter-electrode gap under 70% and 80% self-breakdown voltage DC stress, however, as the inter-electrode gap length has been increased, the  $\beta$  value of  $CO_2$  increased suggesting that by increasing the main inter-electrode gap length, the range of times where a breakdown is likely to occur in a  $CO_2$  filled switch can be reduced.

The value of  $\gamma$ , the minimum time at which the probability of a breakdown event occurring is non-zero is  $\sim 3.4\mu s$  when the inter-electrode gap is stressed with 70% of the self-breakdown voltage of each of the respective gases and  $\sim 3.5\mu s$  when stressed with 80% of the self-breakdown voltage. It was again noted that the smallest  $\gamma$  values were observed from the  $Ar/O_2$  mixture as had been observed in the 2mm inter-electrode gap length.

**Table 4-10 Weibull Parameters for time to breakdown events measured in a 4mm inter-electrode gap for each of the 5 gases tested at 0.2MPa pressure when 70% and 80% of the self-breakdown voltage are applied across the main inter-electrode gap length as DC stress voltage respectively.**

0.2MPa	Air	Nitrogen	60%/40% N <sub>2</sub> /O <sub>2</sub>	90%/10% Ar/O <sub>2</sub>	CO <sub>2</sub>
<b><u>4mm 70% V<sub>br</sub></u></b>					
<u>Scale - <math>\alpha</math></u> <u>(<math>\mu</math>s)</u>	17.42	12.87	N/A	31.87	10.48
95% confidence interval	13.63 – 21.21	9.85 – 15.89		24.87 – 38.87	8.24 – 12.72
<u>Shape - <math>\beta</math></u>	73.20	77.37	N/A	39.48	77.61
95% confidence interval	71.82 – 74.58	75.40 – 79.34		39.07 – 39.89	75.16 – 80.06
<u>Intercept- <math>\gamma</math> (<math>\mu</math>s)</u>	4.29	4.35	N/A	3.68	4.35
95% confidence interval	4.27 – 4.31	4.32 – 4.38		3.66 – 3.70	4.32 – 4.38
<b><u>4mm 80% V<sub>br</sub></u></b>					
<u>Scale - <math>\alpha</math></u> <u>(<math>\mu</math>s)</u>	23.17	N/A	3.59	59.86	7.68
95% confidence interval	17.70 – 28.64		2.79 – 4.39	45.45 – 74.27	5.64 – 9.72
<u>Shape - <math>\beta</math></u>	26.62	N/A	51.61	44.04	92.06
95% confidence interval	26.25 – 26.99		46.89 – 56.33	43.80 – 44.28	87.39 – 96.73
<u>Intercept- <math>\gamma</math> (<math>\mu</math>s)</u>	3.28	N/A	3.94	3.79	4.52
95% confidence interval	3.26 – 3.30		3.86 – 4.03	3.77 – 3.81	4.49 – 4.55

Table 4-10 provides a comparison of the values of the three Weibull parameters obtained for each of the five gases tested under experimental conditions (4mm inter-electrode gap length, 0.1MPa gas pressure and 70% or 80% of the self-breakdown voltage applied as the DC stress across the main gap length).

The value of  $\beta$  under 70% of the self-breakdown voltage and 80% of the self-breakdown voltage applied as DC stress is largest in the switch filled with CO<sub>2</sub>.

The value of  $\gamma$  is again found to be smallest in the Ar/O<sub>2</sub> mixture and largest within the CO<sub>2</sub> under experimental conditions where the inter-electrode gap length is 4mm and the gas pressure within the test cell is 0.2MPa.

#### **4.6 Computational Analysis of Time to Breakdown Results**

As observed within the experimental results resented in Section 4.4, for all 5 gases tested, when the main inter-electrode gap length is stressed with 80% of the self-breakdown voltage of the respective gases, generally it is observed to take a longer period of time before a complete breakdown is observed after the application of a trigger impulse than the switch under experimental conditions where 70% of the self-breakdown voltage is applied as the DC stress across the inter-electrode gap length.

Although seemingly counter-intuitive, it is expected that there will be an observed increase in the time to breakdown measured when a higher percentage of the self-breakdown voltage is applied as DC stress across the main gap of the switch. This experimentally observed result is due to the designed nature of the switch with the application of the positive polarity DC voltage on the upper spherical electrode and the application of a negative trigger impulse voltage on the mid-plane encouraging the initiation of breakdown to occur between the mid-plane triggering electrode and the upper electrode. The initiation of breakdown between the upper electrode and the mid-plane electrode occurs before a complete breakdown occurs across the main gap of the switch.

A net post-initiation voltage as discussed within Section 4.1 is used which is described by Equation (4.1) and when considering magnitudes only, it clearly shows that for the cases where 70% of the self-breakdown voltage and 80% of the self-breakdown voltage are applied as DC stress voltage, the post-initiation voltage. In the initial design phase of the field-distortion switch, the simulation run in Quickfield, simulated a 10kV application on the

high voltage electrode and a -30kV voltage application applied to the mid-plane electrode. These values were chosen as maximum values beyond what would be reasonably being achieved within the switch during experimental procedure. E.g. if the self-breakdown voltage of a gas is 14.28kV,  $V_{br\ 70\%} = 10\text{kV}$ ,  $V_{br\ 80\%} = 11.4\text{kV}$ .

$$V_{post-initiation\ 70\%} = |V_{trigger}| - |V_{br70\%}| = 30\text{kV} - 10\text{kV} = 20\text{kV}$$

$$V_{post-initiation\ 80\%} = |V_{trigger}| - |V_{br80\%}| = 30\text{kV} - 11.4\text{kV} = 18.6\text{kV}$$

Experimentally, this leads to a greater enhanced electric field in the main inter-electrode gap once the breakdown has been initiated between the mid-plane electrode and upper spherical electrode.

If, however, the minimum measured time to breakdown is taken for each of the gases at any gas pressure, multiplied by 0.45kV/ $\mu\text{s}$  (the rate of rise of the voltage impulse) and the dc stress voltage subtracted:

e.g. 4mm inter-electrode gap space, 0.1MPa air

$$V_{min\ post\ init\ 70\%} = t_{br\ min} * 0.45\text{kV}/\mu\text{s} - |V_{br70\%}| = 24.3 * 0.45 - |V_{br70\%}| = 10.9\text{ kV} - 6.7\text{kV} = 4.2\text{ kV}$$

$$V_{min\ post\ init\ 80\%} = t_{br\ min} * 0.45\text{kV}/\mu\text{s} - |V_{br80\%}| = 23.6 * 0.45 - |V_{br80\%}| = 10.6\text{ kV} - 7.7\text{kV} = 2.9\text{ kV}$$

Again, this shows that for the minimum time to breakdown observed, the post-initiation breakdown voltage in the gap stressed with 70% of the self-breakdown voltage will be higher than that in the gap stressed with 80%. A higher post-initiation voltage in the gap stressed with 70% of the self-breakdown voltage means the electric field in the main gap will be larger than in the gap stressed with 80% and so the time to breakdown measured for the gap stressed with 80% can reasonably expected to be longer than the gap stressed with 70%.

Experimental conditions where 70% of the self-breakdown voltage had been applied across the upper electrode, resulting in  $V_{post-initiation70\%} = 20\text{kV}$  on the charged electrodes and 80% of the self-breakdown voltage resulting in  $V_{post-initiation80\%}=18.6\text{kV}$  have been simulated in Quickfield. The resulting electric field strength across the main inter-electrode gap length

(4mm total length from the upper spherical electrode to the grounded, lower electrode) for each of these post-initiation voltages applied across the mid-plane and upper electrode is plotted within Figure 4-35.

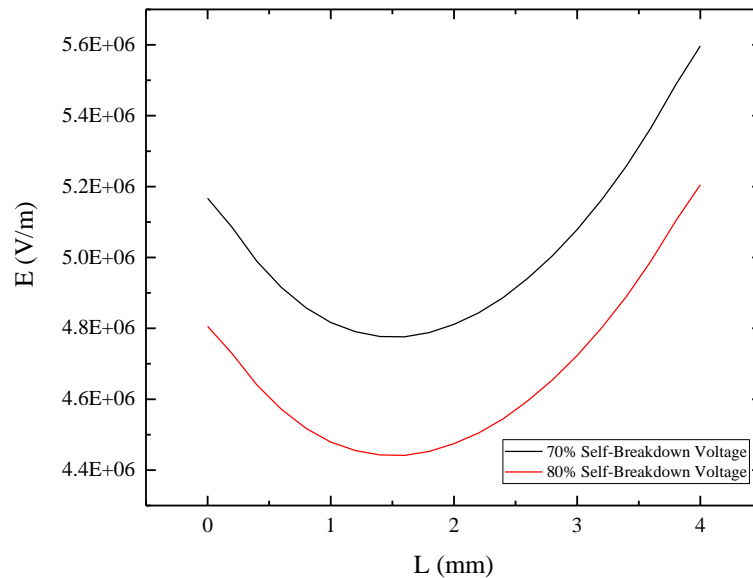


**Figure 4-28 Electric Field Strength within the main inter-electrode gap post-initiation for 70% self-breakdown voltage applied as DC stress and 80% of the self-breakdown voltage applied as DC stress.  $V_{\text{post-initiation}}$  used to model the electric field strength within the main inter-electrode gap of the switch being the net voltage of the trigger impulse minus the DC stress voltage.**

Figure 4-36 presents the electric field strength in the main inter-electrode gap between the spherical electrodes when the net post-initiation voltage after 70% of the self-breakdown voltage had been applied or 80% of the self-breakdown voltage had been applied to the upper electrode as a DC stress voltage prior to the application of the impulse voltage on the mid-plane electrode. It is clearly seen that the net post-initiation voltage after 80% of the self-breakdown voltage had been applied across the switch is lower than the post-initiation voltage after 70% of the self-breakdown voltage had been applied. This lower net-voltage results in lower electric field strength within the main inter-electrode gap for initiation of the complete breakdown between the main electrodes. Since the electric field strength in the main inter-electrode gap is lower post-initiation for the '80% of self-breakdown' condition, it can reasonably be concluded that it will take a longer time to reach a complete breakdown across the gap when the main inter-electrode gap is stressed with 80% of the

self-breakdown voltage than it will when stressed with 70% of the self-breakdown voltage; a result which has been observed experimentally for all gases throughout this chapter.

## 4.7 Conclusions.

This chapter has presented an investigation into the temporal breakdown characteristics of a field-distortion spark gap switch filled with five different gases; air, N<sub>2</sub>, 60%/40% N<sub>2</sub>/O<sub>2</sub>, 90%/10% Ar/O<sub>2</sub> and CO<sub>2</sub>. The switch was triggered with HV impulses with a rate of rise of ~0.45 kV/μs.

The field-distortion spark gap switch was designed based on the electric field in the switch which was modelled using the electrostatic software package QuickField before construction of the switch took place. The design of the switch had been shown to encourage the initiation of breakdown to originate between the mid-plane electrode and the upper, high voltage electrode before complete breakdown occurs within the main inter-electrode gap length.

For the 2mm inter-electrode gap length filled with each of the different gases, a linear increase in the measured time to breakdown was observed as the gas pressure within the switch increases. At the increased inter-electrode gap length of 4mm all gases showed an increase in the measured time to breakdown as the gas pressure within the switch increased, however due to experimental limitations, there was an insufficient range of pressures at which breakdowns were observed to take place to establish any trends.

In each of the gases tested, where it was possible to compare the effect on the time to breakdown that applying 70% or 80% of the self-breakdown voltage potential as a DC stress voltage across the switch had, it was noted that the time to breakdown increased by ~6% - 33% when 80% of the self-breakdown voltage was applied as the DC stress voltage across the switch when compared to stressing the inter-electrode gap length with 70% of the self-breakdown voltage. The difference in the time to breakdown for the different levels of DC stress applied was also observed and found to increase as gas pressure increased for both gap lengths tested and for all gases tested.

The jitter obtained for each of the gases tested was found to be on the  $\mu$ -second timescale as a result of the “slow” voltage rise rate of the impulse ( $0.45 \text{ kV}/\mu\text{s}$ ) applied to the triggering electrode. However, many industrial pulsed power applications require jitter on the nanosecond timescale [34], [142] and, in order to achieve this, a much faster pulse should be applied as a trigger pulse to the mid-plane electrode.

It has been shown within this chapter that if using a field distortion spark gap switch triggered by means of a voltage impulse applied to a mid-plane electrode at a relatively slow voltage rise rate of  $\sim 0.45 \text{ kV}/\mu\text{s}$ , the smallest jitter capabilities were found when the switch was filled with the 90%/10% Ar/O<sub>2</sub> gas mixture. The jitter was calculated to be typically  $< 2 \mu\text{s}$  for 2 mm and 4 mm inter-electrode gap lengths stressed with 70% or 80% of the self-breakdown voltage, whereas the other gases of interest within this investigation showed increased jitter values of up to  $10 \mu\text{s}$  in the case of the CO<sub>2</sub> and N<sub>2</sub> filled switches. The trade-off in this case would be the far-lower self-breakdown voltage capabilities which can be achieved by using the 90%/10% Ar/O<sub>2</sub> mixture. If slightly increased jitter ( $\sim 4 \mu\text{s}$ ) can be tolerated and higher voltage hold-off is of paramount importance, then a switch filled with air would be recommended, as air provides higher voltage hold-off capabilities than the 90%/10% Ar/O<sub>2</sub> mixture, as shown in Chapter 3, and the jitter is only slightly above that of the 90%/10% Ar/O<sub>2</sub> mixture within this investigation.

The next chapter of this thesis discusses an experimental investigation making use of the same field-distortion spark-gap switch and the same inter-electrode gap lengths but triggered with much faster HV voltage impulses with a rate of rise of  $1 \text{ kV}/\text{ns}$ . The DC stress voltage applied across the main gap of the switch will remain at the 70% and 80% of the self-breakdown level of each of the gases at the given gas pressure within the switch. However, the voltage impulse applied to the mid-plane electrode will have a much faster rate of voltage rise-time in an attempt to minimise the jitter of the switch.

## **Chapter 5 . Characterisation of a Field-Distortion Spark Gap switch Triggerred with fast 1kV/ns HV impulses.**

In Chapter 4 of this thesis, a description of the field-distortion spark gap switch and the experimental test set-up was provided alongside the experimental results of an investigation into breakdown characteristics of the switch under triggered conditions when this switch was triggered by applying a -30kV impulse at a rate of  $\sim 0.45\text{kV}/\mu\text{s}$  to the mid-plane electrode. It was found that the time to breakdown and resulting jitter associated with switching was on the  $\mu\text{s}$  timescale. Many pulsed power applications, however, require much lower levels of jitter in their systems typically of the order of a few nanoseconds [143]–[146].

Within this chapter, an experimental investigation into the time to breakdown characteristics and associated jitter of the field distortion spark gap switch triggered with a fast,  $\sim 1\text{ kV/ns}$ , HV impulses is presented. The triggering impulse applied to the mid-plane electrode within this experimental set-up is provided by a Blumlein pulse generator which outputs a  $\sim 30\text{ kV}$  peak voltage pulse over a much shorter ( $\sim 250\text{ ns}$  FWHM) timescale and the triggering mechanism is the only alteration to the experimental set-up that was described in detail in Chapter 4.

Within this chapter, a description of the changes to the trigger pulse forming part of the experimental system is provided. The results of the investigation into the time to breakdown and jitter of the switch when filled with the same 5 gases as have been used in the rest of this experimental investigation. The effect of increasing the gas pressure within the switch across the range  $0.1\text{ MPa} - 0.4\text{ MPa}$  for the different inter-electrode distances ( $2\text{ mm}$  and  $4\text{ mm}$ ) and the effect of different levels of DC stress voltage across the main inter-electrode gap on the time to breakdown and the jitter of the switch is investigated and presented followed by a discussion of the practical applications of the results.

Some results of note presented within this thesis show that for the time to breakdown in a field-distortion spark gap switch triggered by a fast Blumlein impulse, the time to breakdown observed does not statistically change as the gas pressure within the switch increases. It is shown that the level of DC stress voltage applied across the main gap also

has little effect on the measured time to breakdown of the switch for any of the five gases tested.

It is shown within this chapter that by using a Blumlein pulse generator, with a voltage risetime in the nanosecond timescale, to provide the triggering voltage pulse to the mid-plane electrode the jitter of the switch reduces for all gases to nanosecond jitter values. This reduction of jitter to nanosecond timescale levels is ideal for industrial applications. For all gases tested the jitter observed is found to be ~2-3ns however as the gas pressure within the switch is increased within the range 0.1MPa-0.4MPa, the jitter is also observed to increase.

## 5.1 Experimental test set-up

The test-set up for this experimental investigation into time to breakdown characteristics of the field distortion spark gap switch made use of much of the same circuit as was described in Chapter 4. A Glassman high voltage DC power supply (0-60kV) was used to pre-stress the switch via a 1M $\Omega$  charging resistor and a North Star PVM-5 high voltage probe (1000:1 division ratio) (80 MHz nominal bandwidth) monitored the voltage across the main gap of the switch.

In order to create voltage impulses with defined duration and shape, coaxial transmission topologies are commonly used. The duration and shape (including the rise-time of the impulse) is defined by the length of the cables and in order to achieve voltage multiplication, stacks of transmission cables can be used.

The maximum output voltage of a conventional pulse forming line is given by:

$$V_L = V_s \frac{Z_L}{Z_{OUT} + Z_L} \quad (5.1)$$

where  $V_L$  is the load voltage (V);  $V_s$  is the supply voltage (V);  $Z_L$  is the impedance of the load ( $\Omega$ ); and  $Z_{OUT}$  is the output impedance of the impulse generator ( $\Omega$ ) equal to the characteristic impedance of the cable. When  $Z_L$  and  $Z_{OUT}$  are equal, the maximum load voltage can be seen to be half the supply voltage.

A Blumlein is a type of pulse forming network that was patented in 1941 by Alan Blumlein [147] where the magnitude of the output pulse is equal to the input supply voltage. This is

achieved across a matched load, where  $Z_L=2Z_0$ . The Blumlein pulse generator places the load in the centre, between two transmission lines as seen in Figure 5-1, and as such, if the load impedance is twice the characteristic impedance of coaxial cables,  $Z_0$ , Blumlein generators can output a voltage impulse equal to the DC supply voltage.

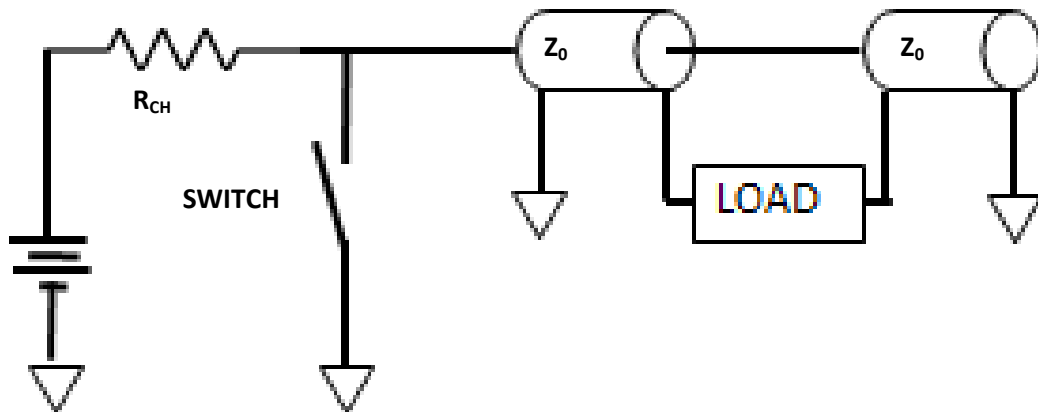


Figure 5-1 Schematic of a Blumlein generator circuit, adapted from [148]

Voltage multiplication can be achieved using Blumlein pulse generators by stacking them in order to obtain double, triple etc the charging voltage [148]. For any kind of transmission line within pulsed power applications where fast, short pulses are required, the characteristic impedance is a key value which can be calculated using Equation 5.2 :

$$Z_0 = \sqrt{\frac{L'}{C'}} \quad (5.2)$$

Where  $L'$  is the inductance of the cable per unit length (H/m) and  $C'$  the capacitance per unit length (F/m).

An ordinary Blumlein topology shown in Fig 5-2 was chosen to provide the triggering voltage impulse to the mid-plane electrode as it allows for very fast (ns) rising voltage impulses.

The single Blumlein pulse generator has a spark switch stressed to  $\sim -30\text{kV}$  before it triggers and provides the  $-30\text{kV}$  voltage impulse rising at a rate of  $\sim 1\text{kV/ns}$  to the mid-plane electrode of the switch.

## 5.2 Methodology

The procedure for carrying out the breakdown experiments with the Blumlein pulse generator was similar to that for the experiments conducted and described within Chapter 4.2, in which the trigger generator producing longer,  $\mu\text{s}$  scale trigger impulses.

The gas switch which controls the firing of the Blumlein voltage impulse is filled with bottled air to  $0.13\text{MPa}$  (absolute) pressure via the gas distribution board and a second Glassman High Voltage DC voltage power supply is used to set the input voltage to  $30\text{kV}$ . This means that as described within Section 5.1 the output pulse of the single Blumlein will also be a maximum of  $-30\text{kV}$ .

The inter-electrode gap length is still considered to be the 'main gap' length and defined from a zero point where a short circuit was observed across the switch. The adjustment of both the upper and lower spherical electrodes beyond this point resulted in a non-zero value of the resistance measured on a digital multimeter.  $2\text{mm}$  increments of inter-electrode gap length were again used (a  $1\text{mm}$  vertical adjustment of both the upper and lower spherical electrodes) to ensure an equidistant spacing between the upper and lower spherical electrodes and the mid-plane triggering electrode as this ensures no breakdown between upper and lower electrode with the mid-plane triggering electrode being favoured due to the geometry of the switch.

The process for carrying out the time to breakdown measurements as previously described involved setting of the inter-electrode gap length, evacuating the test cell of gas and re-filling to atmospheric pressure ( $0.1\text{MPa}$ ) with air and manually applying a DC stress voltage to the upper spherical electrode of 70% or 80% of the self-breakdown voltage for this gas at this pressure, the DC stress voltage is applied to the upper electrode at a rate of  $\sim 2\text{kV/s}$ . The self-breakdown voltages for each gas and pressure combination within this switch topology have previously been measured for the experiments conducted with the  $0.45\text{kV}/\mu\text{s}$  trigger generator (Section 4.4) and thus did not require repeating before this investigation.

### **5.3 'Time to Breakdown' characteristics of the field-distortion switch triggered by a Blumlein pulse generator.**

By using an ordinary Blumlein pulse generator to provide the triggering impulse which initiates breakdown in these experiments, it is seen in the results presented within this section that the total time to breakdown for all gases is on the scale of tens of nanoseconds. The much faster rise-time of the voltage impulse provided by the Blumlein pulse generator ( $\sim 1\text{kV/ns}$ ) results in the decrease in time to breakdown from microsecond timescale measurements taken in Chapter 4 to nanosecond timescale breakdown.

Each data point representing the time to breakdown is an average value of 30 breakdown events initiated. The closed symbols represent the experimental conditions where the main inter-electrode gap length is stressed with 70% of the self-breakdown voltage level and the open symbols the conditions where the main gap length is stressed with 80% of the self-breakdown voltage level. The error bars on each graph again represent the standard deviation in the time to breakdown measurements i.e. the jitter. The gas within the test-cell was evacuated and the switch was filled with fresh gas between each change of inter-electrode gap length tested, each of the gas pressures tested 0.1MPa-0.4MPa (in 0.1MPa increments, at room temperature) or when the level of DC stress applied across the main gap length was changed. The error bars represent the jitter (standard deviation in the time to breakdown) of the switch for the particular gas, gap length and DC stress level applied.

#### **5.3.1 Time to Breakdown for an air-filled switch triggered with 1kV/ns HV impulses.**

The switch test-cell was first filled with bottled air and the time to breakdown measured for gas pressures within the switch between 0.1MPa and 0.4MPa (at increasing 0.1MPa increments) for 2mm and 4mm inter-electrode gap lengths. The effect of the DC stress level applied across the main gap of the switch was again a condition of interest and thus both 70% and 80% of the self-breakdown voltage potential were used as DC stress level conditions. Figure 5-2 presents the time to breakdown in the switch as a function of the gas pressure for a 2mm inter-electrode main gap length in the switch filled with air

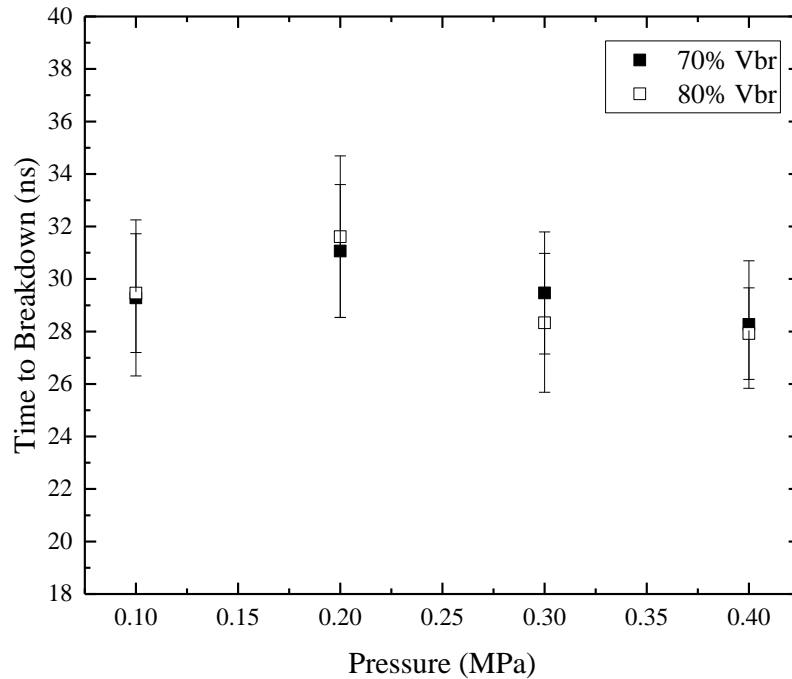


**Figure 5-2 The average time to breakdown measured for a 2mm inter-electrode gap length filled with bottled air as a function of the gas pressure within the switch.**

It was observed that as the gas pressure increased within the test-cell, the measured ‘time to breakdown’ characteristic remained almost unchanged, statistically these data points are not different as their error bars (which represent the standard deviation) overlap. The standard deviation represents the times at which 63% of the time to breakdown events are likely to be observed. The overlapping of the standard deviation error bars for each of the different gas pressures tested within the range 0.1MPa-0.4MPa suggests that there is no significant difference in the measured time to breakdown as the gas pressure increases. This observation that the ‘time to breakdown’ of the switch would not significantly change as the gas pressure within the switch increased (from 0.1MPa to 0.4MPa absolute pressure) was observed for conditions where 70% of the self-breakdown voltage is applied as DC stress across the main gap and also for experimental conditions where 80% of the self-breakdown voltage was applied as the DC stress condition.

For 2mm inter-electrode main gap length experiments conducted, there is no significant impact on the time to breakdown measured by stressing the inter-electrode gap space with

either 70% or 80% of the self-breakdown voltage potential. The difference in the levels of DC stress voltage applied across the gap length resulted in very small changes in the total time to breakdown measured across the switch. The difference in the measured time to breakdown between the gap stressed with 70% and with 80% of the self-breakdown voltage was around 0.5ns-1.1ns, which corresponds to 1-3% of the total time to breakdown measured.

The results seen in Chapter 4 showed that when the system was triggered with a voltage impulse with a much slower voltage rate of rise, 0.45kV/ $\mu$ s, the inter-electrode gap lengths stressed with 80% of the self-breakdown voltage level consistently provided longer total time to breakdown measurements than those of the gap stressed with 70% of the self-breakdown voltage level. However, when triggered by a voltage impulse with a rate of  $\sim$ 1kV/ns neither the 70% level nor the 80% of self-breakdown voltage level applied as DC stress in the resulted in an obvious, consistent, increase in time to breakdown in a 2mm air-filled gap across the range of pressures 0.1MPa – 0.4MPa.

Figure 5-3 shows the time to breakdown as a function of gas pressure for the air-filled switch measured when the inter-electrode gap length is increased from 2mm to 4mm.

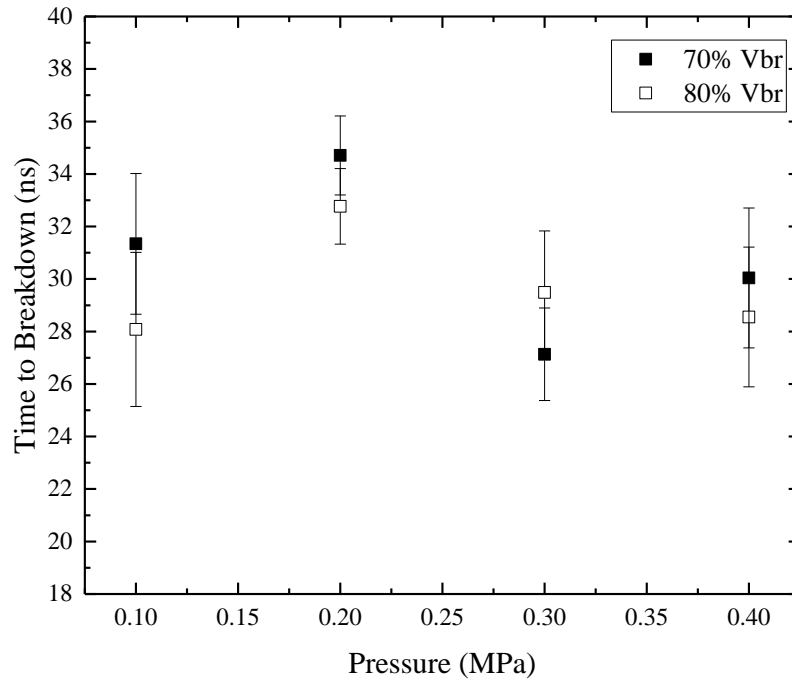


**Figure 5-3 The average time to breakdown measured for a 4mm inter-electrode gap length filled with bottled air as a function of the gas pressure within the switch.**

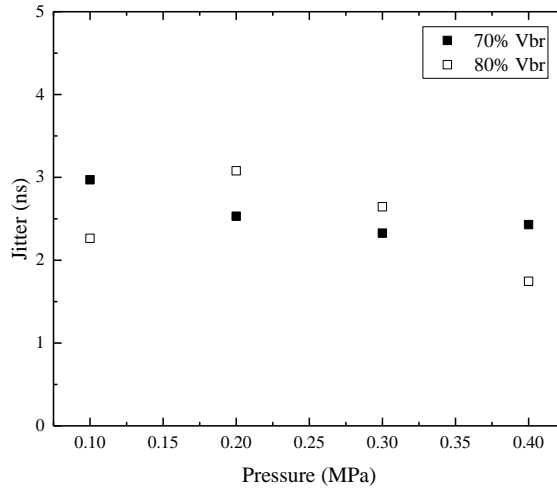
As the inter-electrode gap length was increased to 4mm as shown in Figure 5-3, it is also observed, as was seen in the 2mm gap-space experiments overall, the measured time to breakdown statistically is not different regardless of the gas pressure within the switch, as can be seen by the overlapping standard deviations representing the 63% confidence interval.

A result of note evident within Figure 5-3 is that by increasing the inter-electrode gap length from 2mm to 4mm, the impact of the stress level applied across the gap space has increased the difference in the time to breakdown measurements. It has been calculated from experimental data that when stressed with 70% of the self-breakdown voltage, the total time to breakdown of the 4mm air-filled switch was 1.95-3.26ns longer than the total time to breakdown measured for the inter-electrode gap length stressed with 80% of the self-breakdown voltage, corresponding to a 5-10% increase in the time to breakdown.

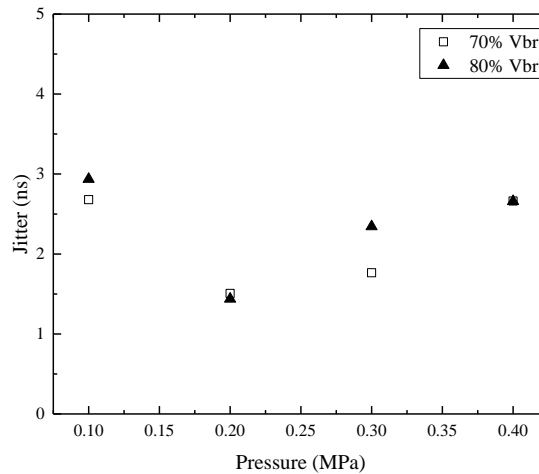
At intermediate pressures between the upper and lower end of the gas pressure range tested (0.1MPa and 0.4MPa), the time to breakdown measurements were seen to fluctuate, however when considering the overall trend of time to breakdown as gas pressure continually increases, the overall influence of the gas pressure on the time to breakdown of the switch is considered. It is clear within the scope of this project, under triggering conditions with a rate of voltage rise of 1kV/ns, for relatively small inter-electrode gap lengths the gas pressure does not much influence the total time to breakdown of an air-filled switch from initial application of trigger impulse to the mid-plane electrode to the point of complete voltage collapse across the main gap.

The other key breakdown characteristic of the switch which is of interest in this investigation is the jitter capability. Determining if triggering the switch with a voltage pulse with a much shorter duration (nanoseconds instead of microseconds) could reduce both the total time to breakdown of the switch as well as the jitter of the switch is of interest.

Previous trigger impulses used to trigger the switch (Chapter 4) provided a voltage pulse over a timescale of  $\sim 185 \mu\text{s}$  and the total time to breakdown of an air-filled switch with gas pressures in the range 0.1MPa-0.4MPa took 10s of  $\mu\text{s}$ . The difference in the total time to breakdown between the two triggering mechanisms is approximately three orders of magnitude due to the Blumlein pulse generator being approximately three orders of magnitude faster. The jitter capabilities ideally should be as small as possible for industrial applications as this provides as much stability and predictability during operation for the switch. Figure 5-4(a) and (b) show the jitter of the air-filled switch triggered by the Blumlein impulse generator as a function of the gas pressure within the switch.



(a)



(b)

**Figure 5-4 The jitter for the field-distortion spark switch when triggered with the Blumlein pulse generator as a function of gas pressure for (a) 2mm and (b) 4mm gap lengths.**

Figure 5-4(a) shows the jitter performance of the 2mm inter-electrode gap length which overall is tending to decrease as the gas pressure increases from 0.1MPa-0.4MPa, suggesting a more predictable operation as the gas pressure increases.

As the inter-electrode gap space was increased to 4mm, the jitter as shown in Figure 5-3(b) did not show a decreasing trend as gas pressure increased. Instead it appears that the jitter

in the air-filled switch reaches a minimum level when the gas pressure within the switch body is at 0.2MPa pressure. At pressures below 0.2MPa or above 0.2MPa, the calculated values for the jitter of the switch were seen to increase.

It can be concluded that in an air-filled field-distortion spark gap switch triggered by a Blumlein pulse generator, the time to breakdown can be reduced to 10s of nanoseconds and the jitter of the switch will be typically < 3ns for gas pressures 0.1MPa-0.4MPa. The gas pressures tested had little effect on the total time to breakdown for either of the inter-electrode gap lengths tested (2mm or 4mm). The level of DC stress applied across the main gap had very little influence on the measured time to breakdown in 2mm gap tests, however in 4mm gap tests, the difference in the measured time to breakdown for a gap stressed with 70% of the self-breakdown voltage is around 5%-25% longer as compared to the gap stressed with 80% of the self-breakdown voltage potential.

It can also be concluded that for smaller inter-electrode gap lengths filled with air i.e. 2mm, the jitter of the switch generally decreases as the gas pressure in the switch increases. However, for increased inter-electrode gap lengths (4mm) an apparent minimum in the calculated jitter is obtained when the gas pressure within the switch is 0.2MPa. This holds true for experimental conditions where the inter-electrode gap length is stressed with 70% or 80% of the self-breakdown voltage potential and thus, the level of DC stress has no apparent influence on the jitter of the switch.

### 5.3.2 Time to Breakdown for a N<sub>2</sub>-filled switch triggered with 1kV/ns HV impulses.

This section presents the results of the experimental investigation into the ‘time to breakdown’ and the jitter characteristics associated with the field-distortion spark gap switch triggered by means of the Blumlein pulse generator when the switch is filled with N<sub>2</sub> gas (99.9% purity).

Figure 5-5 presents the calculated, average time to breakdown measured for each of the gas pressures tested within the range 0.1MPa-0.4MPa.

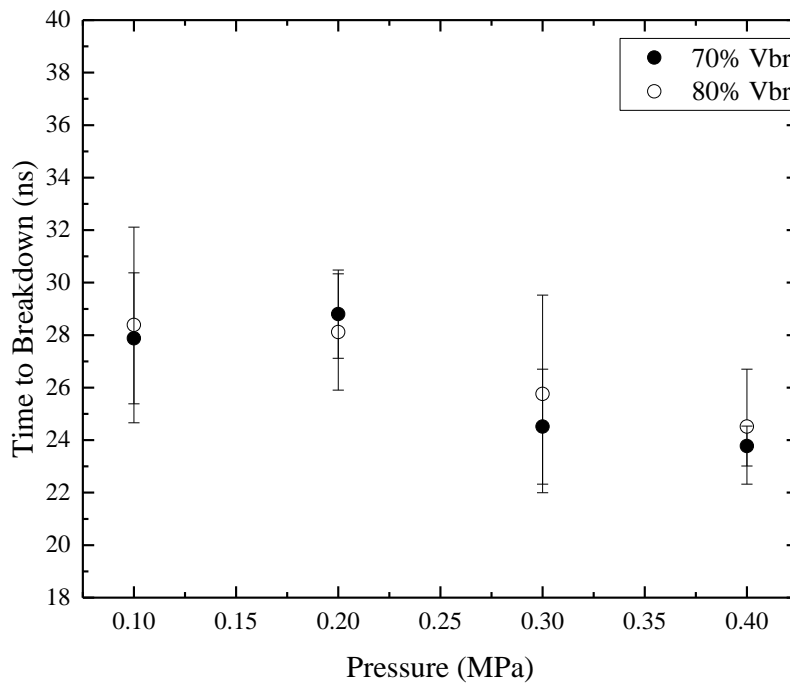


Figure 5-5 The average time to breakdown measured for a 2mm inter-electrode gap length filled with N<sub>2</sub> gas as a function of the gas pressure within the switch.

It can be seen from Figure 5-5 that between 0.1MPa and 0.2MPa gas pressure, there is no statistically significant change in the measured time to breakdown for the increase in gas pressure i.e. as be increasing the gas pressure from 0.1MPa to 0.2MPa, the time to breakdown remains constant. This is confirmed by the overlapping values of the standard

deviation in the time to breakdown as the gas pressure within the switch increases. However, the jitter of the switch decreases as gas pressure increases, a desirable quality of any gas-filled plasma closing switch.

With a 2mm inter-electrode gap space, the influence of the DC stress level applied across the gap length is again found to be small. For all but one of the pressures tested (0.2MPa) in the nitrogen-filled switch, stressed with 80% of the self-breakdown voltage there is a longer time to breakdown measured than under conditions where the gap is stressed with 70% of the self-breakdown voltage. This result was also observed in the breakdown tests presented with the longer trigger voltage impulse applied to the mid-plane electrode in Chapter 4 of this thesis. By stressing the inter-electrode gap length with 80% of the self-breakdown voltage, the time to breakdown was found to be ~1.8%-5% longer than the time to breakdown for the corresponding gas pressure in the switch when the gap was stressed with 70% of the self-breakdown voltage which corresponds to an increase in time to breakdown of 0.5ns-1.2ns respectively. Figure 5-6 presents the time to breakdown results measured in the field-distortion switch filled with N<sub>2</sub> for a 4mm inter-electrode gap length.

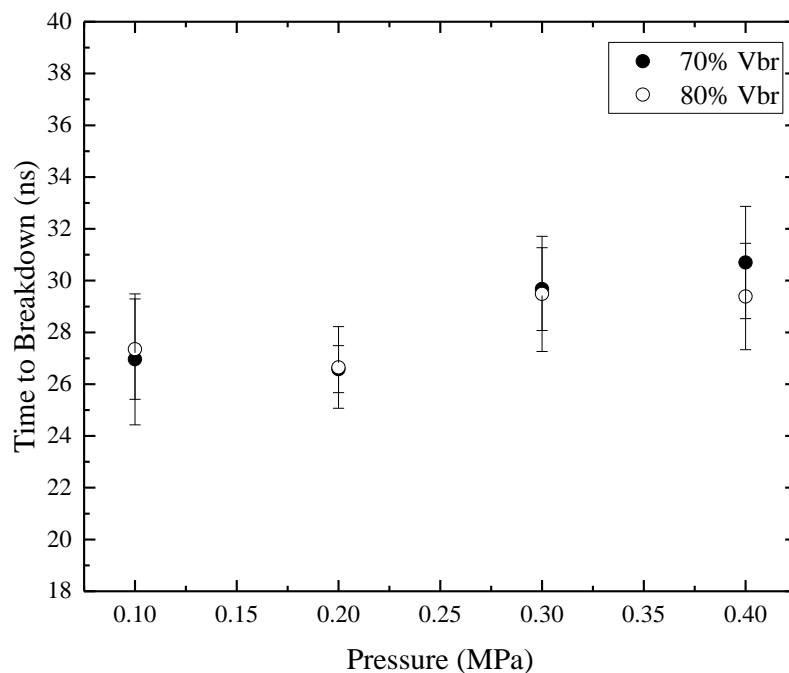
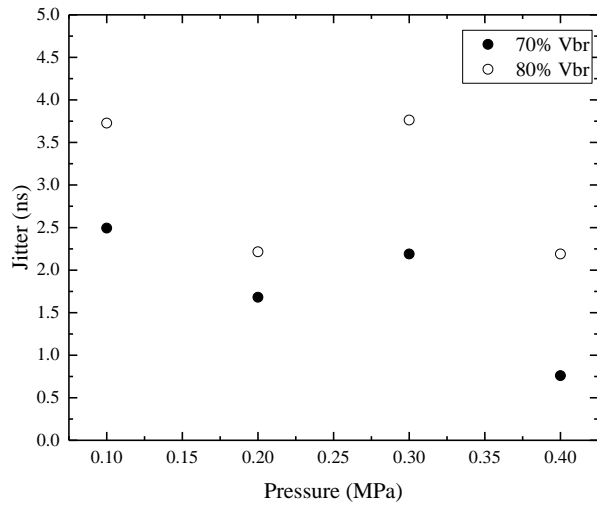


Figure 5-6 The average time to breakdown measured for a 4mm inter-electrode gap length filled with N<sub>2</sub> as a function of the gas pressure within the switch.

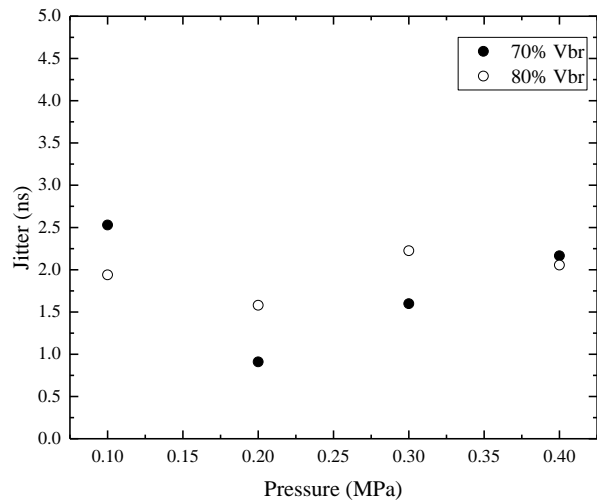
The total time to breakdown for a 4mm, N<sub>2</sub>-filled main gap length, as seen in Figure 5-6, does not change significantly as the gas pressure within the switch increases. The standard deviation of the time to breakdown results within the 4mm gap again shows that there is no significant difference in the time to breakdown as the gas pressure within the switch increases from 0.1MPa to 0.4MPa.

The effect of the DC stress level on the time to breakdown of a 4mm inter-electrode gap space filled with nitrogen is minimal as can also be seen in Figure 5-6. The difference in the time to breakdown calculated for each of the gas pressures 0.3MPa and under at 70% and 80% of the self-breakdown voltage DC stress applied is <1% or < 0.5ns. When the gas pressure within the switch was further increased to the maximum pressure tested, 0.4MPa, it was observed that the switch stressed with 70% of the self-breakdown voltage took longer to breakdown than the gap stressed with 80% of the self-breakdown voltage. The time to breakdown for the 0.4MPa pressure switch stressed with 70% of the self-breakdown voltage was ~1.31ns (~6%) longer than the gap stressed with 80% of the self-breakdown voltage.

The jitter of the switch has been plotted as a function of the gas pressure within the switch and has been plotted separately for each of the two levels of DC stress voltage applied across the gap length to determine any effect on the jitter that these experimental conditions may have. Figure 5-7 presents the jitter of the N<sub>2</sub> filled switch at (a) 2mm and (b) 4mm as a function of the gas pressure within the switch.



(a)



(b)

**Figure 5-7 The calculated Jitter for the field-distortion spark switch filled with N<sub>2</sub> when triggered with the Blumlein pulse generator as a function of gas pressure for (a) 2mm and (b) 4mm inter-electrode gap lengths.**

Figure 5-7(a) shows that the jitter of the 2mm inter-electrode gap length tends to decrease as the gas pressure increases from 0.1MPa-0.4MPa and that although observing an increase

in jitter when the gas pressure is increased between 0.2MPa and 0.3MPa, the jitter was found to be minimum at 0.4MPa (absolute) pressure.

When the inter-electrode gap space was increased to 4mm, the jitter as shown in Figure 5-7(b) did not show a decreasing trend as gas pressure increased. Instead what was observed in terms of jitter for the 4mm inter-electrode gap space filled with N<sub>2</sub> was similar to the results of the air-filled switch presented in section 5.3.1. The jitter was observed to be at a minimum level when the gas pressure within the switch body is at 0.2MPa pressure. At pressures below 0.2MPa or above 0.2MPa, the calculated values for the jitter of the switch were seen to increase.

For both the 2mm and the 4mm inter-electrode gap length filled with N<sub>2</sub>, it was also observed that when the main gap length is stressed with 80% of the self-breakdown voltage, the jitter of the switch is higher than the jitter calculated for conditions where breakdown occurred under 70% of the self-breakdown voltage being applied as a DC stress. Under all experimental conditions considered, the jitter of a nitrogen-filled field distortion gap was found to be between 1-5ns.

It can therefore be concluded that in a N<sub>2</sub>-filled field-distortion spark gap switch triggered by a Blumlein pulse generator, the time to breakdown is reduced to ~27ns in both the 2mm and the 4mm gap length experiments. For the 2mm and 4mm inter-electrode gap lengths, the time to breakdown can be considered to remain constant as the gas pressure within the switch increases when considering the standard deviation of the switch. The level of DC stress applied across the main gap had very little influence on the measured time to breakdown in 2mm gap tests, although the experiments conducted under conditions where the main inter-electrode gap was stressed with 80% of the self-breakdown voltage were found to take 0.5ns-1.2ns longer to breakdown than the gap which for the same gas pressure(s) stressed with only 70% of the self-breakdown voltage, an increase in time to breakdown of 2-5%. In the 4mm inter-electrode gap length tests, however, it was found that for the gap stressed with 80% of the self-breakdown voltage there was no statistical difference in the time to breakdown until the gas pressure in the switch reached 0.4MPa.

It can also be concluded for a N<sub>2</sub>-filled switch that for shorter inter-electrode gap lengths the jitter of the switch generally decreases as the gas pressure in the switch increases. For

4mm inter-electrode gap lengths, the jitter has its minimum value when the gas pressure within the switch is at 0.2MPa.

### **5.3.3 Time to Breakdown for a switch filled with a 60%/40% N<sub>2</sub>/O<sub>2</sub> mixture triggered with 1kV/ns HV impulses.**

This section presents the experimental results obtained when the field-distortion spark gap switch is filled with a gas mixture comprised of 60%/40% N<sub>2</sub>/O<sub>2</sub>. The results of the self-breakdown experiments conducted within Chapter 3 showed this particular gas mixture had a higher voltage hold-off capability than N<sub>2</sub> (99.9% purity) or bottled air with a much smaller standard deviation in breakdown voltages measured. The 60%/40% N<sub>2</sub>/O<sub>2</sub> mixture was also shown to be a reliably and predictably triggered gas in Chapter 4 under the triggered regime when the system was triggered with a voltage impulse with a slower rate of voltage rise.

As before, the time to breakdown across the switch was measured for the 60%/40% N<sub>2</sub>/O<sub>2</sub> mixture at increasing gas pressures within the range 0.1MPa – 0.4MPa (absolute). Breakdown events across the switch were initiated under conditions where the main inter-electrode gap was stressed with 70% and 80% of the self-breakdown voltage and the influence of the level of DC stress across the gap on the total time to breakdown has also been investigated.

Finally within this section, the jitter of the switch when filled with the 60%/40% N<sub>2</sub>/O<sub>2</sub> gas mixture and its dependence on both the gas pressure within the switch and the level of DC stress applied across the gap were investigated as separate breakdown characteristics.

Figure 5-8 presents the time to breakdown results of the 2mm inter-electrode gap length when filled with the 60%/40% N<sub>2</sub>/O<sub>2</sub> gas mixture as the gas pressure within the switch increases.

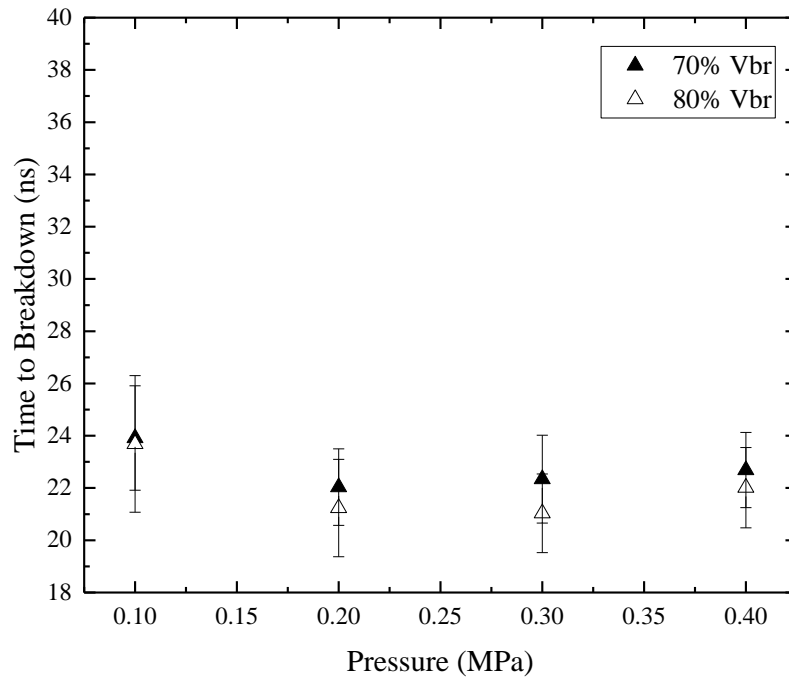


**Figure 5-8** The average time to breakdown measured for a 2mm inter-electrode gap length filled with the 60%/40% N<sub>2</sub>/O<sub>2</sub> gas mixture as a function of the gas pressure within the switch.

It is seen that the average time to breakdown is ~21-23ns with very little change in the time to breakdown as the gas pressure within the switch increases. The overlap of the standard deviation at each pressure suggests that there is no significant difference in the measured time to breakdown.

Figure 5-8 also shows that in the case of a 2mm inter-electrode gap filled with the 60%/40% N<sub>2</sub>/O<sub>2</sub> mixture, when the gap is stressed with 70% of the self-breakdown voltage, it will take longer to breakdown than if the gap is stressed with 80% of the self-breakdown voltage. The difference in the time to breakdown when the gap is stressed with 70% of the self-breakdown voltage has been calculated to be around 0.22-1.31ns longer than the corresponding breakdown events conducted at the same gas pressure under 80% DC stress levels which corresponds to an increase in the time to breakdown of ~0.9%-6%.

Figure 5-9 presents the average time to breakdown in the switch filled with the 60%/40% N<sub>2</sub>/O<sub>2</sub> mixture with a 4mm inter-electrode gap length.

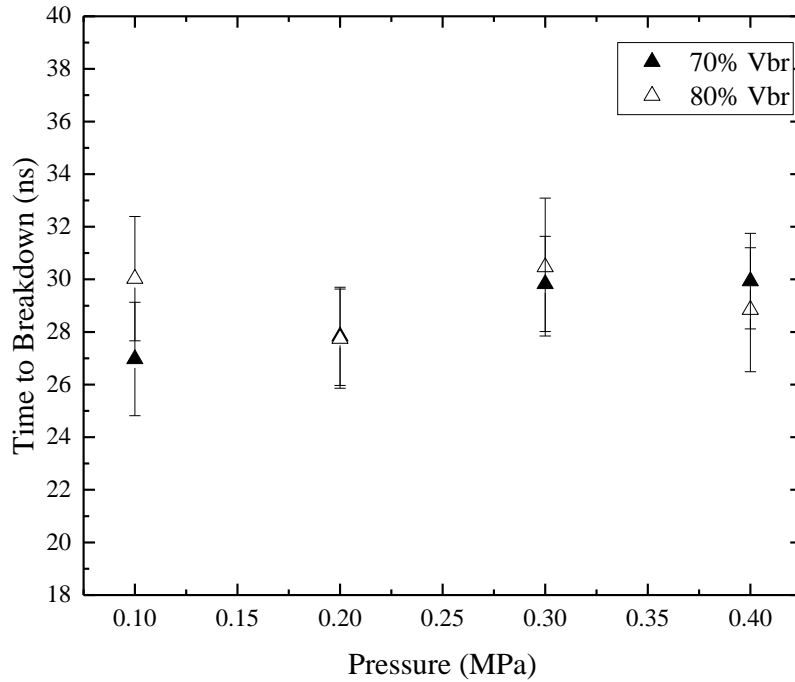


**Figure 5-9** The average time to breakdown measured for a 4mm inter-electrode gap length filled with the 60%/40% N<sub>2</sub>/O<sub>2</sub> gas mixture as a function of the gas pressure within the switch.

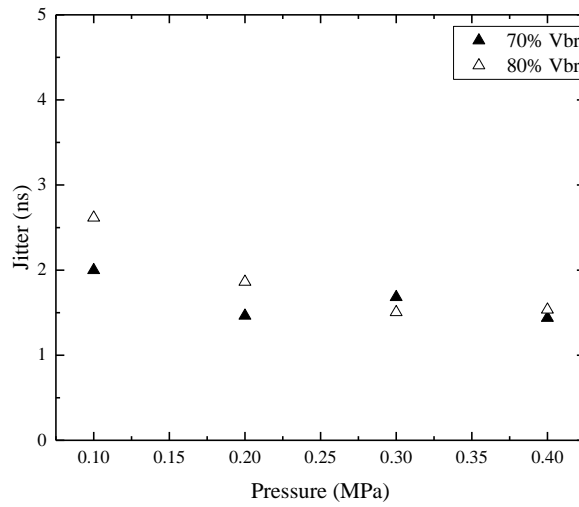
When the inter-electrode gap length within the switch is increased to 4mm, the measured time to breakdown for the gap filled with a mixture comprised of 60%/40% N<sub>2</sub>/O<sub>2</sub> behaves in a different way to 2mm inter-electrode gap length filled with the same gas and the results are presented within Figure 5-9. The measured time to breakdown in a 4mm inter-electrode gap length filled with the 60%/40% N<sub>2</sub>/O<sub>2</sub> mix are similar to those measured when the switch was filled with bottled air or N<sub>2</sub>. It is observed again that as the gas pressure increases within the switch body, there is no statistical difference in the observed time to breakdown measured, again confirmed by the overlapping range of standard deviation at each value of gas pressure.

It is shown in Figure 5-9 that when the gap length is stressed with 70% of the self-breakdown voltage, the time to breakdown measured increases from ~27ns to ~30ns as the gas pressure within the switch is increased from 0.1MPa (absolute) to 0.4MPa (absolute). When the level of DC stress voltage is increased to 80% of the self-breakdown voltage, the time to breakdown measured was not seen to significantly change as the gas

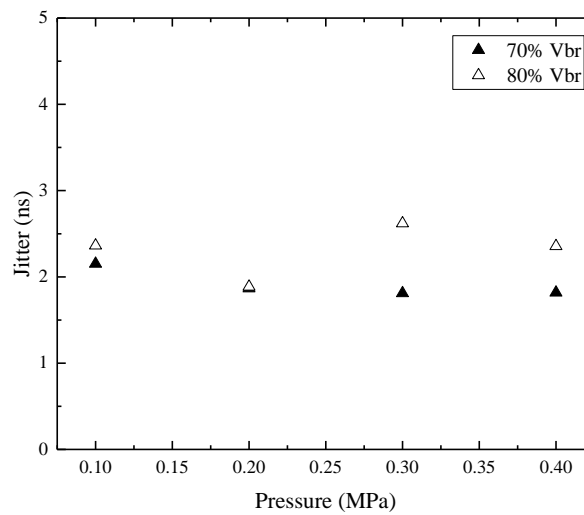
pressure within the switch increased from 0.1MPa to 0.4MPa and remained approximately ~29/30ns regardless of gas pressure within the test cell.

There is a small increase in the time to breakdown when the gap is stressed with 70% of the self-breakdown voltage compared to that where the main inter-electrode gap is stressed with 80% of the self-breakdown voltage. At 0.2MPa there was virtually no difference in the time to breakdown measured for the different levels of DC stress applied across the inter-electrode gap, however for other gas pressures, the increase in the time to breakdown measured is around 2%-11% longer in the 80% DC stress level experiments conducted which corresponds to breakdown events taking 0.5ns-3ns longer respectively.

The jitter for each of the inter-electrode gap lengths tested, both levels of DC stress applied across the gap length and the gas pressure within the switch are presented in Figure 5-10 to determine what effect, if any, changing these experimental parameters would have on the jitter of the switch.



(a)



(b)

**Figure 5-10 The jitter is presented when the field-distortion switch is filled the gas mixture comprised of 60%/40% N<sub>2</sub>/O<sub>2</sub>, the main inter-electrode gap length is (a) 2mm and (b) 4mm.**

Figure 5-10 (a) and (b) present the jitter for the 2mm and 4mm inter-electrode gap lengths filled with the 60%/40% N<sub>2</sub>/O<sub>2</sub> gas mixture respectively. For both gap lengths tested it is seen that the jitter level is < 3ns.

For a 2mm inter-electrode gap length, when the gap space is stressed with either 80% or 70% of the self-breakdown voltage level, the jitter was seen to decrease as gas pressure increased. The gap stressed with 80% of the self-breakdown voltage was calculated to have a higher jitter than the gap stressed with 70% of the self-breakdown voltage for lower pressures. As gas pressure in the switch increases, the jitter levels for 80% stress across the switch decrease and are statistically the same as the jitter of the switch under 70% DC stress voltage application.

When the inter-electrode gap length is increased to 4mm, the jitter calculated remains constant as the gas pressure within the switch is increased. Again it can be noted that the jitter is higher in the switch stressed with 80% of the self-breakdown voltage than the switch conditions stressed with 70% of the self-breakdown voltage although for the 4mm inter-electrode gap results, the difference in jitter is not significant.

In conclusion when the field distortion spark gap switch is filled with a mixture of 60%/40% N<sub>2</sub>/O<sub>2</sub>, the time to breakdown measured in a 2mm inter-electrode gap length remains constant as gas pressure increases and the jitter of the switch which is measured to be low at ~3ns was measured to decrease as the gas pressure increases. The level of DC stress applied across the 2mm inter-electrode gap had very little impact on the key breakdown characteristics of the switch although it was noted that while at lower pressures (0.1MPa and 0.2MPa) the jitter of the switch was higher when the gap was stressed with 80% of the self-breakdown voltage, as the gas pressure increased (0.3MPa – 0.4MPa) the jitter in the switch was statistically the same regardless of the level of DC stress applied across the inter-electrode gap.

At an inter-electrode gap length of 4mm, the time to breakdown was seen to increase as the gap length increased for 70% of the self-breakdown voltage applied as DC stress but for conditions where 80% of the DC stress voltage is applied, the measured time to breakdown remains statistically the same as the gas pressure increases. The jitter in the 4mm gap switch was found to remain at a constant level regardless of gas pressure within the switch.

### 5.3.4 Time to Breakdown for a switch filled with a 90%/10% Ar/O<sub>2</sub> mixture triggered with 1kV/ns HV impulses.

The time to breakdown and the jitter capability of the field distortion spark gap switch when triggered with the Blumlein pulse generator has also been measured for the switch when filled with the gas mixture comprised of 90%/10% Ar/O<sub>2</sub>. In previous breakdown experiments conducted, this gas mixture showed the lowest self-breakdown voltage (Chapter 3) and also had a large spread in breakdown voltages. The time to breakdown measured within Chapter 4 for this gas mixture under a longer voltage impulse applied to the mid-plane electrode provided the shortest time to breakdown of all gases tested, where breakdown was observed, but also showed the smallest jitter of all gases tested. Figure 5-11 presents the measured time to breakdown results for a 2mm inter-electrode gap filled with the 90%/10% Ar/O<sub>2</sub> mixture.

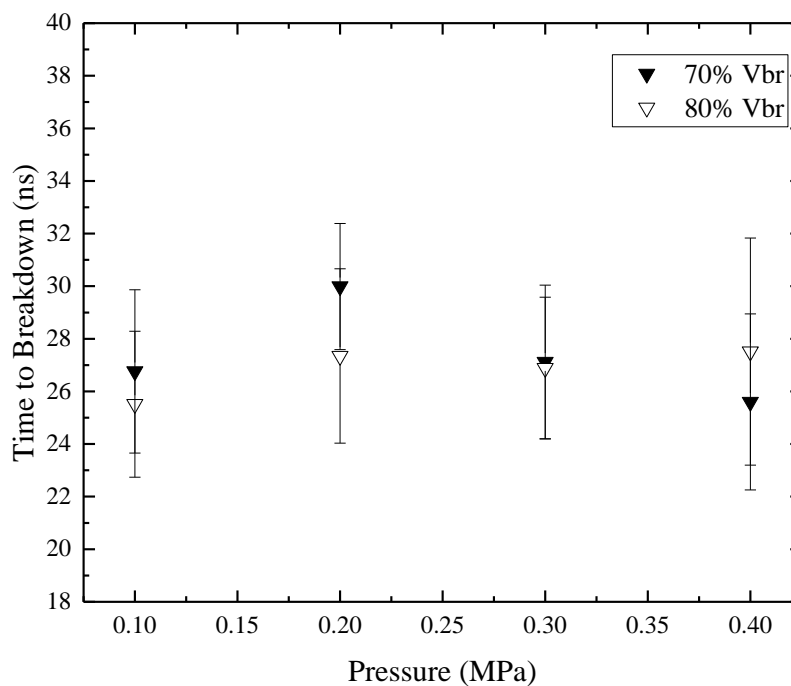
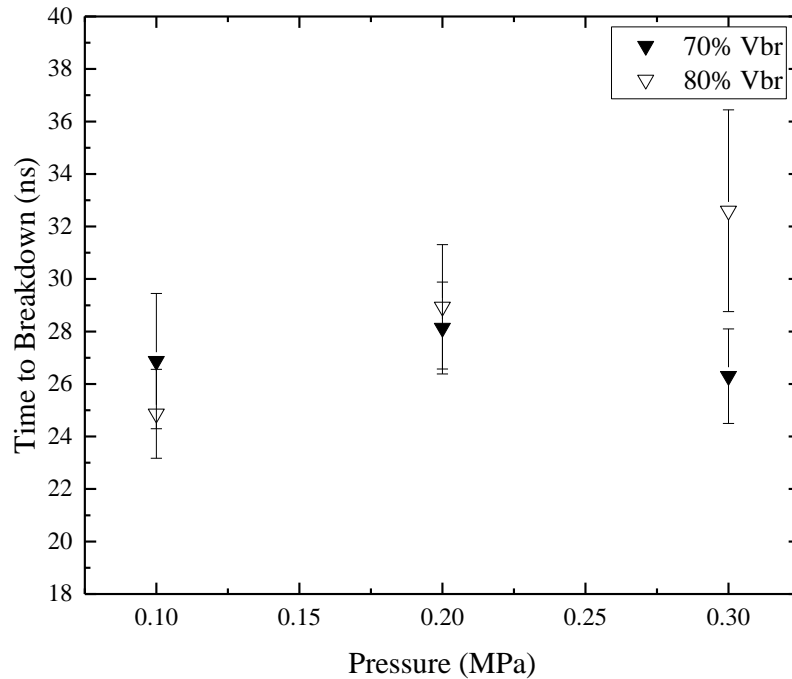


Figure 5-11 The average time to breakdown measured for a 2mm inter-electrode gap length filled with the 90%/10% Ar/O<sub>2</sub> gas mixture as a function of the gas pressure within the switch.

The time to breakdown was measured and is shown in Figure 5-11 to be ~25-28ns across the entire range of gas pressures within the switch and for both 70% and 80% of the self-breakdown voltage applied as a DC stress voltage.

As the gas pressure within the switch was increased from 0.1MPa to 0.4MPa, the measured time to breakdown is not impacted and is statistically considered to remain constant. Once again this conclusion is drawn from the fact that the standard deviation in the mean time to breakdown at each of the gas pressures overlaps which statistically suggests there is no significant difference in the measured time to breakdown at different gas pressures within the switch for this gas mixture. No significant change in the time to breakdown was measured when the DC stress level across the gap was altered from 70% to 80% of the self-breakdown voltage, however it was observed that at lower pressures tested, the gap stressed with 70% of the self-breakdown voltage took longer to reach complete breakdown than the gap stressed with 80% of the self-breakdown voltage potential. Below 0.3MPa, the gap stressed with 70% of the self-breakdown voltage was measured to take 0.2-2.5ns longer to breakdown than under conditions where the gap is stressed with 80% of the self-breakdown voltage for the same gas pressure which corresponds to an increased time to breakdown of 1-10%. The difference in the time to breakdown measured for the gap stressed with 70% with 80% of the self-breakdown voltage is also observed within Figure 5-11 to decrease as pressure increases towards 0.3MPa and as the gas pressure is further increased, the gap stressed with 80% of the self-breakdown voltage was measured to take 2ns longer to breakdown than the 70% stressed gap for the same pressure, an increase of ~7%.

Of the gases tested so far under Blumlein triggered breakdown conditions, when the inter-electrode gap space has been increased to the longer of the gap lengths tested (4mm), the behaviour of the time to breakdown measurements has been significantly changed from the behaviour when the main inter-electrode gap length is shorter (2mm). The time to breakdown measurements for the 4mm inter-electrode gap main gap length when filled with the 90%/10% Ar/O<sub>2</sub> mixture are presented within Figure 5-12 as a function of the gas pressure within the switch.

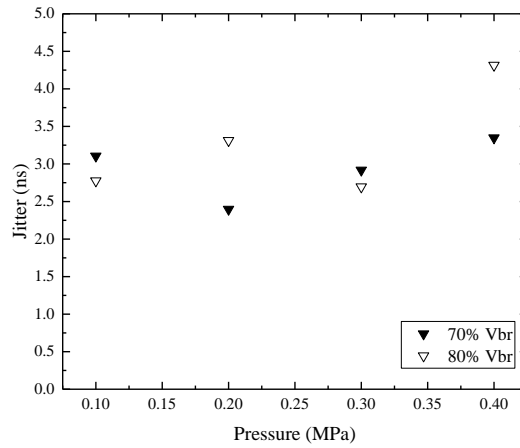


**Figure 5-12 The average time to breakdown measured for a 4mm inter-electrode gap length filled with the 90%/10% Ar/O<sub>2</sub> gas mixture as a function of the gas pressure within the switch.**

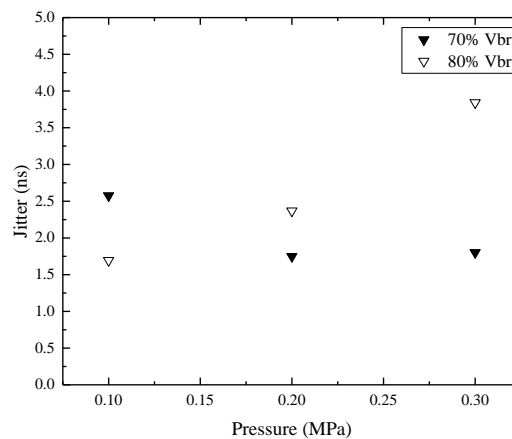
As the gas pressure within the switch body increases, the time to breakdown was measured and can be seen in Figure 5-12 to increase from ~25ns-32ns under experimental conditions where 80% of the self-breakdown voltage was applied as DC stress across the 4mm inter-electrode gap, however due to the large standard deviation in the time to breakdown result as the gas pressure increases, this time to breakdown can again be considered to statistically remain the same as the gas pressure within the switch increases from 0.1MPa-0.3MPa. Under experimental conditions where 70% of the self-breakdown voltage is applied, the time to breakdown measured was found to remain around the same level ~27ns for complete breakdown to occur as the gas pressure within the switch was increased. This time to breakdown remaining statistically unchanged as pressure increases is again confirmed by the overlap of the standard deviation in the time to breakdown values presented.

It can also be clearly seen in Figure 5-12 that the jitter of the switch when filled with the 90%/10% Ar/O<sub>2</sub> mixture is large for all gas pressures tested within the 4mm inter-electrode

gap length. Figure 5-13(a) and (b) presents the behaviour of the jitter calculated for the field-distortion spark gap switch when filled with the 90%/10% Ar/O<sub>2</sub> mixture for the 2mm and 4mm inter-electrode gap length respectively.



(a)



(b)

**Figure 5-13 The jitter is presented when the switch is filled with a mixture of 90%/10% Ar/O<sub>2</sub>, the main inter-electrode gap length is (a) 2mm and (b) 4mm and for both 70% and 80% of the self-breakdown voltage level applied across the main gap as a DC stress voltage.**

Figure 5-13(a) for a 2mm inter-electrode gap length filled with the 90%/10% Ar/O<sub>2</sub> mixture presented jitter that was calculated to be around 2.5ns-4.5ns for gas pressures tested. At pressures between 0.1MPa and 0.3MPa, the jitter is seen to remain around the same level

and the percentage level of DC stress voltage applied across the gap have little impact on the jitter of the switch. However, upon further increasing the gas pressure within the switch to 0.4MPa it was noted that the jitter was seen to increase for both levels of DC stress voltage applied across the gap. No conclusive evidence can be drawn on the influence of the level of DC stress voltage applied across the main inter-electrode gap length of 2mm impacts upon the jitter of a switch filled with the 90%/10% Ar/O<sub>2</sub> mixture as it can be seen that at half of the gas pressures tested, the gap stressed with 70% of the self-breakdown voltage showed higher levels of jitter than the gap stressed with 80% of the self-breakdown voltage and half of the gas pressures tested showed the opposite to be true.

For the jitter calculations carried out on the time to breakdown measurements conducted within the 4mm inter-electrode gap filled with the 90%/10% Ar/O<sub>2</sub> mixture, it can be seen in Figure 5-13(b) that when the gap is stressed with 70% of the self-breakdown voltage potential, the jitter was measured and observed to decrease when the gas pressure was increased from 0.1MPa and 0.2MPa (absolute) pressure. The jitter then remains at a constant value ~1.5ns as the gas pressure increases beyond the 0.2MPa pressure. Under the increased DC stress level conditions where 80% of the self-breakdown voltage is applied across the inter-electrode gap, the jitter is seen to increase almost linearly as the gas pressure within the switch also increases.

In summary, the findings of the experimental investigation into the time to breakdown and jitter characteristics of the field-distortion spark gap switch filled with the gas mixture comprised of 90%/10% Ar/O<sub>2</sub> showed that generally, as the gas pressure within the switch increased, the time to breakdown did not change. The jitter was low for both 2mm and 4mm inter-electrode gap lengths ~2.5-4.5ns and ~1.5-2.5ns respectively. No distinct conclusion can be made as to the influence or impact on the time to breakdown or the jitter of the switch when filled with the 90%/10% Ar/O<sub>2</sub> mixture due to the level of DC stress applied across the main inter-electrode gap as within the experimental restraints of this research project, no distinct trends were discernible from the obtained data.

### **5.3.5 Time to Breakdown for a CO<sub>2</sub>-filled switch triggered with 1kV/ns HV impulses.**

This section presents the time to breakdown data for the field-distortion spark gap switch when filled with CO<sub>2</sub>. CO<sub>2</sub> has been shown previously (Chapter 3 and 4) at the lower pressures of interest within this investigation to provide higher self-breakdown voltages (~6%-75% higher self-breakdown voltage for the same inter-electrode gap length and the same gas pressure) than air, N<sub>2</sub> or the 60%/40% N<sub>2</sub>/O<sub>2</sub> gas mixture but as the gas pressure increases, the self-breakdown performance is comparable to that of air, nitrogen and the 60%/40% N<sub>2</sub>/O<sub>2</sub> mixture. CO<sub>2</sub> has also been shown to have the highest standard deviation in terms of self-breakdown voltage, a less than desirable property for self-breakdown switching applications. When considered within Chapter 4 for triggered switching applications, CO<sub>2</sub> was shown to have comparable time to breakdown as other gases tested, however the jitter was calculated to be marginally higher than that for the other four gases tested.

Figure 5-14 presents the average time to breakdown as a function of the gas pressure within the switch for a 2mm inter-electrode gap length when filled with CO<sub>2</sub>.

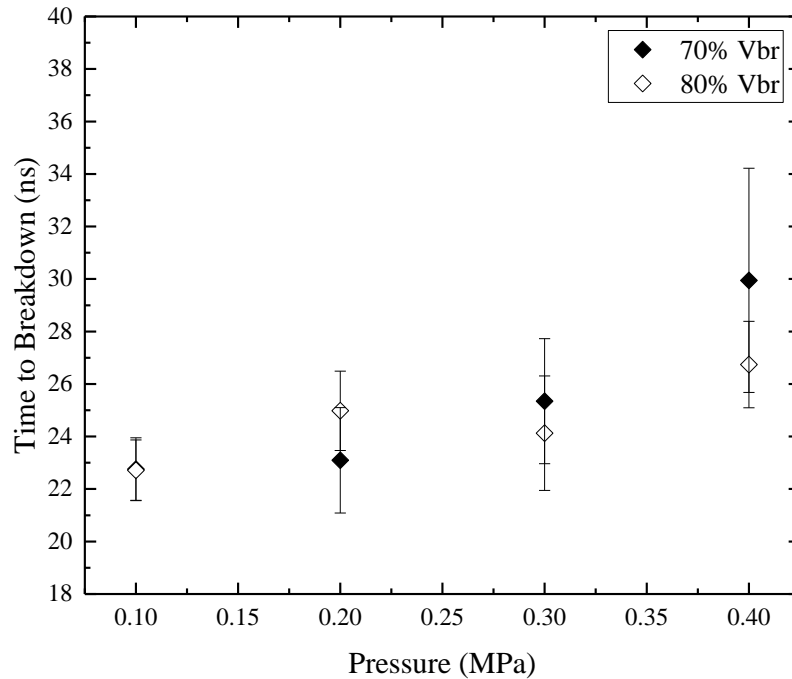


**Figure 5-14 The average time to breakdown measured for a 2mm inter-electrode gap length filled with the CO<sub>2</sub> gas as a function of the gas pressure within the switch.**

Figure 5-14 shows an increase in the measured time to breakdown from ~23ns to ~26-30ns depending upon the level of DC stress applied across the main gap as the gas pressure within the switch increases for a 2mm inter-electrode gap length. At 0.1MPa there is negligible difference in the measured time to breakdown between the gap stressed with 70% and 80% of the self-breakdown voltage. As the gas pressure within the switch increases, however, the difference in the time to breakdown becomes non-negligible and appears that when stressed with 70% of the self-breakdown voltage, the time between initiation of the voltage impulse on the mid-plane triggering electrode and complete voltage collapse across the gap is ~1.2-3.2ns longer (~5-11% longer) than the corresponding time required for breakdown in a gap stressed with 80% of the self-breakdown voltage.

Figure 5-15 presents the time to breakdown measurements in the field-distortion switch filled with CO<sub>2</sub> when the inter-electrode gap length is increased to 4mm.

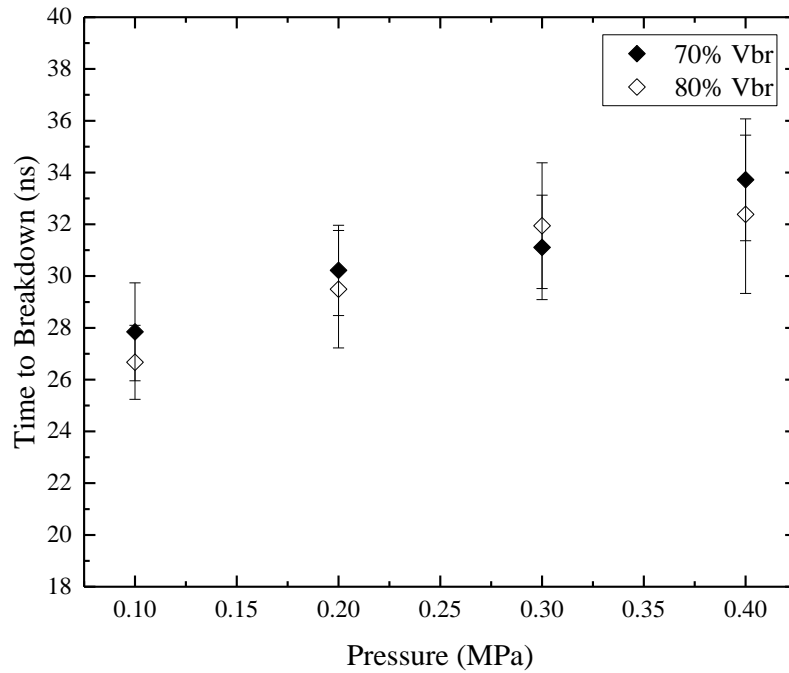
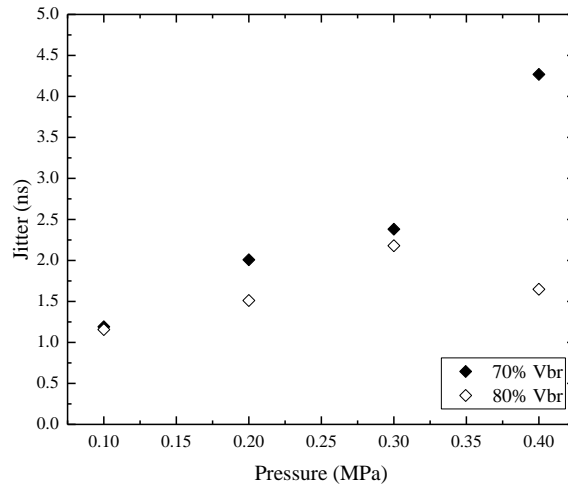


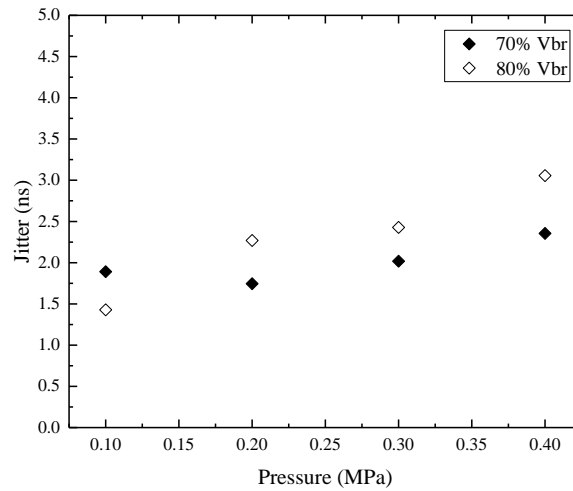
**Figure 5-15** The average time to breakdown measured for a 4mm inter-electrode gap length filled with the CO<sub>2</sub> gas as a function of the gas pressure within the switch.

It can be seen that for CO<sub>2</sub>, the measured time to breakdown is seen to increase as the gas pressure within the switch increases. It can also be reasoned from Figure 5-15 that when stressed with 70% of the self-breakdown voltage level, the measured time to breakdown of a CO<sub>2</sub> filled switch will be longer than that of the switch under the same gas pressure when stressed with 80% of the self-breakdown voltage at higher pressures. On average it was found that under stress equal to 70% of the self-breakdown voltage, the CO<sub>2</sub> filled switch took ~4% longer for breakdown to occur than the measured time when the experimental conditions meant the inter-electrode gap was stressed with 80% of the self-breakdown voltage potential.

As is clear from both Figure 5-14 and Figure 5-15, the standard deviation of the time to breakdown in a CO<sub>2</sub>-filled switch (the jitter of the switch) appears high when compared to the calculated time to breakdown. Figure 5-16(a) and (b) presents the jitter of the switch as a function of the gas pressure for the different inter-electrode gap lengths tested.



(a)



(b)

**Figure 5-16 The jitter is presented when the switch is filled with CO<sub>2</sub>, the main inter-electrode gap length is (a) 2mm and (b) 4mm and for both 70% and 80% of the self-breakdown voltage level applied across the main gap as a DC stress voltage as a function of gas pressure.**

The jitter of a 2mm inter-electrode gap length, as shown in Figure 5-16(a), can be seen to increase as the gas pressure within the test cell increases from 0.1MPa to 0.4MPa. The calculated jitter in all bar one case was found to be < 2.5ns despite the increasing trend as the gas pressure increased. It can also be seen that for all gas pressures tested, the experimental conditions under which the inter-electrode gap distance is stressed with 70%

of the self-breakdown voltage presents the highest jitter values suggesting that for more stable and predictable operation of the switch when the main inter-electrode gap length is 2mm, stressing the gap with 80% of the self-breakdown voltage would provide both the shortest time to breakdown and the lowest jitter.

When the main inter-electrode gap length is increased to 4mm, the jitter is still seen to increase proportionally from 1.5ns to 3ns as the gas pressure within the switch increases. However for this inter-electrode distance it is seen that the gap stressed with 80% of the self-breakdown voltage provided the highest jitter values. For practical applications this may mean that when considering a 4mm inter-electrode gap length filled with CO<sub>2</sub> and triggered by fast-rising impulses, one characteristic may have to be favoured over another, for example, the time to breakdown may be required to be as short as possible and marginally higher jitter levels could be acceptable therefore stressing the 4mm inter-electrode gap with 80% of the self-breakdown voltage would be the optimum solution. If the lowest jitter possible was required for the gap then low pressure CO<sub>2</sub>, stressed with 70% of the self-breakdown voltage would give the lowest jitter at the cost of an increase in the time to breakdown of a few nanoseconds.

This experimental investigation into the time to breakdown and jitter characteristics of the field-distortion spark gap switch filled with CO<sub>2</sub> and triggered by the Blumlein pulse generator have shown a mixture of results from which recommendations for practical applications can be made based upon desired outputs.

Generally, however the jitter of a CO<sub>2</sub> filled switch is comparable if not slightly higher than the other gases tested within this experimental investigation and the time for complete breakdown to occur within the switch is of the order of each of the other gases tested.

### **5.3.6 Jitter Analysis**

The jitter observed for each of the gases is a key characteristic for the performance and reliability of switches. In many areas of pulsed power research, a fundamental aim of the performance of the switch is to minimise the jitter as far as possible.

Table 5-1 contains the average jitter values for each of the inter-electrode gap lengths which have previously been presented within this section.

**Table 5-1 Jitter for the field-distortion spark gap switch when triggered with the Blumlein pulse generator and filled with each of the five different gases.**

<b>Jitter (ns)</b>	<b>Air</b>	<b>N<sub>2</sub></b>	<b>60% N<sub>2</sub> + 40% O<sub>2</sub></b>	<b>90% Ar + 10% O<sub>2</sub></b>	<b>CO<sub>2</sub></b>
<b>2mm</b>	2.43	2.97	1.88	3.27	1.62
<b>4mm</b>	2.56	1.78	1.65	2.94	2.46

As can be seen from Table 5-1 the lowest jitter in the 2mm inter-electrode gap length was demonstrated by the CO<sub>2</sub> filled switch, while in the 4mm gap length, the 60%/40% N<sub>2</sub>/O<sub>2</sub> mixture had the lowest jitter unlike the jitter in the case of triggering impulses with the slower rate of voltage rise presented in Chapter 4 where the 90%/10% Ar/O<sub>2</sub> mixture provided the lowest jitter values. The highest jitter values in the case of the faster Blumlein trigger pulses have been obtained for the air-filled switch and the switch filled with the 90%/10% Ar/O<sub>2</sub> gas mixture.

For all gases tested the jitter was observed to increase as the gas pressure within the switch increased which suggests that for a more reliable and predictable triggering operation, regardless of gas used, if making use of a fast rate of voltage rise impulse, lower gas pressures within the switch are optimal for minimising jitter.

## **5.4 Statistical Analysis**

As with the experimental results in Chapter 4, each of the sets of experimental results obtained for the time to breakdown in the field-distortion spark gap switch when filled with each of the five different gases; air, N<sub>2</sub>, 60%/40% N<sub>2</sub>/O<sub>2</sub>, 90%/10% Ar/O<sub>2</sub> and CO<sub>2</sub> and triggered by the Blumlein pulse generator, presented within Chapter 5.3 have been analysed using a Weibull statistical approach. As discussed in Chapter 4 the Weibull distribution can be used for statistical analysis of unreliability of dielectric systems (breakdown events in gases and liquids). Similar to the Weibull analysis of the time to breakdown in the field distortion switch triggered with slow 0.45 kV/μs impulses, a similar

approach (applying Equation 4.3 to the results obtained within this Chapter) was used in this chapter for statistical analysis of the time to breakdown data in the switch triggered with fast 1kV/ns impulses.

This section presents the Weibull analysis conducted for both the 2mm and 4mm inter-electrode gap lengths stressed with 70% and 80% of the self-breakdown voltage potential and then triggered by the Blumlein pulse generator. A comparison of  $\alpha$  (ns),  $\beta$  and  $\gamma$  (ns) the scale, shape and location parameters for the different combinations of experimental conditions is given and this allows for a direct comparison of all gases tested.

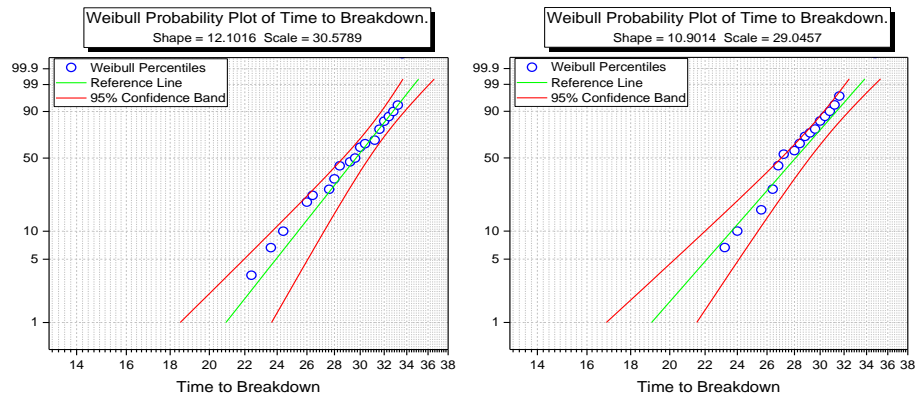
Weibull distribution graphs showing the unreliability of breakdown events occurring for each of the five gases tested; air, N<sub>2</sub>, 60%/40% N<sub>2</sub>/O<sub>2</sub>, 90%/10% Ar/O<sub>2</sub> and CO<sub>2</sub> for each of the gas pressures tested within the range 0.1MPa-0.4MPa are presented. A table of coefficients for each of the respective gas pressures and inter-electrode gap lengths is compiled which provides a direct comparison of the scale and shape coefficients of each of the gases and the 95% confidence intervals for breakdown occurring at a specified time.

#### **5.4.1 Weibull Analysis of a 2mm inter-electrode gap length**

This section presents the Weibull probability plots of breakdown events occurring in a 2mm inter-electrode gap length. The Weibull analysis has been conducted on the measured time to breakdown recorded within a 2mm inter-electrode gap length for each of the five gases tested using Origin Pro graphing software; air, N<sub>2</sub>, 60%/40% N<sub>2</sub>/O<sub>2</sub>, 90%/10% Ar/O<sub>2</sub> and CO<sub>2</sub> at a specified gas pressure under a DC stress application of 70% or 80% of the self-breakdown voltage. A table is provided of the three of the Weibull coefficients for each of the gases at the fixed gas pressure at both levels of DC stress voltage application which allows for a direct comparison of the time to breakdown characteristics of the gases.

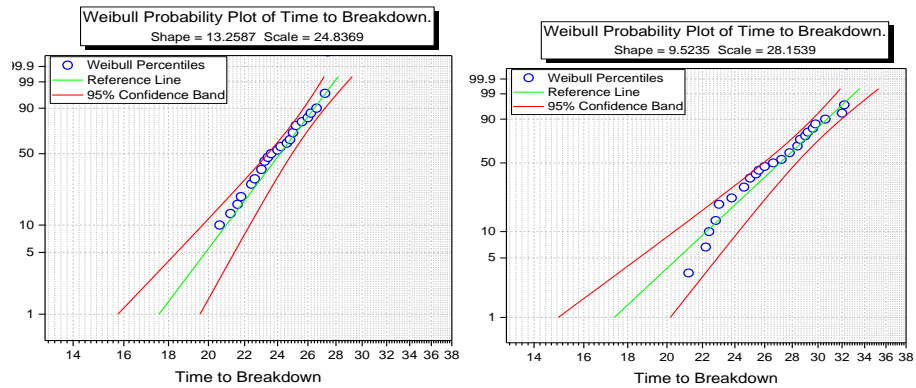
Figure 5-17 and 5-18 provides the Weibull unreliability plots for breakdown events when 70% and 80% of the self-breakdown voltage are applied across the 2mm inter-electrode gap length respectively in a switch filled with (a) air, (b) N<sub>2</sub>, (c) 60%/40% N<sub>2</sub>/O<sub>2</sub>, (d) 90%/10% Ar/O<sub>2</sub> and (e) CO<sub>2</sub> at 0.1MPa. Each open symbol represents a single breakdown event. The green line is a reference line with the parameters of the scale, shape and location extracted

from the Weibull fit line and the red lines on either side represent the 95% confidence bands, that is, the band within which 95% of the breakdown events are predicted to occur.



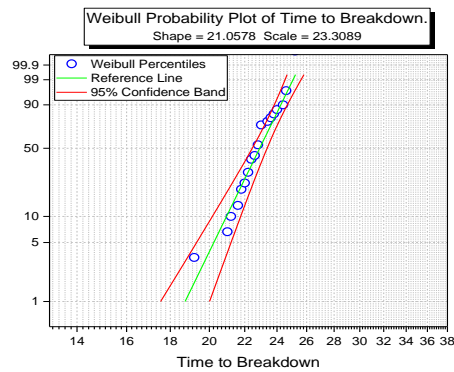
(a)

(b)



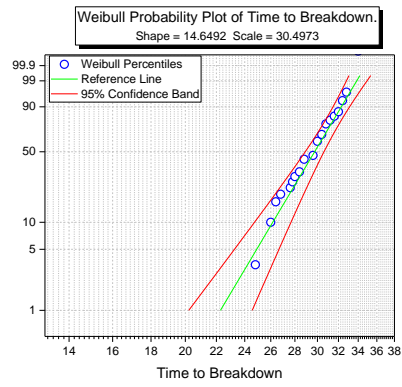
(c)

(d)

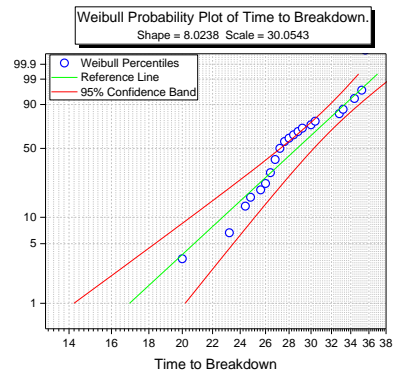


(e)

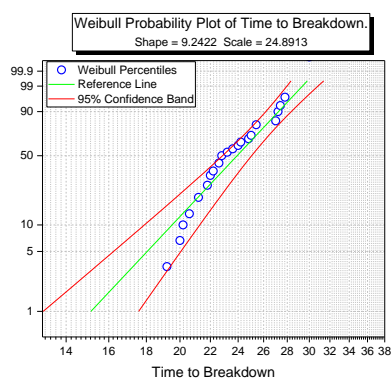
Figure 5-17 Weibull analysis for 70% DC stress applied across 2mm gap at 0.1MPa pressure.



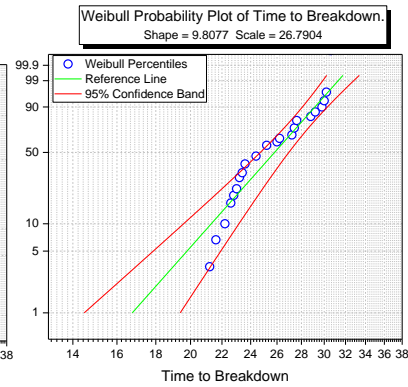
(a)



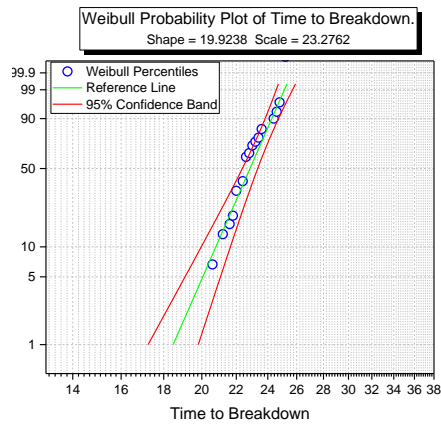
(b)



(c)



(d)



(e)

Figure 5-18 Weibull analysis for 80% DC stress applied across 2mm gap at 0.1MPa pressure.

**Table 5-2 Weibull Parameters for the five gases tested within the 2mm inter-electrode gap space at a gas pressure of 0.1MPa.**

	<b>Air</b>	<b>N<sub>2</sub></b>	<b>60%/40% N<sub>2</sub>/O<sub>2</sub></b>	<b>90%/10% Ar/O<sub>2</sub></b>	<b>CO<sub>2</sub></b>
<b><i>2mm 70% V<sub>br</sub></i></b>					
<b><i>Scale - <math>\alpha</math> (ns)</i></b>	30.58	29.05	24.84	28.15	23.31
95% confidence interval	29.75-31.40	28.17-29.92	24.22-25.45	27.18-29.12	22.95-23.67
<b><i>Shape - <math>\beta</math></i></b>	12.10	10.90	13.26	9.52	21.06
95% confidence interval	9.08-15.12	8.54-13.27	10.09-16.42	7.26-11.79	16.23-25.89
<b><i>Intercept - <math>\gamma</math> (ns)</i></b>	3.42	3.38	3.21	3.34	3.15
95% confidence interval	3.39 – 3.45	3.35 – 3.41	3.19 – 3.23	3.31 – 3.37	3.13 – 3.17
<b><i>2mm 80% V<sub>br</sub></i></b>					
<b><i>Scale - <math>\alpha</math> (ns)</i></b>	30.50	30.05	24.89	26.79	23.28
95% confidence interval	29.81-31.18	28.82-31.29	24.00-25.78	25.89-27.69	22.89-23.66
<b><i>Shape - <math>\beta</math></i></b>	14.65	8.02	9.24	9.81	19.92
95% confidence interval	11.18-18.12	6.16-9.89	7.14-11.34	7.49-12.13	15.39-24.46
<b><i>Intercept - <math>\gamma</math> (ns)</i></b>	3.42	3.40	3.21	3.29	3.15
95% confidence interval	3.40 – 3.44	3.37 – 3.43	3.18 – 3.24	3.26 – 3.32	3.13 – 3.17

As previously discussed within Chapter 4 and outlined within the IEC standard 62539 [141], the value of  $\beta$ , the shape parameter, is related to the range of times over which a breakdown event could occur. The larger the value of  $\beta$ , the smaller the range of potential times where breakdown could be expected to occur, thus, the larger the value of  $\beta$ , the more stable and reliably predictable the time to breakdown is.

As can be seen from Table 5-2, a comparison of the three Weibull parameters obtained from analysis of the time to breakdown measurements in a 2mm inter-electrode gap filled with each of the gases to a pressure of 0.1MPa (absolute), when the test cell is filled with CO<sub>2</sub>, the  $\beta$  value obtained from Weibull analysis is much larger than the value from any of the other gases. This is true for experimental conditions where the main inter-electrode gap length is stressed with 70% of the self-breakdown voltage and when stressed with 80% of the self-breakdown voltage.

The other Weibull parameter of interest is the value of  $\gamma$  which in the context of this experimental investigation is the minimum time at which the probability of a breakdown event occurring is non-zero. It is found that for increasing the level of DC stress applied across the main inter-electrode gap, the minimum time at which a breakdown could occur does not change in three of the gases (air, 60%/40% N<sub>2</sub>/O<sub>2</sub> mixture and CO<sub>2</sub>) and for the other two gases tested (N<sub>2</sub> and 90%/10% Ar/O<sub>2</sub>) the change is found to be  $\sim 10$ s of ps difference. For all five gases tested, the minimum time at which the probability of a breakdown is non-zero was found to be  $\sim 3.13$ - $3.45$ ns in a 2mm inter-electrode gap at a gas pressure of 0.1MPa.

Weibull analysis has been conducted, as in Chapter 4, for both 2mm and 4mm inter-electrode gap distances stressed with both 70% and 80% of the DC self-breakdown voltage of the gas at each pressure. The Weibull breakdown graphs for each gas, inter-electrode gap distance, gas pressure and DC stress voltage level other than 2mm inter-electrode gap distance at 0.1MPa pressure can be found within Appendix 1. The key values of scale  $\alpha$ , shape,  $\beta$ , and the intercept,  $\gamma$ , are presented in the following tables and discussed.

**Table 5-3 Weibull Parameters for the five gases tested within the 2mm inter-electrode gap space at a gas pressure of 0.2MPa.**

	<b>Air</b>	<b>N<sub>2</sub></b>	<b>60%/40% N<sub>2</sub>/O<sub>2</sub></b>	<b>90%/10% Ar/O<sub>2</sub></b>	<b>CO<sub>2</sub></b>
<b><i>2mm 70% V<sub>br</sub> – 0.2MPa</i></b>					
<b><i>Scale - <math>\alpha</math> (ns)</i></b>	11.07	20.17	16.09	14.96	13.37
95% confidence interval	8.07 – 13.43	15.28–25.06	12.32-19.86	11.34-18.58	10.07-16.67
<b><i>Shape - <math>\beta</math></i></b>	32.30	29.57	22.73	31.05	24.00
95% confidence interval	31.33–33.27	29.09–30.04	22.27–23.18	30.37-31.72	23.41-24.59
<b><i>Intercept - <math>\gamma</math></i></b>	3.48	3.39	3.12	3.44	3.18
95% confidence interval	3.45 – 3.51	3.37 – 3.41	3.10-3.14	3.42-3.46	3.16-3.20
<b><i>2mm 80% V<sub>br</sub> – 0.2MPa</i></b>					
<b><i>Scale - <math>\alpha</math> (ns)</i></b>	14.65	8.02	9.24	9.81	19.92
95% confidence interval	11.18-18.11	6.15-9.89	7.13-11.35	7.48-12.14	15.38-24.46
<b><i>Shape - <math>\beta</math></i></b>	30.50	30.05	24.89	26.79	23.27
95% confidence interval	28.81-31.29	28.81-31.29	24.00-25.77	25.89-27.69	22.88-27.69
<b><i>Intercept - <math>\gamma</math></i></b>	3.42	3.40	3.21	3.29	3.15
95% confidence interval	3.30 – 3.43	3.18-3.24	3.18-3.24	3.26-3.32	3.13-3.17

Table 5-3 presents the Weibull parameters obtained by applying the three-parameter Weibull analysis to the time to breakdown measurements of the 2mm inter-electrode gap length filled with each of the five gases respectively to a pressure of 0.2MPa (absolute).

The main parameter value of interest is the value of  $\beta$  which determines the range of times over which a breakdown is likely to occur. The 95% confidence intervals are also shown for each of the Weibull parameter values obtained for each of the gases. At 0.2MPa pressure, the largest value of  $\beta$ , corresponding to the smallest range of times over which breakdown

is likely to occur was found to be in the switch filled with the bottled air for both the 70% and 80% of the self-breakdown voltage level of DC stress applied across the main inter-electrode gap length. This observation of the smallest range of potential 'time to breakdown' measurements observed within the air-filled switch was shown within Chapter 4 when it was seen that the  $\beta$  value of bottled air was statistically one of the largest values observed (air, N<sub>2</sub> and the 60%/40% N<sub>2</sub>/O<sub>2</sub> mixture provided almost identical  $\beta$  values).

It is also of interest to note another observation with the faster triggering impulse application; the  $\beta$  values obtained for the switch filled with the 90%/10% Ar/O<sub>2</sub> mixture are the second largest values of the gases tested under both DC stress level conditions.

The minimum time at which the probability of a breakdown occurring is non-zero for all gases tested at 0.2MPa fell within the range 3.10-3.50ns, the same timeframe as at the lower pressure of 0.1MPa suggesting that by increasing the gas pressure within the switch from 0.1MPa to 0.2MPa there is no impact on the minimum time required before breakdown can be initiated within the switch.

**Table 5-4 Weibull Parameters for the five gases tested within the 2mm inter-electrode gap space at a gas pressure of 0.3MPa.**

	<b>Air</b>	<b>N<sub>2</sub></b>	<b>60%/40% N<sub>2</sub>/O<sub>2</sub></b>	<b>90%/10% Ar/O<sub>2</sub></b>	<b>CO<sub>2</sub></b>
<b><i>2mm 70% V<sub>br</sub> – 0.3MPa</i></b>					
<b><i>Scale - <math>\alpha</math> (ns)</i></b>	12.87	8.35	14.61	9.75	12.43
95% confidence interval	9.93 – 15.81	6.75 - 9.95	11.07-18.14	7.49-12.01	9.35-15.51
<b><i>Shape - <math>\beta</math></i></b>	30.57	25.61	23.13	28.46	26.42
95% confidence interval	29.79-31.35	24.59–26.62	22.60-23.66	27.49-29.42	25.72-27.11
<b><i>Intercept - <math>\gamma</math></i></b>	3.42	3.24	3.14	3.35	3.27
95% confidence interval	3.39-3.45	3.21-3.27	3.12-3.16	3.32-3.38	3.24-3.30
<b><i>2mm 80% V<sub>br</sub> – 0.3MPa</i></b>					
<b><i>Scale - <math>\alpha</math> (ns)</i></b>	12.91	27.48	9.89	12.95	11.43
95% confidence interval	9.70-16.12	23.12-31.71	8.02-11.76	9.76-16.14	8.80-14.06
<b><i>Shape - <math>\beta</math></i></b>	29.51	6.53	21.83	28.01	25.15
95% confidence interval	28.76-30.26	3.47-12.26	21.10-22.56	27.31-28.71	24.42-25.88
<b><i>Intercept - <math>\gamma</math></i></b>	3.38	3.14	3.08	3.33	3.23
95% confidence interval	3.36-3.40	3.17-3.46	3.05-3.11	3.31-3.35	3.20-3.26

Table 5-4 presents the Weibull parameters obtained by applying the three-parameter Weibull analysis to the time to breakdown measurements of the 2mm inter-electrode gap length filled with each of the five gases respectively to a pressure of 0.3MPa (absolute).

The Weibull parameter  $\beta$ , which determines the width of the range of times where breakdown is likely to occur and the corresponding 95% confidence intervals associated with that value are shown within Table 5-4. At 0.3MPa pressure, the largest value of  $\beta$  which corresponds to the smallest range of times over which breakdown is likely to occur

was found to be in the switch filled with the bottled air for both the 70% and 80% of the self-breakdown voltage level of DC stress applied across the main inter-electrode gap length as was observed within the analysis of the time to breakdown measurements at 0.2MPa pressure. For DC stress application across the main inter-electrode gap length of 70% of the self-breakdown voltage and 80% of the self-breakdown voltage, the bottled air time to breakdown provided the smallest value of shape parameter  $\beta$  in the Weibull analysis. The value of  $\beta$  is significantly smaller for the N<sub>2</sub> filled switch at 80% DC stress level than for 70% DC stress level applied across the main inter-electrode gap due the smaller number of breakdown events that were able to be initiated.

The minimum time at which the probability of a breakdown occurring is non-zero for all gases tested at 0.2MPa, the value of the intercept  $\gamma$ , fell within the range 3.05-3.45ns, the same timeframe as both lower pressure of 0.1MPa and 0.2MPa. This result suggests that for a 2mm inter-electrode gap length, the gas pressure within the switch does not have an impact on the minimum time required before breakdown can be initiated within the switch. The probability of a breakdown occurring within the switch at a time shorter than  $\sim 3$ ns is zero for any gas pressure 0.1MPa or above.

**Table 5-5 Weibull Parameters for the five gases tested within the 2mm inter-electrode gap space at a gas pressure of 0.4MPa.**

	<b>Air</b>	<b>N<sub>2</sub></b>	<b>60%/40% N<sub>2</sub>/O<sub>2</sub></b>	<b>90%/10% Ar/O<sub>2</sub></b>	<b>CO<sub>2</sub></b>
<b><i>2mm 70% V<sub>br</sub> – 0.4MPa</i></b>					
<b><i>Scale - <math>\alpha</math> (ns)</i></b>	13.55	37.67	16.97	27.15	8.26
95% confidence interval	10.29-16.81	28.36-46.98	13.01-20.93	25.93-28.37	6.20-10.32
<b><i>Shape - <math>\beta</math></i></b>	29.36	24.13	23.37	7.29	31.79
95% confidence interval	28.65-30.07	23.93-24.33	22.91-23.83	5.68-8.90	30.53-33.04
<b><i>Intercept - <math>\gamma</math></i></b>	3.38	3.18	3.15	3.30	3.46
95% confidence interval	3.36-3.40	3.16-3.20	3.13-3.17	3.25-3.35	3.43-3.49
<b><i>2mm 80% V<sub>br</sub> – 0.4MPa</i></b>					
<b><i>Scale - <math>\alpha</math> (ns)</i></b>	17.17	8.35	12.35	6.66	18.49
95% confidence interval	13.21-21.12	6.75-9.95	9.77-14.93	5.11-8.21	14.06-22.92
<b><i>Shape - <math>\beta</math></i></b>	28.74	25.61	22.79	29.40	27.50
95% confidence interval	28.20-29.28	24.59-26.62	22.18-23.40	27.96-30.84	27.01-30.84
<b><i>Intercept - <math>\gamma</math></i></b>	3.36	3.24	3.13	3.38	3.31
95% confidence interval	3.34-3.38	3.21-3.27	3.10-3.16	3.33-3.43	3.29-3.23

Table 5-5 presents the Weibull parameters obtained by applying the three-parameter Weibull analysis to the time to breakdown measurements of the 2mm inter-electrode gap length filled with each of the five gases respectively to a pressure of 0.4MPa (absolute).

The Weibull shape parameter  $\beta$  that determines the size of the range of times over which a breakdown is likely to occur and the 95% confidence intervals are shown within Table 5-5. At 0.4MPa pressure, the largest value of  $\beta$  which corresponds to the smallest range of times over which breakdown is likely to occur was found to be in the switch filled with CO<sub>2</sub> for the gap stressed with 70% of the self-breakdown voltage, however the value of  $\beta$  for the bottled air filled switch was close in magnitude (31.79 in CO<sub>2</sub> and 29.36 for air). When the

gap was stressed with 80% of the self-breakdown voltage, the value of  $\beta$  was found to be largest for the air-filled switch as has been seen at other gas pressures within the 2mm gap.

The intercept value,  $\gamma$  which corresponds to the minimum time at which the probability of a breakdown event occurring is non-zero falls within the range 3.10-3.40ns when the gas pressure within the switch was 0.4MPa for each of the gases tested.

Overall it has been shown within this section that generally the largest value of the shape parameter,  $\beta$ , which corresponds to a smaller range of potential times where breakdown is likely to occur in a 2mm inter-electrode gap that has been filled with bottled air. This observation held for all gas pressures tested within the range 0.1MPa-0.4MPa and for both levels of DC stress voltage applied across the main gap length which corresponded to either 70% of the self-breakdown voltage level of the respective gas or 80% of the self-breakdown voltage potential of the gas.

The value of  $\gamma$ , the minimum time at which the probability of a breakdown event occurring is non-zero has been shown to fall within the range ~3.10ns-3.5ns for all five gases and has been shown to remain the same regardless of the gas pressure within the switch.

**Table 5-6 Weibull Parameters for gases at 0.1MPa pressure in 4mm gap**

	<b>Air</b>	<b>N<sub>2</sub></b>	<b>60%/40% N<sub>2</sub>/O<sub>2</sub></b>	<b>90%/10% Ar/O<sub>2</sub></b>	<b>CO<sub>2</sub></b>
<b><u>4mm 70% V<sub>br</sub> – 0.1MPa</u></b>					
<i><u>Scale - <math>\alpha</math> (ns)</u></i>	16.90	9.58	13.19	8.78	14.76
95% confidence interval	12.48-21.32	7.57-11.58	10.11-16.27	6.98-10.58	11.36-18.16
<i><u>Shape - <math>\beta</math></u></i>	32.44	28.17	27.99	28.13	28.77
95% confidence interval	31.81-33.06	27.20-29.13	27.29-28.69	27.08-29.18	28.12-29.42
<i><u>Intercept - <math>\gamma</math></u></i>	3.48	3.34	3.33	3.33	3.36
95% confidence interval	3.46-3.50	3.31-3.37	3.31-3.35	3.30-3.36	3.34-3.38
<b><u>4mm 80% V<sub>br</sub> – 0.1MPa</u></b>					
<i><u>Scale - <math>\alpha</math> (ns)</u></i>	9.94	12.41	10.63	14.37	17.11
95% confidence interval	7.63-12.25	9.81-15.01	8.47-12.79	11.16-17.58	13.49-20.73
<i><u>Shape - <math>\beta</math></u></i>	29.44	28.31	31.19	25.69	27.37
95% confidence interval	28.47-30.41	27.56-29.06	30.22-32.16	25.10-26.28	26.84-27.90
<i><u>Intercept - <math>\gamma</math></u></i>	3.34	3.34	3.44	3.25	3.31
95% confidence interval	3.31-3.37	3.41-3.47	3.41-3.47	3.23-3.27	3.29-3.33

Table 5-6 presents the Weibull parameters obtained by applying the three-parameter Weibull analysis to the time to breakdown measurements of the 4mm inter-electrode gap length filled with each of the five gases respectively to a pressure of 0.1MPa (absolute).

At 0.1MPa pressure in the increased gap length of 4mm, the largest value of  $\beta$  which corresponds to the smallest range of times over which breakdown is likely to occur was found to be in the switch filled with the bottled air for the experimental condition when the gap is stressed with 70% of the self-breakdown voltage. When the level of DC stress voltage is increased to 80% of the self-breakdown voltage level, the gas mixture composed of 60%/40% N<sub>2</sub>/O<sub>2</sub> had the largest value of  $\beta$ .

It was noted that the calculated value of  $\beta$ , the shape parameter for each of the gases is close in magnitude for each of the other gases suggesting that the size of the range of times where breakdown may occur is larger for all gases other than air (under 70% of the self-breakdown voltage as a DC stress) or the 60%/40% N<sub>2</sub>/O<sub>2</sub> mix (under 80% of the self-breakdown voltage as DC stress) but similar to each of the other gases.

The minimum time at which the probability of a breakdown occurring is non-zero for all gases tested, the intercept  $y$ , at 0.1MPa, fell within the range 3.23-3.50ns. This is the same minimum time as was observed for the analysis of the 2mm inter-electrode gap length.

**Table 5-7 Weibull Parameters for gases at 0.2MPa pressure in 4mm gap**

	<b>Air</b>	<b>N<sub>2</sub></b>	<b>60%/40% N<sub>2</sub>/O<sub>2</sub></b>	<b>90%/10% Ar/O<sub>2</sub></b>	<b>CO<sub>2</sub></b>
<b><i>4mm 70% V<sub>br</sub> – 0.2MPa</i></b>					
<b><i>Scale - α (ns)</i></b>	27.58	33.04	13.68	14.78	16.37
95% confidence interval	20.92-34.24	25.17-40.91	10.72-16.63	11.55-18.01	12.89-19.85
<b><i>Shape - β</i></b>	35.40	27.01	28.76	29.01	31.06
95% confidence interval	34.98-35.82	26.74-27.28	28.06-29.46	28.36-29.66	30.43-31.69
<b><i>Intercept - γ</i></b>	3.57	3.30	3.36	3.37	3.44
95% confidence interval	3.55-3.59	3.28-3.32	3.34-3.38	3.35-3.39	3.42-3.46
<b><i>4mm 80% V<sub>br</sub> – 0.2MPa</i></b>					
<b><i>Scale - α (ns)</i></b>	26.87	16.27	16.62	12.36	19.23
95% confidence interval	20.35-33.39	12.69-19.85	12.61-20.63	9.59-15.13	14.51-23.95
<b><i>Shape - β</i></b>	33.43	27.42	28.62	30.05	30.35
95% confidence interval	33.02-33.84	26.86-27.98	28.06-29.18	29.25-30.85	29.84-30.86
<b><i>Intercept - γ</i></b>	3.51	3.31	3.35	3.40	3.41
95% confidence interval	3.49-3.53	3.29-3.33	3.33-3.37	3.37-3.43	3.39-3.43

Table 5-7 presents the Weibull parameters obtained by applying the three-parameter Weibull analysis to the time to breakdown measurements of the 4mm inter-electrode gap length filled with each of the five gases respectively to a pressure of 0.2MPa (absolute).

At 0.2MPa pressure in the increased gap length of 4mm, the largest value of β which corresponds to the smallest range of times over which breakdown is likely to occur was found to be in the switch filled with the bottled air for both experimental conditions when the gap is stressed with 70% of the self-breakdown voltage or stressed with 80% of the self-breakdown voltage of the respective gases.

It was again noted that the measured value of  $\beta$ , the shape parameter for each of the gases is close in magnitude for each of the other gases suggesting that the size of the range of times where breakdown may occur is smaller for air than the other gases. All other gases have a range of times where breakdown is likely to occur that are close in size.

The minimum time at which the probability of a breakdown occurring is non-zero for all gases tested, the intercept  $\gamma$ , at 0.2MPa, fell within the range 3.29-3.55ns. Again, this is the same minimum time at which the probability of a breakdown is non-zero as observed with the 2mm inter-electrode gap length at all gas pressures and for the 4mm gap length at 0.1MPa pressure.

**Table 5-8 Weibull Parameters for gases at 0.3MPa pressure in 4mm gap**

	<b>Air</b>	<b>N<sub>2</sub></b>	<b>60%/40% N<sub>2</sub>/O<sub>2</sub></b>	<b>90%/10% Ar/O<sub>2</sub></b>	<b>CO<sub>2</sub></b>
<b><i>4mm 70% V<sub>br</sub> – 0.3MPa</i></b>					
<b><i>Scale - <math>\alpha</math> (ns)</i></b>	16.47	22.82	15.93	15.02	19.71
95% confidence interval	12.63-20.31	17.18-28.46	12.40-19.46	11.57-18.47	15.04-24.38
<b><i>Shape - <math>\beta</math></i></b>	27.97	30.40	30.71	27.16	31.96
95% confidence interval	27.41-28.53	29.96-30.84	30.08-31.33	26.57-27.75	31.43-32.49
<b><i>Intercept - <math>\gamma</math></i></b>	3.33	3.41	3.42	3.30	3.46
95% confidence interval	3.31-3.35	3.39-3.43	3.40-3.44	3.28-3.32	3.44-3.48
<b><i>4mm 80% V<sub>br</sub> – 0.3MPa</i></b>					
<b><i>Scale - <math>\alpha</math> (ns)</i></b>	12.55	13.87	12.15	9.65	11.99
95% confidence interval	9.73-15.37	10.64-17.10	9.41-14.88	7.27-12.03	9.46-14.52
<b><i>Shape - <math>\beta</math></i></b>	30.60	30.54	31.67	34.33	33.12
95% confidence interval	29.80-31.40	29.81-31.27	30.82-32.52	33.16-35.50	32.20-34.04
<b><i>Intercept - <math>\gamma</math></i></b>	3.42	3.42	3.46	3.54	3.50
95% confidence interval	3.39-3.45	3.40-3.44	3.43-3.49	3.51-3.57	3.47-3.53

Table 5-8 presents the Weibull parameters obtained by applying the three-parameter Weibull analysis to the time to breakdown measurements of the 4mm inter-electrode gap length filled with each of the five gases respectively to a pressure of 0.3MPa (absolute)

The Weibull shape parameter  $\beta$ , is shown within Table 5-8. At 0.3MPa pressure in the inter-electrode gap length of 4mm, the largest value of  $\beta$  when the inter-electrode gap is stressed with 70% of the self-breakdown voltage of the respective gases is observed in the CO<sub>2</sub>-filled switch although it should be noted that the  $\beta$  values for all five gases tested are within a small range (27.16-31.96). For the analysis of the time to breakdown results of the inter-electrode gaps that have been stressed with 80% of the self-breakdown voltage of the respective gases, the largest  $\beta$  was found in the 90%/10% Ar/O<sub>2</sub> mixture although again the range of  $\beta$  values for all five gases is small (30.60-34.33). This suggests that the range of times where breakdown is likely to occur is similar for all gases tested at 0.3MPa.

The minimum time at which the probability of a breakdown occurring is non-zero for all gases tested, the intercept  $\gamma$ , at 0.3MPa, fell within the range 3.39-3.57ns. Once again this shows that the minimum time when the probability of a breakdown occurring is non-zero is the same regardless of the inter-electrode gap length or the gas pressure within the switch as  $\sim$ 3.3-3.5ns is the same  $\gamma$  value obtained from the Weibull analysis of all previous results.

The final section presents the analysis of the time to breakdown measurements in the 4mm inter-electrode gap length at 0.4MPa pressure. As no breakdown events were observed for the 90%/10% Ar/O<sub>2</sub> mixture within the 4mm inter-electrode gap length at 0.4MPa pressure, there has been no Weibull analysis for this gas and thus only the Weibull analysis of the time to breakdown measurements in the other four gases; air, N<sub>2</sub>, 60%/40% N<sub>2</sub>/O<sub>2</sub> and CO<sub>2</sub> is presented.

**Table 5-9 Weibull Parameters for gases at 0.4MPa pressure in 4mm gap**

	<b>Air</b>	<b>N<sub>2</sub></b>	<b>60%/40% N<sub>2</sub>/O<sub>2</sub></b>	<b>90%/10% Ar/O<sub>2</sub></b>	<b>CO<sub>2</sub></b>
<b><i>4mm 70% V<sub>br</sub> – 0.4MPa</i></b>					
<i>Scale - α (ns)</i>	10.65	13.84	16.88	N/A	15.71
95% confidence interval	8.37-12.93	10.80-16.88	13.09-20.67		12.11-19.31
<i>Shape - β</i>	31.30	31.74	30.8	N/A	34.80
95% confidence interval	30.33-32.27	30.99-32.49	30.21-31.39		34.07-35.53
<i>Intercept - γ</i>	3.44	3.46	3.43	N/A	3.55
95% confidence interval	3.41-3.47	3.44-3.48	3.41-3.45		3.53-3.57
<b><i>4mm 80% V<sub>br</sub> – 0.4MPa</i></b>					
<i>Scale - α (ns)</i>	10.40	12.11	12.5	N/A	13.99
95% confidence interval	8.17-12.63	9.66-14.56	9.61-15.39		13.97-14.01
<i>Shape - β</i>	29.79	30.40	29.97	N/A	33.68
95% confidence interval	28.84-30.74	29.57-31.23	29.17-30.77		32.90-34.46
<i>Intercept - γ</i>	3.39	3.41	3.40	N/A	3.52
95% confidence interval	3.36-3.42	3.38-3.44	3.37-3.43		3.50-3.54

Table 5-9 presents the Weibull parameters obtained by applying the three-parameter Weibull analysis to the time to breakdown measurements of the 4mm inter-electrode gap length filled with each of the five gases respectively to a pressure of 0.4MPa (absolute).

The Weibull shape parameter  $\beta$  values are shown within Table 5-9. At 0.4MPa pressure in the inter-electrode gap length of 4mm, the largest value of  $\beta$  when the inter-electrode gap is stressed with either 70% of the self-breakdown voltage or with 80% of the self-breakdown voltage of the respective gases, was found with the switch filled with CO<sub>2</sub>. As has been observed previously however, the values of  $\beta$  for the other gases tested were

close in magnitude suggesting that when considering the range of times where a breakdown is likely to occur, all gases have a similar size of spread.

The  $\gamma$  value obtained from the Weibull analysis which is the minimum time at which the probability of a breakdown event occurring being non-zero at 0.4MPa gas pressure within the 4mm gap, in agreement with all other gas pressures tested was found to be within the range 3.36-3.57ns. This shows that the minimum time when the probability of a breakdown occurring is non-zero is the same regardless of the inter-electrode gap length or the gas pressure within the switch within the scope of this experimental investigation and can reasonably be deduced to hold true for gap lengths and pressures above those tested within the scope of this work.

## 5.5 Conclusions

Investigating the breakdown characteristics of the field distortion gap filled with five different gases and triggered by a Blumlein impulse generator, some interesting results have been shown throughout this chapter.

The field-distortion spark gap switch which had previously been used within Chapter was utilised in a similar experimental test set-up this time triggered by a Blumlein pulse generator which provides a 30kV voltage impulse to the mid-plane electrode with a FWHM  $\sim$ 280ns, far quicker than the 185 $\mu$ s that had previously been investigated (Chapter 4). When filled with five different gases; bottled air, N<sub>2</sub> (BOC Ltd, 99.9% purity), 60%/40% N<sub>2</sub>/O<sub>2</sub> mixture, 90%/10% Ar/O<sub>2</sub> mixture and CO<sub>2</sub>, the time taken between the initiation of the trigger impulse and the complete breakdown across the main inter-electrode gap was measured as the 'time to breakdown'.

It has been shown throughout this chapter that the 'time to breakdown' characteristic of the switch when plotted as a function of the gas pressure within the switch does not significantly change as the gas pressure increases within the range 0.1MPa-0.4MPa for either the 2mm or the 4mm inter-electrode gap length tested. The total time to breakdown was found to be  $\sim$ 26-30ns for all gases tested although the gas mixture of 60%/40% N<sub>2</sub>/O<sub>2</sub> did generally provide the shortest time to breakdown of all gases tested when compared directly to the other gases.

It was observed that not only did the gas pressure have little effect on the measured time to breakdown; the level of DC stress applied across the main inter-electrode gap had little influence on the time required between initiation of the voltage impulse on the trigger plane and complete voltage collapse across the main electrode gap. This is unlike the results observed in Chapter 4 where it was observed that stressing the gap with 80% of the self-breakdown voltage of the respective gas would result in a longer time to breakdown; no discernible trend was observed when stressing the gap with 70% or 80% of the self-breakdown voltage of the gases.

The other key breakdown characteristic which has been investigated for industrial applications is the jitter of the switch as it is generally wished to minimise the switch jitter within a system to allow for more predictable and reliable triggering applications. This is mainly due to the large number of triggered switches that can be used within the voltage erection stage of pulsed power systems such as in Marx generators. In order to have synchronisation of the switches, that is, in order for the switches to trigger at the same time so that the output voltage impulse across the load is of the correct magnitude and occurs at the required time, the jitter of each of the switches should be low. It was seen that when triggering with the Blumlein pulse generator, the jitter was on the scale of  $\sim 2\text{-}3\text{ns}$  generally, 3 orders of magnitude lower than the jitter observed in Chapter 4 when the rate of voltage rise applied to the trigger plane was  $0.45\text{kV}/\mu\text{s}$ . It was observed from the experimental results however, that as the gas pressure within the test cell increased, the jitter generally was also seen to increase in all gases tested. The jitter observed within this chapter is in line with the required levels and the levels of jitter reported in many other studies into jitter of closing switches [34], [142]–[144], [146], [149]–[151].

A three-parameter Weibull statistical analysis has been conducted on all the time to breakdown data and it was shown for the shape parameter  $\beta$  which determines the size of the range of times where breakdown may occur (the larger the value of  $\beta$ , the smaller the range of times over which a breakdown is likely to be observed) was found to be similar for all gases at the same pressure. The values of  $\beta$  showed negligible change in between those from the experiments conducted under a DC stress voltage equal to 70% of the self-breakdown voltage or 80% of the self-breakdown voltage. The Weibull analysis also showed that the value of  $\gamma$  (the minimum time at which the probability of a breakdown occurring is

non-zero) does not change with respect to DC stress level, inter electrode gap length or gas pressure within the switch.

In conclusion, by triggering the field distortion spark gap switch with a Blumlein pulse generator with a fast rate of voltage rise as compared with the trigger generator where the rate of voltage rise was  $0.45\text{kV}/\mu\text{s}$ , the time to breakdown and jitter have been seen to reduce from  $\mu\text{s}$  to ns. There is little influence on the time to breakdown as a result of the gas pressure within the switch although the jitter has been observed to increase as the gas pressure also increases. For optimum performance in practical systems where either a field-distortion switch is being used with one of the five gases that have been investigated, the gas mixture of 60%/40%  $\text{N}_2/\text{O}_2$  provided marginally faster times to reach complete breakdown and the jitter values observed within this switch were the smallest values of all the gases tested.

For the evidence presented within this chapter, if designing a system and requiring switches to operate with the fastest breakdown times and low jitter under a range of inter-electrode gap distances, the gas mixture comprising 60%/40%  $\text{N}_2/\text{O}_2$  is recommended (of those tested within this investigation).

## Chapter 6. Plasma Channel Characteristics

One of the key objectives of this research is to develop a computational model of a 12-stage practical Marx Generator which would enable modelling of the wave-shapes of output HV impulses across different loads under the experimental conditions when plasma closing switches of the generator are filled with different gases. The actual 12-stage Marx generator which is being modelled in the present project is a part of the charging system in a larger pulsed power system [59], [60]. Therefore, a comprehensive PSpice model of the Marx generator would allow optimization of operational performance of the practical pulsed power system. The switches within the computational model of the Marx generator are desired to accurately describe the performance of the self-breakdown spark-gap switch which has been previously used in experimental investigations presented within Chapters 3, 4 and 5. In order to build a computational model of a pulsed power system including these plasma closing switches, the electrical characteristics of the plasma channel which is formed within the switch during the breakdown event need to be known e.g. the resistance of the plasma channel, inductance of the plasma channel and an estimation of the energy deposited into the plasma channel. With this data, simulation of the plasma can be conducted.

Within this chapter, an investigation of the temperature of the plasma in the breakdown channel formed in the spark switch filled with the six gases; air, N<sub>2</sub>, 60%/40% N<sub>2</sub>/O<sub>2</sub>, 90%/10% Ar/O<sub>2</sub>, CO<sub>2</sub> and SF<sub>6</sub>, has been conducted by means of plasma emission spectroscopy. The optical spectrum of light emitted by breakdown plasma channels in different gases has been obtained and analyzed. The plasma temperature in the switch is related to the energy deposited into the plasma channel during a breakdown event [77], [82], [152]. By evaluating the temperature of the plasma that forms within the inter-electrode gap length, it is possible to evaluate the conductivity of the plasma, which then will be used in the computational model of the Marx generator.

The temperature of the plasma that forms within the switch can be obtained by using the Boltzmann approach which links the optical emission to the plasma temperature in the case of the thermalized plasma. Then, using the Spitzer approximation, it is possible to evaluate the plasma conductivity. Thus, the values of plasma temperature and conductivity in

different gases can be obtained and then used in the computational model of a 12-stage Marx generator in PSpice (Chapter 8).

Further key characteristics obtained within this chapter for each of the six gases of interest; are the resistance and inductances of the breakdown plasma channels which have been obtained by monitoring the post-breakdown current waveforms and extracting relevant information pertaining to the experimental set-up and subtracting any known resistance values in the experimental set-up which are provided by the other elements of the circuit.

## 6.1. Plasma Temperature Evaluation

To obtain the plasma temperature for different gases, light emitted during breakdown was directed through a fiber optic into a spectrometer (OceanOptics HR4000) and optical emission spectra were registered and analysed. The Boltzmann approach to obtaining the temperature of the plasma was selected for the purpose of this project. This approach which is based on the assumption of the partial local thermodynamic equilibrium (LTE) in plasma channel has been discussed in literature and found to be an appropriate method for obtaining the average plasma temperature in spark discharges [153]–[159].

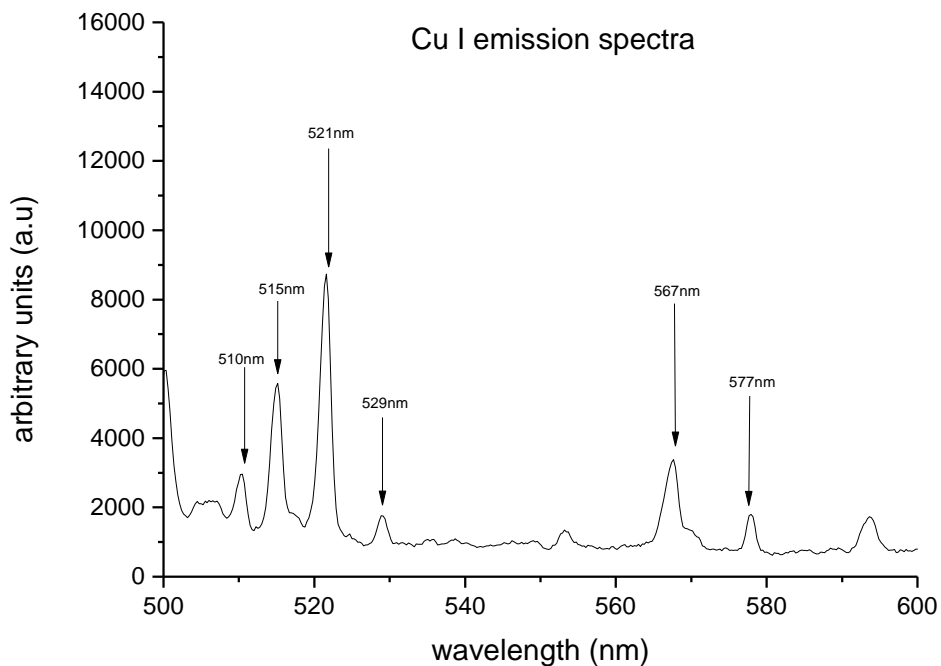
In the Boltzmann approach the relative peak values of the optical emission lines of specific elements are linked with the plasma temperature through the following Equation 6.1:

$$\ln\left(\frac{\lambda I}{A g_u}\right) = C - \frac{E_i}{kT} \quad (6.1)$$

where  $I$  is the relative intensity of a specific emission line with the wavelength,  $\lambda$ ,  $A$  is Einstein's transitional probability for this emission line,  $g_u$  the statistical weight of the upper level,  $E_i$  is the energy of the upper level (in eV) for the specific element,  $k$  is Boltzmann's constant and  $T$  is the temperature of a plasma. The values of the transitional probability, statistical weight of the upper level and the energy of the upper level ( $A$ ,  $g_u$  and  $E_i$ ) are all known spectroscopic constants for specific elements which can be obtained from [160], [161].

Breakdown tests were conducted using the same circuit set-up as outlined in Chapter 3 with the self-breakdown voltage analysis of the gases. An OceanOptics HR4000 spectrometer with fibre optic cable was placed at the 25mm diameter quartz window which was installed into the side of the self-breakdown switch. The SpectraSuite software was used to analyse the light emission spectra during breakdown events.

The tests using the self-breakdown switch described in Chapter 3 were conducted for each of the six gases; air, N<sub>2</sub>, 60%/40% N<sub>2</sub> /O<sub>2</sub>, 90%/10% Ar/O<sub>2</sub>, CO<sub>2</sub> and SF<sub>6</sub> at a range of pressures from 0.1MPa-0.4MPa. The inter-electrode gap spacing was altered from 1mm-9mm in 1mm increments. The optical emission spectra of five breakdown events were captured on the SpectraSuite software and saved for analysis. Due to the high percentage of copper in the brass electrodes within the self-breakdown switch, copper Cu I emission lines at 6 wavelengths; 510.55nm, 515.32nm, 521.82nm, 529.25 nm, 567.02nm and 577.21nm are easily identified in the optical emission spectra of spark discharges and these lines have been selected for the use in Equation 6.1 in order to obtain the plasma temperature.



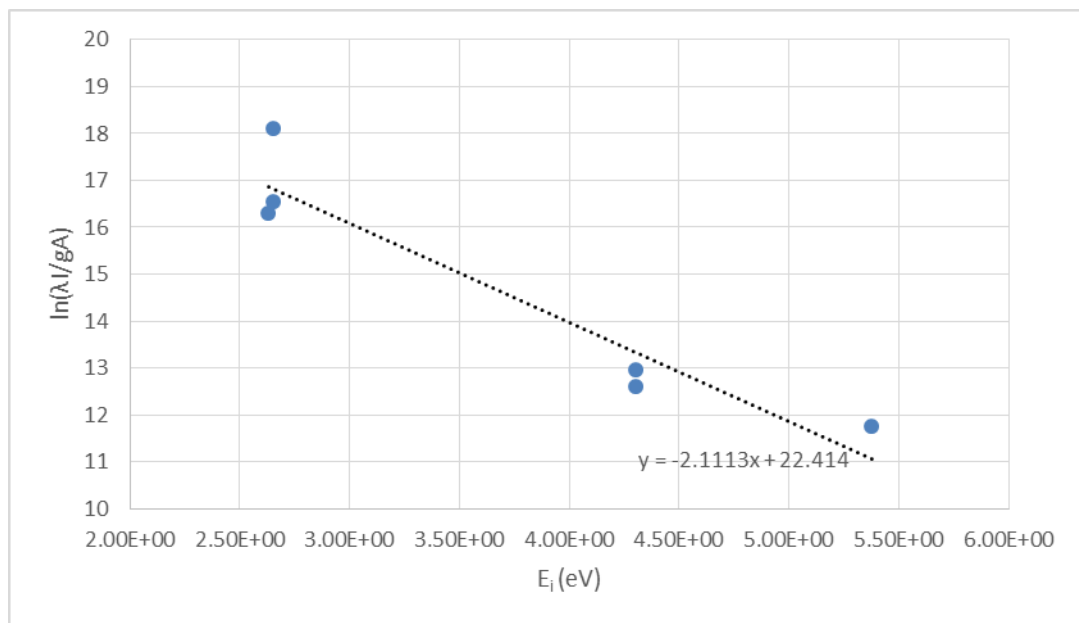
**Figure 6-1** Optical emission spectrum from 500-600nm in a 1mm air-filled self-breakdown switch at 0.1MPa pressure. The high percentage of copper in the brass electrodes allows for analysis of the Cu I emission spectrum where there are 6 peaks at wavelengths within the 500-600nm range.

Figure 6-1 shows the emission spectrum between 500nm-600nm for the breakdown event in the 1mm inter-electrode gap in the air-filled self-breakdown switch at 0.1MPa.

**Table 6-1 Spectroscopic constants for Cu I, copper emissions at wavelengths between 500-600nm [160].**

	510nm	515nm	521nm	529nm	567nm	577nm
$g_i A (10^8 /s)$	0.051	4.7	5.8	3.2	0.014	0.054
$E_i (eV)$	2.65	4.31	4.31	5.38	2.65	2.63

Table 6-1 **Error! Reference source not found.** provides the relevant spectroscopic constants for the copper optical emission spectral lines that have been analysed within this work. For each spectrum obtained, the relative peak intensities of the spectral lines at the identified wavelengths have been obtained and then used in Equation 6.1. For a given spectrum the logarithmic term of Equation 6.1 is plotted versus  $E_i$ , and a straight line of best fit through the points will be obtained. The slope of this best fit lines allows the temperature of plasma, T, to be obtained.



**Figure 6-2 An example of a Boltzmann plot obtained from one breakdown event occurring within the air-filled switch at 0.1MPa with a 1mm inter-electrode gap length.**

Figure 6-2 shows one of the five Boltzmann plots for the air-filled switch at 0.1MPa with a 1mm inter-electrode gap space. The natural logarithm of the product of the emitted wavelength and relative intensity of the emission at that wavelength divided by Einstein's transitional probability and the statistical weight of the upper energy level is plotted against the energy of the upper level. A line of best fit is applied through the experimental data points on the graph with Equation:

$$y = -ax + b \quad (6.2)$$

when  $y = \ln\left(\frac{\lambda I}{gA}\right)$ ,  $x = -\frac{1}{kT}$ ,  $a = E_i$  and  $b = C$ . Using the Microsoft Excel software,

the temperature of the plasma channel formed during a breakdown event can be obtained from the gradient of the best-fit line applied to the data points. E.g within the experimentally obtained results presented within Figure 6-2 it was found to have a gradient of -2.11 which corresponds to a plasma channel temperature of ~5,490 K.

It has been discussed [157] that the value of the spectroscopic constants used within the Boltzmann spectroscopic analysis of the temperature of the plasma channel are important as incorrectly evaluated constants can result in incorrect estimations of temperature. This investigation into the temperature of the plasma channels formed during the breakdown events conducted is concerned with any overall trends in temperature as the product  $pd$  increases as any significant change in temperature of the plasma temperature as a function of  $pd$  will correspond to significant changes in the conductivity of the plasma in the switch depending upon the inter-electrode gap length and the gas pressure within the switch, a consideration which would need to be made for developing the computational model.

The outlined Boltzmann method of evaluating the temperature of the plasma channel during breakdown events has been deemed appropriate for the investigation as this approach provides a relatively straightforward method of extracting and comparing the temperature of the plasma channels formed in different gases.

The symbols in each graph are an average temperature value which has been extracted from the analysis of 5 emission spectra. The error bars associated with each symbol represents the standard deviation in the temperature of the plasma channel extracted.

### 6.1.1. Temperature of Air Plasma Channels

This section presents the results of the experimental investigation into the temperature of the plasma channel formed during a breakdown event initiated within a self-breakdown switch that has been filled with bottled air.

As outlined previously, 5 optical emission spectra were obtained for each combination of inter-electrode gap length from 1mm-9mm (in 1mm increments) and gas pressures within the range of 0.1MPa-0.4MPa (increasing in pressure by increments of 0.1MPa). Each of the saved spectra waveforms were analysed and the relative peak intensities of emissions at the wavelengths in the region 500nm-600nm that correspond to copper Cu I emissions lines were plotted according to Equation 6.1 with the logarithmic term versus the energy term. The analytical function (Equation 6.2) was used to fit the experimental data using the best fit procedure in the Microsoft Excel software, as outlined in Section 6.1, to extract a temperature of the plasma.

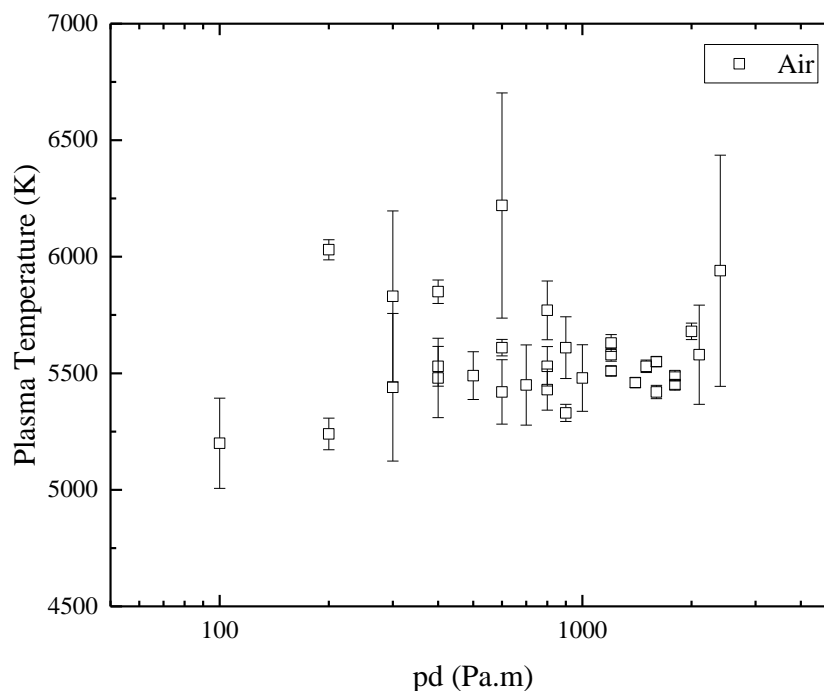


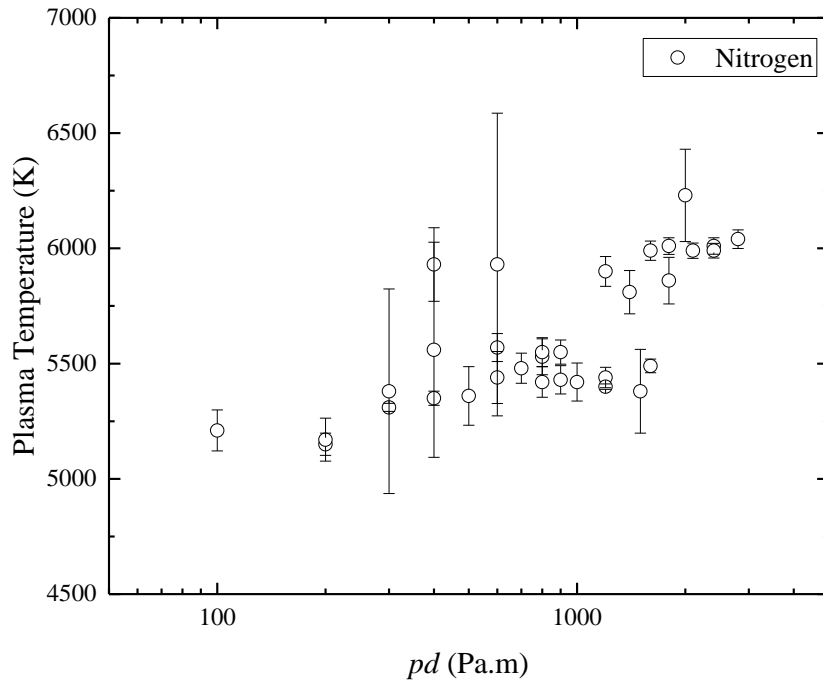
Figure 6-3 Temperature of the plasma channel formed during breakdown in an air-filled self-breakdown switch as a function of the product of the gas pressure and the inter-electrode gap spacing.

Figure 6-3 shows the temperature of the plasma channel formed in an air-filled switch as the product of the inter-electrode gap length and the gas pressure  $pd$  increases. It is seen that generally, the temperature of the plasma channel formed within the air-filled switch remains within the range 5250-6750K for all values of  $pd$  within the switch.

As the product  $pd$  increases for the air-filled switch, there is no obvious discernible trend in terms of the temperature of the plasma channel formed during breakdown, extracted by using the Boltzmann Equation which suggests that within the range of  $pd$  values tested within this investigation, the plasma temperature remains almost constant. A constant plasma temperature over all values of  $pd$  within the switch, as will be discussed within Section 6.2, suggests a constant average value for the conductivity of the plasma in the breakdown channel for the range of  $pd$ 's and energies available in discharge used in the present study.

### **6.1.2. Temperature of $N_2$ Plasma Channels**

As with the experiments conducted in section 6.1.1 where the self-breakdown switch was filled with bottled air and the light emissions of 5 breakdown events were obtained using the SpectraSuite software, the light emission spectra for 5 breakdown events for each inter-electrode gap length and gas pressure combination were again obtained for the switch filled with  $N_2$  gas (99.9% purity, BOC Ltd). The average value and the standard deviation for the temperature are presented as a function of the product  $pd$  in Figure 6-4.



**Figure 6-4 Temperature of the plasma channel formed during breakdown in an N<sub>2</sub>-filled self-breakdown switch as a function of the product of the gas pressure and the inter-electrode gap spacing..**

When the light emission spectra of the switch filled with N<sub>2</sub> gas is analysed, it can be seen from Figure 6-4 that the range of temperatures extracted from the optical emissions analysed using the Boltzmann for breakdown events within the N<sub>2</sub> plasma channels is ~5250-6250K.

As was observed for the temperature of the plasma channel extracted from the breakdown events in the air-filled switch and again seen for the N<sub>2</sub> breakdown events within Figure 6-4, the temperature of the plasma channels formed during the breakdown events does not appear to be significantly affected by altering the product  $pd$  within the switch. This constant temperature of the plasma channel formed during breakdown, independent of the product  $pd$  will allow for the calculation of a conductivity of the plasma channel based upon a constant temperature within Section 6.2.

### 6.1.3. Temperature of 60%/40% N<sub>2</sub>/O<sub>2</sub> Plasma Channels

This section presents the plasma temperature as a function of the product  $pd$  for the plasma channel formed during breakdown in a switch filled with the 60%/40% N<sub>2</sub>/O<sub>2</sub> gas mixture. Figure 6-5 shows the average temperature extracted from the 5 emissions obtained from each combination of inter-electrode spacing and gas pressure.

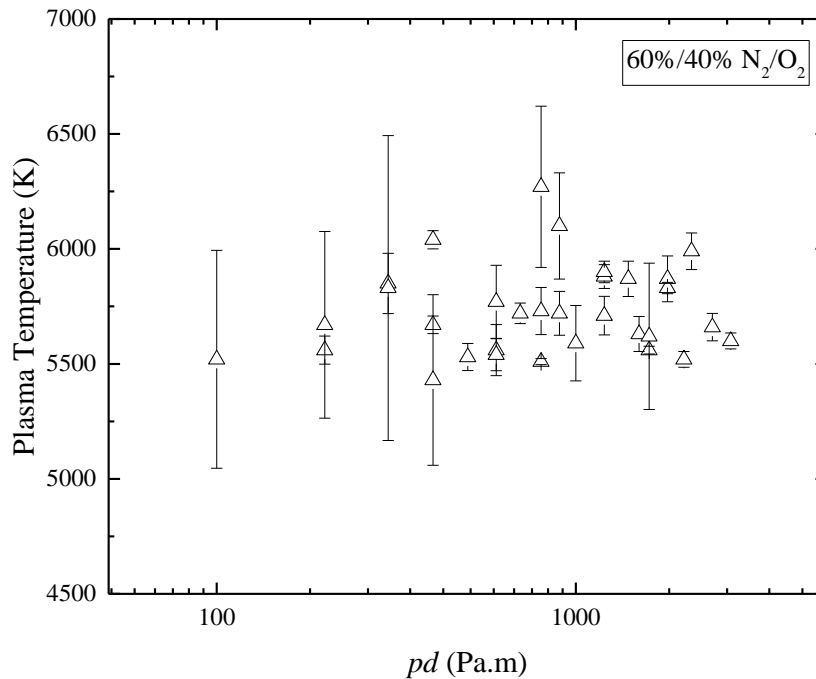


Figure 6-5 Temperature of the plasma channel formed during breakdown in a switch filled with a 60%/40% N<sub>2</sub>/O<sub>2</sub> gas mixture as a function of the product of the gas pressure and the inter-electrode gap spacing.

Figure 6-5 shows the average temperature of the plasma channel formed during breakdown in the switch filled with the 60%/40% N<sub>2</sub>/O<sub>2</sub> gas mixture as a function of the product  $pd$ . In line with the results obtained for air and N<sub>2</sub> filled switches previously discussed, for  $pd$  values within the range  $\sim 100$ - $3000$  Pa.m, the temperature of the plasma channel formed during breakdown is seen to fall within the range  $\sim 5,500$ - $6,250$ K. It can also be seen from Figure 6-5 that as the value of  $pd$  increases within the switch, the temperature of the plasma in the channel formed between the electrodes remains almost unchanged.

#### 6.1.4. Temperature of 90%/10% Ar/O<sub>2</sub> Plasma Channels

The average value of the 5 temperatures extracted for each combination of gap space and gas pressure are presented within Figure 6-6 when the switch was filled with the 90%/10% Ar/O<sub>2</sub> mixture.

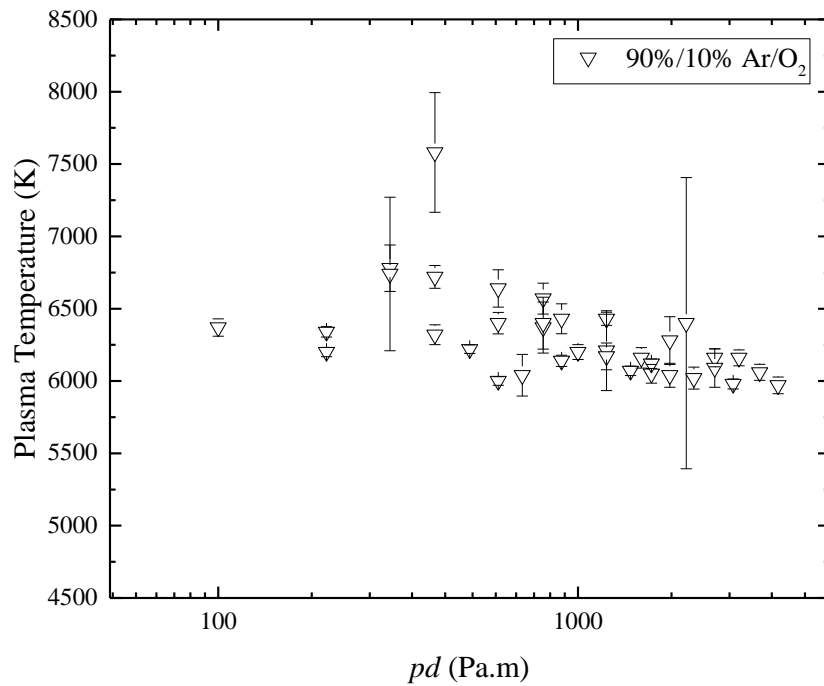


Figure 6-6 Temperature of the plasma channel formed during breakdown in a switch filled with a 60%/40% N<sub>2</sub>/O<sub>2</sub> gas mixture as a function of the product of the gas pressure and the inter-electrode gap spacing.

Figure 6-6 presents the obtained temperatures of the plasma within the switch when filled with the 90%/10% Ar/O<sub>2</sub> mixture as a function of the product  $pd$  with the switch. It can be seen that generally the temperatures measured across the range of  $pd$  values within this investigation are  $\sim 6,000$ - $7,750$ K and as the product  $pd$  increases, the temperature again was observed to remain almost constant.

It is also observed for the 90%/10% Ar/O<sub>2</sub> mixture, in line with the other gases tested that the temperature of the plasma channel formed during a breakdown event remains relatively unchanged as  $pd$  increases.

### 6.1.5. Temperature of CO<sub>2</sub> Plasma Channels

This section presents the results of the experimental investigation into the temperature of the plasma channel formed during breakdown events when the plasma closing switch is filled with CO<sub>2</sub> gas.

Figure 6-8 presents the temperature of the plasma channels formed during breakdown in a CO<sub>2</sub>-filled switch.

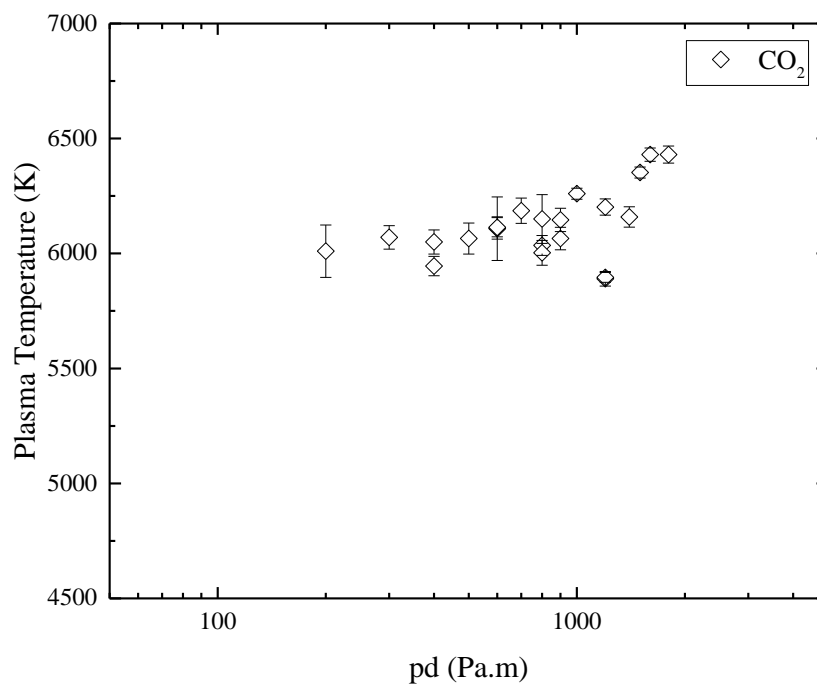


Figure 6-7 Temperature of the plasma channel formed during breakdown in a switch filled with a CO<sub>2</sub> gas mixture as a function of the product of the gas pressure and the inter-electrode gap spacing.

As can be seen by the results of the optical investigation into the average temperature of the plasma presented within Figure 6-8 as a function of the product  $pd$  within the switch,

for a CO<sub>2</sub> filled switch the range of temperatures of the plasma for the  $pd$  values of interest is  $\sim 5,750$ - $6,500$ K. This temperature range is slightly higher than that of the air, N<sub>2</sub> and 60%/40% N<sub>2</sub>/O<sub>2</sub> filled switches which may correspond to the slightly higher self-breakdown voltage capabilities observed for CO<sub>2</sub> as discussed within Chapter 3.

Generally it is seen within Figure 6-7 that as the value of  $pd$  increases, the temperature of the plasma channel formed during breakdown remains constant across the range of  $pd$  values of interest within this investigation. This again will allow within Section 6.2 an evaluation of the conductivity of the plasma channel to be made using only a constant temperature for the entire  $pd$  range within this investigation.

### 6.1.6. Temperature of SF<sub>6</sub> Plasma Channels

The final gas to be evaluated for the temperature of the plasma channels formed during breakdown events is SF<sub>6</sub>. The average value of the 5 emissions for each inter-electrode gap length and gas pressure when the switch was filled with SF<sub>6</sub> has been plotted within Figure 6-8.

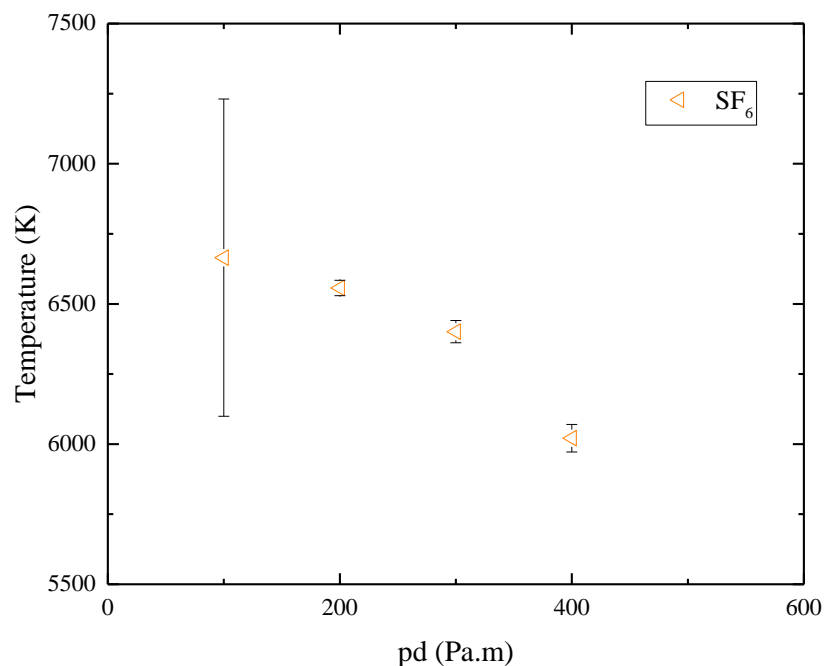


Figure 6-8 Temperature of the plasma channel formed during breakdown in a switch filled with SF<sub>6</sub> as a function of the product of the gas pressure and the inter-electrode gap spacing.

Figure 6-8 shows the temperature of the plasma channels formed during breakdown events in a switch filled with SF<sub>6</sub> gas. It can be seen from Figure 6-8 that for the range of  $pd$  values of interest within this investigation where breakdown events were able to be initiated within a switch filled with SF<sub>6</sub> gas, the temperature of the plasma channel that forms during a breakdown event, in line with all other gases tested is within the range of 6,000-6,500K.

SF<sub>6</sub> has been shown within Chapter 3 to have the highest self-breakdown voltage potential of all the 6 gases tested however it was also shown to have the largest standard deviation in self-breakdown voltage of the gases tested.

### 6.1.7 Comparison of Plasma Temperature of all gases

This section provides a direct comparison of the temperatures extracted using the Boltzmann method outlined within Section 6.1 for the plasma channels formed during breakdown events in all six of the gases tested within this experimental investigation.

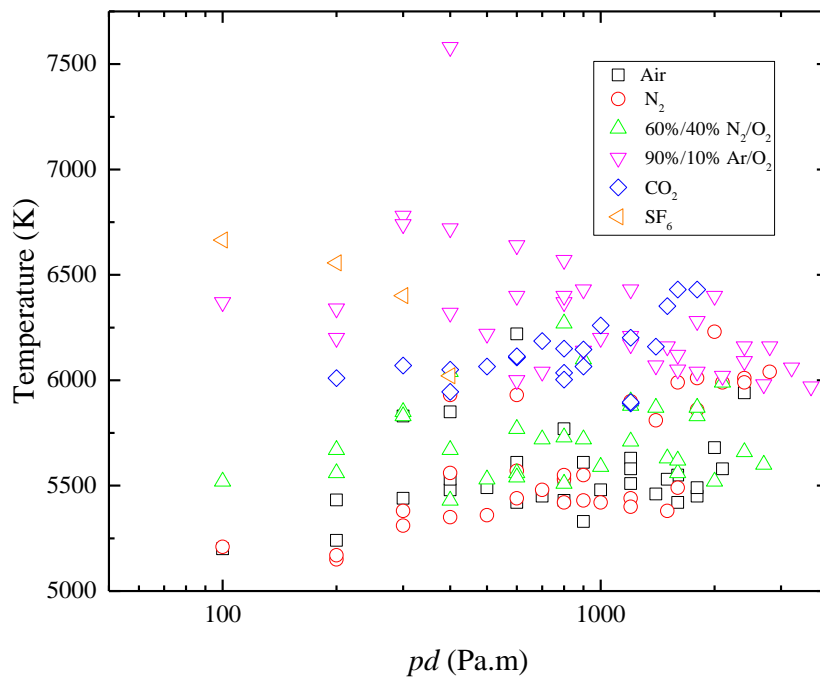


Figure 6-9 The temperature of the plasma channel formed for each of the six gases tested; air, N<sub>2</sub>, 60%/40% N<sub>2</sub>/O<sub>2</sub>, 90%/10% Ar/O<sub>2</sub>, CO<sub>2</sub> and SF<sub>6</sub> as a function of the product  $pd$  within the switch.

Figure 6-9 provides a comparison of the obtained temperatures of each of the gases of interest within this investigation

Initial expectations for analysis of the temperature of the plasma channel formed during the breakdown event within a spark gap switch were that the gases which were shown within Chapter 3 to provide the highest voltage hold-off capability of all six gases tested would correspondingly also result in the highest temperatures extracted by using the Boltzmann method of temperature analysis. This result was expected as the self-breakdown voltage required to initiate breakdown across the switch is related to the energy applied across the inter-electrode gap by:

$$E = \frac{1}{2}CU^2 \quad (6.3)$$

where  $U$  is the breakdown voltage,  $C$  the capacitance of the circuit and  $E$  the energy applied into the circuit and thus a higher self-breakdown voltage requires more energy applied to initiate breakdown.

Since the energy applied across the inter-electrode gap length is related to the breakdown voltage by Equation 6.3 and the temperature of the plasma channel formed has been seen for air,  $N_2$ , the 60%/40%  $N_2/O_2$  gas mixture and  $CO_2$  to increase under conditions where the self-breakdown voltage for each gas at the same  $pd$  value is higher. Thus, it would be expected that for a switch filled with the 90%/10%  $Ar/O_2$  mixture which has been shown within Chapter 3 to have the lowest self-breakdown voltage, the temperature evaluated by optical emission and application of the Boltzmann Equation would be the lowest of all the gases tested. However, it can be seen from Section 6.1.6 and Figure 6-9 that the temperature of the plasma channel formed during breakdown events when the switch is filled with the 90%/10%  $Ar/O_2$  mixture is actually higher than the temperatures found in the air,  $N_2$ , 60%/40%  $N_2/O_2$  and  $CO_2$  filled switches for the same  $pd$  values.

Figure 6-9 provides a direct comparison of the average constant temperature of the plasma which forms inside the channels during the breakdown events across the full range of  $pd$  values of interest within this investigation for all six gases/gas mixtures tested within this investigation. It is clearly seen that that temperature of the plasma channels formed in the air and  $N_2$  are almost identical for the same  $pd$  values while the temperature for the 60%/40%  $N_2/O_2$  gas mixture is ~7-8% higher than the plasma temperatures extracted for

the air and N<sub>2</sub> filled switch for the same  $pd$  values. As for the 90%/10% Ar/O<sub>2</sub> mixture, the highest temperatures of the plasma channels formed during breakdown events were observed for this gas mixture and are observed to be ~13-16% higher than the temperature of the air or N<sub>2</sub> filled plasma channels formed at the same  $pd$  values.

The temperature of the plasma channel in the 90%/10% Ar/O<sub>2</sub> mixture is higher than in any of the other gases tested, although seemingly due to the lower self-breakdown voltage required to initiate breakdown within the switch filled with this gas mixture, this can possibly be explained due to some components of the temperature which cannot be directly measured from the Boltzmann method applied within this investigation. Dutton has shown [162] that for the same  $E/N$  values, characteristics such as the drift velocity of Argon is higher than the drift velocity of CO<sub>2</sub> and other gases of interest within this investigation. This higher drift velocity for the same  $E/N$  values contributes to the observation of the higher plasma channel temperature in the 90%/10% Ar/O<sub>2</sub> than the other gases tested despite the observation within Chapter 3 that the self-breakdown voltage of the 90%/10% Ar/O<sub>2</sub> mixture is significantly lower.

Despite this, the difference in the temperatures of the plasma channels formed during breakdown events for all of the gases tested was found to be <1000K or < 16% across the entire range of  $pd$  values within this investigation. In addition to this, it has also been observed that as the value of  $pd$  changes, there is no significant change in the temperature of the plasma channel formed during a breakdown event for each of the gases. Now that there is an estimation of the plasma temperature that has been observed to remain constant for the range of  $pd$  within this investigation, the conductivity of the plasma channel formed during a breakdown event can be calculated using temperatures of ~5500K-6500K.

## 6.2 Conductivity of Plasma in Breakdown Channel

So far within this chapter, a description of the theoretical and experimental approach taken in order to estimate the temperature of the plasma in a breakdown channel formed in different gases within a self-breakdown spark gap switch by means of analysing optical emissions has been provided. It has been shown that for the range of inter-electrode gap lengths within the switch (1 mm – 9 mm) and gas pressures (0.1 MPa - 0.4 MPa) of interest within this investigation, the resulting  $pd$  values (the product of the inter-electrode gap length and the gas pressure) result in corresponding plasma channel temperatures during breakdown events of ~5,500-6,500K depending upon the gas within the switch.

Knowledge of the temperature of the plasma formed during a breakdown event is essential in order to estimate the conductivity of the plasma in the channel. The conductivity of the plasma is a fundamental parameter which is needed in order to evaluate the resistance of the plasma channel which is used in the development of the computational model in order to accurately describe the output of spark gap switches. The spark gap switches which are accurately described and modelled can then be used within the models of other, larger pulsed power systems such as a Marx Generator as will be discussed within Chapter 8 of this thesis. In order to obtain the conductivity of the plasma, the Spitzer model, which says that the resistance of a plasma will decrease in proportion to the electron temperature as  $T^{-3/2}$  [163] was used. The Spitzer conductivity of the plasma as described by Equation 6.3, below can be used:

$$\sigma_{sp} = \frac{\gamma_E T^{3/2}}{38.0 \times Z \times \ln \Lambda} \quad (6.3)$$

where  $\gamma_E$  takes into account electron-electron scattering and takes the value 0.582 when  $Z$ , the mean ionic charge is equal to 1 [164],  $T$  is the absolute temperature of the plasma channel formed during a breakdown event, which has been obtained previously within this chapter from experimental investigations (K), and  $\Lambda$  is the Coulombic logarithmic term

which is a factor that takes into account the long range interactions between two charged particles within the plasma channel formed during the breakdown and is given by:

$$\ln \Lambda = \ln \left( \frac{1.24 \times 10^7 \times T^{3/2}}{n_e^{1/2}} \right) \quad (6.4)$$

and  $n_e$  is the number of electrons per unit volume (MKS).

A reasonable estimation of the number of electrons per unit volume within the plasma channel formed during breakdown in the self-breakdown switch and is  $\sim 10^{14} \text{ cm}^{-3}$ [165].

By using the temperatures at either end of the range from 5,500K-6,500K as were extracted experimentally earlier in Equation 6.3, the spritzer conductivity of the plasma channel formed during breakdown events was calculated to be:

$$\sigma_{SP5500K} \approx 4.7 \times 10^3 \frac{1}{\Omega.m} \quad , \quad \sigma_{SP6500K} \approx 6 \times 10^3 \frac{1}{\Omega.m}$$

and so for a 1,000K difference in temperature, a change in conductivity of  $\sim 20\%$  can be classed as a small change due to the approximations made of quantities such as number of electrons per unit volume within the calculation and limitations on accuracy of temperature measurement. For this reason, the conductivity of the plasma channel is taken as

$$\sigma_{SP} \sim 10^3 \frac{1}{\Omega.m}$$

across the full range of plasma temperatures extracted experimentally. This observation of the conductivity of the plasma channel holding a value of  $\sim 10^3 \Omega\text{m}^{-1}$  for breakdown events occurring in all gases tested across the full range of  $pd$  values of interest allows for an approximately constant value of plasma conductivity  $\sim 10^3 \Omega\text{m}^{-1}$  to be employed within the computational model developed within Chapter 8. This obtained value of conductivity for the plasma in the breakdown channel for gases with temperatures in the range 5,500K-6,500K fits well with data available in literature where other groups have estimated plasma conductivity for similar temperature ranges and found obtained values in the region

of  $10^3 \Omega\text{m}^{-1}$ , however some groups have reported conductivities as low as  $10^2 \Omega\text{m}^{-1}$  in  $\text{SF}_6$  [164].

### 6.3 Discussion

This chapter has presented an experimental investigation into the temperature of the plasma channel which is formed within the main inter-electrode gap length during a breakdown event. By obtaining the light emission spectra produced when a plasma channel is formed within the main inter-electrode gap length during a breakdown event, it is possible to analyse the spectra and by use of the Boltzmann approach, extract the temperature of the plasma temperature which has formed.

It has been shown within this chapter that for all six gases of interest within this investigation; air,  $\text{N}_2$ , 60%/40%  $\text{N}_2/\text{O}_2$ , 90%/10%  $\text{Ar}/\text{O}_2$   $\text{CO}_2$  and  $\text{SF}_6$ , the temperature of the plasma channels which form during breakdown events are in the region of  $\sim 5,500\text{K}$ - $6,500\text{K}$ . By calculating the temperature of the plasma channels formed during breakdown events for all gases of interest within this investigation, the temperatures extracted were then able to be used to estimate the conductivity of the produced plasma channel as  $\sim 10^3 \Omega\text{m}^{-1}$ .

This value of the conductivity of the produced plasma channel holds across the full range of gases and temperatures extracted which then will allow, in the development of the computational model within Chapter 8, a constant value for plasma conductivity to be used.

## Chapter 7. Plasma Channel Characteristics

### 7.1 Post Breakdown Characteristics

One of the main objectives of this research project is to develop a computational model of a plasma closing switch which would describe the dynamic post-breakdown characteristics such as resistance, of the switch. This computational model of a plasma closing switch with the dynamic resistance will then be used within models of larger pulsed power systems to accurately describe their outputs allowing for optimization of full pulsed power systems or within the development phase of new systems yet to be built.

In order to develop such a computational model which will provide output results as close to practical experimental results as possible, some operational characteristics of the plasma closing switch need to be known in order to be built into the model, such as the conductivity of post breakdown plasma (which was obtained from optical emission analysis within Chapter 6), resistance and inductance of the plasma channel formed during breakdown events. The resistance and inductance parameters of the plasma channel which are investigated within this chapter are required in order to better aid the development of the computational model which is fully described within Chapter 8. The conductivity of the plasma channel formed have already been investigated and discussed within Chapter 6 and as such, the focus of this chapter remains on estimating the resistance of the plasma channel as well as the inductance of the plasma channel formed during breakdown.

It is shown within this chapter that by setting up a basic self-breakdown DC charged switch circuit and analyzing the post-breakdown current waveforms in the switch, values for both the constant resistance and the inductance of the plasma channel formed during breakdown events can be extracted from experimental data. This analysis is based on representation of the post-breakdown circuit as a lumped  $R-L-C$  circuit with constant values of  $R$ ,  $L$ , and  $C$ , solving the Kirchhoff Equation for this model circuit and matching the analytical solution with the experimental post-breakdown wave-forms.

This method is chosen as it is shown within literature [166] to be a valid method for calculating the post-breakdown plasma resistance within plasma closing switches filled with different gases including air. Based upon the method described within the literature, by

assuming the post-breakdown plasma resistance to be a constant value, it has been possible to obtain values of resistance of the plasma channel formed within different gases for different inter-electrode gap distances.

## **7.2 Test-set-up and methodology**

This section describes the experimental test set-up used to obtain the waveforms of the post-breakdown current that flows through the breakdown channel which is established across the inter-electrode gap in the gas-filled self-breakdown switch. A self-breakdown switch and the experimental set-up, as with the tests conducted to obtain the temperature of the plasma channel formed during breakdown described within Chapter 6, is utilised within this investigation. The switch is filled with gases, bottled air, N<sub>2</sub>, 60%/40% N<sub>2</sub>/O<sub>2</sub>, 90%/10% Ar/O<sub>2</sub>, CO<sub>2</sub> and SF<sub>6</sub> at 0.1MPa (all gases obtained from BOC Ltd,).

Figure 7-1 provides a schematic of the experimental test set-up used within the post-breakdown analysis of the switch characteristics, specifically the resistance and inductance of the plasma channel formed during a breakdown event.

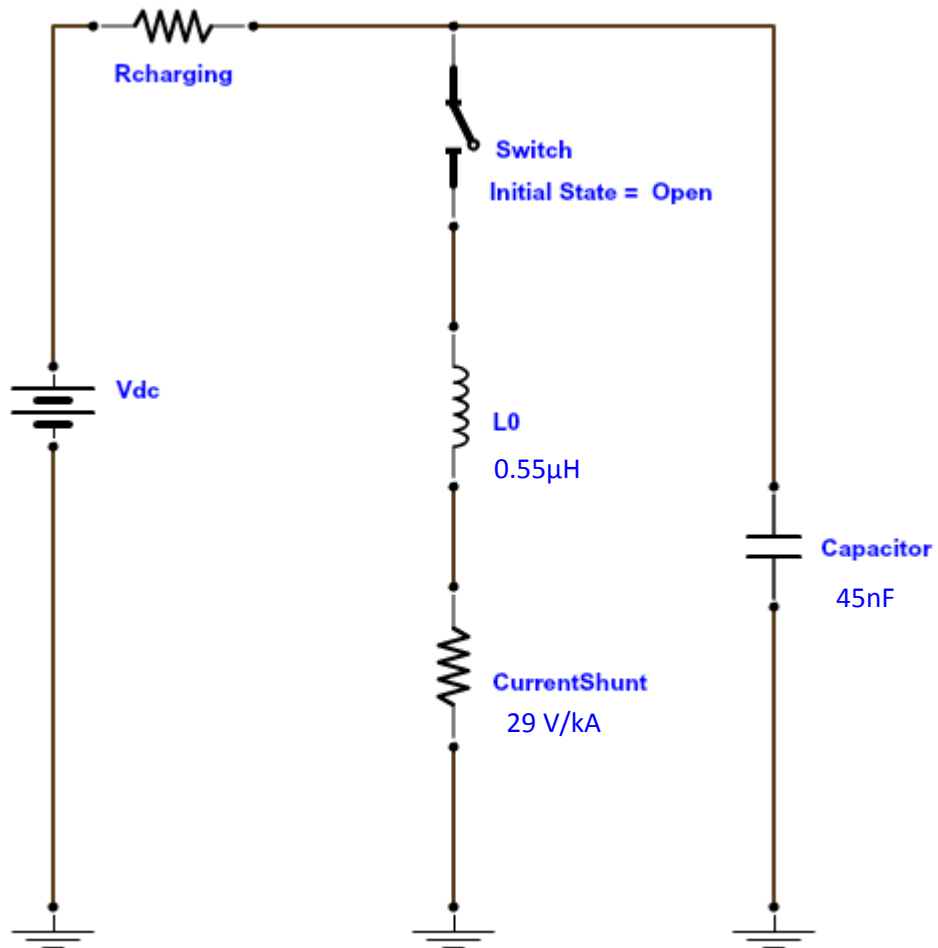
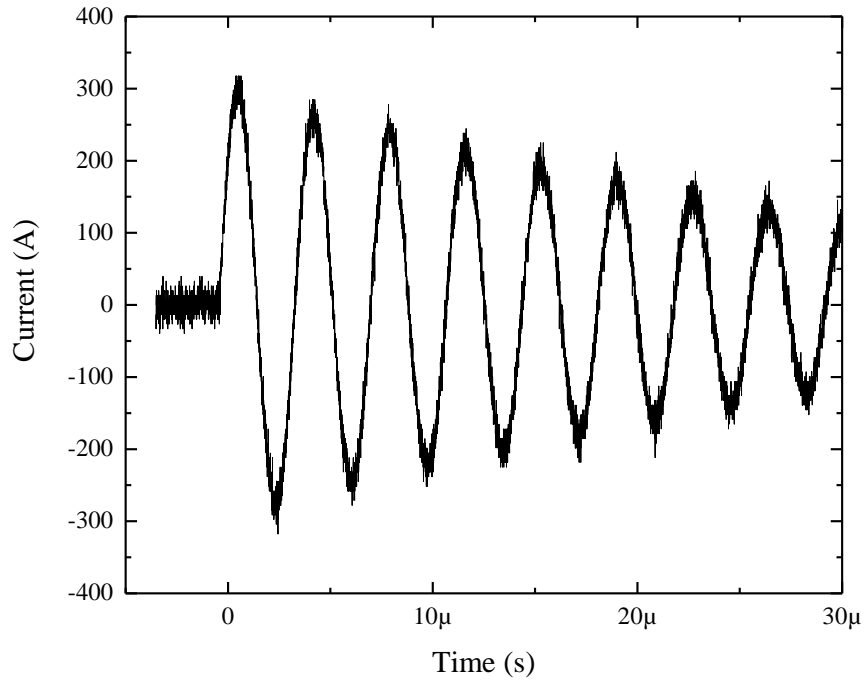


Figure 7-1 A schematic of the experimental set-up to obtain the post-breakdown current waveforms

A Glassman 100 kV high voltage DC power supply was used to apply the charging voltage across the switch via a 1M $\Omega$  charging resistor at a rate  $\sim$ 2kV/sec. A 0.55 $\mu$ H inductor and current shunt (29 V/kA) were positioned in series with the spark switch. A 45nF high voltage capacitor (Maxwell Ltd) was located in parallel to the spark gap switch in the circuit and charged through 1 M $\Omega$  current limiting protection resistance. A North Star PVM-5 high voltage probe (division ratio 1000:1, 80 MHz bandwidth) was used within the experimental procedure to monitor the voltage applied across the inter-electrode gap to ensure complete collapse of voltage across the switch had occurred. Both the current shunt and the PVM-5 probe were attached to a Tektronix TDS-3054 (500MHz, 5GS/s) oscilloscope to monitor the waveforms of the post-breakdown current and voltage across the switch respectively throughout the experimental procedure.

In obtaining the required waveforms for analysis of the plasma channel characteristics, the inter-electrode gap lengths used within these experiments ranged from 1mm-4mm (1mm, 2mm, 3mm and 4mm inter-electrode gap length) in order to analyse the effect of smaller inter-electrode gap lengths on the plasma resistance and inductance. Once the required inter-electrode gap length was set, the test cell was evacuated of gas via the gas distribution board (the same as utilised within Chapters 3 – 6 for evacuating and re-filling of the test cell with different gases/ gas mixtures) and re-filled with the required gas to 0.1MPa pressure (absolute). After the inter-electrode gap length has been set and the test-cell filled with the required gas, the DC voltage applied to the upper spherical electrode via the charging resistor was manually increased at a rate of  $\sim 2\text{kV/s}$  until a breakdown event was observed on the screen of the oscilloscope as monitored by the North Star high voltage probe. A current waveform which corresponded to the current flowing through the plasma channel created during the breakdown event was also shown on the oscilloscope screen and saved for analysis. A current waveform was obtained for three breakdown events conducted at each of the inter-electrode gap distances between 1mm-4mm listed and the waveforms analysed to extract characteristics of the plasma channel formed during the breakdown.

A typical example of the transient current in the air-filled switch is shown in Figure 7-2.



**Figure 7-2. Experimentally obtained post-breakdown current waveform from a plasma channel formed in the 1mm inter-electrode gap length in the air-filled switch at 0.1MPa with a breakdown voltage of 4.6kV.**

The current waveform in the circuit was analysed using the lumped RLC circuit model; the Kirchhoff Equation for this model circuit is:

$$\frac{d^2 I(t)}{dt^2} + \frac{1}{L} \frac{d(I(t)R_{total})}{dt} + \frac{I(t)}{LC} = 0 \quad (7.1)$$

where  $I(t)$  is the transient current,  $R_{total}$  is the total resistance of the circuit including the plasma resistance,  $C$  is the capacitance and  $L$  is the total inductance of the circuit.

In the experimental set-up, the plasma channel developed during the closure of the switch is used as the resistive load, the capacitance provided by a 45nF capacitor,  $C$ , and the resistance is the total resistance of the system which can be considered to be composed of two individual components, the circuit component  $R_{circuit}$  of the resistance and the

resistance provided by the plasma channel formed during breakdown  $R_{plasma}$  (assuming that this resistance is constant, this approximation can be used for description of the post-breakdown transient oscillations in the spark channel [70], [166]). The total overall resistance is a sum of the two individual components:

$$R_{total} = R_{circuit} + R_{plasma} \quad (7.2)$$

When breakdown occurs in the switch and the plasma channel formed between the upper and lower spherical electrodes, a transient process can be observed within the RLC circuit and the oscillating current can be monitored (Figure 7-2).

### 7.3 Results

For the purposes of the analytical approach taken within this chapter it was assumed that the resistance and inductance of the plasma channel formed during breakdown are constant and did not alter over time, therefore allowing the current flowing through the channel to be described by the solution of the Kirchoff Equation (7.1):

$$I = I_0 \exp(-\alpha t) \sin(\omega t) \quad (7.3)$$

where  $I_0$  is a constant related to the maximum peak current, (A),  $\alpha$  is the attenuation constant (1/sec) and  $\omega$  is the angular frequency (in rad/sec) all of which can be obtained from the experimental waveform as shown in Figure 7-2.

The current waveforms were obtained using the current shunt, these waveforms have been analysed using Equation (7.3) to extract values of  $\alpha$ , the attenuation constant and  $\omega$ , the angular frequency from the relative peak amplitudes of the oscillations of the current waveform.

The analysis procedure followed to obtain the values of resistance and inductance of the breakdown plasma was as follows; three breakdown events for each inter-electrode gap length within the switch when filled with each of the six different gases: air, N<sub>2</sub>, 60%/40% N<sub>2</sub>/O<sub>2</sub>, 90%/10% Ar/O<sub>2</sub>, CO<sub>2</sub> and SF<sub>6</sub> at 0.1MPa were initiated and the post-breakdown current waveforms were obtained and analysed. Peak current values,  $I_n$ , have been obtained for each sinusoidal current wave-form at

$$\omega t = (\pi/2 + n\pi), \text{ where } n=0, 1, 2, 3 \dots, \quad (7.4)$$

at these values of  $\omega t$  Equation (7.3) becomes:

$$I_n = I_0 \exp(-\alpha t) \quad (7.5)$$

$I_n$  values are used to obtain the averaged attenuation constant and the angular frequency,  $\omega$ , of the oscillations in the current flowing through the plasma channel produced during breakdown events.

In order to obtain  $\alpha$  for each wave-form, two peak currents,  $I_n$  (Equation 7.5) for  $n_1$  and  $n_2$  should be measured, and then divided by each other. This results in Equation 7.6 which allows calculation of  $\alpha$ :

$$\frac{I_1}{I_2} = \exp(\alpha(t_2 - t_1)) = \exp(\alpha \Delta t) \quad (7.6)$$

where  $\Delta t$  is the time difference between two time moments which correspond to Equation 7.4.

During the calculation of the resistance of the plasma channel, the post-breakdown current waveforms were analysed and by using the values of the subsequent relative peaks of the current oscillations, a value of  $\alpha$ , the attenuation coefficient is extracted by using

$$\alpha = \frac{\ln\left(\frac{I_1}{I_2}\right)}{\Delta t} \quad (7.7)$$

Where  $I_1$  is the relative peak magnitude of the current at point  $t_1$ ,  $I_2$  is the relative peak magnitude of the current at point  $t_2$  and  $\Delta t$  is the time elapsed between  $t_1$  and  $t_2$ . The value of the attenuation constant is later used in Equation (7.9) in order to obtain a value for the total resistance of the circuit.

For each wave-form, at least 6 current peaks have been measured and used for calculation of the attenuation coefficient  $\alpha$  for different time intervals  $\Delta t$ . Then the obtained 3 (at least) values of the attenuation coefficient have been averaged and  $\alpha$  for specific gas and specific inter-electrode distance have been calculated. Three individual current post-breakdown wave-forms for each gas and gap have been obtained and for each of these wave-form the attenuation coefficient have been obtained. The average of these three individual  $\alpha$  coefficients have been used in further analysis of the constant plasma resistance.

From the average value of the angular frequency obtained from the current waveforms, the inductance of the plasma channel formed during breakdown event can be calculated by using Equation 7.8:

$$L = \frac{1}{\sqrt{\omega^2 C}} \quad (7.8)$$

Once a value for the inductance,  $L$ , of the plasma channel formed during a breakdown has been evaluated, this is then used to evaluate the total resistance  $R_{total}$  of the circuit by making use of Equation 7.9:

$$R_{TOTAL} = 2L\alpha \quad (7.9)$$

Additional assumptions made within this analysis in addition to the constant value of the plasma resistance are:

1. the energy deposition into the plasma channel,  $E$  is a continuous process and directly proportional to time and
2. the radius of the plasma channel is also directly proportional to the energy delivered into the plasma channel.

The resistance of the plasma channel is then, for any specified inter-electrode gap length given by Equation 7.10:

$$R_{plasma} = k \frac{\ell}{E^3} \quad (7.10)$$

Where  $\ell$  is the inter-electrode gap length and  $k$  is a constant which describes the ratio of the change in total resistance of the experimental set-up (factoring in the circuit resistance as well as the differences in the resistance of the plasma channel due to the change in inter-electrode gap-lengths) to the corresponding energy of the plasma channel at a given inter-electrode gap length, and can be obtained from Equation 7.11:

$$k = \frac{\Delta R_{total}}{\left( \frac{\ell_1}{E_1^3} - \frac{\ell_2}{E_2^3} \right)} \quad (7.11)$$

where  $\Delta R_{TOTAL}$  is the difference between the total resistance for two different inter-electrode gap lengths (which can be calculated using Equation 7.7 for each of the inter-electrode gap distances ( $\ell_1$  and  $\ell_2$ ) required).

The post-breakdown current waveforms for three breakdown events in each of the inter-electrode gap lengths between 1 mm and 4 mm was analysed and the angular frequency and attenuation coefficients extracted. From these values, the inductance of the plasma channel formed during the breakdown event is obtained and the overall, total resistance of the circuit is evaluated as well as an estimated value for the resistance of the plasma channel which is formed at each inter-electrode gap length between 1 mm and 4 mm.

### ***7.3.1 Resistance and Inductance of Plasma Channel***

As previously outlined, three breakdown events were initiated for each inter-electrode gap length between 1mm and 4mm and the characteristics of the current waveform extracted in order to obtain further information such the values of the relative peaks of the current oscillations and the corresponding time at which they occur are used to evaluate the attenuation constant  $\alpha$  (1/sec), and the angular frequency  $\omega$  (rad/sec).

Using the value the angular frequency of the current waveform, it is possible to evaluate the inductance of the plasma channel formed during the breakdown event using Equation (7.8).

Table 7-1 provides the values of the inductance of the plasma channels formed during breakdown events at each of the inter-electrode gap lengths within the range 1mm-4mm for each of the 6 gases of interest within this investigation at 0.1MPa gas pressure.

**Table 7-1 Average inductance value extracted by analysing the angular frequency of the post-breakdown current waveform in an air-filled switch.**

Inter-electrode gap length (mm)	Air	N <sub>2</sub>	60%/40% N <sub>2</sub> /O <sub>2</sub>	90%/10% Ar/O <sub>2</sub>	CO <sub>2</sub>	SF <sub>6</sub>
1	7.74 μH	7.19 μH	7.13 μH	7.20 μH	7.17 μH	7.20 μH
2	7.72 μH	7.16 μH	7.16 μH	7.17 μH	7.18μH	7.20 μH
3	7.73 μH	7.14 μH	7.18 μH	7.17 μH	7.22 μH	7.20 μH
4	7.73 μH	7.17 μH	7.18 μH	7.16 μH	7.15 μH	7.13 μH

By using experimental waveforms to obtain and analyse the post-breakdown current waveforms and extract the inductance for each of the gases, the inductance of the plasma channels formed during breakdown for each of the gases can be compared. It is seen within Table 7-1 that the inductance of the plasma channels formed is ~7.20μH for all gases (except air where the inductance of the plasma channels formed was found to be slightly higher at ~7.73μH).

Once the value of inductance of the plasma channel has been estimated, using Equations 7.5 - 7.7, the values for the total resistance of the circuit and thus a value for the resistance of the plasma channels formed during breakdown in each of the inter-electrode gap lengths can also be estimated.

Table 7-2 provides the obtained values of the total resistance,  $R_{total}$ , of the system (circuit components and the resistance of the plasma channel formed during a breakdown) and the extracted value of the resistance of the plasma channel,  $R_{pl}$ , formed during breakdown events conducted within the self-breakdown switch when filled with each of the six different gases of interest within this experimental investigation.

**Table 7-2 Total resistance of the RLC circuit has been evaluated from Plasma Resistance value extracted from analysis of the post-breakdown current waveforms in the self-breakdown switch filled with each of the six different gases of interest within this investigation.**

Inter-electrode gap length (mm)	Air		N <sub>2</sub>		60%/40% N <sub>2</sub> /O <sub>2</sub>		90%/10% Ar/O <sub>2</sub>		CO <sub>2</sub>		SF <sub>6</sub>	
	R <sub>tot</sub> (Ω)	R <sub>pl</sub> (mΩ)	R <sub>tot</sub> (Ω)	R <sub>pl</sub> (mΩ)	R <sub>tot</sub> (Ω)	R <sub>pl</sub> (mΩ)	R <sub>tot</sub> (Ω)	R <sub>pl</sub> (mΩ)	R <sub>tot</sub> (Ω)	R <sub>pl</sub> (mΩ)	R <sub>tot</sub> (Ω)	R <sub>pl</sub> (mΩ)
1	0.44	30	0.48	82	0.48	50	0.53	49	0.48	45	0.44	97
2	0.41	(12)	0.43	(23)	0.44	(31)	0.48	(46)	0.44	(7)	0.35	(1)
3	0.40	(30)	0.41	(37)	0.42	(29)	0.46	(62)	0.43	(23)	0.35	(4)
4	0.38	(10)	0.38	(12)	0.40	(8)	0.43	(33)	0.42	(6)	0.36	(2)

It can be seen that within the assumptions of lumped  $R-L-C$  model used to obtain the constant plasma resistance,  $R_{pl}$ , and following the assumptions imposed on the energy deposited into the plasma channel and its radius outlined previously, namely that the resistance of the plasma channel is constant over time, it is possible to obtain values of plasma resistance for these inter-electrode gap lengths.

The values of plasma resistance for the air, 60%/40% N<sub>2</sub>/O<sub>2</sub> mixture, 90%/10% Ar/O<sub>2</sub> mixture and CO<sub>2</sub> filled gaps with 1mm inter-electrode gap length, as shown in Table 7-2 have similar values, typically  $\sim(30-50)$  mΩ. However, the plasma resistance values calculated for the 1mm inter-electrode gap length when the switch filled with N<sub>2</sub> or SF<sub>6</sub> were higher  $\sim(80-100)$  mΩ.

As the inter-electrode gap length increased from 1mm to 4mm, the changes observed in the obtained plasma resistance of the formed plasma channels are more stochastic between gases and between inter-electrode gap lengths. This is due to the limitations of the approach used to estimate the resistance of the plasma channel and the number of assumptions that were made in order to estimate the energy deposited into the plasma channel. As the inter-electrode gap length increases to lengths longer than 1mm, this method of extracting values of the resistance of the plasma channel that forms during breakdown in each of the gases may not be as reliable due to the previous assumptions

made in order to extract values of the plasma resistance. For this reason, while the calculated values of plasma resistance provide a reasonable approximation (i.e. the right order of magnitude), the exact values cannot be confirmed and have been placed in brackets to denote this. It is also observed that as the inter-electrode gap length increases, the resistance of the plasma channel formed decreases for all gases tested at 0.1MPa.

#### **7.4 Discussion**

It has been shown within this chapter that by constructing a simplified *RLC* circuit, it is possible to describe the post-breakdown current that flows through the system using the Kirchoff Equation. By making some basic assumptions about the energy deposited into the plasma channel, e.g. the energy deposited is proportional to time and that the radius of the plasma channel is also proportional to the energy deposited, it is possible to extract information from the current waveforms in order to estimate the value of resistance of the plasma that forms during a breakdown event.

It has been shown within this chapter that by using the Kirchoff approach it is possible to estimate the angular frequency and the attenuation of the post-breakdown current waveforms. From the values obtained of the angular frequency and attenuation of the current oscillations, it was possible to estimate the inductance of the plasma that forms within the inter-electrode gap spacing for all gases of interest and for gap distances of 1mm – 4mm. It was shown that inductances were in the region of  $\sim 7.2\text{-}7.7\mu\text{H}$ . This value of inductance estimated from the Kirchoff Equation is twice the ‘worst tolerable’ value presented within [60] when modelling replacement switches within the Marx bank of the Mevex machine. This value of  $7.2\text{-}7.7\mu\text{H}$  estimated from experimental data, however, is likely a total inductance value taking into account all components of the circuit and not just the switch itself.

From the value of the inductance as well as the other waveform parameters analytically obtained, it has also been possible to extract values for the resistance of the plasma that forms within the switch during a breakdown event. It has been shown that for a 1mm inter-electrode gap distance, the range of plasma resistances is of the order of  $\sim 30\text{-}100\text{ m}\Omega$  across all gases tested within this investigation. This value of plasma resistance was seen to decrease as the inter-electrode gap length increases and although the exact values obtained through the method outlined within this chapter were not considered to be

accurate due to the dependence on the difference between values extracted from two waveforms at a time, the order of magnitude of the plasma resistance (a few m $\Omega$ ) seems consistent and can be used to give a reasonable estimation as to the order of magnitude that can be expected of the plasma resistance as the inter-electrode gap length increases.

The Kirchhoff approximation, used within this chapter to extract the attenuation and angular frequency information from the post-breakdown current waveforms and, as a result, to be able to obtain values of inductance and resistance of the post-breakdown plasma has been outlined, however, a few assumptions had to be made in order to be able to apply this method. In assuming that the resistance of the plasma channel remains constant over time, it is also assuming that at the point of breakdown occurring the radius of the plasma channel is instantaneously formed. This is not the case as an instantaneous formation of a plasma channel of a fixed radius is physically impossible. Instead, the radius of the plasma channel will change and the resistance of the plasma channel will change dramatically, particularly over the first quarter of the post-breakdown current oscillation.

This change in plasma resistance over the first quarter of the post-breakdown current oscillation is of great importance as the resistance can change by orders of magnitude during this first quarter oscillation. The next chapter of this thesis takes the constant-resistance values obtained here for the plasma that forms during a breakdown event and uses them to develop a computational model that describes the output of a 12-stage Marx Bank system and then expands the constant-value model to include the more detailed analysis of plasma resistance over the first quarter of the post-breakdown current oscillation.

## **Chapter 8. Computational Model: 12 Stage Marx Generator**

The development of a computational model which describes and models the output of current Marx bank systems or a computational model that can be used to design and predict the output of any future Marx bank systems by making use of temporal breakdown characteristics such as the time dependent (transient) inductance and resistance of plasma channels formed obtained from experimental breakdown events within different gases was a fundamental aim of this research project.

Within this chapter a discussion on the development of a constant-value plasma resistance model is presented from an electronic circuit containing a single plasma closing switch model, the standard approach to modelling plasma channels, through to the full 12 stage Marx bank model within the computational software package PSpice. The constant resistance model is then adapted and expanded to take into account the real-life, time dependent nature of the plasma channel that develops within the switch and a model which considers these temporal characteristics is developed. Once a single stage switch with temporal characteristics has been developed, this too was expanded into a full 12 stage Marx generator model.

Several different approaches to estimating the transient resistance of the plasma channel formed during a breakdown event have been suggested [80]. The properties of spark-discharge plasmas have been of interest depending upon the physical characteristics of the gas used within the system such as pressure, gas type and temperature. The constant value of the plasma resistance initially used within the model developed within section 8.1.1 is a value extracted from experimental results obtained in section 7.3.1. The approach taken to describe the time-dependent resistance adapted from the above mentioned studies is discussed within section 8.2.

The computational models described within this chapter have been developed and are run using physical, experimentally obtained values from the experimental test set-up alongside values of plasma channel characteristics experimentally obtained earlier within this thesis.

## 8.1 Constant Resistance Model

### 8.1.1 Development of Computational Model

In order to simulate the characteristics of a plasma closing switch within a larger pulsed power system such as those in use at AWE [59], [60], [167], a model describing breakdown events in a single stage pulsed power system was developed within the computational software package PSpice. A simplistic model that represents the plasma channel which forms within the switch was created from lumped elements within an electric circuit as shown from Figure 8-1.

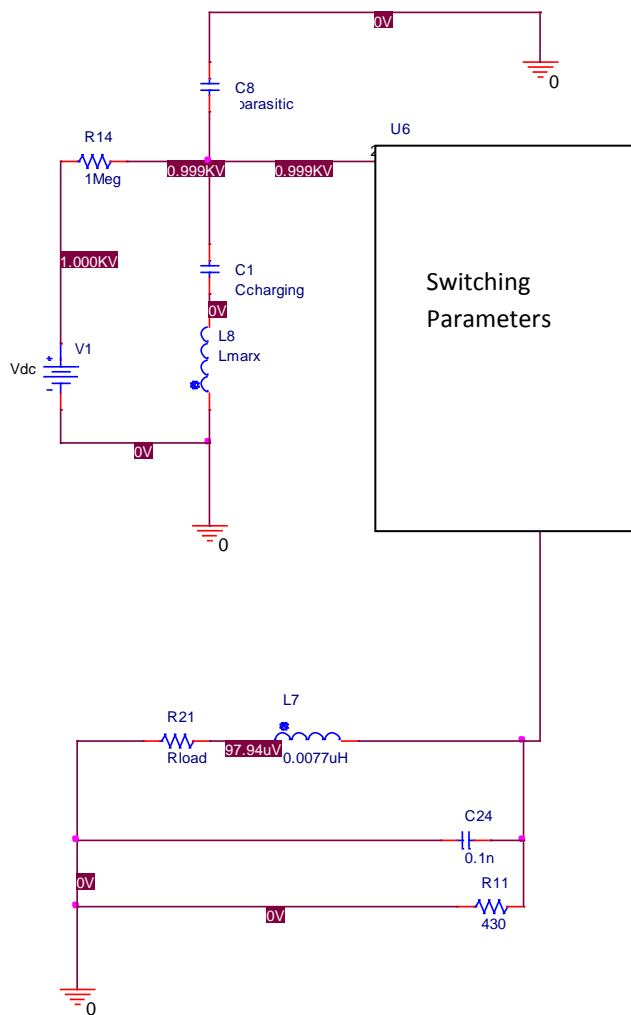


Figure 8-1 Simulated circuit with Plasma closing switch parameters.

It can be seen from Figure 8-1 that the circuit has a  $1\text{ M}\Omega$  charging resistor which acts as a current limiter and effectively decouples the DC charging circuit from the plasma post-breakdown event. Many of the values used within the charging elements and load elements were provided from [60]. The charging resistor has the same value,  $1\text{ M}\Omega$ , as was used in experimental tests previously described within this thesis (Chapter 3-7). The open-circuit, pre-breakdown impedance of the switch was specified to be  $1000\text{ M}\Omega$ , a switch closure time of  $1\text{ ns}$  was specified and the switch has a closed circuit impedance of  $0.01\Omega$ . The charging capacitor within the system denoted within Figure 8-1 as  $C_{\text{charging}}$  is  $250\text{ nF}$ . The inductance in series with that capacitor,  $L_{\text{marx}}$  represents the inductance of the Marx bank circuit. The total inductance of the system has been evenly distributed across the twelve stages of the Marx generator e.g a total inductance of the Marx bank equal to  $1.32\mu\text{H}$  corresponds in the simulation to twelve evenly distributed inductors at each switching stage with inductance values of  $0.11\mu\text{H}$ . This total circuit inductance has been varied in the simulations presented within this chapter and thus the inductance values presented within this chapter are presented as the value at each stage of the Marx bank. Also included within the model are parasitic capacitances to ground with values of  $0.01\text{ nF}$  at each stage of the Marx bank. These parasitic capacitances are typically  $\sim 2\%$  of the capacitance of the gap within the switch and parasitic capacitances of this nature have been shown to give more accurate results [7], [72].

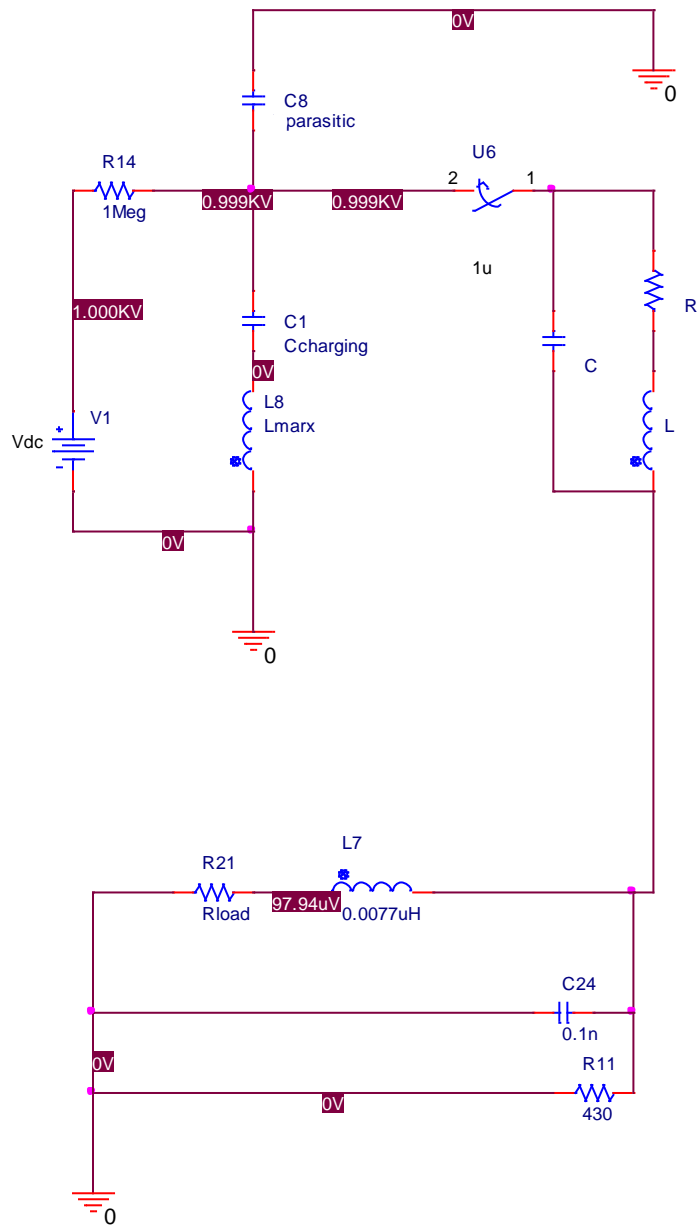


Figure 8-2 Single switch circuit model with the parameters of the plasma channel that forms during a breakdown event modelled after the switch by a lumped element RLC system.

From Figure 8-2 the constant value, lumped element, plasma parameters, R, L and C, can be seen. The post-breakdown plasma channel itself is described with basic resistance, inductance and capacitance (RLC) elements. Once the single gap switch elements had been put into place within the model, the values of the resistance of the plasma channel and the total inductance provided by the physical switch must be inserted in order to run the simulation to achieve as accurate results as possible.

Firstly, when evaluating the inductance of the switch topologies, including the inductance provided by the plasma channel formed during a breakdown event, some assumptions are made in order to be able to evaluate the inductance of the switches used within the experimental work conducted within this thesis. The analytical Equations provided [168], [169] were used to estimate the self-inductance of the switch in its post-breakdown state in which switch components such as electrodes and the breakdown plasma channel are simulated as straight, rod-shaped conductors have been used:

$$L = 2l \left[ \ln \left( \frac{2l}{a} \right) - 0.75 \right] \quad (8.1)$$

where  $L$  is the estimated inductance of the switch in nH,  $l$  is the length of a straight rod-shaped conductor (in cm) with a radius  $a$  (in cm). The inductance of the self-breakdown switch which has been utilised within Chapters 3 and 7 for evaluation of self-breakdown voltages and estimations of resistance of plasma channel, has been calculated. The schematic of the switch is shown again within Figure 8-3 in order to further illustrate the dimensions which have been used within Equation 8.1 in order to calculate the inductance of the switch.

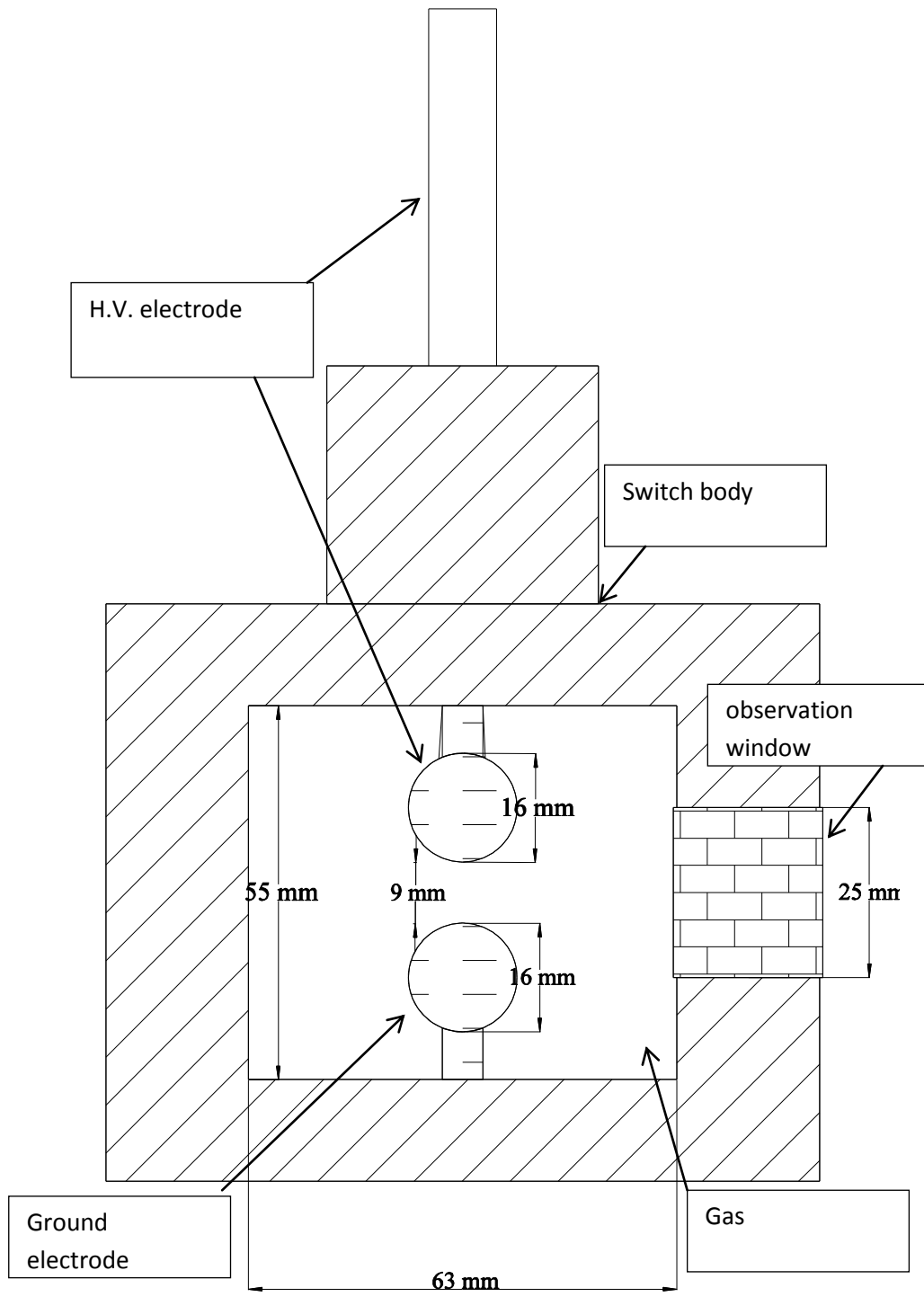


Figure 8-3 Topology of the self-breakdown switch used.

By using the dimensions of the switch topology in Figure 8-3 within Equation 8.1, this gives a total switch inductance value of  $\sim 65\text{nH}$  (the value of inductance contributed by a 9mm inter-electrode gap length with radius of 2mm is  $\sim 3\text{nH}$ ). These values of inductance are

then used within the PSpice model as the switch parameter inductance values in order to, as accurately as possible, under the assumptions made (i.e. not changing over time) describe the performance of the plasma closing switch.

In addition to the value of inductance required within the computational model of the plasma closing switch, a value of the resistance of the plasma channel that forms during a breakdown event is also required. It has been shown from experimental evaluation that the resistance of the plasma channel that forms within the inter-electrode gap length of a self-breakdown switch, estimated from Chapter 7, was in the range of 10s of m $\Omega$  when the length of the plasma channel is 1mm and decreases towards a few m $\Omega$  as the inter-electrode gap length increases towards 4mm (the limit of the experimental work conducted). Values for the constant plasma resistance of the order of 1m $\Omega$ -100m $\Omega$  have been deemed reasonable from experimental results and are therefore used within the development of this computational model of a single switch.

The development of a model of a single switch does give practical information as to the realistic, expected, output of a larger pulsed power systems where multiple switches are used since a single switch model within an electric circuit can describe the performance of only one switch (described by a lumped RLC circuit with constant resistance and inductance values). Once this single switch model within the electrical circuit was found to run without error however, it was possible to expand the model to incorporate 12 switches which would be charged in parallel and then by closing of the switches, would discharge in series – creating a computational model of a 12 stage Marx generator.

By using a switch inductance value of 65nH, plasma resistance values between 1 m $\Omega$  and 100 m $\Omega$ , it is possible with a full 12 stage model to see the effect of changing certain key characteristics of the plasma channel on the output of a 12-stage Marx bank system. Factors of operation of the switch such as risetime of the voltage impulse, the peak output voltage, pulsed power system run-time and dV/dt are of interest and were investigated with the use of this computational model.

### **8.1.2 Computational Results – Constant Resistance Model**

Initial simulations using constant value plasma characteristics which were run, modelled a 12-stage Marx bank system with a 60kV charging voltage in order to be able to compare the output of the developed model to the output of the Marx bank used in erecting AWE's Mevex machine [60] which charge the electrodes of their switches to +/- 30kV. Different values of plasma resistance and overall inductance of the Marx system were modeled in order to gain a better understanding of the influence of these characteristics on key output parameters such as peak output voltage, runtime of the system and  $dV/dt$ .

Presented within this section are the results of the output of the 12-stage Marx system across a load as the constant-value parameters of the plasma switches are varied. The resistance of the plasma was set at  $1m\Omega$  and  $100m\Omega$ , the overall inductance of the Marx bank was distributed evenly across the 12 stages. These results are compared and contrasted to observe the influence on the output of the Marx bank of changing the characteristics of the plasma switches and the system.

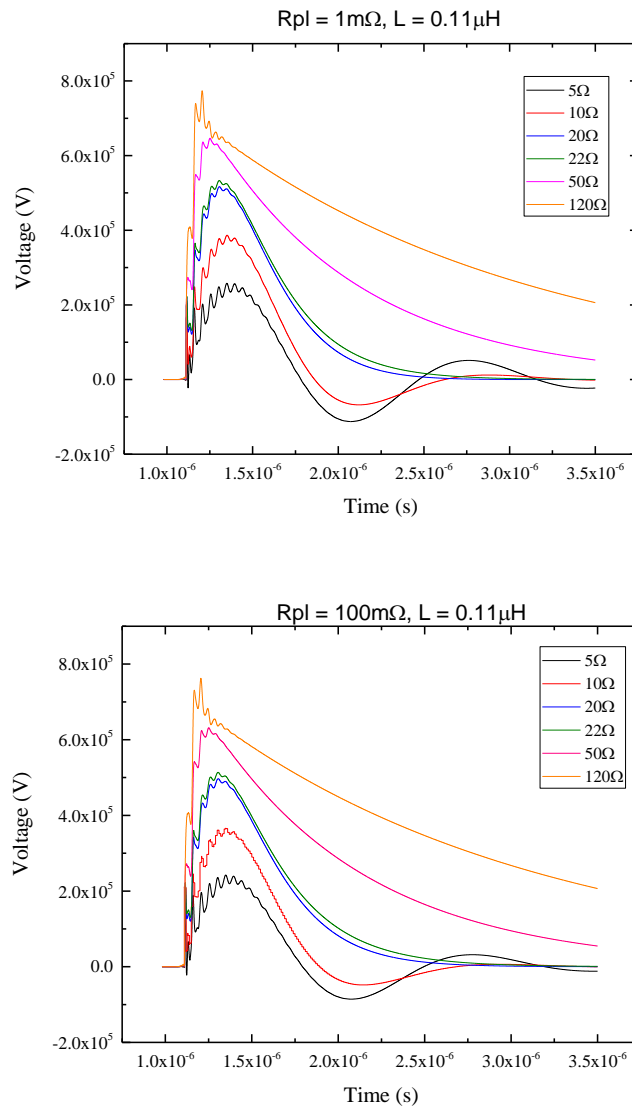


**Figure 8-4 Peak Voltage output of the 12-stage Marx bank as a function of time for 1mΩ and 100mΩ plasma channel resistance respectively.**

Initial simulations run within the constant-value characteristic model were for fixed value values of plasma resistance at 1mΩ and 100mΩ for values of load resistance from 5Ω-120Ω, again from [60] which simulate situations where the system would be underdamped, critically damped and overdamped as can be seen by the output waveforms within Figure 8-4. The peak output voltage of the 12-stage Marx generator model shown within Figure 8-4 is under modelled conditions for a total Marx inductance equal to 1.32μH.

It is seen within Figure 8-5 that a total inductance of  $1.32\mu\text{H}$ , a  $60\text{kV}$  charging voltage to the system, the peak voltage output observed is determined by the load resistance only. In terms of the peak voltage output across any specified load, for the simulations run with a plasma resistance value of  $1\text{m}\Omega$  were not significantly different from the output results presented by the simulations run when the plasma resistance was equal to  $100\text{m}\Omega$ .

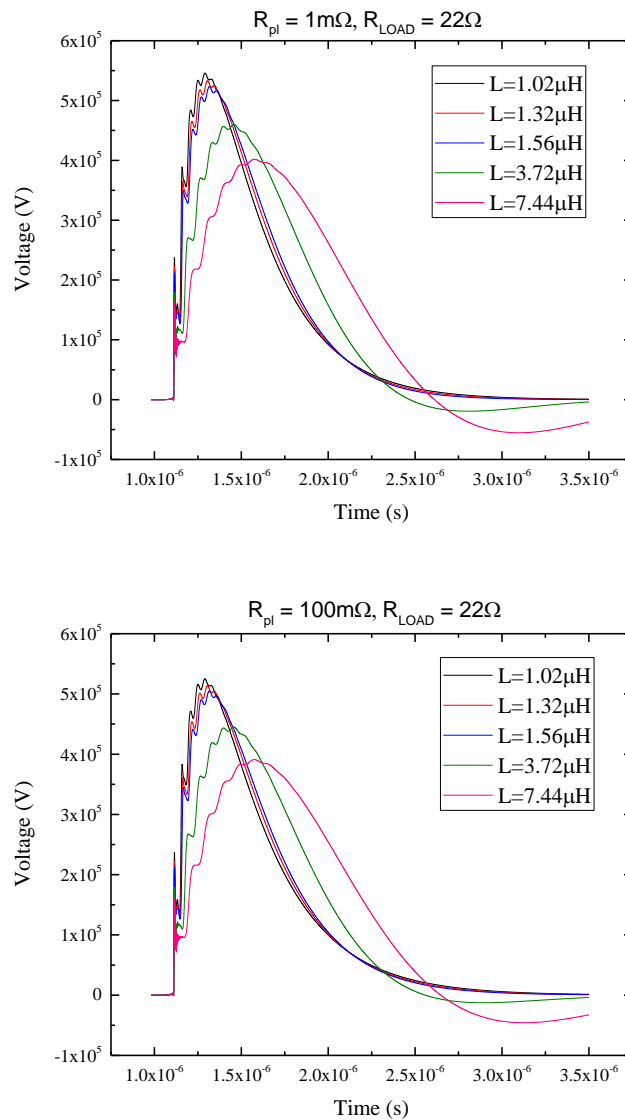


**Figure 8-5 The peak voltage across the 12-stage marx bank over time for only the  $22\Omega$  load resistance at the output of the 12 stage system.**

For a  $22\Omega$  load resistance (the typical load resistance of a diode in a flash radiography experiment) at the output of the 12-stage Marx generator, the waveforms within Figure 8-6

provide a means of observing the influence of the overall, total Marx generator inductance on the peak output voltage of the system. It can be seen that for total inductance values of  $1.02\mu\text{H}$ ,  $1.32\mu\text{H}$  and  $1.56\mu\text{H}$  that there is very little change in the peak voltage achieved or the time taken to achieve this peak voltage. For a total inductance value equal to  $3.72\mu\text{H}$  which has been deemed as the ‘worst tolerable’ inductance value for any potential Mevex replacement design [60]) the peak output voltage achieved is  $\sim 20\%$  lower than the peak voltage achieved for the inductances within the ‘expected inductance’ range. It has also been observed that for the inductance values equal to  $3.72\mu\text{H}$ , the time taken to reach peak voltage is  $\sim 48\%$  longer than the time taken to reach the equivalent peak output voltage when the inductance values are equal to  $1.02\mu\text{H}$ .

In addition to the impact on both the peak output voltage and the time taken to reach the peak output voltage by the inductance of the Marx system, it was again noted that for simulations run where the resistance of the plasma channel is equal to  $1\text{m}\Omega$  or  $100\text{m}\Omega$ , there was negligible difference in the output waveforms obtained.

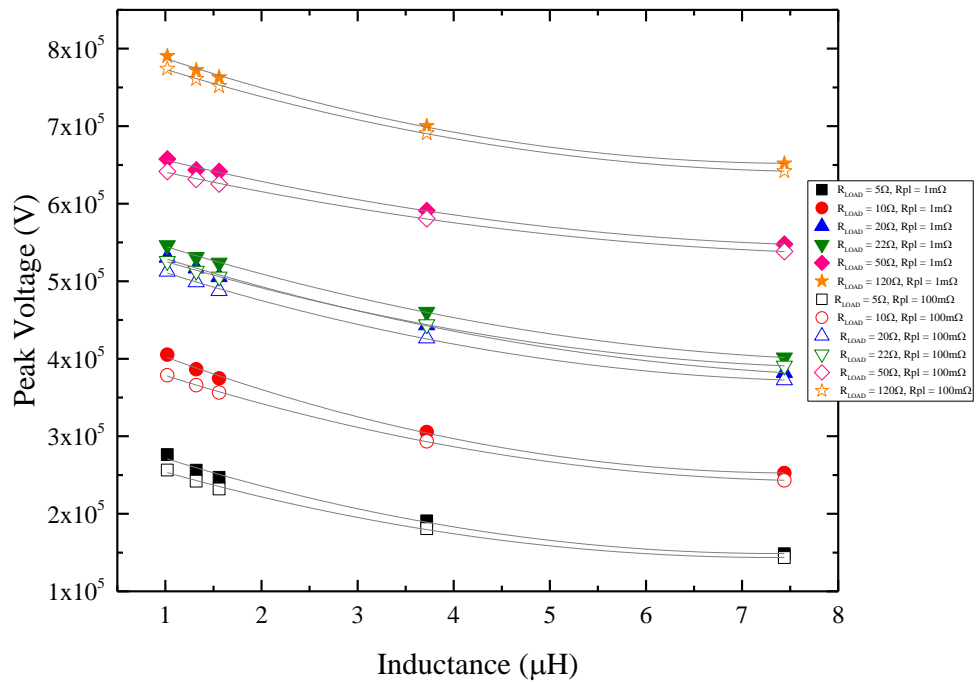


**Figure 8-6 Peak voltage across the resistive load, charged with 60kV DC as a function of the inductance of the Marx bank itself.**

The peak voltage output of the 12-stage Marx for different load resistances has been presented as a function of increasing inductance values (per stage) in Figure 8-6 across all values of load resistance of interest and for both 1mΩ and 100mΩ plasma resistance values. It is observed within Figure 8-6 that as the inductance of each stage of the Marx increases the peak output voltage decreases as is expected and observed from previous simulations shown in Figure 8-5. It is shown here that the difference in the peak output voltage when the plasma resistance is equal to 1mΩ and when it is equal to 100mΩ is typically very small ~3-7% and decreases as inductance increases.

Within these results, a second order polynomial Equation:

$$V_{pk} = AL^2 + BL + C \quad (8.2)$$

has been applied to fit the obtained data where  $A$ ,  $B$  and  $C$  are coefficients extracted from the fitting procedure,  $L$  is inductance at each stage (in μH) and  $V_{pk}$  is given in Volts. The extracted coefficients from the data obtained from the simulations are presented within **Error! Reference source not found..**

**Table 8-1 Coefficients from the second order polynomial fitting applied to the peak voltage output data as a function of the inductance at each stage of the 12-stage Marx bank system**

	<b>A</b>	<b>B</b>	<b>C</b>	<b>R<sup>2</sup></b>
$R_L = 5\Omega / R_{pl} = 1m\Omega$	$3 \times 10^3$	$-44 \times 10^3$	$291 \times 10^3$	0.99
$R_L = 5\Omega / R_{pl} = 100m\Omega$	$2.7 \times 10^3$	$-40 \times 10^3$	$313 \times 10^3$	0.99
$R_L = 10\Omega / R_{pl} = 1m\Omega$	$3.5 \times 10^3$	$-52 \times 10^3$	$451 \times 10^3$	0.99
$R_L = 10\Omega / R_{pl} = 100m\Omega$	$2.8 \times 10^3$	$-45 \times 10^3$	$420 \times 10^3$	0.99
$R_L = 20\Omega / R_{pl} = 1m\Omega$	$2.4 \times 10^3$	$-43 \times 10^3$	$570 \times 10^3$	0.99
$R_L = 20\Omega / R_{pl} = 100m\Omega$	$2.7 \times 10^3$	$-44 \times 10^3$	$552 \times 10^3$	0.99
$R_L = 22\Omega / R_{pl} = 1m\Omega$	$2.4 \times 10^3$	$-43 \times 10^3$	$585 \times 10^3$	0.99
$R_L = 22\Omega / R_{pl} = 100m\Omega$	$2.4 \times 10^3$	$-41 \times 10^3$	$564 \times 10^3$	0.99
$R_L = 50\Omega / R_{pl} = 1m\Omega$	$1.9 \times 10^3$	$-33 \times 10^3$	$687 \times 10^3$	0.99
$R_L = 50\Omega / R_{pl} = 100m\Omega$	$1.7 \times 10^3$	$-30 \times 10^3$	$669 \times 10^3$	0.99
$R_L = 120\Omega / R_{pl} = 1m\Omega$	$3.1 \times 10^3$	$-47 \times 10^3$	$832 \times 10^3$	0.99
$R_L = 120\Omega / R_{pl} = 100m\Omega$	$2.7 \times 10^3$	$-43 \times 10^3$	$814 \times 10^3$	0.99

The coefficients *A*, *B* and *C* of the fitting Equation (Equation 8.2) that are presented within Table 8-1 were obtained by fitting a second order polynomial fit to the obtained data in Figure 8-6 within OriginPro 2015 computational software package. Each of the values *A*, *B* and *C* are constant, dimensionless values while the final column of Table 8-1 provides the  $R^2$  values associated with the fitting lines applied to the data. The  $R^2$  values are the coefficients of determination and a measure of the closeness of fit to actual data.  $R^2$  values of 0.99 allow for a level of in the accuracy of the applied fit to the obtained results from PSpice.

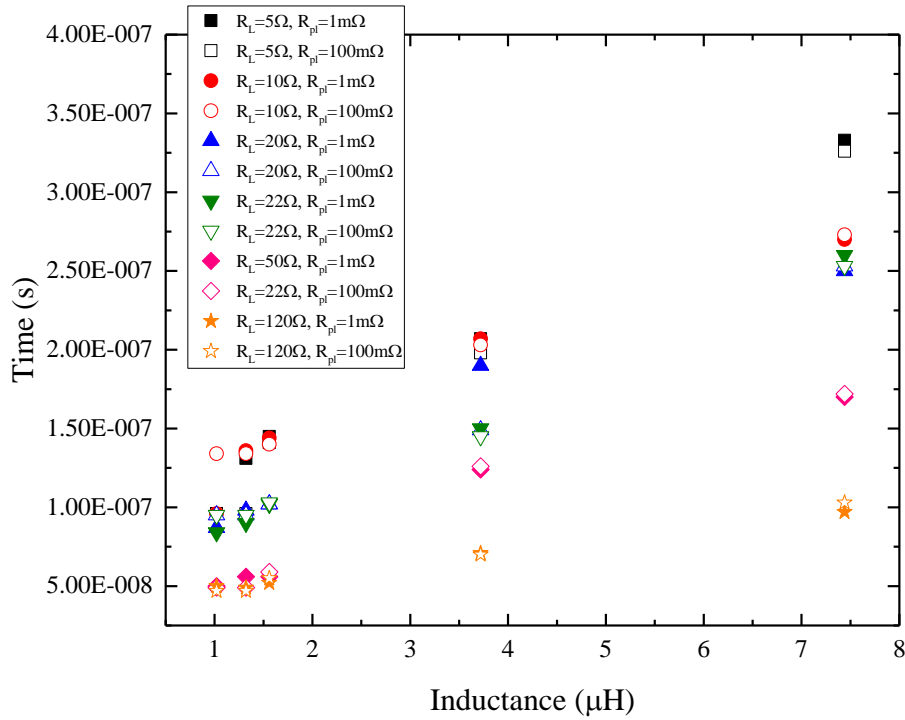


**Figure 8-7 Runtime of the 12-stage Marx bank system versus the inductance at each of the 12 stages of the Marx bank system. The runtime of the simulation being defined as the time to reach 80% of the peak output voltage from the time that the final switch in the 12-stage Marx system closes as defined by the user input.**

The runtime of the system is defined within this investigation as the time from the closure of the final switch to the time when the voltage has reached 80% of the peak magnitude. A delay of  $0.01\mu s$  between the closure of the first switch and the closure of each subsequent switch has been built into the model as this is a more realistic representation of functional systems which experience delay between the closure of each switch [23]. Switches do not all switch at the same time. As a result, the runtime of the Marx has also been investigated within this project as a function of the inductance (at each stage of the Marx) and is presented within Figure 8-8.

The runtime of the pulsed power system increases with inductance of the system and is observed within Figure 8-8, is shorter for higher values of load resistance,  $R_L$ . It was again observed that the difference in the runtime between simulations run for a plasma resistance  $R_{pL}=1m\Omega$  and a plasma resistance of  $R_{pL}=100m\Omega$  was small, typically  $<1\%$ .

Another quantity of interest is  $dV/dt$ , that is the change in voltage from 0 to 80% of the peak voltage over the time taken to reach that voltage as a function of the inductance of the Marx.

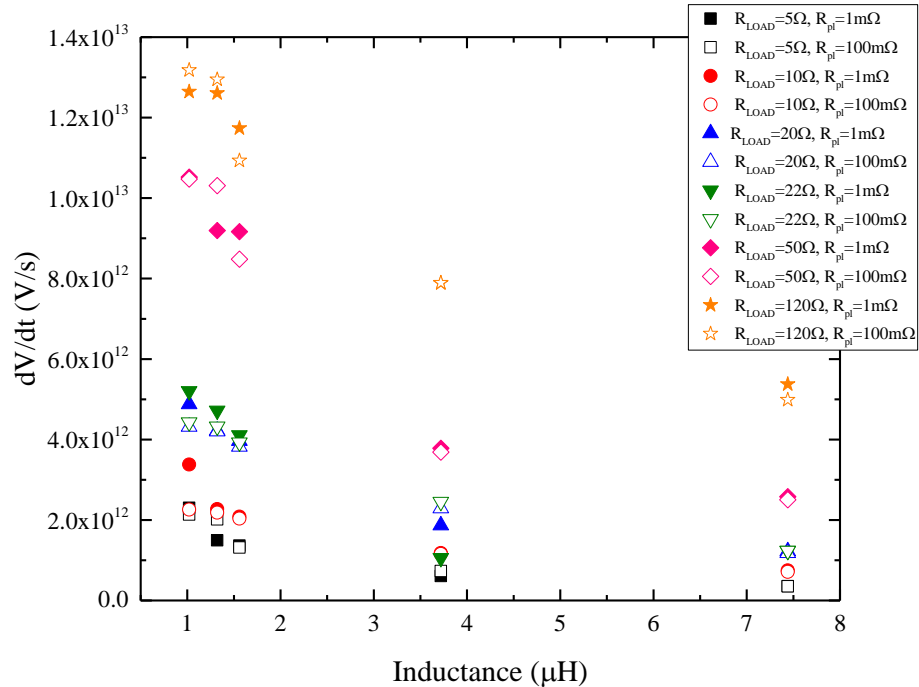


**Figure 8-8**  $dV/dt$  versus inductance of the Marx system (per stage) at each of the load resistances of interest within this investigation. For each load resistance, at each of the inductance values run within the simulation, the plasma resistance has been simulated at both 1mΩ (solid colour shapes) and 100mΩ (empty shapes).

The  $dV/dt$  quantity was evaluated as the voltage change from 0V to 80% of the peak voltage over the runtime of the system. It can be seen from Figure 8-9Figure 8-8 that as the inductance of each stage of the Marx increases (and thus the total inductance of the Marx system increases),  $dV/dt$  decreases which suggests that the change in voltage will be smaller over time for higher inductances within the system. Systems with high inductance will have smaller changes in voltage over the same timeframe, a result which is already observed from Figure 8-6Figure 8-5.

### 8.1.3 Conclusions

The development of a computational model within PSpice software of a plasma closing switch which uses constant values for characteristics of the plasma closing switch parameters such as the plasma resistance and inductance has been described. The plasma closing switch model has been utilised within a 12-stage Marx bank model, which includes all the values of Marx bank inductances, charging capacitances, stray capacitances and charging resistors that would be associated with physical experimental systems.

The peak output voltage for a  $22\Omega$  load resistance shows similar peak voltages and duration of oscillation with the computational and experimental results over long periods of time ( $\mu\text{s}$ ) presented within [60]. It also showed good agreement with the simulations where the inductance of the Marx bank was varied over an 'expected' to 'worst tolerable' range. From this range of inductances of the 12-stage Marx bank ( $1.02\mu\text{H}$ ,  $1.32\mu\text{H}$ ,  $1.56\mu\text{H}$ ,  $3.72\mu\text{H}$  and  $7.44\mu\text{H}$ ) it was possible to observe the effect of inductance on the characteristics of the Marx bank such as the peak output voltage, the runtime (defined as the time from the closure of the final switch in the system to the time where 80% of the peak voltage magnitude is reached) and  $dV/dt$  across the resistive load of the system.

The peak output voltage across the load was found to decrease as the inductance of the Marx bank increased and from the computational data obtained, a fitting has been suggested to allow for future calculations of peak voltage of systems where inductance values and load resistance values are known and also may fall within the range tested within these simulations. The runtime of the system was found to increase as the inductance increased which leads to the observation that  $dV/dt$ , that is rate of change of voltage over time, decreases as inductance of the Marx increases.

The developed computational model that replicates the operation of a plasma closing switch over time that uses constant values for characteristics such as the resistance and inductance within the switch, this can be used to describe transient processes over long periods of time which are used within applications such as arc switching and within the power industry. However, for many applications within pulsed power, the first quarter of the current oscillation is the key area of interest, as this is the time interval in which the resistance changes (by orders of magnitude) from its maximum value to some very small

value. In order to more accurately model this first quarter of the current oscillation, a model which considers dynamic parameters of the plasma channel must be developed.

## 8.2 Dynamic Resistance Model

In the previous section, a constant resistance approach was taken in order to develop a computational model of a plasma closing switch which could then be incorporated within a larger pulsed power system. In order to more accurately describe the performance of a gas-filled plasma closing switch, the temporal characteristics of the switch need to be taken into account, such as the time-dependent resistance of the plasma channel that forms during a breakdown event, as this will more accurately describe the characteristics of the current oscillations during the first quarter oscillation. Many different approaches have been taken throughout the years in estimating the resistance contributed by the plasma channel that forms during a breakdown event [73]–[75], [77]–[82], [170], [171]. All the models outlined relate the resistance of the plasma channel to the current flow either by relating the resistance to the inverse integral of the current or by relating the resistance of the plasma to the inverse exponential of the current. Both of these approximations focus on the first quarter of the current oscillation post-breakdown event when the resistance changes (by orders of magnitude) from an open circuit to the minimum value as the current reaches its peak magnitude. As the current flowing through the plasma channel will depend upon the radius of the plasma channel, which changes with time. The hydrodynamic model proposed by Braginskii [82] for the arc radius has been shown to match reasonably well with experimental investigations [83] and as such, the following ‘Braginskii’ Equation has been used for approximating the radius of the plasma channel over time:

$$a^2(t) = \left( \frac{4}{\pi^2 \rho_0 \zeta} \right)^{1/3} \frac{1}{\sigma} \int i^{2/3} dt = C_{brag}^{1/3} \sigma^{-1/3} \int i^{2/3} dt \quad [\mu\text{m}] \quad (8.2)$$

where  $a(t)$  is the radius of the plasma channel,  $i$  is the current flowing through the channel,  $t$  is the time,  $\zeta$  is a constant associated with the gas,  $\sigma$  is the conductivity of the gas,  $C_{brag}$  is a

phenomenological constant which is characteristic for each specific gas [82] and  $\rho_0$  is the gas density. By making use of this expression for the radius of the plasma channel, the time-dependent resistance of the plasma channel that forms during a breakdown event can be given by Equation 8.3, known as the Braginskii Equation.

$$R_{plasma} = \frac{l}{C_{brag}^{\frac{1}{3}} \sigma^{\frac{4}{3}} \pi \int I^{\frac{2}{3}} dt} \quad (8.3)$$

Where  $l$  is the length of the plasma channel (m),  $\sigma$  is the conductivity of the plasma channel ( $(\Omega.m)^{-1}$ ) and  $I$  is the current flowing through the plasma channel. The Braginskii Equation for estimating the resistance of the plasma channel within the switch during a breakdown event has been chosen as the most suitable description above those equations for the resistance Equations (2-12 – 2-20) is that in many of the alternative equations, constants of proportionality are present. The constants of proportionality in these equations have been obtained either theoretically or by fitting constants to data under prescribed and constrained experimental conditions.

This time dependent resistance (Equation 8.3) is utilised within the transient, time dependent model of the spark gap switch. By taking into account the time dependent resistance, this is designed to provide a more accurate description of the actual resistance within the plasma channel that forms during a breakdown event which will change value over time instead of taking a constant value at the point of breakdown. Therefore, the next step in developing the computational model was to replace the single constant value resistor with a system where the resistance of the plasma channel is described by Equation 8.3.

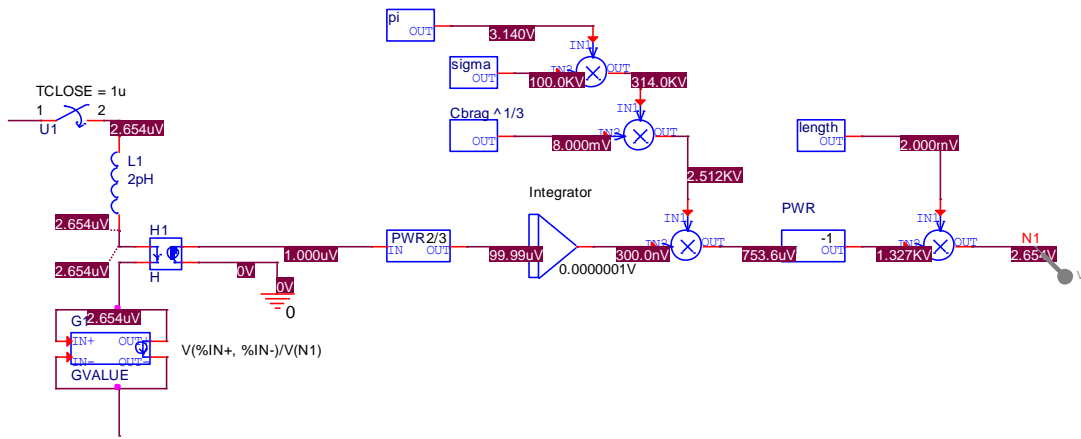


Figure 8-9 shows the expanded model of the plasma closing switch which now has the time-dependent resistance as described by Equation 8.3.

The circuit diagram within Figure 8-10 shows the method of modelling Equation 8.3 within the PSpice software package. Each of the elements which make up the dynamic resistance model are shown within Figure 8-11 and described individually as to their purpose within this model.

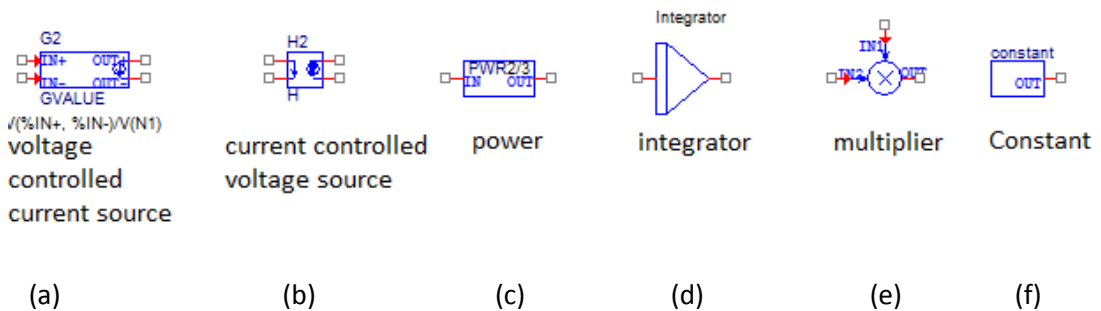


Figure 8-10(a)-(f) circuit components from the PSpice library that are utilised in order to model the time dependent resistance of the plasma channel which forms during a breakdown event within the switch.

The components Figure 8-10(a)-(f) are circuit components from the PSpice library which are used in building a computational model of a plasma closing switch which incorporates dynamic characteristics into the development of the model. Figure 8-10(a) is a voltage dependent current source which takes a voltage input and outputs a current equal to it with some proportionality determined by the expression 'value'. Figure 8-10(b) shows a current controlled voltage source which is placed in-line with the plasma channel components. This current controlled voltage source takes current and represents it as a

voltage signal with no negative impact on current waveform. The circuit shown within Figure 8-11 is a self-consistent model in which the dynamic plasma resistance is dependent upon the current and the current in turn is dependent upon the plasma resistance. Figure 8-10(c) is a power function and raises the input to a specified power, Figure 8-10(d) is an integrator function, Figure 8-10(e) a mathematical multiplier which multiplies the two inputs together and Figure 8-10(f) is a user-defined constant value.

Each of these components are brought together in order to model the dynamic resistance as described by Equation (8.3).

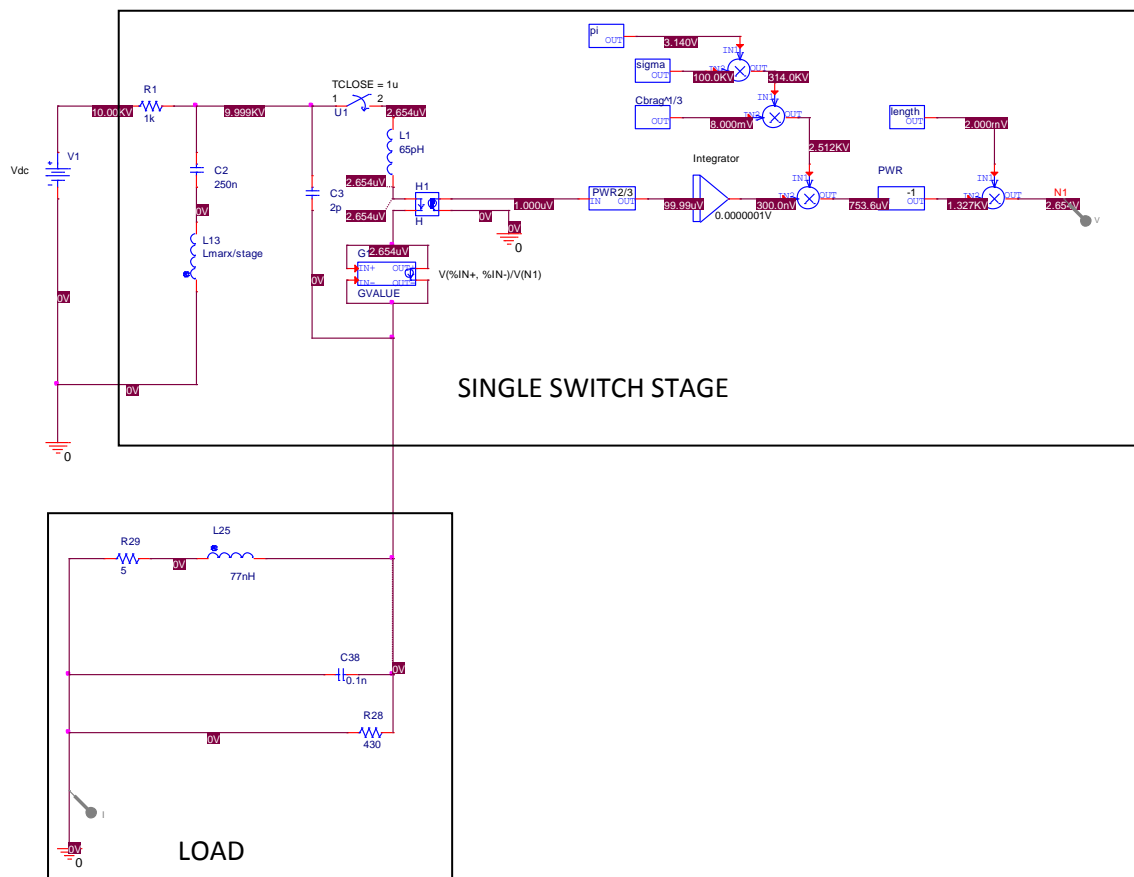
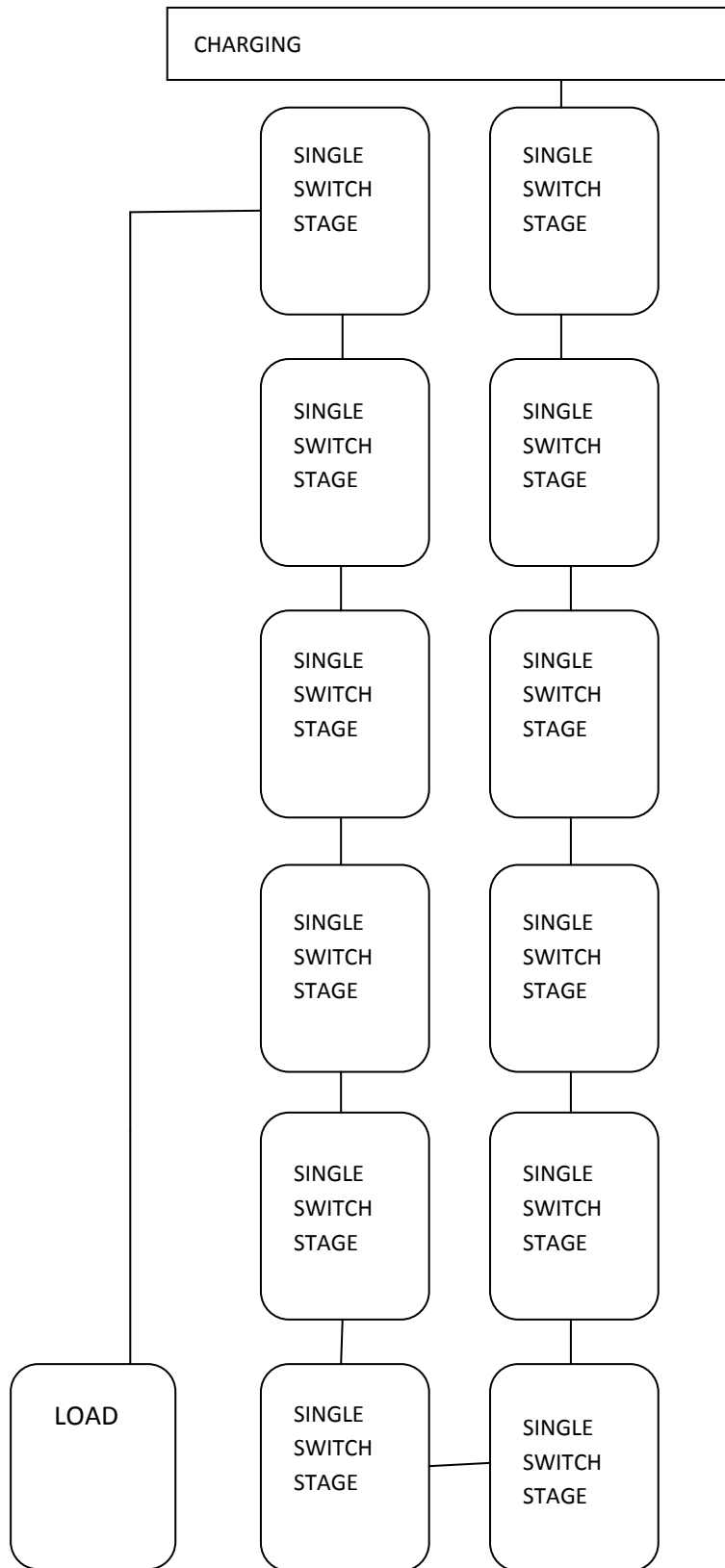


Figure 8-11 shows the schematic of a single switch model which incorporates the dynamic plasma parameters of the resistance into the model.

As with the constant resistance model within Section 8.1, a single switch does not give much useful information pertaining to the operation of larger pulsed power systems where

multiple switches are utilised in practice. In order to be able to accurately replicate systems which use multiple switches, a model containing multiple switches should be developed.

As previously discussed within Section 8.1 where a 12 switch system which replicates a 12-stage Marx bank generator was developed, so too in the dynamic resistance model is a system developed which contains 12 stages each containing the components shown within Figure 8-10 in place to model the resistance of the plasma channel. The full 12-stage dynamic Marx bank model which has been developed is shown within Figure 8-13.



**Figure 8--12 A block diagram of a 12-stage Marx bank model which has been developed that contains the components within each switch stage to more accurately describe the dynamic properties of the switch.**

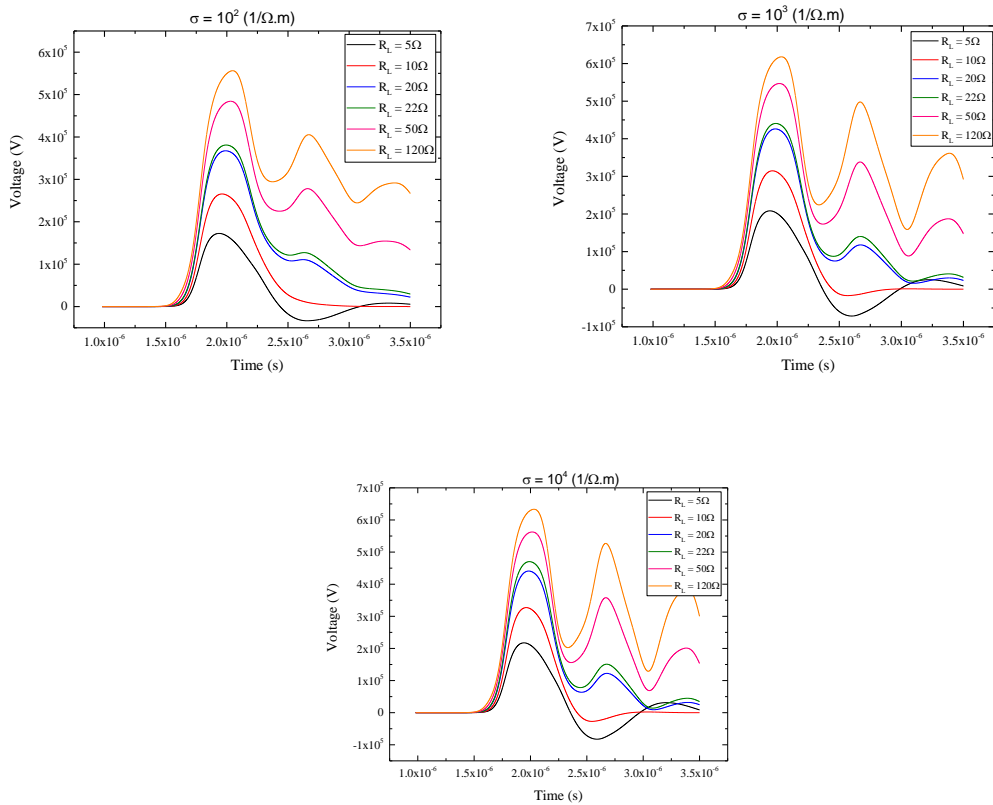
Within this model of the 12-stage Marx generator, the same charging voltage (60kV) is applied through a 1k $\Omega$  charging resistor in the circuit. The parameters that are altered within this simulation are the load resistance (the same values of load resistance as used within Section 8.1 of 5 $\Omega$ , 10 $\Omega$ , 20 $\Omega$ , 22 $\Omega$ , 50 $\Omega$  and 120 $\Omega$  were simulated) and the conductivity of the plasma (which has previously been calculated within Chapter 6).

Key output characteristics, such as the peak output voltage, the runtime of the system and dV/dt, are again of interest with this dynamic characteristic model and are monitored and compared as parameters are altered within the computational model.

### **8.2.1 Computational Results – Dynamic Resistance**

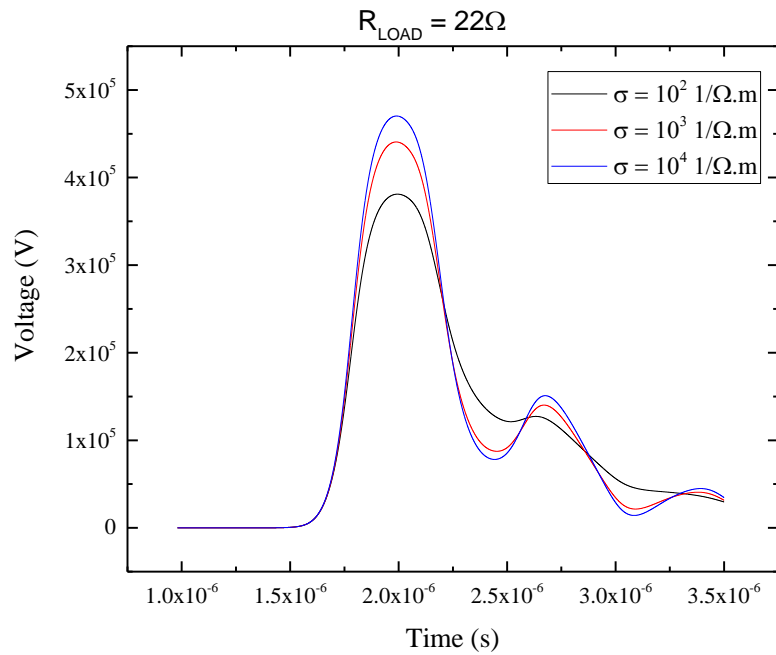
As has already been calculated within Chapter 6 of this thesis from an evaluation of the optical emissions within the switches, a value of the conductivity of the plasma  $\sim 10^3$  ( $\Omega\cdot\text{m}$ )<sup>-1</sup> was estimated by making use of the Boltzmann approach. It has been observed from literature that for plasma temperatures  $\sim 5000\text{K}$ , it is possible to measure a conductivity of plasma as low as  $\sim 10^2$  ( $\Omega\cdot\text{m}$ )<sup>-1</sup> [172] or as temperature of plasma increases, the conductivity of the plasma can also increase towards  $\sim 10^4$  ( $\Omega\cdot\text{m}$ )<sup>-1</sup> and beyond. Within the simulations conducted within this investigation, plasma conductivities of  $10^2$ ,  $10^3$  and  $10^4$  ( $\Omega\cdot\text{m}$ )<sup>-1</sup> are used to determine the sensitivity of the output characteristics such as the peak voltage output, the runtime of the system and dV/dt across the resistive load on the conductivity of the plasma.

With a DC charging voltage of 60kV applied and plasma conductivities within the range  $10^2$ - $10^4$  ( $\Omega\cdot\text{m}$ )<sup>-1</sup>. The first of the output characteristics of interest with this dynamic characteristic model is that of the peak output voltage across the resistive load.



**Figure 8--13 Peak voltage output of the 12 stage marx bank which incorporated the dynamic resistance model over time for different output load resistances. Each of the three graphs shows different conditions where the value of conductivity of plasma was altered between  $\sim 10^2 - 10^4$  1/Ω.m**

It can be seen from Figure 8-14 that for each of the values of plasma conductivity, the peak output voltage will vary depending upon the load resistance at the output of the Marx generator as was observed within Section 8.1 in the constant value model. Within the results shown, regardless of the conductivity of the plasma it is evident that the higher the load resistance, the more oscillations there will be on the voltage waveform. For a direct view of the effect that a difference in the plasma conductivity will have on the peak output voltage, the waveforms for the 22Ω load resistance were directly compared and are shown within Figure 8-15.



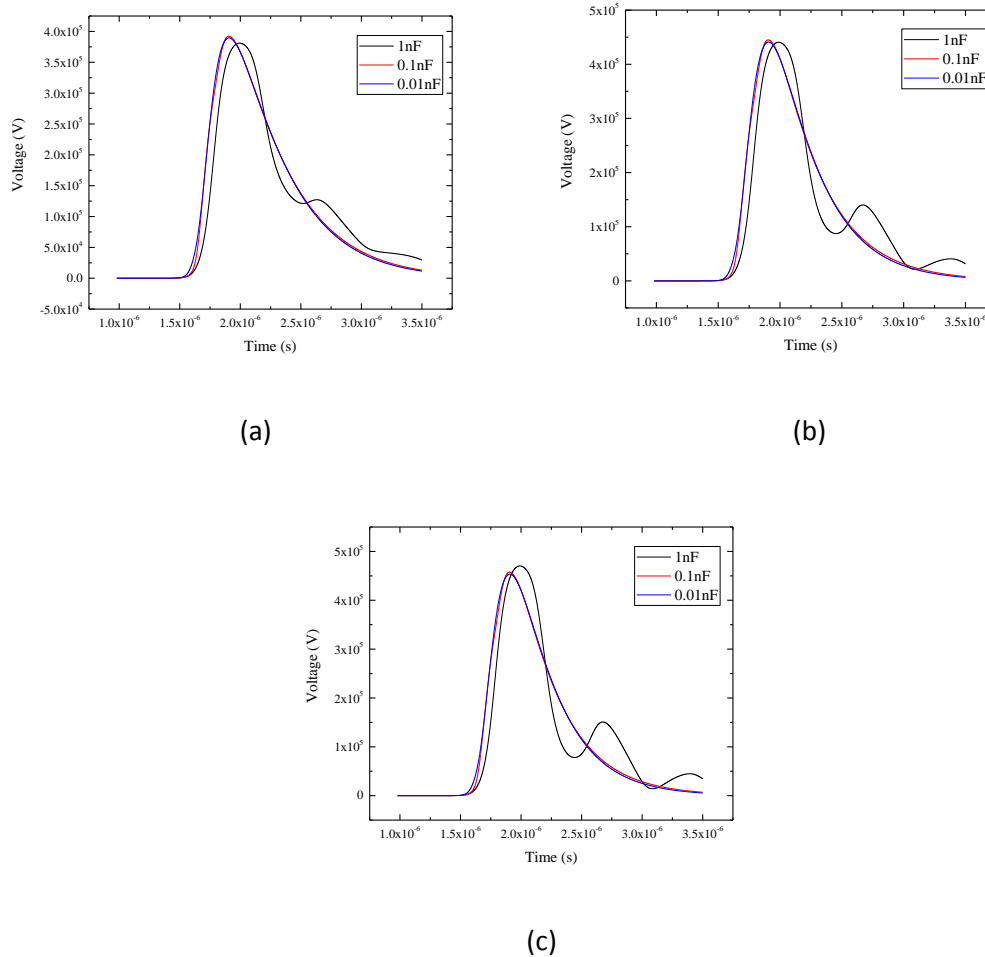
**Figure 8-14 Peak voltage versus time for a 22Ω load resistance at each of the 3 different plasma conductivity values covering the range of reasonable plasma conductivities seen to correspond to plasma temperatures 5500K-6500K and above from literature.**

Figure 8-15 shows peak voltage output over time of the 12-stage Marx generator model and the influence of the conductivity of the plasma in the switch on the peak voltage output. It can be seen that for higher conductivity of plasma in the switch, the peak output value will also be higher. The peak voltage output of the Marx generator is ~16% higher when the conductivity of the plasma is  $10^3 (\Omega.m)^{-1}$  than when the conductivity is  $10^2 (\Omega.m)^{-1}$  and a further 7% higher when the conductivity increases to  $10^4 (\Omega.m)^{-1}$ .

Another observation from within Figure 8-14 is that as the conductivity of the plasma increases, further oscillations in the voltage waveform become more prominent. While this dynamic model was created due to an interest by the industrial partners of this project in, primarily, the behaviour over the first quarter of any voltage or current oscillations, any oscillations that appear at later time-points may be of importance in other applications where the whole waveform is considered.

One other consideration within the model is the effect on results of any stray capacitances to ground. Stray capacitances have been included within the model, however the value of

these stray capacitances are not well known and have also been estimated from literature values [72]. As such, the  $22\Omega$  load resistance with conductivity values of  $10^2$ ,  $10^3$  and  $10^4$   $(\Omega.m)^{-1}$  were re-run with values of each of the stray capacitances to ground of 1nF, 0.1nF and 0.01nF.



**Figure 8-15(a)-(c) the effect of varying the parasitic capacitance to ground on the peak output voltage waveforms for plasma conductivities of (a)  $10^2$ , (b)  $10^3$  and (c)  $10^4$   $1/\Omega.m$  respectively.**

In terms of the effect on peak output voltage, the sensitivity of the 12-stage Marx model that incorporates dynamic characteristics on the value of the parasitic capacitances to ground is seen to be small. For all values of plasma conductivity, when the parasitic capacitances within the model had values of 0.1nF or 0.01nF, there was virtually no difference at all in the peak output voltage and the waveforms were almost identical in terms of temporal conditions too. For plasma conductivity of  $10^2$   $(\Omega.m)^{-1}$ , the peak output voltage with 1nF stray capacitance to ground peak output voltage was seen to be  $\sim 3\%$

lower than the peak output voltage observed for the 0.1nF and the 0.01nF stray capacitances and for conductivity of  $10^4(\Omega.m)^{-1}$ , the 1nF stray capacitance voltage waveform showed an increase in peak voltage of  $\sim 2.5\%$  compared to the peak voltage output when simulated with stray capacitances with values of 0.1nF or 0.01nF. The 1nF stray capacitance values for all plasma conductivity values showed oscillations on the voltage waveform beyond the first voltage peak and these oscillations become more prominent as the conductivity of plasma increases. In addition to this, for 1nF values of stray capacitance, it can be seen within Figure 8-15(a)-(c) that it takes a longer amount of time to reach the peak voltage than if the stray capacitances were 0.1nF or 0.01nF.

After these observations, it was decided to fix the value of the stray capacitances within the rest of the simulations in this investigation at 1nF as this allows for some degree of flexibility and 'worst tolerable' values to be obtained. The conductivity of the plasma channel measured within experimental conditions in Chapter 6 provided a value of  $10^3(\Omega.m)^{-1}$  which when considering Figure 8-16(b) showed no change in peak voltage when changing the stray capacitance value over two orders of magnitude. The time taken to reach peak voltage is observed to take longer when the stray capacitance is 1nF than when the stray capacitance is 0.1nF or 0.01nF, however any times taken to determine the runtime of the system can then be considered to be over-estimations or 'longest expected time' to reach the peak voltage.

Once the peak voltage output of the 12-stage Marx generator had been analysed for different values of plasma conductivity, the runtime of the system was also analysed in a similar way to that described within Section 8.1.2.

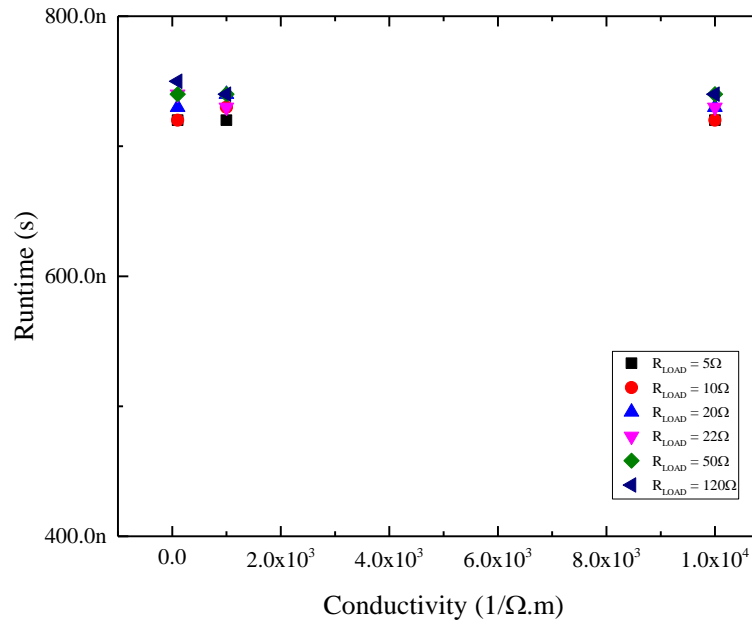


**Figure 8-17** The runtime of the 12-stage dynamic Marx generator model vs conductivity of plasma within the switch.

The runtime of the system is again defined (the same definition from Section 8.1.2) as the time difference between the closure of the final switch in the system (user defined within this computational model at 1.11μs. The first switch closes after a 1μs delay and a further delay time of 0.01μs between each switch closing and the closure of the previous switch) and the time at which the voltage reaches 80% of its peak magnitude.

It can be seen from the results of the runtime of the system plotted as a function of increasing conductivity as shown within Figure 8-17 that there for each value of plasma conductivity, there is an increase in the runtime of the system as the load resistance increases, however this increase in runtime is typically very small. As the conductivity of the plasma channel increases from  $10^2 (\Omega.m)^{-1}$  to  $10^4 (\Omega.m)^{-1}$  there has been no discernible change in the runtime of the system due to the change in plasma conductivity. As the conductivity of the plasma channel increases, the runtime of the system remained constant at ~720ns -740ns across all values of load resistance of interest within this investigation.

This result shows that the runtime of any model and therefore, in theory, any practical pulsed power generators developed will not be sensitive to the gas used within the

switches of the plasma that forms within the switches. This gives greater flexibility and means that certainly for runtimes, an estimation of the conductivity within the plasma would be sufficient rather than requiring precise measurements. With that being said, the runtime of the system not changing will then have an impact on the rate of rise of voltage across the load of the system which is another key characteristic in many applications.

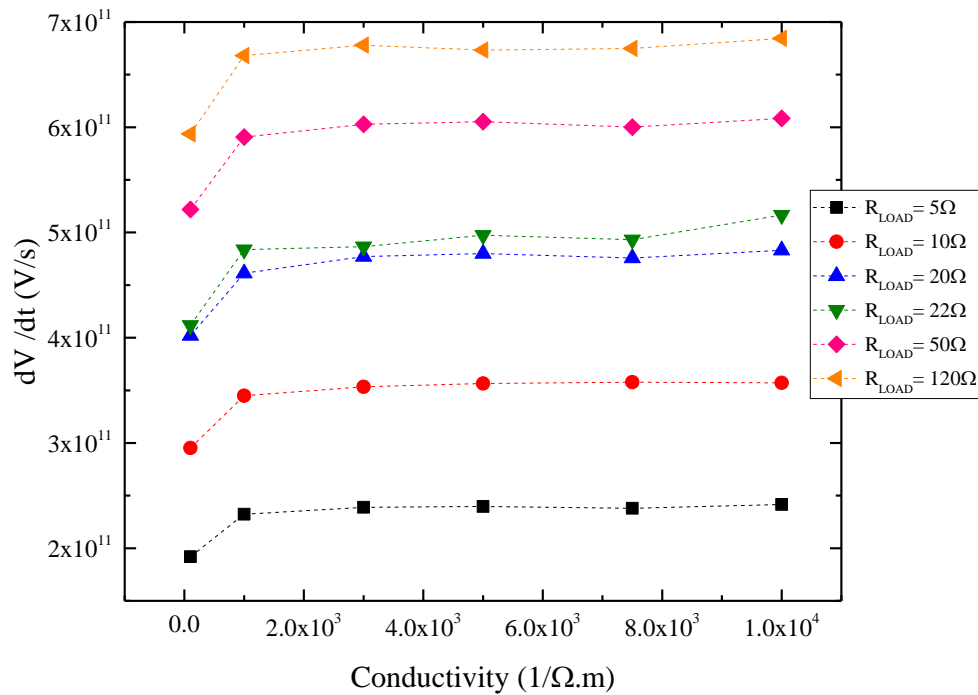


Figure 8-18  $dV/dt$  vs Conductivity of Plasma for each individual load resistance value.

Presented within **Error! Reference source not found.** is the rate of voltage rise across the load for different load resistances of the 12-stage Marx system as a function of the plasma conductivity within the switch. The  $dV/dt$  value was calculated for the voltage to change from 0V to 80% of the peak voltage and the time over which this change took place, i.e. the runtime of the switch. It is seen within Figure 8-18 that when the conductivity changes from  $10^2 (\Omega.m)^{-1}$  to  $10^3 (\Omega.m)^{-1}$  the  $dV/dt$  value increases for all values of load resistance beyond the Marx generator, however for any value of plasma resistance between  $1 \times 10^3 (\Omega.m)^{-1}$  and  $1 \times 10^4 (\Omega.m)^{-1}$  there does not appear to be any significant difference in  $dV/dt$ . This again suggests that for plasma conductivities that cover a wide range (corresponding to a wide range of plasma temperatures) there is little sensitivity within the model (or practical

systems) on the  $dV/dt$  to this parameter which allows for greater flexibility in practical settings. This also does not depend on the gas within the switch.

### 8.3 Discussion and Conclusions

Within this section, two computational models have been developed and run with important characteristics observed in both cases.

A constant plasma resistance model which models the breakdown plasma resistance and inductance parameters has been seen to depict the working characteristics of a 12 stage Marx generator over  $\mu s$  timescales. The peak voltage output of the 12-stage Marx generator model showed similar voltage magnitude to both the simulations and the experimental results presented within [60].

The key changes within this model were the values of plasma resistance or the value of the Marx generator inductance which was evenly distributed across the twelve stages of this model. It was seen that for plasma resistance values of  $1m\Omega$  and  $100m\Omega$  (values of plasma resistance which had previously been obtained from experimental results in Chapter 7) that no significant difference was observed on any of the key output characteristics monitored within this investigation.

The value of the inductance of the Marx generator, however, does play a more significant role in determining the output characteristics of the Marx generator. The peak voltage across the load was found to decrease as the inductance of the system increased and a fitting has been suggested to allow for future prediction of peak voltages which can be obtained for future models or systems with inductance and resistance values that fall within the range investigated within this project without the need to re-run or build entire models. In addition to this it was also found that the runtime of the system will increase as the inductance of the system increases – this will be of use for applications looking to minimise inductance knowing that this also minimises runtime but will also allow for maximum peak voltage. The  $dV/dt$  of the Marx generator was found to decrease as the inductance of the switch increases. As discussed within [6], the recovery rate of switches can sometimes lead to  $dV/dt$  constraints within switches depending upon the application and so would need to be considered as high  $dV/dt$  applications can result in switch closure.

All of these results for the constant-value resistance and inductance model showed good agreement with previously investigated works with similar experimental conditions over long ( $\mu\text{s}$ ) timescales. Many applications are primarily concerned, however, with the behaviour over the first quarter of the current oscillation and have no real concern for the behaviour beyond this. For this reason, a more accurate model over this first quarter of the voltage waveform was required and for this, a model that described the resistance of the plasma channel with dynamic parameters was developed.

The dynamic resistance model is a self-consistent model that can be altered to include details of the conductivity of the plasma channel and the associated gas constants obtained using the Braginskii approach for the specific gas which fills the switch as an insulating medium. In Chapter 7 of this thesis it has been calculated using the Boltzmann approach that for plasma temperatures in the range of 5500-6500K, the conductivity of the plasma within the switch is  $\sim 10^3(\Omega\cdot\text{m})^{-1}$  for the gases of interest within this study [173] although this can be as low as  $10^2(\Omega\cdot\text{m})^{-1}$  [172] and so changes to the output parameters of the Marx for conductivity values in the range  $10^2$ - $10^4(\Omega\cdot\text{m})^{-1}$  were simulated.

It was found that as the conductivity of the plasma increases, the peak voltage that can be achieved also increases, however an appearance of oscillations in the voltage waveform at higher values of conductivity beyond the initial voltage peak may play a factor for any applications looking for smooth voltage waveforms on longer timescales. The runtime of the system was investigated again, this time for the dynamic model, and was found to remain constant regardless of the value of conductivity of the plasma channel. A useful finding for practical applications as it allows for more freedom in physical experimental conditions if the runtime of the system does not depend on the conductivity measurement. It was also seen that the  $dV/dt$  of the dynamic model while increasing initially when the conductivity increases from  $10^2(\Omega\cdot\text{m})^{-1}$  to  $10^3(\Omega\cdot\text{m})^{-1}$ , beyond this value of conductivity, there was no evidence of change in  $dV/dt$  at higher conductivity values.

One final consideration with this dynamic resistance model was the effect of parasitic capacitances to ground within the model. It has been shown within some studies that the value of these capacitances can affect the voltages within the system [72] however values of stray capacitances across two orders of magnitude were simulated (1nF, 0.1nF and 0.01nF) and little difference was noted in terms of peak voltage waveforms output. The peak voltage magnitude changed <3% for the  $10^2(\Omega\cdot\text{m})^{-1}$  and  $10^4(\Omega\cdot\text{m})^{-1}$  conductivity plasma

simulations, however it was noted that the time take to reach the peak output voltage was slightly longer for the 1nF stray capacitances than for the 0.1nF or 0.01nF capacitances. For this reason, all simulations in the dynamic simulation model were left with 1nF stray capacitance values as this allowed for a “longest expected” timeframe value to be obtained.

It is possible therefore from the results of the two models created to suggest options that may be worth investigating further in terms of real-life practical experiments depending upon the application and required output of the Marx generator that would be needed.

## Chapter 9. Conclusions and Future Work.

### 9.1 Conclusions

The main aims of this thesis were to characterise plasma closing switches when filled with different gases and to use the experimental results to develop a computational model that would describe the operational working of a plasma closing switch that could be used within a model of a larger pulsed power system.

The focus of the research came from filling two commonly used plasma closing switch topologies with environmentally friendly gases and comparing the operational characteristics to those when the switches were filled with the conventionally used SF<sub>6</sub>. Throughout the course of the research project, the operational characteristics of a self-breakdown topology switch and a field distortion spark gap switch were examined when filled with air, N<sub>2</sub>, 60%/40% N<sub>2</sub>/O<sub>2</sub>, 90%/10% Ar/O<sub>2</sub>, CO<sub>2</sub> and SF<sub>6</sub>, up to 0.4MPa. The experimental novelty of this work lies in the use of the 60%/40% N<sub>2</sub>/O<sub>2</sub> gas mixture, and the 90%/10% Ar/O<sub>2</sub> gas mixture within the switches. These gas mixtures, in these percentages have not been considered for plasma closing switches previously as potential alternatives to SF<sub>6</sub> gas. The other gases used, air, N<sub>2</sub> and CO<sub>2</sub> while having been considered as alternative gases for SF<sub>6</sub> or having been used within mixtures with SF<sub>6</sub>, have not been characterised in as much detail for switching purposes. In the present work for the first time a comprehensive investigation into the operational performance of self-breakdown and triggered switches filled with these gases has been conducted. Experimental investigation and statistical analysis of the breakdown data allowed for characterisation of the breakdown characteristics and operational parameters of the switches filled with these gases. Based on the comprehensive optical emission spectroscopy study the characteristics of the plasma channels in these gases have been obtained which allowed for estimation of the plasma conductivity and resistivity of the plasma channels which is necessary for the development of the computational model of the Marx generator. No previous computational model takes into account the transient characteristics of the plasma channel that forms during breakdown process within plasma closing switches, particularly one

developed from the results of an experimental investigation into characteristics of plasma closing switches filled with different gases.

An extensive literature review was conducted into various aspects of pulsed power, including: the history of pulsed power, some large pulsed power systems and the switches they use, the basic principles of gas breakdown, approaches to modelling the transient processes within plasma closing switches are described and a discussion on the most commonly used gases within plasma closing switches is provided. As SF<sub>6</sub> is still one of the most commonly used gases within the switches of pulsed power systems, despite the environmental concerns associated with its usage, it was discussed that any plasma closing switch topology should operate on comparable levels when filled with any potential replacement gas as they do when filled with SF<sub>6</sub> and so key operational characteristics of plasma closing switches are discussed within Chapter 2 also as this formed the foundation from which this research project grew and the direction taken.

An experimental test set-up was designed and constructed to investigate the self-breakdown voltage and the spread in self-breakdown voltage of different gases; air, N<sub>2</sub>, 60%/40% N<sub>2</sub>/O<sub>2</sub>, 90%/10% Ar/O<sub>2</sub> CO<sub>2</sub> and SF<sub>6</sub> in a sphere-sphere topology switch for gas pressures 0.1 MPa – 0.4 MPa and for a range of inter-electrode gap distances from 1 mm – 9 mm. It was found that although SF<sub>6</sub> provided the highest self-breakdown voltage capabilities, it also showed a large spread in self-breakdown voltage which is not a desirable property in practical applications as a large spread in self-breakdown voltage means a wider range of values where breakdown may occur. This then means that a breakdown event occurring at a specific voltage cannot be relied upon as a wide range of voltages over which breakdown can occur makes breakdown rather unpredictable. It was also observed that the self-breakdown voltage values of SF<sub>6</sub> could be achieved in air, N<sub>2</sub> and the 60%/40% N<sub>2</sub>/O<sub>2</sub> mixture by increasing the *pd* value by a not unreasonable amount (an increase in pressure of 0.1 - 0.3 MPa) and this would also give an added advantage of smaller spread in self-breakdown voltage for any of these other gases. Another novelty of this research arose from the comparison of the self-breakdown voltage for all the gases tested within this self-breakdown switch to the classic Paschen breakdown curves where available. The classic Paschen curves for air, SF<sub>6</sub>, N<sub>2</sub> and Ar have been obtained for ideal, perfectly uniform electric field conditions. Although it was not expected to be accurate within a sphere-sphere topology switch which does not have ideal uniform field conditions, it was found

that the self-breakdown voltages of the gases were close to the classic Paschen breakdown curves, although an allometric fitting gave a closer fitting. This allows for fitting lines to be applied to the self-breakdown data of the gases where no previous Paschen breakdown curves were available, particularly the gas mixtures, and so, equations describing the self-breakdown voltage as a function of  $pd$  of all six gases are suggested.

Following on from the self-breakdown voltage, a field distortion spark gap switch was designed and constructed and triggered with two different trigger impulses, a 'slow' and a 'fast' voltage impulse, to investigate the time to breakdown of the switch and the corresponding jitter of the switch when filled with each of the six gases. Triggered switches are an important part of pulsed-power systems as they allow for precision over the timing of the triggering of switches which is not possible with self-breakdown switches. Two inter-electrode gap distances (2 mm and 4 mm) were stressed with 70% or 80% of the DC self-breakdown voltage before a -30kV voltage impulse was applied to the mid-plane trigger electrode. Under the 'slow' trigger voltage impulse, the -30kV impulse is applied to the trigger electrode at a "slow" rate of  $\sim 0.45\text{kV}/\mu\text{s}$ . It was found that for all gases, the time to breakdown of the switch, defined as the time between the application of the voltage impulse until complete voltage collapse across the main inter electrode gap, was on the  $\mu\text{s}$  time scale and increased as gas pressure increased. When the 2mm inter-electrode gap space was set, the time to breakdown was found to increase linearly as the gas pressure within the switch increased for all gases. However at 4 mm inter-electrode gap spacing, due to experimental limitations, insufficient data was available to comment on the trend of the increase. It was also found within this experimental study that stressing the main inter-electrode gap length with 80% of the DC self-breakdown voltage will result in an increase in time to breakdown over the gap when stressed with 70% of the DC self-breakdown voltage. The jitter of the switch, defined as the standard deviation in the time to breakdown was also found to be of the order of a few  $\mu\text{s}$  and increased as gas pressure increased, however many applications require ns jitter or better and, therefore, the next logical step was to attempt to reduce the jitter to ns-timescale levels.

The field distortion spark switch was again utilised, this time triggered with a 'fast'  $\sim 1\text{kV}/\text{ns}$  -30kV voltage impulse applied to the mid-plane electrode. It was found that the time to breakdown for each individual gas does not significantly change as gas pressure increased from 0.1 MPa to 0.4 MPa in either the 2 mm or 4 mm inter-electrode gap space, nor did

stressing the gap with 70% or 80% of the DC self-breakdown voltage level yield any discernible trend under these breakdown conditions investigated. The time to breakdown and the jitter when the 'fast' voltage impulse is applied was found to have reduced from  $\mu\text{s}$  to ns timescales, a far more practical and comparable timeframe for each of the gases to the conventional  $\text{SF}_6$  filled switches currently used. It was found that for the field distortion switch triggered under both the 'slow' and 'fast' voltage impulses, no breakdown events were able to be initiated when the switch was filled with  $\text{SF}_6$ .

Within the design of the self-breakdown switch, a quartz window was installed into the side of the body to allow for the analysis of optical emissions produced during a breakdown event. This was conducted in order to extract a value of the temperature of the plasma that forms during a breakdown event and, by using the Spitzer approximation, it was possible to evaluate the conductivity of the plasma. The Boltzmann approach to obtaining the temperature was conducted using the associated assumptions as this is a method which was found to be an appropriate approximation from literature. Cu I emissions were identified within the emission spectra between 500 nm and 600 nm and their relative intensities (alongside spectroscopic constants) plotted as a function of the energy. The temperature was extracted for each gas at a range of  $pd$  values and found to be  $\sim 5,500\text{K}$ - $6,500\text{K}$ . By using this range of temperatures within the Spitzer equation for conductivity it was possible to extract a value of plasma conductivity  $\sim 10^3 (\Omega\cdot\text{m})^{-1}$  which was found to be in line with other literature estimations of plasma conductivity for plasma temperatures of  $\sim 5000\text{K}$ - $6000\text{K}$ .

As part of characterising the plasma closing switches in order to develop an accurate computational model, one of the fundamental components that should be known is the resistance and inductance of the switches. The next step was then to consider the post-breakdown current waveforms and extract useful information from that in order to estimate the inductance and resistance values when the switch is filled with different gases. An RLC circuit with constant values of R, L and C was used and this allowed for the solution of the Kirchhoff equation to be matched with experimental results.

Post-breakdown current waveforms were obtained for 1 mm – 4 mm inter-electrode gap spacing of the self-breakdown switch and the relative peaks of the current waveforms used in order to determine the angular frequency  $\omega$  and the attenuation constant  $\alpha$ . Once these had been determined from experimental waveforms, and from values of circuit

parameters, it was possible to extract values of the inductance and resistance of the circuit. The total resistance was assumed to be made up from circuit parameters and the plasma resistance and on the basis of estimated values e.g. the resistance of the circuit elements, it was possible to obtain values of the plasma resistance at each inter-electrode gap length.

These values of inductance and resistance were then used within the development of the computational model of a single spark gap switch – initially assuming the resistance doesn't change over time – and then expanding one switch up to a 12-stage Marx bank model. It was shown that the value of the plasma resistance does not have a significant effect on the peak output voltage across the load, nor does the plasma resistance value have a significant influence on the runtime of the system. However, as the overall inductance of the 12-stage Marx generator increases the run-time increased and  $dV/dt$  decreased.

When the model was then adapted from a constant-value resistance model to a dynamic resistance model, the Braginskii equation was used as this was an equation derived empirically instead of fit to an experimental data set. The conductivity of the plasma channel as previously obtained from optical emission spectroscopy and literature was used within this computational model and found that the peak output voltage increased ~16% when the conductivity increased by an order of magnitude from  $10^2$  to  $10^3$  ( $\Omega.m$ )<sup>-1</sup> and a further 7% when increased from  $10^3$  to  $10^4$  ( $\Omega.m$ )<sup>-1</sup>. Values of stray capacitances to ground which may exist in practical systems, were included within the model and were found to have very little effect on the peak output voltage, however oscillations within the voltage waveform beyond the first voltage peak were apparent for stray capacitances of 0.1nF and smaller. A change in conductivity was found to have no impact on the runtime or  $dV/dt$  of the 12-stage Marx model with dynamic characteristics included. The results of this investigation show that the conductivity plays little role in the runtime or the  $dV/dt$  of the system. It had previously been shown that the conductivity of each of the gases tested did not vary greatly and as such, practical Marx systems should not be sensitive in terms of  $dV/dt$  or runtime to gas type or change of gas type.

From all experimental results obtained it would be recommended that if considering plasma closing switches operating with  $pd$  values within the range in this investigation, gas mixture comprised of 60%/40% N<sub>2</sub>/O<sub>2</sub> could be considered to replace SF<sub>6</sub> in current systems with minimal to no retrofitting, provided that the system could withstand increased gas pressures or the inter-electrode gap distance could be increased. This is due to the self-

breakdown results showing it to have the highest voltage hold-off capabilities after SF<sub>6</sub> with the smallest spread in self-breakdown voltage and the field distortion results showing it to have some of the lowest jitter values of the gases test. The extraction of plasma conductivity value showed that there was no significant change in conductivity between any of the gases and no significant change in conductivity as  $pd$  increased either.

## 9.2 Future Work

The research conducted within this project considered two plasma closing switch topologies commonly used in industrial applications and considered some of their key operational characteristics when filled with different gases in place of the conventionally used SF<sub>6</sub>. From the results presented within this thesis there is scope for future work to be conducted in the move towards using environmentally friendly alternatives to SF<sub>6</sub> in switches for pulsed power applications.

The self-breakdown switch used within this investigation made use of only sphere-sphere topology electrodes in studying the breakdown voltage and spread in breakdown voltage of the 5 gases tested in comparison to SF<sub>6</sub>. It was identified that all bar one of the gases had similar voltage hold-off potentials and, although lower than the voltage hold-off capability of SF<sub>6</sub> for the same  $pd$  values, for a small increase in  $pd$  the breakdown voltage was the same as SF<sub>6</sub> but with smaller spread of the breakdown voltage. All of the tests conducted were done for pressures between 0.1MPa and 0.4MPa. This leaves significant room for investigation of the same gases at pressures below atmospheric pressure or above 0.4MPa within self-breakdown switches.

Within the second part of this investigation where a field distortion switch was constructed and investigations carried out under two different triggering mechanisms, there is also scope for further work to be conducted, expanding upon the research presented within this thesis. It was shown that the level of DC stress before the trigger impulse is applied can have an influence on the time to breakdown so further levels of stress could be considered to find an optimum level of DC stress voltage prior to application of impulse voltage. It was also only possible to initiate breakdown in 2mm and 4mm inter-electrode gap spacing under a small range of gas pressures, again this would allow for further work to be

conducted at a wider range of inter-electrode gap distances and gas pressures. It was also noted within the literature review at the start of this thesis that the shape of trigger electrode can play a role in the time to breakdown and other characteristics of this switch. Changing the edge profile of the mid-plane trigger electrode would therefore result in changes to the field profile and thus the ultimate breakdowns occurring between the electrodes within the switch and this could influence the behaviour within different gases.

Each of these sets of tests were conducted with different gases in a single switch. A future expansion of this work could also be to build a Marx generator using several switches filled with these gases and investigate the operation of the Marx generator with multiple switches filled with any possible alternative gas as it is not likely that it will only ever be one switch utilised at a time.

Finally, the last section of this thesis developed two different computational models of an industrial 12-stage Marx generator, one of which included a dynamic model for the resistance of the plasma within the plasma closing switch. A future development of this would be to take the computational model and adapt it within the simulation of the full pulsed power system and assess how the whole system runs, with the Marx generator model at the voltage erection stage compared to the physical output of the machine itself.

## Chapter 10. Publications

C. McGarvey, I. V. Timoshkin, S. J. MacGregor, M. P. Wilson, M. J. Given, and M. A. Sinclair, "Characterisation of a plasma closing switch filled with environmentally friendly gases," *IEEE Pulsed Power Conference*. Ieee, pp. 1–1, Jun-2013.

C. McGarvey, I. V. Timoshkin, S. J. MacGregor, M. P. Wilson, M. J. Given, and M. A. Sinclair, "Breakdown characteristics of plasma closing switches filled with different gases," in *International Conference on Gas Discharges and their Applications*, 2014, pp. 398–401.

C. McGarvey, I. V. Timoshkin, S. J. MacGregor, M. P. Wilson, M. J. Given, and M. A. Sinclair, "An experimental and analytical study of plasma closing switches filled with environmentally friendly gases" in *IEEE Pulsed Power Conference*, 2015, pp. 1–6.

## Chapter 11. References

- [1] European-Union, "Regulation (EU) No 517/2014 of the European Parliament and of the Council of 16 April 2014 on fluorinated greenhouse gases and repealing Regulation (EC) No 842/2006," 2014.
- [2] W. A. Stygar, M. E. Cuneo, D. I. Headley, H. C. Ives, R. J. Leeper, M. G. Mazarakis, C. L. Olson, J. L. Porter, T. C. Wagoner, and J. R. Woodworth, "Architecture of petawatt-class z-pinch accelerators," *Phys. Rev. Spec. Top. - Accel. Beams*, vol. 10, no. 3, p. 30401, Mar. 2007.
- [3] J. R. Woodworth, J. A. Alexander, F. R. Gruner, W. A. Stygar, M. J. Harden, J. R. Blickem, G. J. Dension, F. E. White, L. M. Lucero, H. D. Anderson, L. F. Bennett, S. F. Glover, D. Van Devalde, and M. G. Mazarakis, "Low-inductance gas switches for linear transformer drivers," *Phys. Rev. Spec. Top. - Accel. Beams*, vol. 12, no. 6, p. 60401, Jun. 2009.
- [4] J. C. Martin, "THE PRE HISTORY OF PULSED POWER," in *IEE Colloquium on Pulsed Power*, 1995.
- [5] G. A. Mesyats, *PULSED POWER*. Springer, 2005.
- [6] G. Schaefer, M. Kristiansen, and A. Guenther, "Gas Discharge Closing Switches." Springer US, Boston, MA, 1990.
- [7] H. Bluhm, *Pulsed Power Systems*. Springer Berlin Heidelberg, 2006.
- [8] A. Van Arsdall, "Pulsed Power at Sandia National Laboratories: The first forty years," Albuquerque, New Mexico, 2007.
- [9] J. C. Martin, "Pulsed Power For Fusion," in *IEEE Pulsed Power Conference*, 1979, pp. 2–8.
- [10] H. W. Lee, S. K. Kang, S. K. Kwon, I. H. Won, H. C. Kwon, H. Y. Kim, J. K. Lee, and H. W. Lee, "Enhancement of microwave plasma characteristics for biomedical applications using pulse modulation method," in *IEEE Conference on Plasma Science*, 2013, pp. 312–315.
- [11] S. R. Rajulapati, F. A. Husain, S. B. Ananthapadmanabha, K. H. Schoenbach, and S. Xiao, "Nanosecond Biphasic Pulse Generators for Biomedical Applications," in *IEEE Conference on Plasma Science*, 2013, pp. 593–596.
- [12] T. Masuoka, T. Kawakami, T. Kiyoshima, C. Asada, Y. Nakamura, K. Teranishi, and N. Shimomura, "Effect of Pulsed Discharges on Mycelium Growth of *Sparassis Crispa*," in *IEEE Pulsed Power Conference*, 2015, pp. 67–71.
- [13] V. Tran, T. Park, H. Choi, and J. Choi, "High Efficiency and Reliability Pulsed Power System for Medical Lasers With the Digital Controller li . Circuit Descriptions and Basic," pp. 223–228, 2015.
- [14] S. Matsubara, A. Nakagawa, S. Kuniyasu, K. Teranishi, Y. Uto, and N. Shimomura,

- "Investigation of effect of applied nanosecond pulsed electric fields on tumor," *Dig. Tech. Pap. Int. Pulsed Power Conf.*, vol. 2015–Octob, pp. 374–378, 2015.
- [15] T. Sugai, T. Maruyama, W. Jiang, and A. Tokuchi, "Investigation of Capacity Enlargement of a Reactor for Water Treatment By Pulsed Streamer Discharge," in *IEEE Pulsed Power Conference*, 2015, pp. 9–13.
- [16] H. Akiyama, T. Sakugawa, T. Namihira, K. Takaki, Y. Minamitani, and N. Shimomura, "Industrial applications of pulsed power technology," *IEEE Trans. Dielectr. Electr. Insul.*, vol. 14, no. 5, pp. 1051–1064, 2007.
- [17] M. P. Wilson, L. Balmer, M. J. Given, S. J. MacGregor, and I. V. Timoshkin, "Optimization of the spark gap parameters for high power ultrasound applications," *Conf. Rec. Int. Power Modul. Symp. High Volt. Work.*, pp. 306–309, 2006.
- [18] I. V. Timoshkin, J. W. Mackersie, and S. J. MacGregor, "Plasma channel miniature hole drilling technology," *IEEE Trans. Plasma Sci.*, vol. 32, no. 5 I, pp. 2055–2061, 2004.
- [19] S. Qin, I. V. Timoshkin, M. MacLean, M. P. Wilson, S. J. MacGregor, M. J. Given, J. G. Anderson, and T. Wang, "Pulsed electric field treatment of microalgae: Inactivation tendencies and energy consumption," *IEEE Trans. Plasma Sci.*, vol. 42, no. 10, pp. 3191–3196, 2014.
- [20] J. R. Beveridge, K. Wall, S. J. MacGregor, J. G. Anderson, and N. J. Rowan, "Pulsed electric field inactivation of spoilage microorganisms in alcoholic beverages," in *IEEE Pulsed Power Conference*, 2004, vol. 92, no. 7, pp. 1138–1143.
- [21] A. Guenther, M. Kristiansen, and T. Martin, "Opening switches," in *Advances in pulsed power technology : Opening Switches*, New York: Plenum Press, 1987, p. 7.
- [22] J. R. Macdonald, M. A. Schneider, J. B. Ennis, F. W. Macdougall, and X. H. Yang, "High Energy Density Capacitors," in *IEEE Electrical Insulation Conference*, 2009, no. June, pp. 306–309.
- [23] W. J. Carey and J. R. Mayes, "Marx generator design and performance," in *Conference Record of the Twenty-Fifth International Power Modulator Symposium*, 2002, pp. 625–628.
- [24] J. C. Martin, *JC Martin on pulsed power*. New York: Plenum Press, 1996.
- [25] S. N. Laboratories, "Sandia Z accelerator: How it Works." [Online]. Available: [http://www.sandia.gov/z-machine/about\\_z/how-z-works.html](http://www.sandia.gov/z-machine/about_z/how-z-works.html).
- [26] A. A. Kim, B. M. Kovalchuk, V. A. Kokshenev, A. V. Shishlov, N. A. Ratakhin, V. I. Oreshkin, V. V. Rostov, V. I. Koshelev, and V. F. Losev, "Review of high-power pulsed systems at the Institute of High Current Electronics," *Matter Radiat. Extrem.*, vol. 1, no. 4, pp. 201–206, 2016.
- [27] I. C. London, "MAGPIE." [Online]. Available: <http://www.imperial.ac.uk/plasma-physics/magpie/magpie-basics/>.
- [28] T. R. Burkes, J. P. Craig, M. O. Hagler, M. Kristiansen, and W. M. Portnoy, "A review

- of high-power switch technology," *IEEE Trans. Electron Devices*, vol. 26, no. 10, pp. 1401–1411, Oct. 1979.
- [29] P. Cong, G. Zhang, L. Sheng, T. Sun, H. Wu, Z. Zeng, and A. Qiu, "Reproducibility of Microsecond Self-Breakdown Water Switch With Negative Field Enhancement," *IEEE Trans. Plasma Sci.*, vol. 41, no. 2, pp. 355–359, 2013.
- [30] S. J. Macgregor, S. M. Turnbull, and A. Tuema, "Self-closing water switch for load decoupling," in *IEE Colloquium on Pulsed Power*, 1997.
- [31] P. M. Barnes, K. Harries, T. E. James, and J. Philpott, "Multiple-Arc 100-kV 2.0MA solid dielectric switch," in *Proceedings of the Institution of Electrical Engineers*, 1970, pp. 255–260.
- [32] R. A. Dougal, G. Morris, and G. D. Volakakis, "Low-Loss , High-Repetition-Rate Vacuum Switching," *IEEE Trans. Plasma Sci.*, vol. 19, no. 5, pp. 976–988, 1991.
- [33] H. Uhm and T. Lee, "High-energy x-ray emission in vacuum spark discharge.," *Physical review. A*, vol. 40, no. 7. pp. 3915–3919, 01-Oct-1989.
- [34] A. Larsson, S. Member, D. Yap, and Y. W. Lim, "Time Jitter Study of a Corona-Stabilized Closing Switch," *IEEE Trans. Plasma Sci.*, vol. 40, no. 10, pp. 2646–2652, 2012.
- [35] X. B. X. Bian, L. W. L. Wang, J. M. K. Macalpine, Z. G. Z. Guan, J. H. J. Hui, and Y. C. Y. Chen, "Positive corona inception voltages and corona currents for air at various pressures and humidities," *IEEE Trans. Dielectr. Electr. Insul.*, vol. 17, no. 1, pp. 63–70, 2010.
- [36] J. M. Koutsoubis and S. J. MacGregor, "Effect of gas type on high repetition rate performance of a triggered, corona stabilised switch," *IEEE Transactions on Dielectrics and Electrical Insulation*, vol. 10, no. 2. pp. 245–255, Apr-2003.
- [37] W. Rogowski, "Die elektrische Festigkeit am Rande des Plattenkondensators," *Arch. Fur elektrotechnik*, vol. 12, no. 1, pp. 1–15, 1923.
- [38] S. M. Turnbull, S. J. MacGregor, and J. Harrower, "the Repebility of Spheresphere Spark Gap Columns," *Electr. Eng.*, pp. 23–26, 1997.
- [39] C. McGarvey, I. V. Timoshkin, S. J. MacGregor, M. P. Wilson, M. J. Given, and M. A. Sinclair, "Characterisation of a plasma closing switch filled with environmentally friendly gases," *IEEE Pulsed Power Conference. Ieee*, pp. 1–1, Jun-2013.
- [40] C. McGarvey, I. V. Timoshkin, S. J. MacGregor, M. P. Wilson, M. J. Given, and M. A. Sinclair, "Breakdown characteristics of plasma closing switches filled with different gases," in *International Conference on Gas Discharges and their Applications*, 2014, pp. 398–401.
- [41] C. McGarvey, I. V. Timoshkin, S. J. Macgregor, M. P. Wilson, M. J. Given, and M. A. Sinclair, "An experimental and analytical study of plasma closing switches filled with environmentally friendly gases.," in *IEEE Pulsed Power Conference*, 2015, pp. 1–6.
- [42] A. C. Mermigkas, I. V. Timoshkin, M. J. Given, and M. P. Wilson, "Effect of corona

stabilisation in atmospheric air in DC and impulse conditions,” in *Technological Plasma Workshop*, 2011.

- [43] M. E. Savage and B. S. Stoltzfus, “High reliability low jitter 80 kV pulse generator,” *Phys. Rev. Spec. Top. - Accel. Beams*, vol. 12, no. 8, pp. 1–13, 2009.
- [44] J. R. Woodworth, J. a. Alexander, W. a. Stygar, L. F. Bennett, H. D. Anderson, M. J. Harden, J. R. Blickem, F. R. Gruner, and R. White, “Low inductance switching studies for Linear Transformer Drivers,” *2009 IEEE Pulsed Power Conf.*, pp. 250–254, Jun. 2009.
- [45] H. Bo and H. Min, “Numerical simulation of gas breakdown process in field distortion switch,” *Proc. 6th Int. Conf. Prop. Appl. Dielectr. Mater. (Cat. No.00CH36347)*, vol. 1, pp. 391–394, 2000.
- [46] S. Hussain and M. Zakauallah, “Reliable Field Distortion Spark Gap for Plasma Focus,” *Plasma Sci. Technol.*, vol. 9, no. 4, pp. 1–5, 2007.
- [47] G. Stewart, M. P. Wilson, I. V. Timoshkin, M. J. Given, and S. J. Macgregor, “The Suitability of N<sub>2</sub> to Replace SF<sub>6</sub> in a Triggered Spark-Gap Switch for Pulsed Power Applications,” in *44th International Universities’ Power Engineering Conference*, 2009, pp. 1–6.
- [48] J. R. Mayes, W. J. Carey, W. C. Nunnally, and L. Altgilbers, “Sub-nanosecond jitter operation of Marx generators,” in *IEEE Pulsed Power Conference*, 2002, vol. 1, pp. 471–474.
- [49] B. Pashaie-Awal, “A new design concept for field distortion triggered spark gaps,” Texas Tech University, 1986.
- [50] P. F. Williams and F. E. Peterkin, “Triggering in trigatron spark gaps: A fundamental study,” *J. Appl. Phys.*, vol. 66, no. 9, p. 4163, 1989.
- [51] F. E. Peterkin and P. F. Williams, “Triggering of Trigatron Spark Gaps,” Lincoln, Nebraska, 1989.
- [52] a H. Guenther and J. R. Bettis, “The laser triggering of high-voltage switches,” *J. Phys. D. Appl. Phys.*, vol. 11, no. 12, pp. 1577–1613, 1978.
- [53] K. R. Lechien, W. A. Stygar, M. E. Savage, P. E. Wakeland, V. Anaya, D. S. Artery, M. J. Baremore, D. E. Bliss, R. Chavez, G. D. Coombs, J. P. Corley, P. A. Jones, A. K. Kipp, B. A. Lewis, J. A. Lott, J. J. Lynch, G. R. McKee, S. D. Ploor, K. R. Prestwich, S. A. Roznowski, D. C. Spencer, S. D. White, and J. R. Woodworth, “6.1-MV, 0.79-MA laser-triggered gas switch for multimodule, multiterawatt pulsed-power accelerators,” *Phys. Rev. Spec. Top. - Accel. Beams*, vol. 13, no. 3, pp. 1–11, 2010.
- [54] A. Larsson, S. Member, D. Yap, J. Au, and T. E. Carlsson, “Laser Triggering of Spark Gap Switches,” vol. 42, no. 10, pp. 2943–2947, 2014.
- [55] F. Hegeler, M. C. Myers, M. F. Wolford, J. D. Sethian, and A. M. Fielding, “Low jitter, high voltage, repetitive laser triggered SF<sub>6</sub> gas insulated spark gaps,” *Proc. 2012 IEEE Int. Power Modul. High Volt. Conf. IPMHVC 2012*, pp. 128–131, 2012.

- [56] J. R. Blickem, Z. R. Wallace, V. Anaya, J. P. Corley, J. A. Lott, and K. C. Hodge, "Laser Triggered Gas Switches Utilising Beam Transport Through 1M $\Omega$ -cm Deionized Water," in *IEEE Pulsed Power Conference*, 2005.
- [57] O. Frolov, K. Kolacek, V. Bohacek, J. Straus, J. Schmidt, and V. Prukner, "Gas-filled laser-triggered spark gap," *Czechoslov. J. Phys.*, vol. 54, no. S3, pp. C309–C313, Mar. 2004.
- [58] L. Arantchouk, A. Houard, Y. Brelet, J. Carbonnel, J. Larour, Y. B. André, and A. Mysyrowicz, "A simple high-voltage high current spark gap with subnanosecond jitter triggered by femtosecond laser filamentation," *Appl. Phys. Lett.*, vol. 102, no. 16, pp. 1–4, 2013.
- [59] A. Jones, S. Briscall, J. Buck, S. Clough, G. Cooper, L. Rickard, J. Mclean, R. Provis, M. Sinclair, A. Steeden, and T. Williams, "Replacement Marx Generator for the Mevex X-ray Machines," in *IEEE Pulsed Power Conference*, 2013.
- [60] S. Briscall, S. Clough, G. Jeffries, R. Raspin, K. Wales, K. Webb, and S. Wise, "Characterization of the Mevex Replacement Marx and the associated design of a resistive load," in *IEEE Pulsed Power Conference*, 2013, p. 2723.
- [61] L. L. Alston, *High Voltage Technology*. Oxford: Oxford University Press, 1968.
- [62] S. Brown, *Elementary Processes in gas discharge plasma*. Cambridge, 1961.
- [63] M. S. Naidu and V. Kamaraju, *High Voltage Engineering*. McGraw-Hill, 1995.
- [64] V. . Atrazhev, I. V. Timoshkin, S. J. MacGregor, M. J. Given, and M. P. Wilson, "Analysis of Breakdown Characteristics of Vapors in Micro-Bubbles Formed in Insulating Mineral Oils Under Electrical Stress," in *International Conference on Gas Discharges and Their Applications*, 2010, pp. 338–341.
- [65] F. Paschen, "Ueber die zum Funkenübergang in Luft, Wasserstoff und Kohlensäure bei verschiedenen Drucken erforderliche Potentialdifferenz," *Ann. Phys.*, vol. 273, no. 5, pp. 69–96, 1889.
- [66] E. Husain and R. S. Nema, "Analysis of Paschen Curves for Air, N<sub>2</sub> and SF<sub>6</sub> using the Townsend Breakdown Equation," *IEEE Trans. Electr. Insul.*, vol. 17, no. 4, pp. 350–353, 1982.
- [67] M. G. Hogg, I. V. Timoshkin, S. J. McGregor, M. P. Wilson, and M. J. Given, "Polarity effects on breakdown of short gaps in a point-plane topology in air," *IEEE Trans. Dielectr. Electr. Insul.*, vol. 22, no. 4, pp. 1815–1822, 2015.
- [68] D. B. Go and D. A. Pohlman, "A mathematical model of the modified Paschen's curve for breakdown in microscale gaps," *J. Appl. Phys.*, vol. 107, no. 10, 2010.
- [69] W. J. Carey, A. J. Wiebe, and R. D. Nord, "Characterization of Paschen Curve Anomalies At High P \* D Values," in *IEEE Pulsed Power Conference*, 2011, pp. 741–744.
- [70] W. D. Greason, "Methodology to study the resistance of spark discharges," *IAS '97. Conf. Rec. 1997 IEEE Ind. Appl. Conf. Thirty-Second IAS Annu. Meet.*, vol. 3, pp. 1907–

1913, 1997.

- [71] W. D. Greason, "Methodology to study the resistance of spark discharges," *IEEE Transactions on Industry Applications*, vol. 35, no. 2. pp. 359–365, 1999.
- [72] C. Burkhart and M. Kemp, "Pulsed Power Engineering Advanced Topologies," *US Particle Accelerator School Lecture Slides*, 2009. [Online]. Available: [http://uspas.fnal.gov/materials/09VU/PPE\\_AdvancedTopologies.pdf](http://uspas.fnal.gov/materials/09VU/PPE_AdvancedTopologies.pdf).
- [73] A. E. Vlastós, "Restrike channel resistance of thin exploding wires," *J. Appl. Phys.*, vol. 40, no. 12, pp. 4752–4760, 1969.
- [74] S. . Barannik, "Resistance and Inductance of a gas arc," *Sov. Phys. Tech. Phys.*, vol. 19, pp. 1449–1453, 1975.
- [75] M. J. Kushner, W. D. Kimura, and S. R. Byron, "Arc resistance of laser-triggered spark gaps," *Journal of Applied Physics*, vol. 58, no. 5. p. 1744, 1985.
- [76] T. P. Sorensen and V. M. Ristic, "Rise time and time-dependent spark-gap resistance in nitrogen and helium," *J. Appl. Phys.*, vol. 48, no. 1, p. 114, 1977.
- [77] T. Hussey, K. Davis, J. M. Lehr, N. Roderick, R. Pate, and E. Kunhardt, "Dynamics of nanosecond spark-gap channels," in *IEEE Pulsed Power Conference*, 1999, pp. 1171–1174.
- [78] M. . Popovic, "Investigation of the beginning of high current discharges in pulsed arcs," *Proc. Int. Conf. Gaseous Discharges*, pp. 32–36, 1974.
- [79] R. Rompe and W. Weitzel, "Über das Toeplesche funkengastz," *Phys. Rev.*, vol. 122, p. 636, 1944.
- [80] T. G. Engel, A. L. Donaldson, and M. Kristiansen, "The Pulsed Discharge Arc Resistance and its Functional Behavior," *IEEE Trans. Plasma Sci.*, vol. 17, no. 2, pp. 323–329, Apr. 1989.
- [81] M. Toepler, "Zur Kenntnis der Gesetze der Gleitfunkenbildung," *Ann. Phys.*, vol. 326, no. 12, pp. 193–222, 1906.
- [82] S. I. Braginskii, "Contribution to the theory of the development of a spark channel," *Sov. Phys. -JEPT*, vol. 34, no. 7, pp. 1068–1074, 1958.
- [83] B. L. Maas, "Arc Current, Voltage and Resistance in a High Energy, Gas Filled Spark Gap," Texas Tech University, 1985.
- [84] A. E. Vlastós, "The resistance of sparks," *J. Appl. Phys.*, vol. 43, no. 4, pp. 1987–1989, 1972.
- [85] R. Sinton, R. Van Herel, W. Enright, and P. Bodger, "Observations of the long distance exploding wire restrike mechanism," *J. Appl. Phys.*, vol. 108, no. 5, 2010.
- [86] G. . Vorob'yev and G. A. Mesyats, "Technique of shaping high voltage nanosecond pulses," 1971.
- [87] T. H. Martin, "ENERGY LOSSES IN SWITCHES," in *IEEE Pulsed Power Conference*,

1993, pp. 463–470.

- [88] N. H. Malik and A. H. Qureshi, "A review of electrical breakdown in mixtures of SF<sub>6</sub> and other gases," *IEEE Trans. Electr. Insul.*, vol. EI-14, no. 1, pp. 1–13, 1979.
- [89] S. Woo, D. Jeong, K. Seo, and J. Kim, "A Study on Dielectric Strength and Insulation Property of SF<sub>6</sub> / N<sub>2</sub> Mixtures for GIS," *J. Int. Counc. Electr. Eng.*, vol. 2, no. 1, pp. 104–109, 2012.
- [90] L. E. Kline, "Dielectric properties for SF<sub>6</sub> and SF<sub>6</sub> mixtures predicted from basic data," *Journal of Applied Physics*, vol. 50, no. 11. p. 6789, 1979.
- [91] L. G. Christophorou and R. J. Van Brunt, "SF<sub>6</sub>/N<sub>2</sub> mixtures: basic and HV insulation properties," *IEEE Trans. Dielectr. Electr. Insul.*, vol. 2, no. 5, pp. 952–1003, 1995.
- [92] S. L. Moran and L. W. Hardesty, "High-repetition-rate hydrogen spark gap," *IEEE Trans. Electron Devices*, vol. 38, no. 4, pp. 726–730, Apr. 1991.
- [93] P. Widger, "Investigation into CF<sub>3</sub>I-CO<sub>2</sub> Gas Mixtures for Gas-Insulated Distribution," Cardiff University, 2014.
- [94] L. Xuandong, W. Hu, and L. Xiaoang, "Multichannel Discharge Characteristics of Gas Switch Gap in SF<sub>6</sub>-N<sub>2</sub> or SF<sub>6</sub>-Ar Gas Mixtures Multichannel Discharge Characteristics of Gas Switch Gap in SF<sub>6</sub> -N<sub>2</sub> or SF<sub>6</sub> -Ar Gas Mixtures Under Nanosecond Triggering Pulses \* Experimental setup and Experiment."
- [95] J. Martin, "Nanosecond pulse techniques," *Proc. IEEE*, vol. 80, no. 6, pp. 934–945, 1970.
- [96] R. B. Sandler, "Technology of Fast Spark Gaps," no. September, 1989.
- [97] L. Shondeep, C. Energy, C. Energy, and R. Cited, "United States Patent [191," 1995.
- [98] United-Nations, "United Nations Framework on Climate Change," 1997. [Online]. Available: [http://unfccc.int/kyoto\\_protocol/items/2830.php](http://unfccc.int/kyoto_protocol/items/2830.php).
- [99] European-Union, "EU legislation to control F-gases," 2006. [Online]. Available: [https://ec.europa.eu/clima/policies/f-gas/legislation\\_en](https://ec.europa.eu/clima/policies/f-gas/legislation_en).
- [100] L. E. Kline, "Dielectric properties for SF<sub>6</sub> and SF<sub>6</sub> mixtures predicted from basic data," *J. Appl. Phys.*, vol. 50, no. 11, p. 6789, 1979.
- [101] B. G. Camilli, "Gas-Insulated Power Transformers," vol. 1960, no. 3288, 1960.
- [102] T. Rokunohe, Y. Yagihashi, F. Endo, and T. Oomori, "Fundamental insulation characteristics of air; N<sub>2</sub>, CO<sub>2</sub>, N<sub>2</sub>/O<sub>2</sub>, and SF<sub>6</sub>/N<sub>2</sub> mixed gases," *Electr. Eng. Japan*, vol. 155, no. 3, pp. 9–17, May 2006.
- [103] K. Mardikyan, S. Seker, O. Kalenderli, and E. Ayaz, "Breakdown Strength of Air and AIR+SF<sub>6</sub> in Rod-sphere gap and breakdown voltage estimation using artificial neural network.," in *International Conference on Electrical and Electronics Engineers.*, 1999, pp. 135–139.
- [104] S. S. P. Berzak L F, Dorfman S E, "Paschen's Law in Air and Noble Gases," *Vasa*, 2008.

- [105] K. Mardikyan, S. Seker, and E. Ayaz, "Breakdown strength estimation of air and a mixture of air+SF6 using artificial neural network approach," *Adv. Model. Anal. B*, vol. 43, no. 1–2, pp. 1–14, 2000.
- [106] O. Farish and S. J. Macgregor, "The development of fast single-shot and repetitively-operated SF6 closing switches for pulsed power applications," in *Gaseous Dielectrics IX*, 2001, pp. 271–284.
- [107] T. Kawamura, S. Matsumoto, M. Hanai, and Y. Murayama, "SF6/N2 Mixtures for HV Equipment and Practical Problems," in *Gaseous Dielectrics VIII*, 1998, pp. 333–343.
- [108] AIRGAS, "Safety Data Sheet SF6," 2009.
- [109] ICF Consulting, "Byproducts of Sulfur Hexafluoride (SF6 ) Use in the Electric Power Industry," 2002.
- [110] J. M. Koutsoubis and S. J. MacGregor, "Effect of gas type on high repetition rate performance of a triggered, corona stabilised switch," *IEEE Trans. Dielectr. Electr. Insul.*, vol. 10, no. 2, pp. 245–255, Apr. 2003.
- [111] L. Christophorou, J. Olthoff, and D. Green, "Gases for electrical insulation and arc interruption: possible present and future alternatives to pure SF6," 1997.
- [112] C. S. Gas, "Concorde Specialty Gases , Inc . PRODUCT SPECIFICATIONS SHEET :," p. 648.
- [113] United-Nations, "Doha Amendment." [Online]. Available: [http://unfccc.int/kyoto\\_protocol/doha\\_amendment/items/7362.php](http://unfccc.int/kyoto_protocol/doha_amendment/items/7362.php).
- [114] United-Nations, "Paris Agreement," 2016. [Online]. Available: [http://unfccc.int/paris\\_agreement/items/9485.php](http://unfccc.int/paris_agreement/items/9485.php).
- [115] R. S. Nema, S. V Kulkarni, and E. Husain, "Calculation of Sparking potentials of SF6 and SF6-gas mixtures in Uniform and non-uniform Electric fields.," no. 1, pp. 70–75, 1982.
- [116] W. Khechen and J. Laghari, "Breakdown studies of SF 6/argon gas mixtures," *Electr. Insul. IEEE ...*, vol. 24, no. 0, pp. 1141–1146, 1989.
- [117] S. Park, C. Hwang, N.- Ryul, K. Lee, and C. Huh, "Breakdown Characteristics of SF 6 / CF 4 Mixtures in Test Chamber and 25 . 8kV GIS," no. August, 2007.
- [118] J. Dutton, F. Harris, and D. Hughes, "Electrical breakdown of N 2 O, SF 6 and N 2 O/SF 6 mixtures," *Proc. Inst. Electr. ...*, vol. 121, no. 3, pp. 223–226, 1974.
- [119] S. J. Macgregor, I. D. Chalmers, and G. Street, "The switching properties of sf6 gas mixtures," in *IEEE Pulsed Power Conference*, 1989, pp. 510–513.
- [120] X. Q. Qiu, I. D. Chalmers, and P. Coventry, "A study of alternative insulating gases to SF 6," *J. Phys. D. Appl. Phys.*, vol. 32, no. 22, pp. 2918–2922, 1999.
- [121] J. Devins, "Replacement gases for SF6," *Electr. Insul. IEEE Trans.*, vol. EI-15, no. 2, pp. 81–86, 1980.

- [122] M. S. Kamarudin, M. Albano, P. Coventry, N. Harid, and a. Haddad, "A survey on the potential of CF3I gas as an alternative for SF6 in high voltage applications," *Univ. Power Eng. Conf. (UPEC), 2010 45th Int.*, pp. 1–5, 2010.
- [123] L. Chen, P. Widger, M. Kamarudin, H. Griffiths, and a Haddad, "CF3I Gas Mixtures: Breakdown Characteristics and Potential for Electrical Insulation," *IEEE Trans. Power Deliv.*, vol. 8977, no. c, pp. 1–1, 2016.
- [124] J. Wada, G. Ueta, S. Okabe, and M. Hikita, "Dielectric properties of gas mixtures with per-fluorocarbon gas and gas with low liquefaction temperature," *IEEE Trans. Dielectr. Electr. Insul.*, vol. 23, no. 2, pp. 838–847, 2016.
- [125] L. P. Rosa and R. Schaeffer, "Global warming potentials.," *Energy Policy*, 1995. .
- [126] M. Koch and C. M. Franck, "High Voltage Insulation Properties of HFO1234ze," *IEEE Trans. Dielectr. Electr. Insul.*, vol. 22, no. 6, pp. 3260–3268, 2015.
- [127] M. S. Kamarudin, "Gas Mixtures on the Breakdown Characteristics in Uniform and Non- Uniform Field Configurations," 2013.
- [128] H. Kasuya, Y. Kawamura, H. Mizoguchi, Y. Nakamura, S. Yanabu, and N. Nagasaki, "Interruption capability and decomposed gas density of CF3I as a substitute for SF6 gas," *IEEE Trans. Dielectr. Electr. Insul.*, vol. 17, no. 4, pp. 1196–1203, 2010.
- [129] L. Chen, "Investigation on the Feasibility of Trifluoroiodomethane for applications in gas-insulated lines," Cardiff University, 2015.
- [130] K. Feser, "Breakdown Behaviour of Air Spark-Gaps with Non-Homogeneous Field at Bias Voltages," *Bull. ASE*, vol. 62, p. 320, 1971.
- [131] M. Klas and Š. Matejčík, "Dc Breakdown in Air , Oxygen and Nitrogen At Micrometer Separations," vol. 2.
- [132] J. Novak and R. Bartnikas, "Quantitative model of a short-gap breakdown in air," in *International Symposium on Discharges and Electrical Insulation in Vacuum*, 1996, pp. 60–64.
- [133] P. Pongsri, a. Pruksanubal, and N. Tanthanuch, "Lightning impulse breakdown voltage of nitrogen and air under rod-plane gap," *2012 9th Int. Conf. Electr. Eng. Comput. Telecommun. Inf. Technol.*, pp. 1–4, May 2012.
- [134] L. Ledernez, F. Olcaytug, and G. Urban, "Inter-Electrode Distance and Breakdown Voltage in Low Pressure Argon Discharges," *Contrib. to Plasma Phys.*, vol. 52, no. 4, pp. 276–282, May 2012.
- [135] M. Radmilović-Radjenović and B. Radjenović, "Modelling of a low-pressure argon breakdown in combined fields," *Plasma Sources Sci. Technol.*, vol. 15, no. 1, pp. 1–7, Feb. 2006.
- [136] C. Torres, P. G. Reyes, F. Castillo, and H. Martínez, "Paschen law for argon glow discharge," *J. Phys. Conf. Ser.*, vol. 370, p. 12067, Jun. 2012.
- [137] L. LedernezP, "A modification of Paschen law for Argon," in *International Conference*

on *Phenomena and Ionized Gases*, 2009, pp. 0–2.

- [138] AWE, “Discovery 23,” no. July, 2012.
- [139] M. P. Wilson, M. J. Given, I. V. Timoshkin, S. J. MacGregor, T. Wang, M. A. Sinclair, K. J. Thomas, and J. M. Lehr, “Impulse-driven surface breakdown data: A weibull statistical analysis,” *IEEE Trans. Plasma Sci.*, vol. 40, no. 10 PART 1, pp. 2449–2456, 2012.
- [140] M. Wilson and M. Given, “Weibull statistical analysis of impulse-driven surface breakdown data,” *IEEE Trans. Plasma Sci.*, vol. 40, no. 10, pp. 2449–2456, 2011.
- [141] IEEE, “IEC 62539 ‘Guide for the Statistical Analysis of electrical insulation breakdown data,’” 2007.
- [142] A. Larsson, S. Member, D. Yap, and Y. W. Lim, “Time Jitter Study of a Small V / n Switch,” vol. 40, no. 10, pp. 2653–2657, 2012.
- [143] C. Frost, T. Martin, R. Focia, and J. Schoenberg, “Ultra-low-jitter repetitive solid state picosecond switching,” in *12th International Pulsed Power Conference*, 1999, pp. 291–294.
- [144] Y. Chen, J. Dickens, J. Mankowski, and M. Kristiansen, “Optimization of a low jitter, 50 kV, 100 Hz triggered spark gap with high pressure gas mixtures,” *IEEE Trans. Dielectr. Electr. Insul.*, vol. 16, no. 4, pp. 971–978, Aug. 2009.
- [145] A. Larsson and S. Member, “Gas-Discharge Closing Switches and Their Time Jitter,” vol. 40, no. 10, pp. 2431–2442, 2012.
- [146] Y. Chen and J. Mankowski, “Low-jitter triggered spark gap with high-pressure gas mixtures,” *IEEE Trans. Plasma Sci.*, vol. 36, no. 5, pp. 2546–2553, 2008.
- [147] A. Blumlein, “UK Patent 589127,” 1941.
- [148] I. C. Somerville, S. J. MacGregor, and O. Farish, “An efficient stacked-Blumlein HV pulse generator,” *Meas. Sci. Technol.*, vol. 1, pp. 865–868, 1990.
- [149] A. Larsson, “Gas-Discharge Closing Switches and Their Time Jitter,” *IEEE Transactions on Plasma Science*, vol. 40, no. 10, pp. 2431–2442, Oct-2012.
- [150] B. Hutsel and D. Sullivan, “Characterization of Runtime and jitter on a laser triggered Spark gap switch,” in *IEEE International Conference on Plasma Science*, 2007, pp. 110–113.
- [151] Y. Chen and J. Mankowski, “Jitter and recovery rate of a triggered spark gap with high pressure gas mixtures,” *IEEE Int. Conf. Plasma Sci.*, pp. 254–257, 2007.
- [152] S. G. Koutoula, I. V. Timoshkin, M. D. Judd, S. J. MacGregor, M. P. Wilson, M. J. Given, T. Wang, and E. I. Harrison, “A Study of Energy Partition during Arc Initiation,” *IEEE Trans. Plasma Sci.*, vol. 44, no. 10, pp. 2137–2144, 2016.
- [153] A. Sarani, A. Y. Nikiforov, and C. Leys, “Atmospheric pressure plasma jet in Ar and Ar/H<sub>2</sub>O mixtures: Optical emission spectroscopy and temperature measurements,” *Phys. Plasmas*, vol. 17, no. 6, p. 8pp, 2010.

- [154] S. Yalcin, D. R. Crosley, G. P. Smith, and G. W. Faris, "Influence of ambient conditions on the laser air spark," *Appl. Phys. B Lasers Opt.*, vol. 68, no. 1, pp. 121–130, 1999.
- [155] I. Prysiashnevych, V. Chernyak, S. Olzewski, and V. Yukhymenko, "Plasma properties of transverse blowing ARC under atmospheric pressure," *Chem. List.*, vol. 102, no. 16 SPEC. ISS., pp. 1403–1407, 2008.
- [156] S. Gershman, A. Belkind, and K. Becker, "Optical emission diagnostics of the plasma channel in a pulsed electrical discharge in a gas bubble," *IEEE Pulsed Power Conf.*, pp. 838–840, 2009.
- [157] B. Li and H. Li, "Discussion on emission spectroscopy measurements from a dense electrothermal launcher plasma," *Proc. 19th Int. Symp. Ballist.*, no. May, pp. 7–11, 2001.
- [158] T. Billoux, V. Boretskij, Y. Cressault, A. Gleizes, P. Teulet, and A. Veklich, "Emission spectrum of the electric arc discharge in CO<sub>2</sub> between copper electrodes," pp. 1–4.
- [159] Fridman, "Optical diagnostics of atmospheric pressure air plasmas," *Plasma Sources Sci. Technol.*, vol. 12, no. 2, p. 125, 2003.
- [160] C. H. Corliss and W. R. Bozman, "Experimental Transition Probabilities for Spectral Lines of Seventy Elements," United States Department of Commerce, Washington DC, 1962.
- [161] NIST, "NIST Spectral Database." [Online]. Available: [http://physics.nist.gov/cgi-bin/ASD/lines1.pl?spectra=cu&low\\_wl=500&upp\\_wn=&upp\\_wl=600&low\\_wn=&unit=1&submit=Retrieve+Data&de=0&java\\_window=3&java\\_mult=&format=0&line\\_out=0&en\\_unit=0&output=0&bibrefs=1&page\\_size=15&show\\_obs\\_wl=1&show\\_calc\\_wl=1&order\\_out=0](http://physics.nist.gov/cgi-bin/ASD/lines1.pl?spectra=cu&low_wl=500&upp_wn=&upp_wl=600&low_wn=&unit=1&submit=Retrieve+Data&de=0&java_window=3&java_mult=&format=0&line_out=0&en_unit=0&output=0&bibrefs=1&page_size=15&show_obs_wl=1&show_calc_wl=1&order_out=0).
- [162] J. Dutton, "A Survey of Electron Swarm Data," *J. Phys. Chem. Ref. Data*, vol. 4, no. 3, pp. 577–856, 1975.
- [163] L. Spitzer, "No Title," 1956. [Online]. Available: <http://www.ipp.mpg.de/1766097/spitzer>.
- [164] H. Dienemann, K. Hinz, and H.-J. Freyer, "Electrical Conductivity in Sulphur hexafluoride," *J. Phys. D. Appl. Phys.*, vol. 18, pp. 2207–2219, 1985.
- [165] M. Janda, V. Martisovits, L. Dvornic, and Z. Machala, "Measurement of the electron density in Transient Spark discharge," *Plasma Sources Sci. Technol.*, vol. 23, 2014.
- [166] W. D. Greason and S. Member, "Methodology to Study the Resistance of Spark Discharges," vol. 35, no. 2, pp. 359–365, 1999.
- [167] A. Jones, S. Briscall, J. Buck, S. Clough, G. Cooper, G. Jeffries, L. Rickard, J. Mclean, R. Provis, M. Sinclair, A. Steeden, K. Webb, and T. Williams, "X-RAY MACHINES," pp. 3–6, 2013.
- [168] F. W. Grover, "Inductance Calculations: Working Formulas and Tables." Dover Publications, NY, p. 286, 1946.

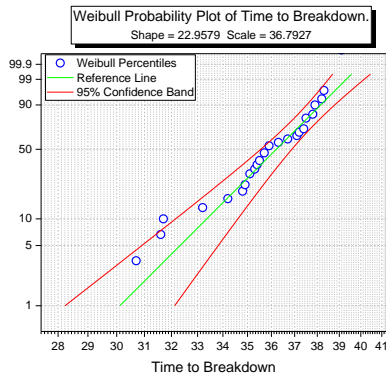
- [169] C. S. Walker, *Capacitance, Inductance and Crosstalk Analysis*. Boston, MA: Artech House, 1990.
- [170] H. Hess, "Zur Funkenkonstante nach Rompe und Weizel," *Beiträge aus der Plasmaphysik*, vol. 13, no. 3. pp. 131–136, 1973.
- [171] D. M. Barrett, S. R. Byron, E. a. Crawford, D. H. Ford, W. D. Kimura, and M. J. Kushner, "Low-inductance capacitive probe for spark gap voltage measurements," *Rev. Sci. Instrum.*, vol. 56, no. 11, p. 2111, 1985.
- [172] M. N. Plooster, "Numerical Simulation of Spark Discharges in Air," *Phys. Fluids*, vol. 14, no. 10, pp. 2111–2123, 1971.
- [173] P. W. Schreiber and A. M. Hunter, "Electrical conductivity and total emission coefficient of air plasma," *AIAA J.*, vol. 11, no. 6, pp. 815–821, 1973.

## **Appendix 1. Weibull Graphs**

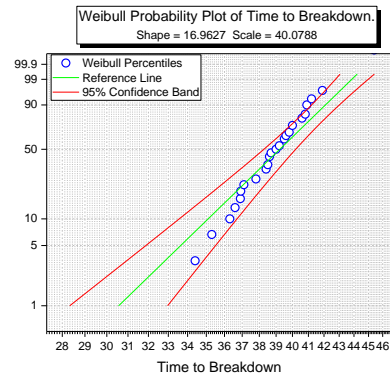
### **1A. Field-Distortion Gap triggered with 0.45kV/ $\mu$ s HV impulse**

The remaining Weibull graphs for the field-distortion spark switch stressed with 70% and 80% of the self-breakdown voltage, filled with gas pressures 0.15MPa-0.4MPa, with inter-electrode gap lengths of 2mm and 4mm and triggered with a voltage impulse applied at a rate of 0.45kV/ $\mu$ s presented within Chapter 4 are presented in Figure 12-1 – Figure 12-8.

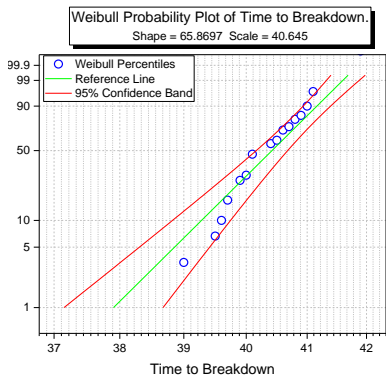
The vertical axis represents the unreliability (%) and the horizontal axis is the time to breakdown (ns). Each of the open circle symbols plotted on the graph represent breakdown events occurring at a specified time. The green line on each graph is a reference line with parameters of the shape and scale extracted from the Weibull fit of the plotted open symbols. The red lines on either side of the green line represent the 95% confidence band, that is, the band within which 95% of the breakdown events are predicted to occur.



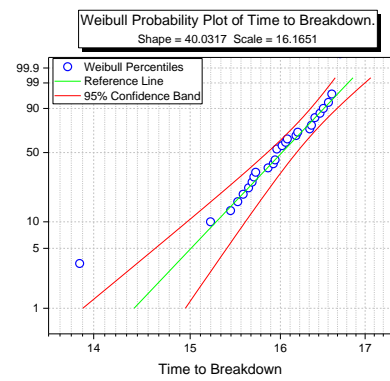
(a)



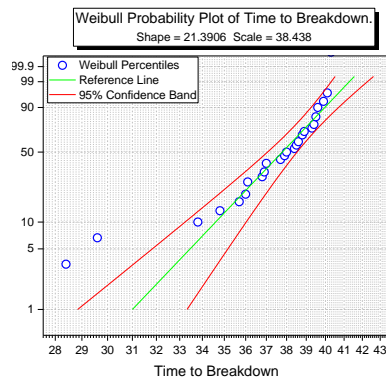
(b)



(c)

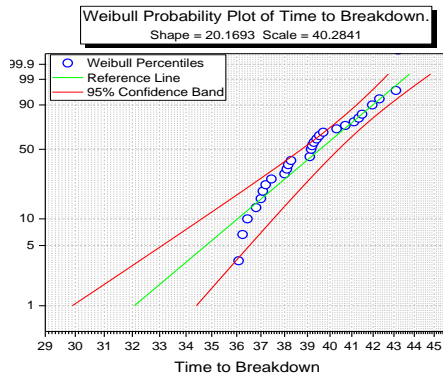


(d)

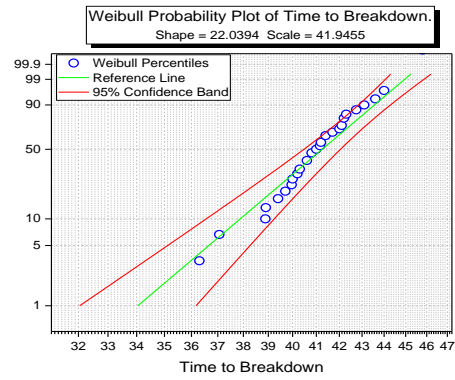


(e)

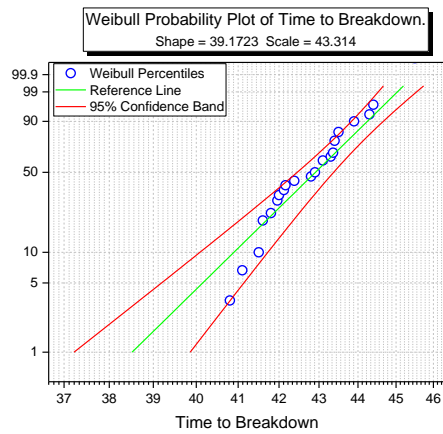
**Figure 12-1 Weibull analysis graphs for a 2mm inter-electrode gap length at 0.2MPa (a) Air (b) N<sub>2</sub> (c) 60%/40% N<sub>2</sub>/O<sub>2</sub> (d) 90%/10% Ar/O<sub>2</sub> (e) CO<sub>2</sub> with 70% of the self-breakdown voltage applied across the main inter-electrode gap length as DC stress.**



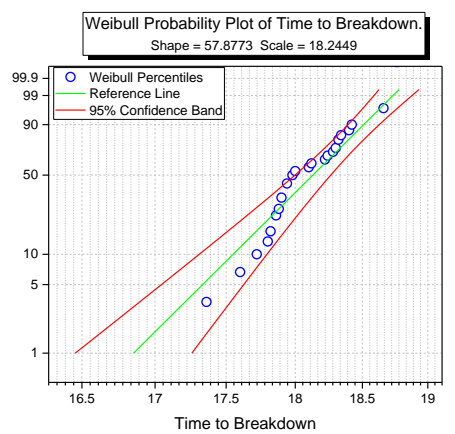
(a)



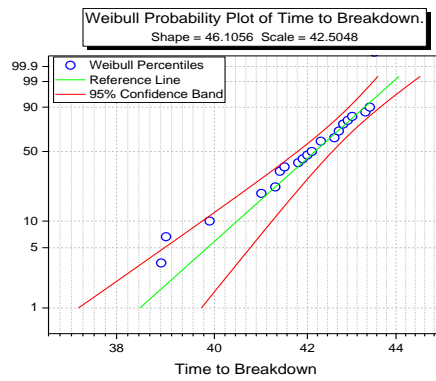
(b)



(c)

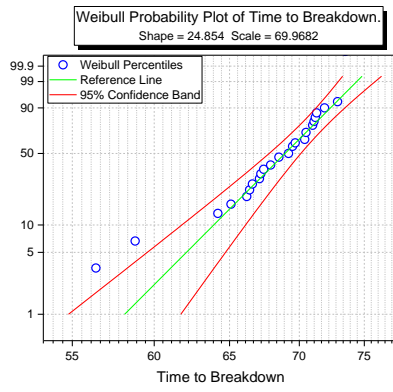


(d)

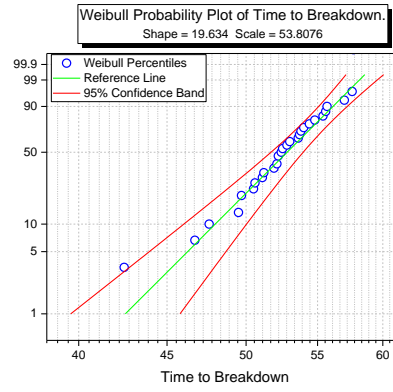


(e)

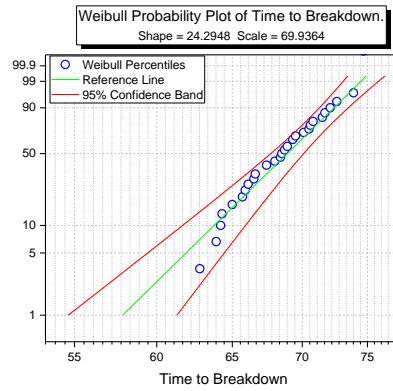
Figure 12-2 Weibull analysis graphs for a 2mm inter-electrode gap length at 0.2MPa (a) Air (b) N<sub>2</sub> (c) 60%/40% N<sub>2</sub>/O<sub>2</sub> (d) 90%/10% Ar/O<sub>2</sub> (e) CO<sub>2</sub> with 80% of the self-breakdown voltage applied across the main inter-electrode gap length as DC stress.



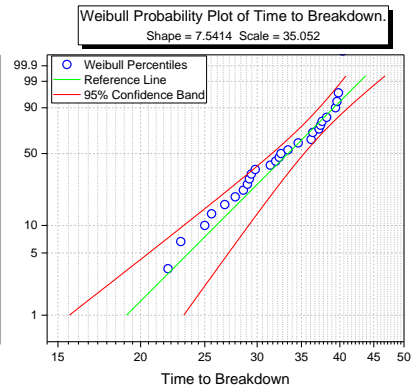
(a)



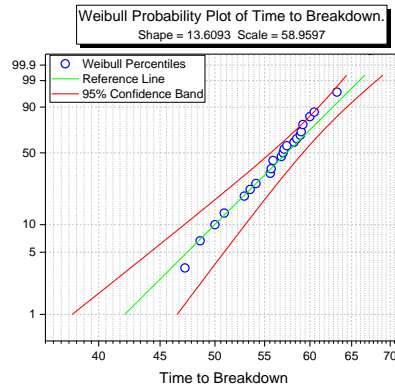
(b)



(c)

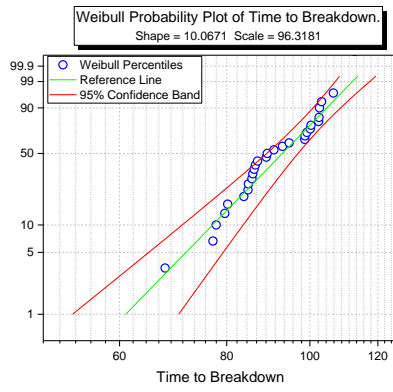


(d)

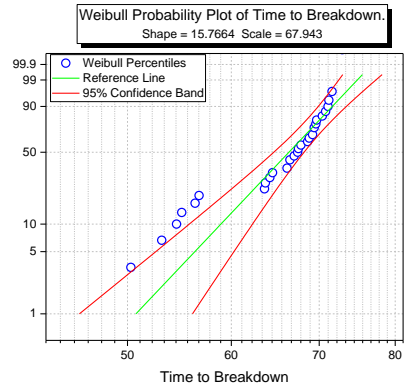


(e)

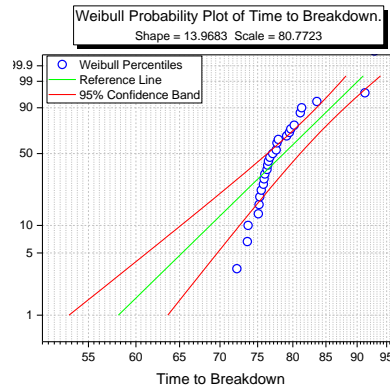
**Figure 12-3 Weibull analysis graphs for a 2mm inter-electrode gap length at 0.3MPa (a) Air (b) N<sub>2</sub> (c) 60%/40% N<sub>2</sub>/O<sub>2</sub> (d) 90%/10% Ar/O<sub>2</sub> (e) CO<sub>2</sub> with 70% of the self-breakdown voltage applied across the main inter-electrode gap length as DC stress.**



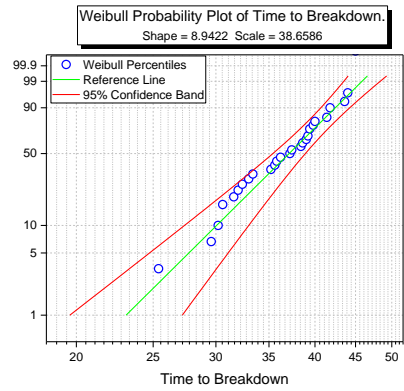
(a)



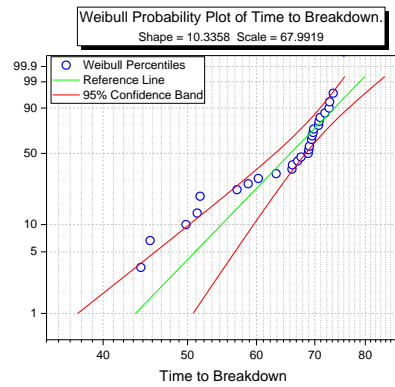
(b)



(c)

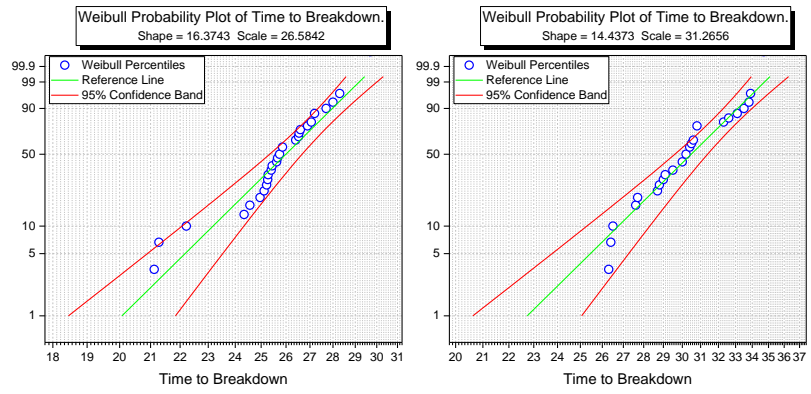


(d)



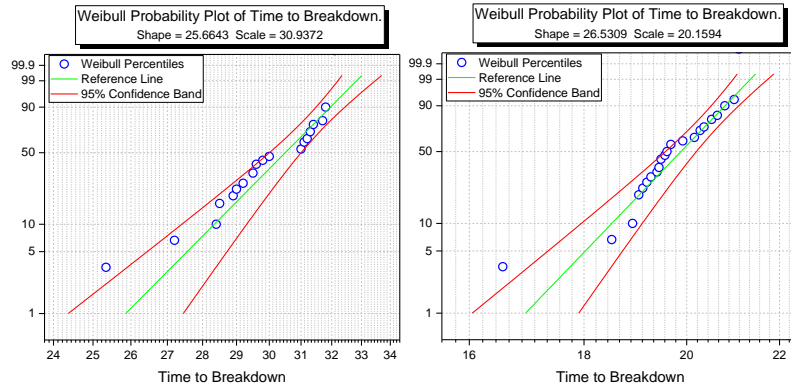
(e)

**Figure 12-4 Weibull analysis graphs for a 2mm inter-electrode gap length at 0.3MPa (a) Air (b) N<sub>2</sub> (c) 60%/40% N<sub>2</sub>/O<sub>2</sub> (d) 90%/10% Ar/O<sub>2</sub> (e) CO<sub>2</sub> with 80% of the self-breakdown voltage applied across the main inter-electrode gap length as DC stress.**



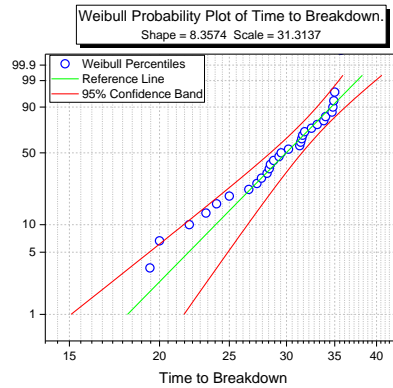
(a)

(b)



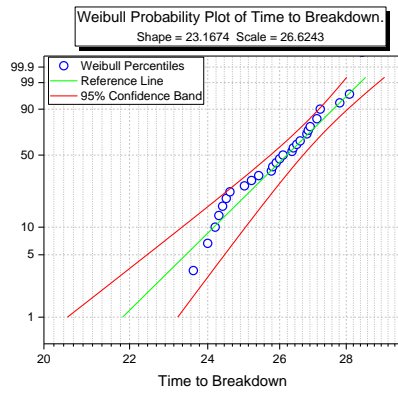
(c)

(d)

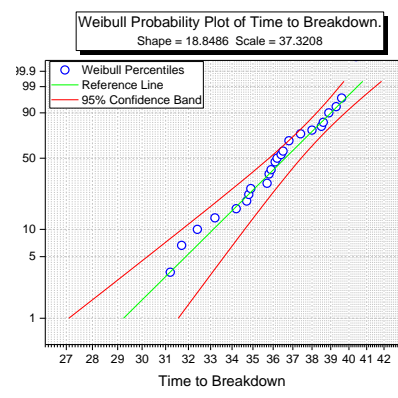


(e)

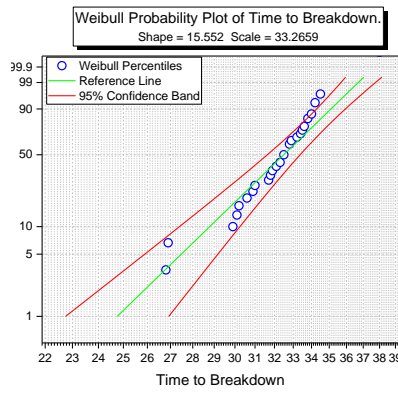
**Figure 12-5 Weibull analysis graphs for a 4mm inter-electrode gap length at 0.1MPa (a) Air (b) N<sub>2</sub> (c) 60%/40% N<sub>2</sub>/O<sub>2</sub> (d) 90%/10% Ar/O<sub>2</sub> (e) CO<sub>2</sub> with 70% of the self-breakdown voltage applied across the main inter-electrode gap length as DC stress.**



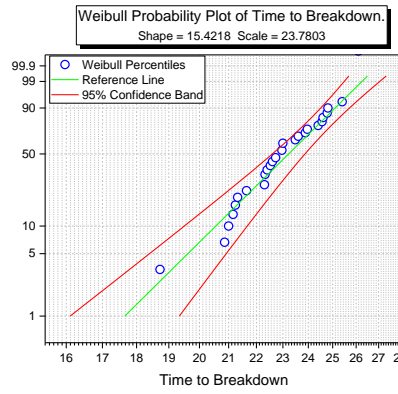
(a)



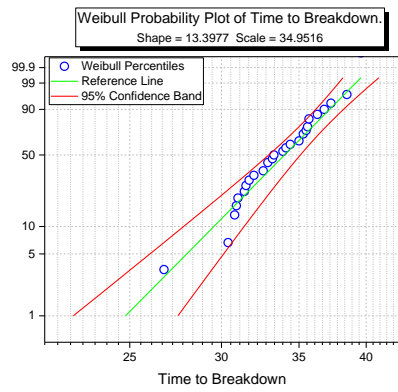
(b)



(c)

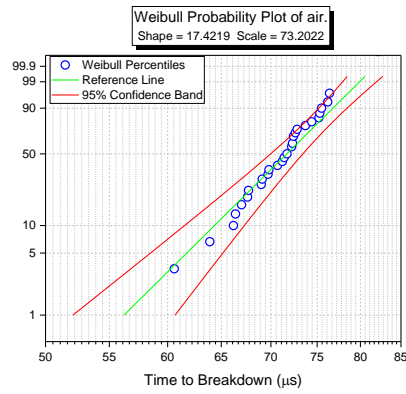


(d)

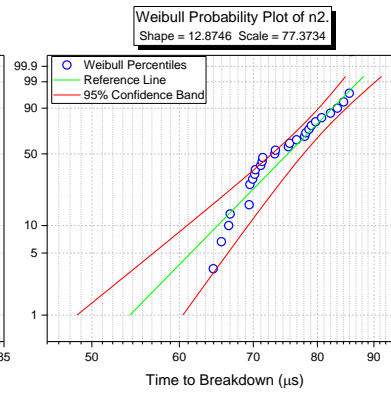


(e)

**Figure 12-6 Weibull analysis graphs for a 4mm inter-electrode gap length at 0.1MPa (a) Air (b) N<sub>2</sub> (c) 60%/40% N<sub>2</sub>/O<sub>2</sub> (d) 90%/10% Ar/O<sub>2</sub> (e) CO<sub>2</sub> with 80% of the self-breakdown voltage applied across the main inter-electrode gap length as DC stress.**

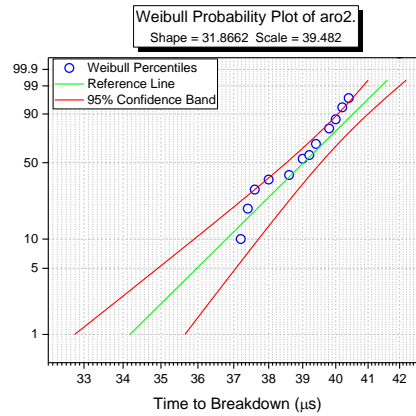


(a)



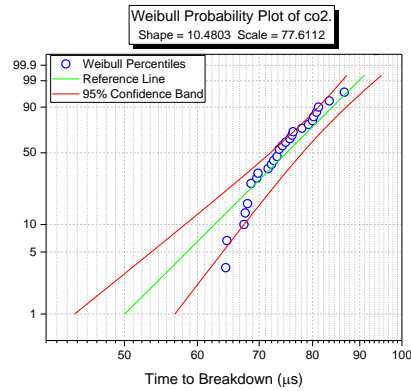
(b)

No breakdown events



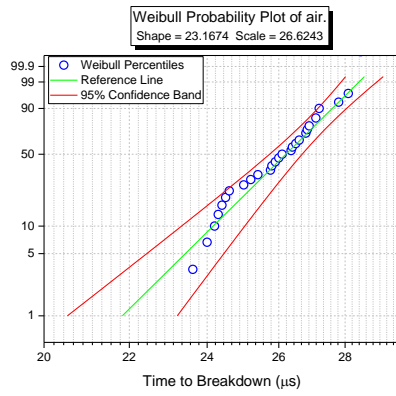
(c)

(d)



(e)

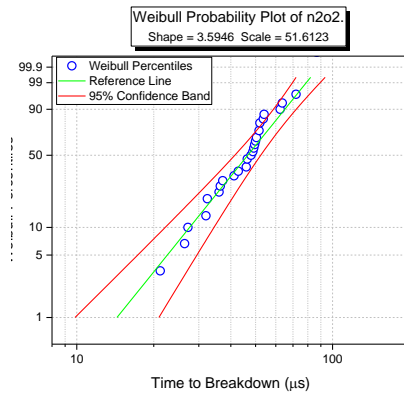
Figure 12-7 Weibull analysis graphs for a 4mm inter-electrode gap length at 0.2MPa (a) Air (b) N<sub>2</sub> (c) 60%/40% N<sub>2</sub>/O<sub>2</sub> (d) 90%/10% Ar/O<sub>2</sub> (e) CO<sub>2</sub> with 70% of the self-breakdown voltage applied across the main inter-electrode gap length as DC stress.



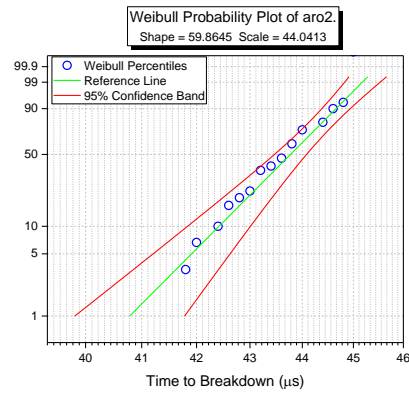
No Breakdown events

(a)

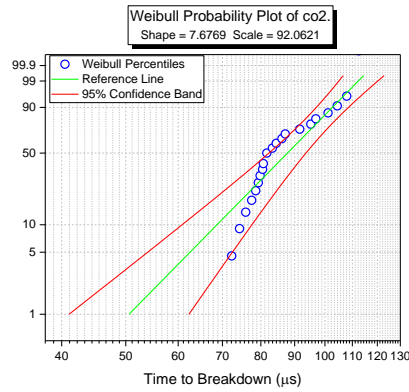
(b)



(c)



(d)



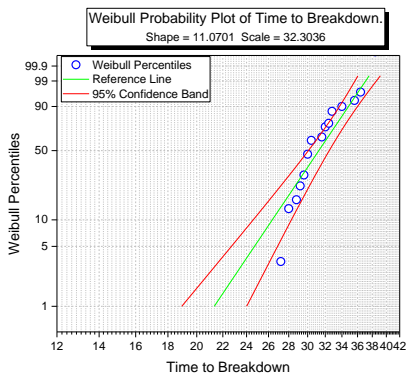
(e)

Figure 12-8 Weibull analysis graphs for a 4mm inter-electrode gap length at 0.2MPa (a) Air (b) N<sub>2</sub> (c) 60%/40% N<sub>2</sub>/O<sub>2</sub> (d) 90%/10% Ar/O<sub>2</sub> (e) CO<sub>2</sub> with 80% of the self-breakdown voltage applied across the main inter-electrode gap length as DC stress.

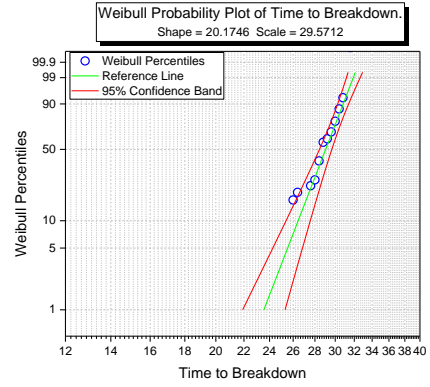
## **1B. Field-Distortion Gap triggered with 1 kV/ns triggering**

The remaining Weibull graphs for the field-distortion spark switch stressed with 70% and 80% of the self-breakdown voltage, filled with gas pressures 0.15MPa-0.4MPa, with inter-electrode gap lengths of 2mm and 4mm and triggered with a voltage impulse applied at a rate of ~1kV/ns presented within Chapter 5 are presented in Figure 12-9 – Figure 12-22.

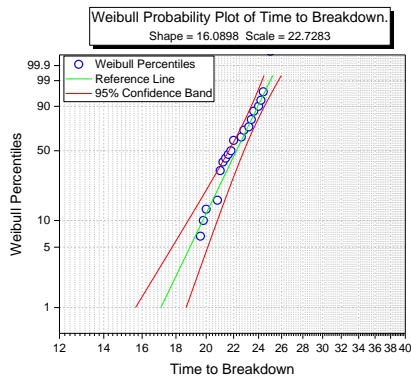
The vertical axis represents the unreliability (%) and the horizontal axis is the time to breakdown (ns). Each of the open circle symbols plotted on the graph represent breakdown events occurring at a specified time. The green line on each graph is a reference line with parameters of the shape and scale extracted from the Weibull fit of the plotted open symbols. The red lines on either side of the green line represent the 95% confidence band, that is, the band within which 95% of the breakdown events are predicted to occur.



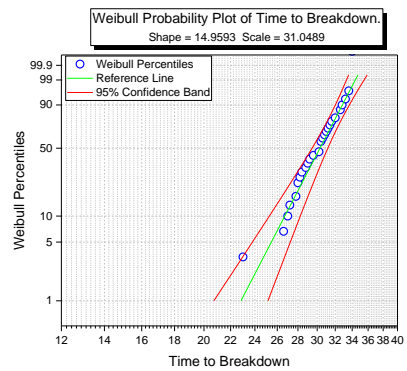
(a)



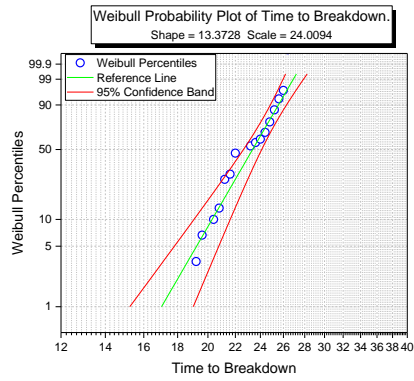
(b)



(c)

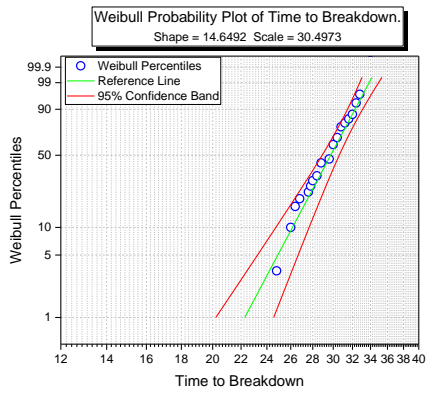


(d)

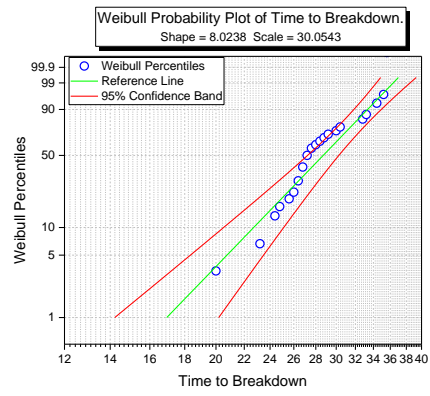


(e)

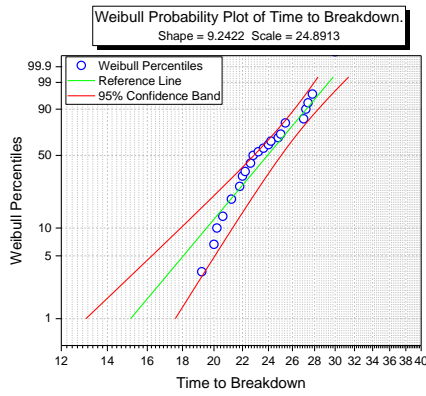
Figure 12-9 Weibull analysis for 70% DC stress applied across 2mm gap at 0.2MPa pressure.



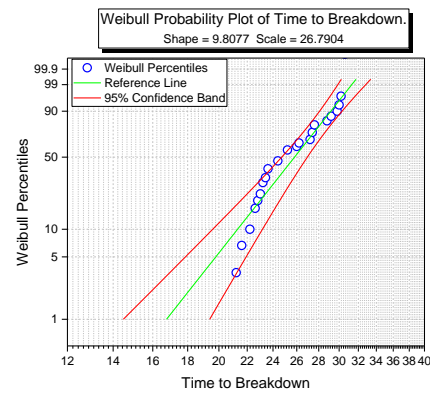
(a)



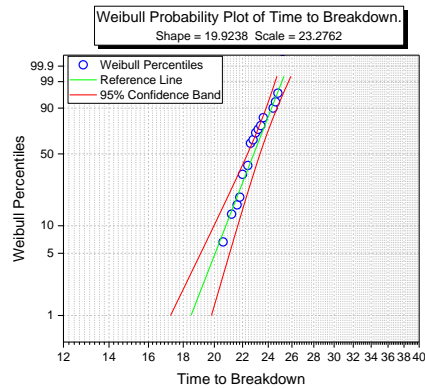
(b)



(c)

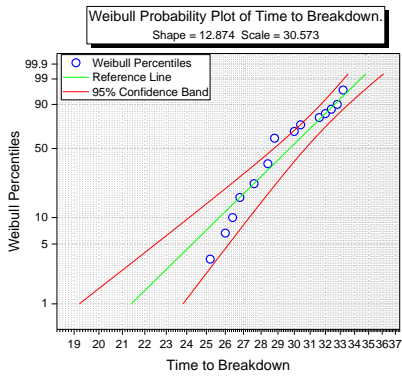


(d)

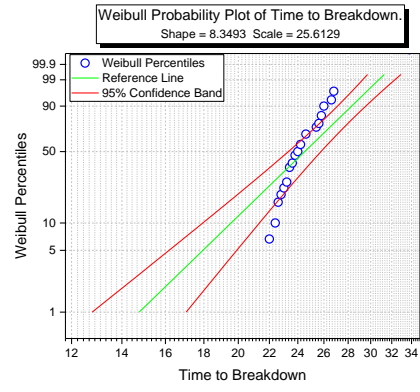


(e)

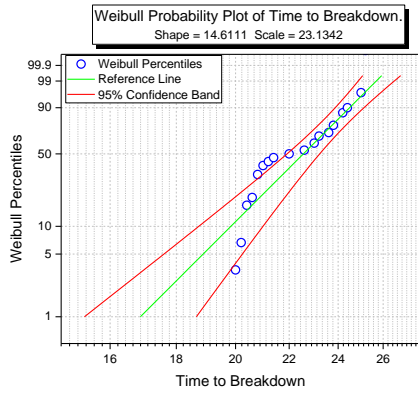
Figure 12-10 Weibull analysis for 80% DC stress applied across 2mm gap at 0.2MPa pressure.



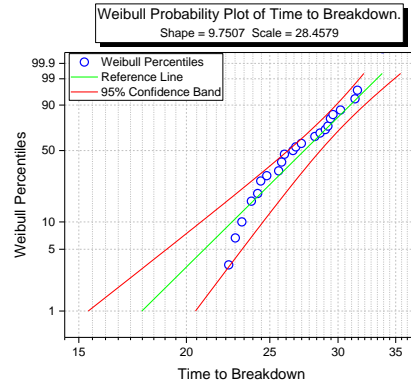
(a)



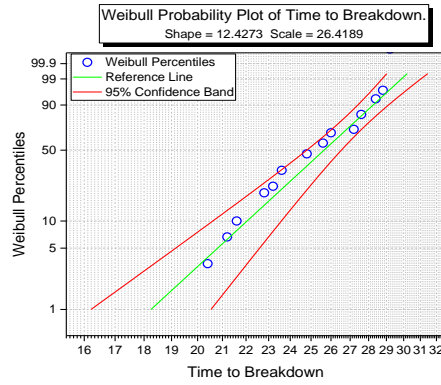
(b)



(c)



(d)



(e)

Figure 12-11 Weibull analysis for 70% DC stress applied across 2mm gap at 0.3MPa pressure.

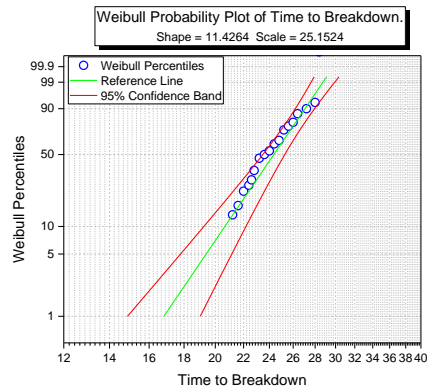
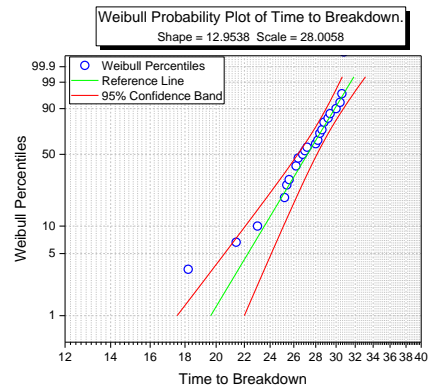
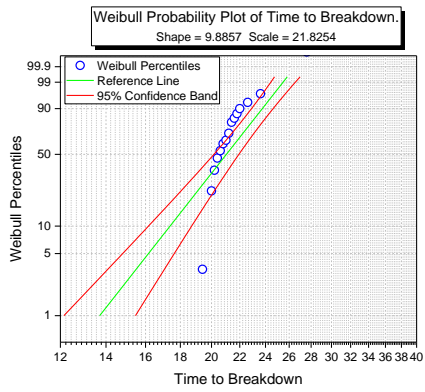
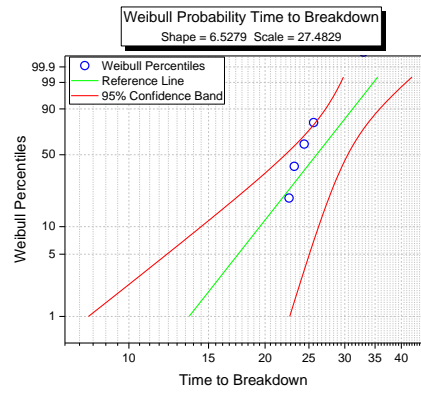
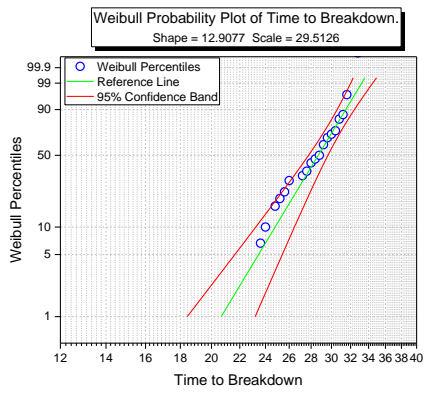


Figure 12-12 Weibull analysis for 80% DC stress applied across 2mm gap at 0.3MPa pressure.

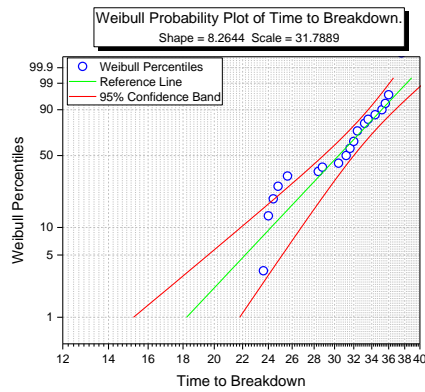
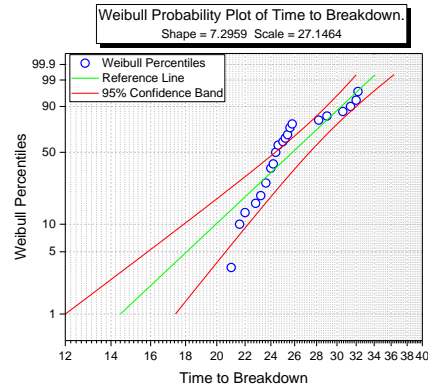
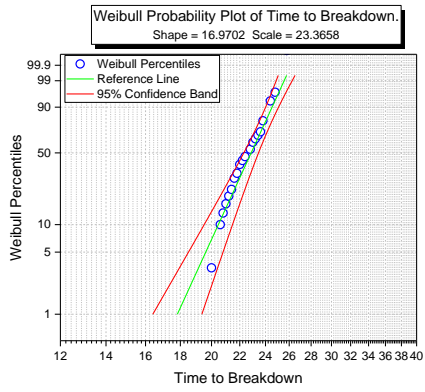
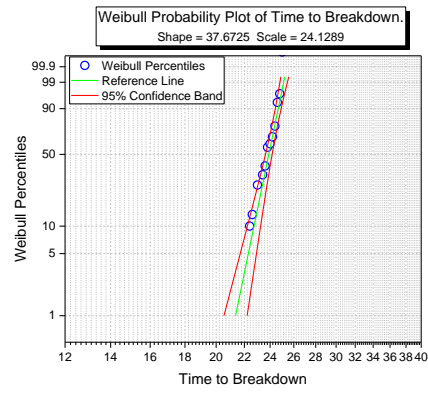
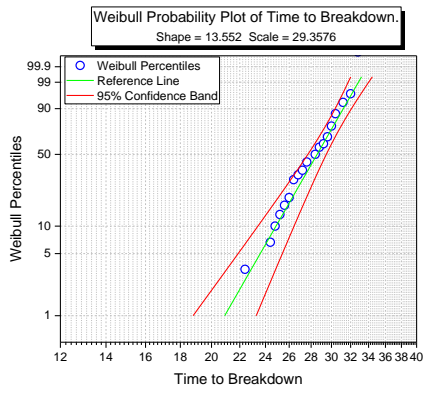


Figure 12-13 Weibull analysis for 70% DC stress applied across 2mm gap at 0.4MPa pressure.

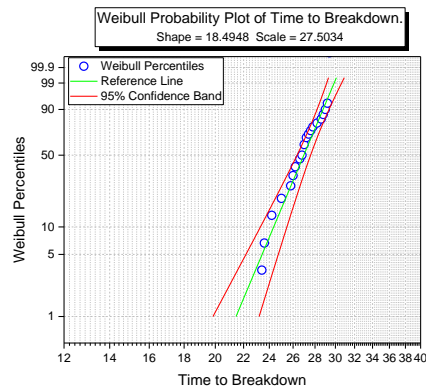
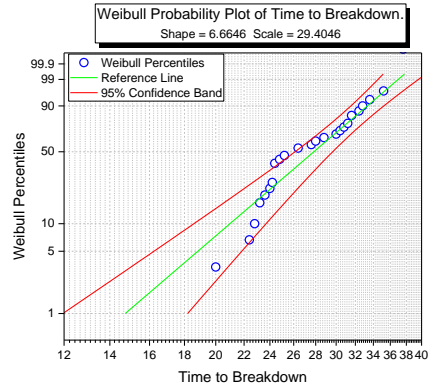
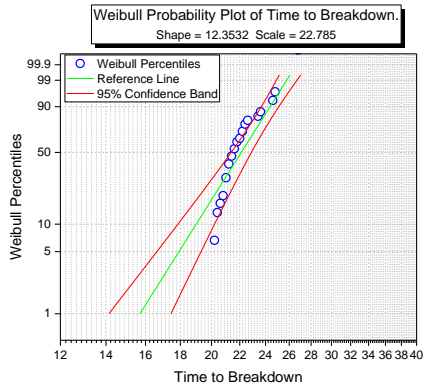
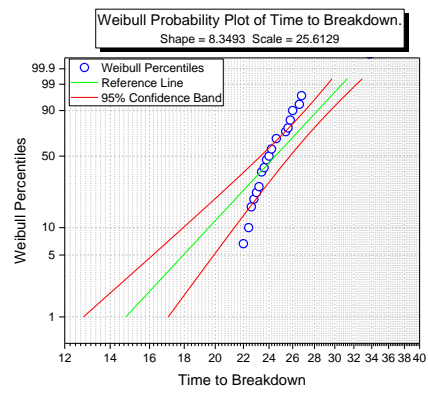
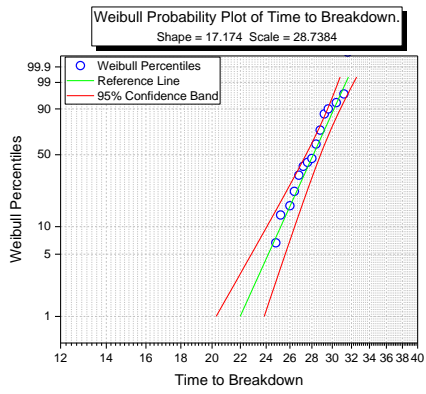


Figure 12-14 Weibull analysis for 80% DC stress applied across 2mm gap at 0.4MPa pressure.

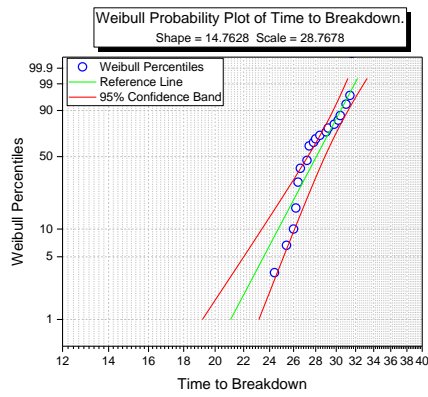
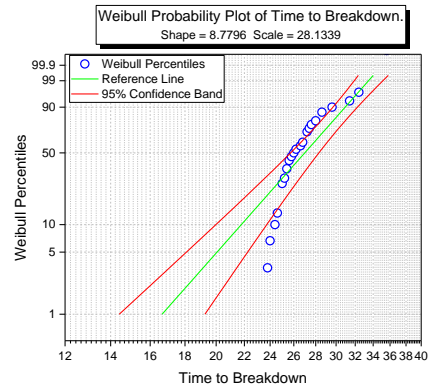
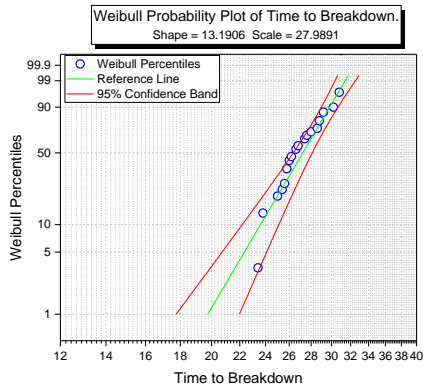
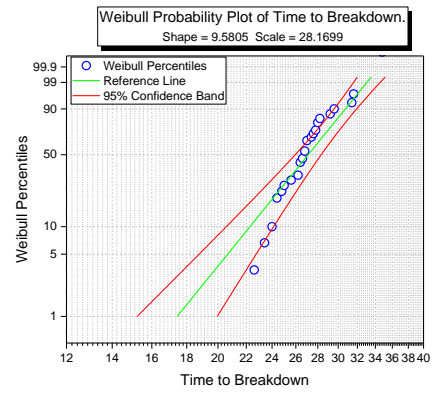
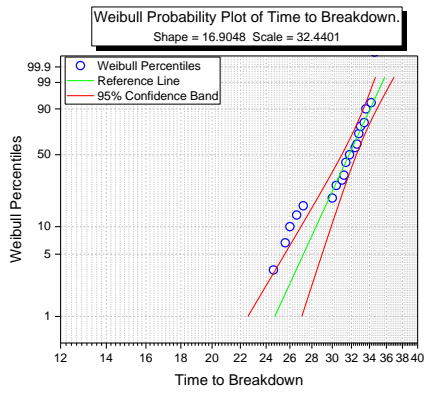


Figure 12-15 Weibull analysis for 70% DC stress applied across 4mm gap at 0.1MPa pressure.

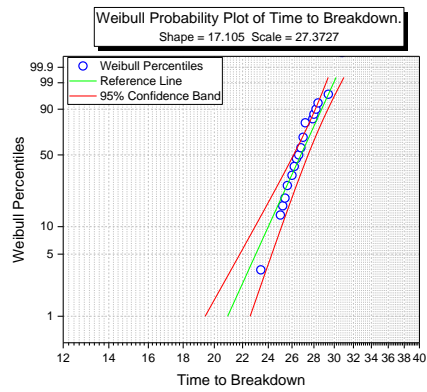
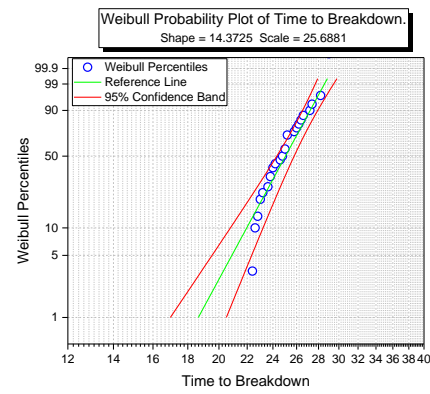
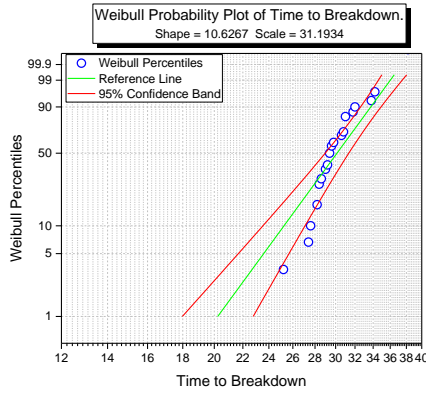
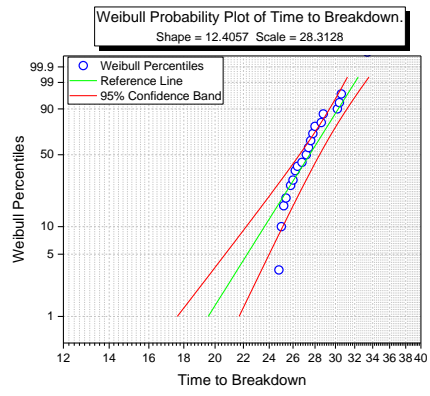
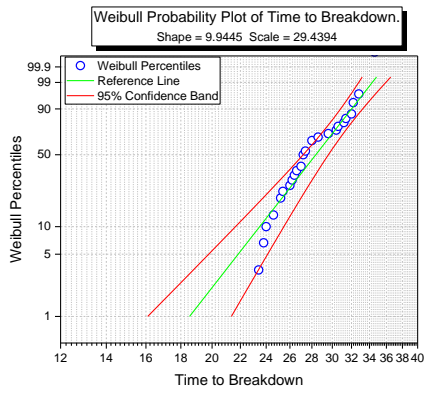


Figure 12-16 Weibull analysis for 80% DC stress applied across 4mm gap at 0.1MPa pressure.

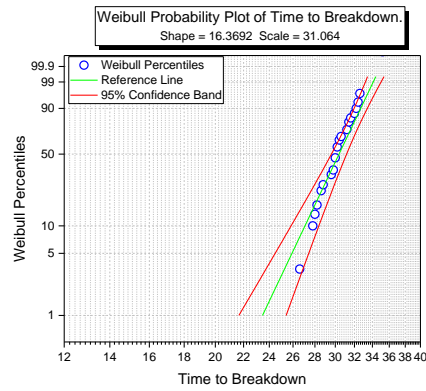
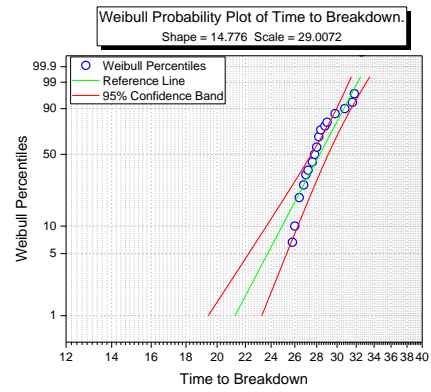
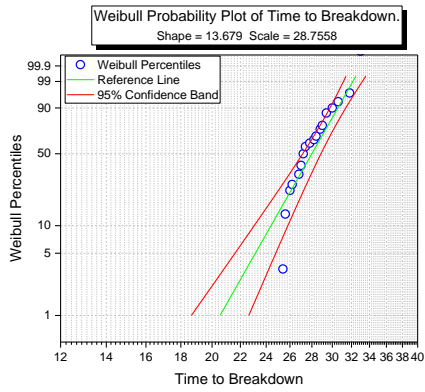
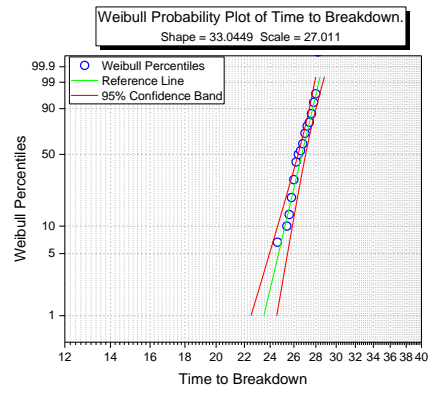
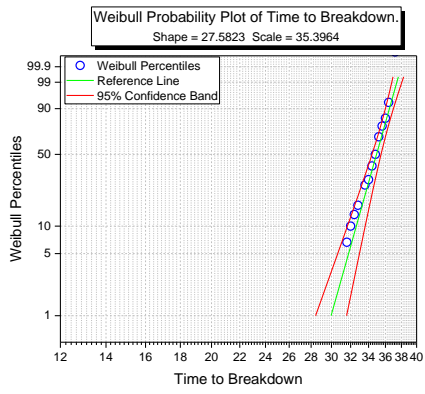


Figure 12-17 Weibull analysis for 70% DC stress applied across 4mm gap at 0.2MPa pressure.

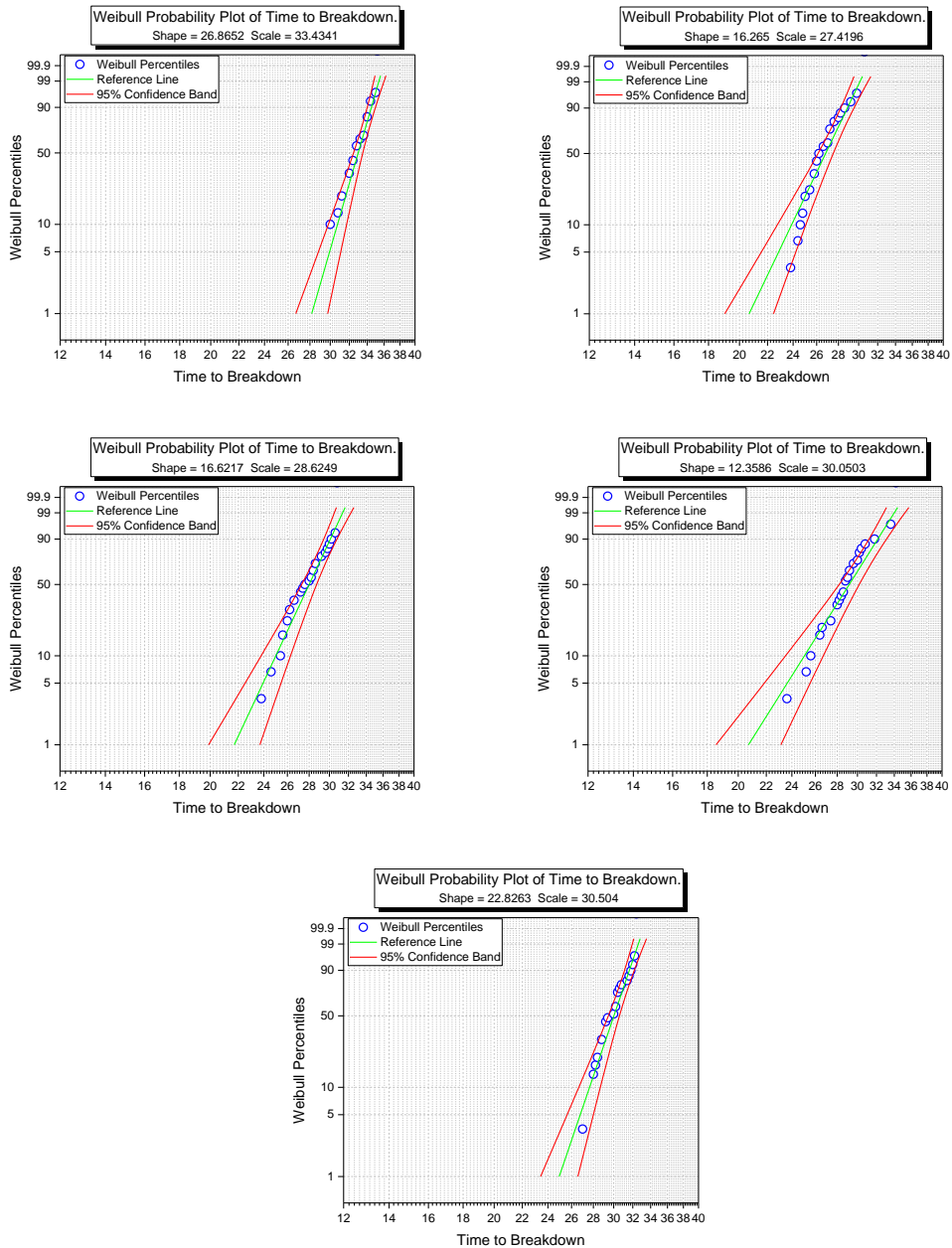


Figure 12-18 Weibull analysis for 80% DC stress applied across 4mm gap at 0.2MPa pressure.

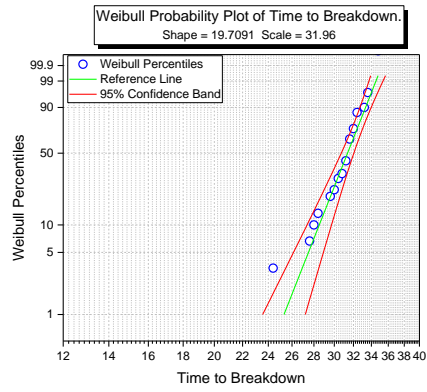
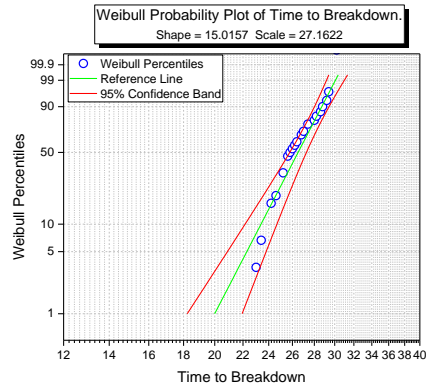
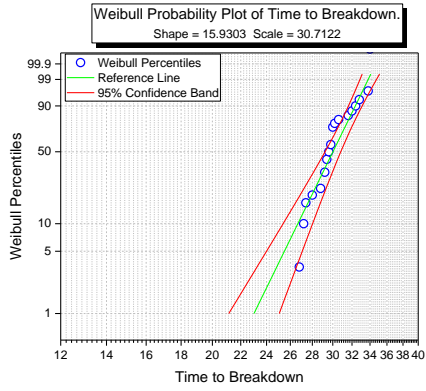
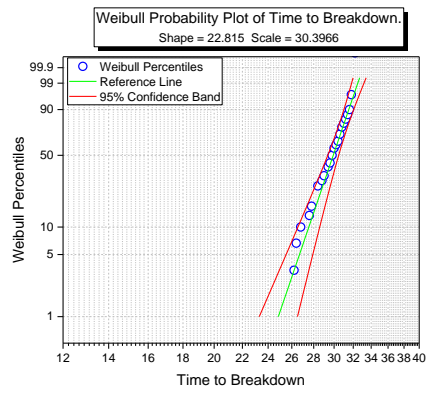
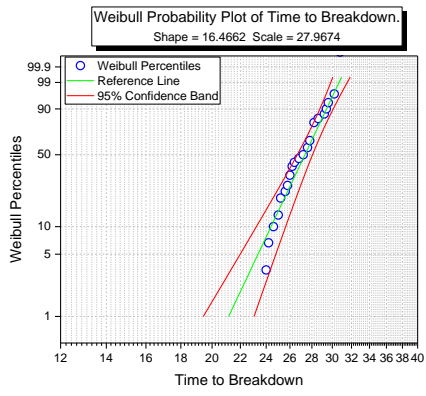


Figure 12-19 Weibull analysis for 70% DC stress applied across 4mm gap at 0.3MPa pressure.

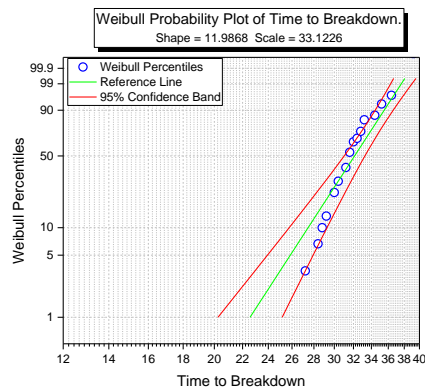
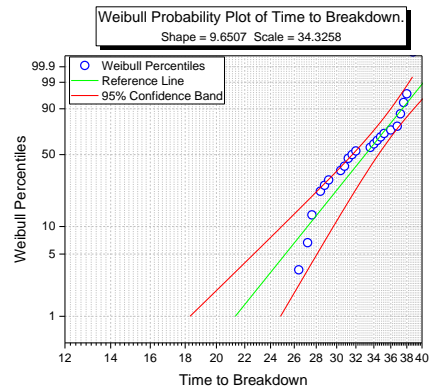
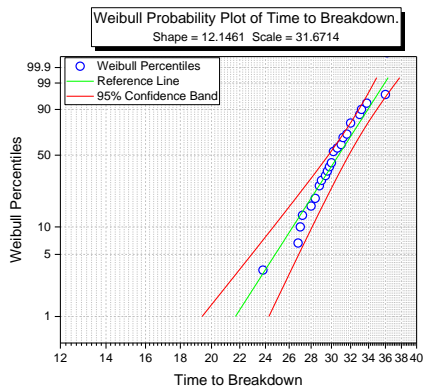
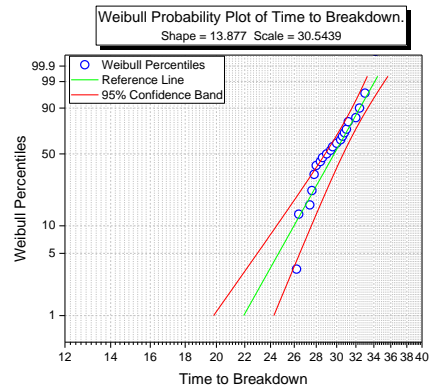
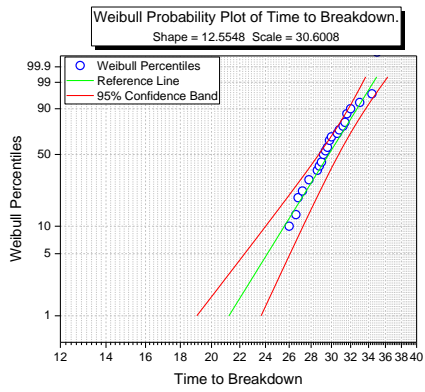
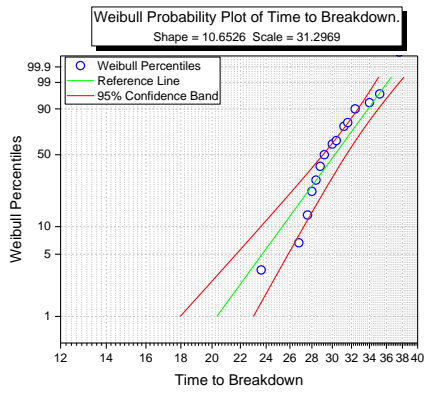
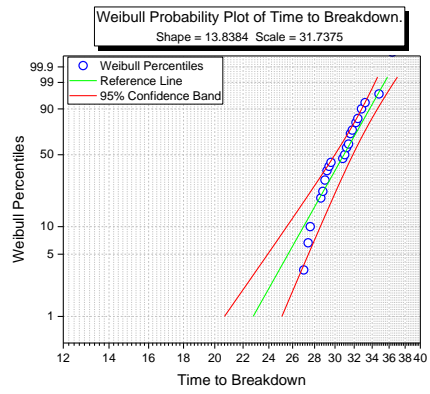


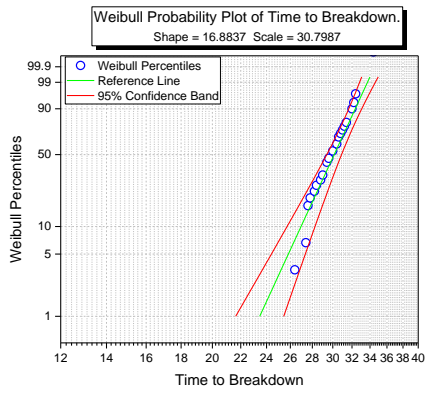
Figure 12-20 Weibull analysis for 80% DC stress applied across 4mm gap at 0.3MPa pressure.



(a)

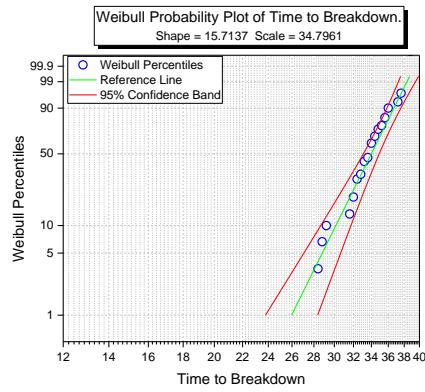


(b)



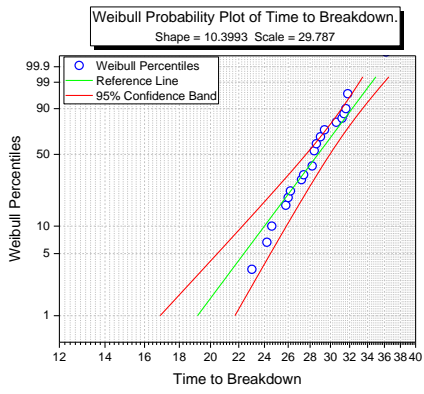
(c)

(d)

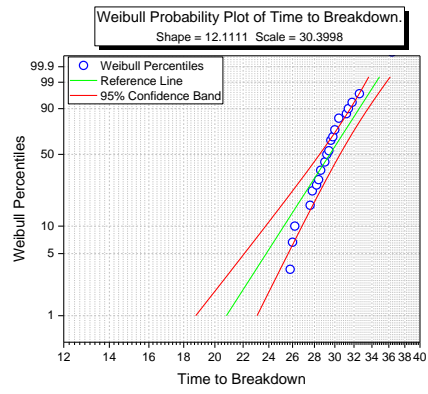


(e)

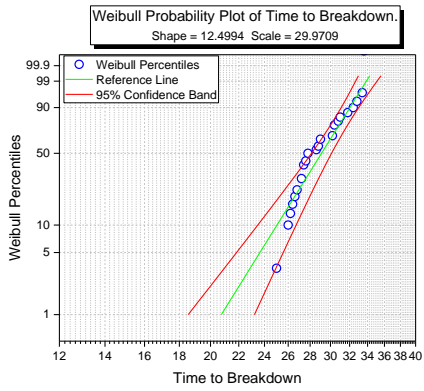
Figure 12-21 Weibull analysis for 70% DC stress applied across 4mm gap at 0.4MPa pressure.



(a)

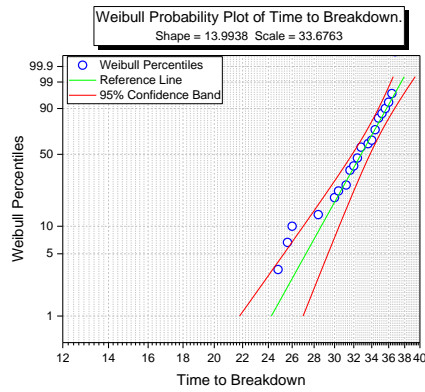


(b)



(c)

(d)



(e)

Figure 12-22 Weibull analysis for 80% DC stress applied across 4mm gap at 0.4MPa pressure.